University of Kentucky
UKnowledge

Theses and Dissertations--Chemistry | Chemistry

2012

ORGANOMETALLIC HETEROCYCLES AND ACENE-QUINONE COMPLEXES OF RUTHENIUM, IRON AND MANGANESE

Uttam Raj Pokharel
University of Kentucky, rajuttam@hotmail.com

Right click to open a feedback form in a new tab to let us know how this document benefits you.

Recommended Citation
Pokharel, Uttam Raj, "ORGANOMETALLIC HETEROCYCLES AND ACENE-QUINONE COMPLEXES OF RUTHENIUM, IRON AND MANGANESE" (2012). *Theses and Dissertations--Chemistry*. 6.
https://uknowledge.uky.edu/chemistry_etds/6

This Doctoral Dissertation is brought to you for free and open access by the Chemistry at UKnowledge. It has been accepted for inclusion in Theses and Dissertations--Chemistry by an authorized administrator of UKnowledge. For more information, please contact UKnowledge@lsv.uky.edu.

STUDENT AGREEMENT:

I represent that my thesis or dissertation and abstract are my original work. Proper attribution has been given to all outside sources. I understand that I am solely responsible for obtaining any needed copyright permissions. I have obtained and attached hereto needed written permission statements(s) from the owner(s) of each third-party copyrighted matter to be included in my work, allowing electronic distribution (if such use is not permitted by the fair use doctrine).

I hereby grant to The University of Kentucky and its agents the non-exclusive license to archive and make accessible my work in whole or in part in all forms of media, now or hereafter known. I agree that the document mentioned above may be made available immediately for worldwide access unless a preapproved embargo applies.

I retain all other ownership rights to the copyright of my work. I also retain the right to use in future works (such as articles or books) all or part of my work. I understand that I am free to register the copyright to my work.

REVIEW, APPROVAL AND ACCEPTANCE

The document mentioned above has been reviewed and accepted by the student's advisor, on behalf of the advisory committee, and by the Director of Graduate Studies (DGS), on behalf of the program; we verify that this is the final, approved version of the student's dissertation including all changes required by the advisory committee. The undersigned agree to abide by the statements above.

Uttam Raj Pokharel, Student

Dr. John P. Selegue, Major Professor

Dr. John E. Anthony, Director of Graduate Studies

ORGANOMETALLIC HETEROCYCLES AND ACENE-QUINONE COMPLEXES OF RUTHENIUM, IRON AND MANGANESE

DISSERTATION

A dissertation submitted in partial fulfillment of the

requirements for the degree of Doctor of Philosophy in the

College of Arts and Science

at the University of Kentucky

By

Uttam Raj Pokharel

Lexington, Kentucky

Director: Dr. John P. Selegue, Professor of Chemistry

Lexington, Kentucky

2012

Copyright © Uttam Raj Pokharel 2012

ABSTRACT OF DISSERTATION

ORGANOMETALLIC HETEROCYCLES AND ACENE-QUINONE COMPLEXES OF RUTHENIUM, IRON AND MANGANESE

A variety of organometallic-fused heterocycles and acene quinones were prepared and characterized. This work was divided into three parts: first, the synthesis of 5,5-fused heterocyclic complexes of tricarbonylmanganese and (1',2',3',4',5'-pentamethylcyclopentadienyl)ruthenium; second, the synthesis of 1,2-diacylcyclopentadienyl p-cymene complexes of ruthenium(II); and third, synthesis of cyclopentadienyl-fused polyacenequinone complexes of ruthenium, iron and manganese.

The first examples of the convenient, versatile and symmetric cyclopentadienyl-fused heterocycle complexes of (1',2',3',4',5'-pentamethylcyclopentadienyl)ruthenium(II) and tricarbonylmanganese(I) were synthesized starting from (1,2-dicarbophenoxycyclopentadienyl)sodium. The sodium salt was transmetalated using $[MnBr(CO)_5]$ and 1/4 $[Ru(\mu3\text{-}Cl)(Cp^*)]_4$ to give $[Mn(CO)_3\{\eta^5\text{-}C_5H_3(CO_2Ph)_2\text{-}1,2\}]$ and $[Ru\{\eta^5\text{-}C_5H_3(CO_2Ph)_2\text{-}1,2\}(Cp^*)]$. The diester complexes were saponified under basic conditions to obtain the corresponding dicarboxylic acids. The dicarboxylic acids were used to synthesize unique cyclopentadienylmetal complexes including diacyl chlorides, anhydrides, thioanhydrides and p-tolyl imides of ruthenium and manganese.

Similarly, a series of 1,2-diacylcyclopentadienyl-p-cymene cationic complexes of ruthenium were synthesized using thallium salt of 2-acyl-6-hydroxyfulvene and $[Ru(\eta^6\text{-p-cymene})(\mu\text{-}Cl)Cl]_2$ in a 2:1 ratio with an intension of converting them into heterocycle-fused cationic sandwich complexes. However, our attempts of ring closing on 1,4-diketons with sulfur or selenium were unsuccessful. A methodology involving the synthesis of metallocene-fused quinone complexes was employed starting from pentamethylruthenocene-1,2-dicarboxylic acids. The diacyl chloride was prepared in situ from the dicarboxylic

acids and used for Friedel-Crafts acylation. We observed single-step room-temperature diacylation of aromatics, including benzene, o-xylene, toluene, 1,4-dimethoxybenzene and ferrocene with pentamethylruthenocene-1,2-diacyl chloride to obtain the corresponding quinone complexes. Similarly, we synthesized mononuclear and binuclear γ-quinones by aldol condensation of 1,2-diformylcyclopentadienylmetal complexes with cyclohexane-1,4-dione or 1,4-dihydroxyarenes.

The third methodology involves the Friedel-Crafts acylation of ferrocene with 2-carbomethoxyaroyl chlorides followed by saponification, carbonyl reduction, and ring closing by second Friedel-Crafts acylation to give Ferrocene-capped anthrone-like tricyclic and tetracyclic ketones. The oxidation of the ketones gave [3,4-c]-fused α-quinone complexes of iron. The oxidative and reductive coupling, enolization and C-alkylation of the anthrone complex were studied. Solvolysis of α-carbinol gave α-ferrocenylcarbenium salt, which underwent dimerization on treatment with non-nucleophilic base. We were successful to trap the in situ generated trimethylsilyl enol ether of ferrocene-anthrone using dienophiles like N-phenylmaleimide or dimethylacetylenedicarboxylate under Diels-Alder conditions.

KEYWORDS: Pentamethylruthenocene, cymantrene, ferrocene, Aldol condensation, Friedel-Crafts acylation

Uttam Raj Pokharel

04/09/2012

ORGANOMETALLIC HETEROCYCLES AND ACENE-QUINONE COMPLEXES OF RUTHENIUM, IRON AND MANGANESE

By

Uttam Raj Pokharel

Dr. John P. Selegue

Director of Dissertation

Dr. John E. Anthony

Director of Graduate Studies

04/09/2012

Date

To

My parents

ACKNOWLEDGEMENTS

First and foremost, I would like to acknowledge and express my deepest gratitude to my advisor, Professor John P. Selegue. His guidance, advice and limitless patience over the past five and half years have been unbelievably helpful and motivational. To join his research group was one of the best decisions I have ever taken in my academic life. He has not only taught me the vital hands-on laboratory techniques but he has also trained me how to be an independent and creative researcher.

In addition, I express my sincere thanks to my Ph.D. committee, Professors John Anthony, Folami Ladipo and Douglas Kalika for their support and criticism throughout my doctoral studies. Professors Selegue and Anthony have a unique alliance in designing the current project. I feel very fortunate to have Dr. Ladipo in my committee who has been abundantly helpful, and has assisted me in numerous ways throughout this work.

Within the group, I would like to acknowledge all my colleagues, Rituraj, Mahendra, Deepshikha, Bidhya, Surya and Ilya for their friendliness and creating an excellent working environment. I must thank former group members Dr. Tice, Dr. Wallace, Dr. Blankenbuehler, and Mr. Truong who led the groundwork for my research.

I am thankful to Dr. Sean Parkin, who worked on all of my crystals and solved the single crystal X-ray analysis for each crystal structure presented in this dissertation. Thanks to Mr. John Layton for all the time and help acquiring NMR data and to Dr. Jack Goodman for analyzing mass spectra of my compounds.

I would like to express my special appreciation to my parents for everything that they have given to me without any hope of return. I am grateful to my brothers, sisters and their family for their love, continued support and encouragement throughout my academic life. My endless appreciation goes to my life-partner, Bandana, and daughter, Shradha, for always standing on my side and all the sacrifices they have made to contribute to my successful doctoral studies.

Table of Contents

ACKNOWLEDGEMENTS iii

List of Tables vi

List of Figures viii

List of Schemes x

List of Abbreviations and Symbols xii

Chapter 1: Introduction to Organic Semiconducting Materials 1

1.1.Organometallic Complexes of Fused-Ring Polyacenes 9

1.2. Metallocene-Fused Heterocycles 15

Chapter 2: The Synthesis, Characterization and Reactivities of 5,5-Fused Heterocyclic Complexes of Manganese and Ruthenium 18

2.1. Introduction 18

2.2. Experimental 19

2.1. Results and Discussion 39

2.1.1. Synthesis 39

2.1.2. Spectroscopy. 46

2.1.3. Structure. 50

2.3. Summary 89

Chapter 3: Synthesis and Characterization of 1,2-Diacylcyclopentadienyl p-Cymene Complexes of Ruthenium(II) 92

3.1. Introduction 92

3.2. Experimental 94

3.3. Results and Discussion 103

3.3.1. Synthesis. 103

3.3.2. Spectroscopy. 106

3.3.3. Structure. 108

3.4. Summary 113

Chapter 4: Synthesis, Characterization, and Reactivity of Some Metallocene-Fused Acene-Quinone Complexes 114

Introduction 114

4.1. Friedel-Crafts Acylation 116

4.1.1. Experimental 117

4.1.2. Results and Discussion 126

4.1.2.1 Synthesis. 126
4.1.2.2. Spectroscopy. 130
4.1.3.3. Electrochemistry. 132
4.1.3.4. Structure. 136
4.1.4. Summary..... 151

4.2. Aldol Condensation 152
4.2.1. Experimental 154
4.2.2. Results and discussion 160
4.2.2.1. Synthesis. 160
4.2.2.2. Spectroscopy. 163
4.2.2.3. Structure. 164
4.2.4. Summary..... 168

Chapter 5: Synthesis and Characterization of Ferrocene-Fused Acene-Quinone Complexes……170

5.1. Introduction 170

5.2. Experimental 172

5.3. Results and Discussion 198
5.3.1. Synthesis and Characterization. 198
5.3.2. Electrochemistry..... 222
5.3.3. Structure. 224
5.3.3.1. Dimerized lactones. 225
5.3.3.2. Quinones. 226
5.3.3.3. Reduced quinones..... 228
5.3.3.4. Fc-Hydroxyanthrone. 229
5.3.3.5. Monobenzyl anthrone. 230
5.3.3.6. Trimethylsilyl enol ether adducts..... 231

5.4. Summary 280

References……283

Vita……..289

List of Tables

Table 2.1. Selected ^{1}H and ^{13}C NMR data (ppm) for 1–13a 48
Table 2.2. Selected ^{1}H and ^{13}C NMR data (ppm) for 1, 2b, 3b, 8, and 10b–13b ..49
Table 2.3. Selected IR absorption frequencies of ruthenium and manganese complexes 50
Table 2.4. Crystal Data and Structure Refinement for Compounds 3a and 6a.....62
Table 2.5. Crystal Data and Structure Refinement for Compounds 10a and 15a…….....63
Table 2.6. Crystal Data and Structure Refinement for Compounds 3b, 11b and 12b 64
Table 2.7. Crystal data and structure refinement for 13a and 13b.....65
Table 2.8. Bond Distances [Å] and Angles [°] for 3a.....66
Table 2.9. Bond Distances (Å) and Angles [°] for 6a 70
Table 2.10. Bond Distance (Å) and Angle [°] of 10a 72
Table 2.11. Bond lengths [Å] and angles [°] for 13a 76
Table 2.12. Bond lengths [Å] and angles [°] for 15a 78
Table 2.13. Bond lengths [Å] and Angles [°] for 3b.....81
Table 2.14. Bond lengths [Å] and Angles [°] for 11b.....84
Table 2.15. Bond lengths [Å] and Angles [°] for 12b.....86
Table 2.16. Bond lengths [Å] andbond angles [°] for 13 87
Table 3.1. Selected NMR and IR (Nujol) Data of 3a-d.....107
Table 3.2. Crystal Data and Structure Refinement for Compound 3a.....110
Table 3.3. Bond angle [°] and bond distance [Å] of compound 3a.....111
Table 4.1. Selected ^{1}H NMR and ^{13}C NMR (ppm) data in $CDCl_3$ and IR data of complexes 3a-7 131
Table 4.2. Electrochemical data of complexes 3a, 3b and 4 showing oxidation .136
Table 4.3. Electrochemical data of complexes 3a, 3b and 4 showing reduction.136
Table 4.4. Crystal data and structure refinement for 3a, 3b and 6.....141
Table 4.5. Bond lengths [Å] and angles [°] for 3a.....142
Table 4.6. Bond lengths [Å] and Angles [°] for 3b 144

Table 4.7. Bond lengths [Å] and Angles [°] for 4 148
Table 4.8. Selected data of ^{1}H NMR, ^{13}C NMR and IR of complexes 8-13.....164
Table 4.9. Crystal Data and Structure Refinement for Compound 8a.....166
Table 4.10. Bond Distances (Å) and bond angles [°] for 8a.....167
Table 5.1. Comparison of ^{1}H and ^{13}C NMR of carbinol 8a and carbenium ion 20a..218
Table 5.2. Electrochemical data of complexes 7a and 7b showing half oxidation and half reduction.....224
Table 5.3. Crystal Data and Structure Refinement for Compounds 5a and 5b...242
Table 5.4. Crystal Data and Structure Refinement for Compounds 7a and 7b...243
Table 5.5. Crystal Data and Structure Refinement for Compounds 9a and 11a.244
Table 5.6. Crystal Data and Structure Refinement for Compounds 13a, 14a and 20a 245
Table 5.7. Crystal Data and Structure Refinement for Compounds 18a and 19a247
Table 5.8. Bond Distances (Å) and Bond Angles [°] for 5a 248
Table 5.9. Bond Distances (Å) and Bond Angles [°] for 5b 252
Table 5.10. Bond Distances (Å) and Bond Angles [°] for 7a 255
Table 5.11. Bond Distances (Å) and Bond Angles [°] for 7b 257
Table 5.12. Bond Distances (Å) and Bond Angles [°] for 9a 259
Table 5.13. Bond Distances (Å) and Bond Angles [°] for 11a 261
Table 5.14. Bond Distances (Å) and Bond Angles [°] for 13a 263
Table 5.15. Bond Distances (Å) and bond angles [°] for 14a.....267
Table 5.16. Bond Distances (Å) and bond angles [°] for 18a.....269
Table 5.17. Bond Distances (Å) and bond angles [°] for 19a.....274
Table 5.18. Bond Distances (Å) and Bond Angles [°] for 20a 277

List of Figures

Figure 1.1. Regioisomeric coupling patterns in poly(alkylthiophene)s 3
Figure 1.2. Chemical structures of some thiophene-based semiconducting polymers and oligomers 4
Figure 1.3. Soluble retro Diels-Alder pentacene precursors 5
Figure 1.4. Some functionalized acene molecules 6
Figure 1.5. Arrangements of pentacenes in the solid state:..... 7
Figure 1.6. Some substituted anthradithiophenes 8
Figure 1.7. Haptotropic rearrangement of fluorenyl complexes 10
Figure 1.9. Ring slippage of metal center from η^5-Cp to η^6-arene 12
Figure 1.10. Fluorenyl complexes of zirconium tethered in ansa-fashion 12
Figure 1.11. Dibenzo- and tetrabenzo-fluorenyl complexes of transition metals 13
Figure 1.12. Indenyl and benz[*f*]indenyl complexes of transition metals. 14
Figure 1.13. Some organometallic complexes prepared by the Selegue group . 17
Figure 2.1. Molecular Structure of [Ru{η^5-$C_5H_3(CO_2H)_2$-1,2}(Cp*)] 3a..... 54
Figure 2.2. Molecular structure of [Ru{η^5-$C_5H_3(CO_2Me)_2$-1,2}(Cp*)] 6a..... 55
Figure 2.3. Molecular structure of [Ru{$C_5H_3(CO)_2O$-1,2}(Cp*)] 10a..... 56
Figure 2.4. Molecular structure of [Ru{$C_5H_3(CO)_2S$-1,2}(Cp*)] 13a 57
Figure 2.5. Molecular structure of [Ru{η^5-C_5H_3(COOH)(CONCyCONHCy)-1,2}(Cp*)] 15a..... 58
Figure 2.6. Molecular structure of [$Mn(CO)_3${η^5-$C_5H_3(CO_2H)_2$-1,2}] 3b 59
Figure 2.7. Molecular structure of [$Mn(CO)_3${η^5-$C_5H_3(CO)_2N$-4-$C_6H_4CH_3$-1,2}] 11b 60
Figure 2.8. Molecular structure of [$Mn(CO)_3${η^5-$C_5H_3(CO_2Cl)_2$-1,2}] 12b 60
Figure 2.9. Molecular structure of [$Mn(CO)_3${η^5-$C_5H_3(CO)_2S$}] 13b..... 61
Figure 3.1. Targeted n-doped heterocycle-fused sandwich complexes of ruthenium(II)..... 93
Figure 3.2. Resonance structures of 2-acyl-6-hydroxyfulvenes[121] 104
Figure 4.1. The desired acene precursors, metallocene acenes and free acenes 115

Figure 4.2. Numbering scheme in benz[*f*]indenyl ligands 120
Figure 4.3. Disordered molecular structure of [Ru{η^5-$C_5H_3(COCHOH)C_6H_3CH_3$-1,2}(Cp*)] (6) 125
Figure 4.4. Cyclic voltammogram of [Ru{η^5-$C_5H_3(CO)_2C_6H_4$-1,2}(Cp*)] (3a) vs. Ag/Ag+ in 0.1 M Bu_4NPF_6/CH_2Cl_2 at scan rate of 50 mV/sec..... 134
Figure 4.5. Cyclic voltammogram of [Ru{η^5-$C_5H_3(CO)_2C_6H_3CH_3$-1,2}(Cp*)] (3b)135
Figure 4.6. Cyclic voltammogram of [Ru{η^5-$C_5H_3(CO)_2C_5H_3$(Fc)-1,2}(Cp*)] (4)..135
Figure 4.7. Molecular structure of [Ru{η^5-$C_5H_3(CO)_2C_6H_4$-1,2}(Cp*)] (3a) 139
Figure 4.8. Molecular structure of [Ru{η^5-$C_5H_3(CO)_2C_6H_3CH_3$-1,2}(Cp*)] (3b).. 140
Figure 4.10. Molecular structure of [Ru{η^5-$C_5H_3(CH_2OH)_2$-1,2}(Cp*)] (8a) 165
Figure 5.5. ORTEP diagram of C32H26FeO (15a)..... 209
Figure 5.3. X-ray crystal structure of $C_{36}H_{26}Fe_2O_2$ (17a) 211
Figure 5.4. Canonical structures of ferrocenylmethyl free radical..... 212
Figure 5.6. ^{1}H NMR of 20a in acetone-d_6. 217
Figure 5.7. Canonical structures of ferrocenylcarbenium ion 20a$^+$ 218
Figure 5.8. ORTEP diagram of complex $C_{36}H_{30}Fe_2$ (22a)..... 221
Figure 5.9. Cyclic voltammogram of $C_{18}H_{12}FeO_2$ (7a) 223
Figure 5.10. The electrochemical reduction of ferrocene-fused quinones 224
Figure 5.11. Packing of quinone 7b molecules on their lattice along a-axis 228
Figure 5.12. Molecular structure of $C_{36}H_{26}Fe_2O_4$ (5a) 232
Figure 5.13. Molecular structure of $C_{44}H_{30}Fe_2O_4$ (5b)..... 233
Figure 5.14. Molecular structure of $C_{18}H_{18}Fe$ (9a) 234
Figure 5.15. Molecular structure of $C_{36}H_{28}Fe_2$ (11a)..... 235
Figure 5.16. Molecular structure of $C_{18}H_{16}FeO_2$ (13a) 236
Figure 5.17. Molecular structure of $C_{25}H_{20}FeO$ (14a) 237
Figure 5.18. Molecular structure of $C_{36}H_{26}Fe_2O_2$ (17a) 238
Figure 5.19. Molecular structure of $C_{31}H_{29}FeNO_3Si$ (18a) 239
Figure 5.20. Molecular structure of $C_{27}H_{28}FeO_5Si$ (19a)..... 240
Figure 5.21. Molecular structure of $C_{36}H_{26}Fe_2O_2$ (20a) 241

List of Schemes

Scheme 2.1. Synthesis of heterocycle-fused cyclopentadienylmetal complexes..19
Scheme 2.2. Synthesis of 1',2',3',4',5'-pentamethylruthenocene-1,2-dicarboxylic acid 3a, cymantrene-1,2-dicarboxylic acid 3b and their heterocyclic derivatives 40
Scheme 2.3. Proposed mechanism of ketonic cleavage in 1,2-diacyl ketone complexes 42
Scheme 2.4. Synthesis of pentamethylruthenocene-1,2-dicarboxylic anhydride using DCC 44
Scheme 2.5. Proposed mechanism of N-acylation via four-membered cyclic tetrahedral intermediate..... 45
Scheme 3.1. Synthesis of 1,2-diacylmetallocene complexes 92
Scheme 3.2. Synthesis of 1,2-diacylcyclopentadienylp-cymene complexes of ruthenium(II) 105
Scheme 4.1. Proposed synthetic scheme of organometallic acene complexes..117
Scheme 4.2. Synthesis of acene-quinone complexes of ruthenium and their derivatives 128
Scheme 4.3. Mechanism showing selectivity of *o*-xylene for double acylation . 129
Scheme 4.4. Resonating structures of bimetallic quinone complex after acidification..... 130
Scheme 4.5. Proposed synthetic schemes of organometallic quinone complexes…….....153
Scheme 4.6. Synthesis of Cp-capped mononuclear and binuclear quinone complexes 162
Scheme 5.1. Target Fc-fused acenes and their synthetic precursors..... 172
Scheme 5.2. Synthesis of ferrocene-fused quinone complexes 199
Scheme 5.3. Synthesis of Fc-anthraquinone by two-step Friedel-Crafts acylation ..... ……201
Scheme 5.4. Equilibration of *o*-carboxybenzoylferrocene and its cyclic tautomer 202

Scheme 5.5. Proposed mechanism of dimerization of keto-acid under acidic condition 203
Scheme 5.6. Reactions of Fc-anthrone 206
Scheme 5.7. Proposed mechanism of reductive coupling 207
Scheme 5.8. The oxidative coupling and cycloaddition of trimethyl silyl enol ether 210
Scheme 5.9. The proposed mechanism of oxidative coupling and cycloaddition of 16a 213
Scheme 5.10. Solvolysis of 2,3-ferroindenol and subsequent dimerization 215
Scheme 5.11. Solvolysis of carbinol and reactions of ferrocenylcarbenium ion. 216
Scheme 5.12. Attempts to deprotonate of α-ferrocenylcarbenium salt 20a 219
Scheme 5.13. Proposed mechanism of coupling of benz[*f*]indenyl complex of iron 222

List of Abbreviations and Symbols

General

Å	angstrom, 10^{-10} m
[°]	degrees
η^5	pentahapto
Anal.	Analytical
BDT	Benzo[1,2-*b*:4,5-*b'*]dithiophene
n-BuLi	n-butyllithium, $CH_3(CH_2)_3Li$
^{t}Bu	*tertiary* butyl, $C(CH_3)_3$
18-Crown-6	1,4,7,10,13,16-Hexaoxacyclooctadecane
Calcd	calculated
Cp	cyclopentadienyl
Cp*	1,2,3,4,5-Pentamethylcyclopentadiene
d_{calc}	calculated density, Mg/m^3
DMAD	dimethylacetylenedicarboxylate
°C	degree Celsius
dec	decomposed
EI MS	electron impact mass spectrometry
Fc	ferrocenyl
g	grams
GCMS	gas chromatography-mass spectrometry
GOF	goodness of fit
h	hours
Hz	hertz, s^{-1}

kJ	kilojoules
LDA	Lithium diisopropylamide
LiHMDS	Lithium hexamethyldisilazide
M^+	molecular ion
Me	methyl, CH_3
mg	milligrams
min	minutes
mL	milliliters
mmol	millimoles
mp	melting point
MS	mass spectra
m/z	mass-to-charge ratio
Ph	phenyl
R	R-factor (for X-ray crystallography)
Rw	weighted R-factor
s	seconds
t	time
T	temperature
THF	tetrahydrofuran, C_4H_8O
Tol	tolyl, $CH_3C_6H_3$

For nuclear magnetic resonance (NMR) spectra

δ	chemical shift (in parts per million)

d	doublet
dt	doublet of triplet
J	coupling constant
m	multiplet
NMR	nuclear magnetic resonance
ppm	parts per million
q	quartet
s	singlet
sept	septet
t	triplet
td	triplet of doublets

For infrared (IR) spectra

ATR	Attenuated total reflectance
br	broad
cm^{-1}	wavenumbers
FT IR	Fourier Transform Infrared Spectra
s	strong
w	weak

Chapter 1: Introduction to Organic Semiconducting Materials

Semiconducting materials based on organic polymers and small molecules have been a subject of intense investigation for the past few decades. Polycyclic aromatic hydrocarbons and oligomers/polymers involving aromatic heterocycles have spurred much curiosity as they are the most widely studied organic π-conjugated materials for organic optoelectronic applications (light-emitting diodes, field-effect transistors, photovoltaics, etc.).[1-4] These materials have emerged as viable candidates for the charge transport layer of organic electronic devices owing to their extended conjugation, which lowers the energy gap between the HOMO (highest occupied molecular orbital) and LUMO (lowest unoccupied molecular orbital).

Organic semiconducting materials present us with the opportunity for solution-phase fabrication (e.g., spin coating, inkjet printing and screen printing) opening an avenue of wet chemistry in materials developments. Similarly, the weak intermolecular interactions of organic molecules in comparison to their inorganic counterparts allow fabrication by physical or chemical vapor deposition at low temperature on flexible substrate like plastics. These advantages of organic materials not only contribute to making future technological devices thinner, smaller and more flexible but they may also lower the manufacturing cost of electronics. The advantages of these systems may fulfill the increasing demand for inexpensive, wide-area coverage, flexible devices that can be

processed at much lower substrate temperature than the inorganic-based semiconductors.[5]

As the optimized charge-carrier mobility of organic semiconducting materials in field effect transistor studies so far is in range of amorphous silicon (0.1–1 $cm^2 \bullet V^{-1} \bullet s^{-1}$), these materials might be suitable candidate in applications like identification tags, electronic barcodes or active matrix display elements. A major problem in use of organic semiconductors is the shelf life of organic compounds as they undergo degradation upon the action of atmospheric oxygen, humidity, and light or the combinations of these stress factors.[2]

One important class of organic semiconductors is polyheterocycles, in particular polythiophene and polypyrrole. These heterocycles exhibit very good environmental stability in addition to interesting electronic properties. Their stability is due to the ability of the heteroatom to stabilize positive charge in the p-doped state.[6] A practical difficulty associated with incorporating these polyheterocycles into electronic materials is their poor solubility in common organic solvents. The insolubility of the materials makes them difficult to purify and process. However, the problem can be overcome through the introduction of alkyl chains and other solubilizing functional groups.

Facile substitution at the 3- and 4- positions of thiophene has led to the creation of polythiophene/oligothiophene derivatives with improved solubility. Since 3-alkylthiophenes are not mirror-symmetric monomers, there are three possible coupling patterns of dimeric subunits in polymer chains when thiophene

building blocks are connected solely in 2- and 5- positions (Figure 1.1). There are 2,5' (head-to-tail, HT), 2,2' (head-to-head, HH) and 5,5' (tail-to-tail, TT) coupling. Regioregular functionalization has an additional benefit of creating a more highly ordered polymer, which decreases the band gap and increases the conductivity in comparison to their regioirregular analogs (Figure 1.1).[5,7]

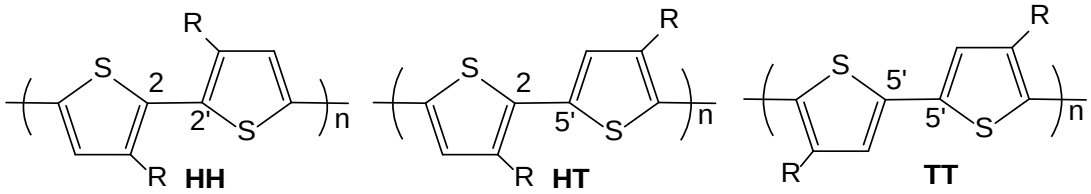

Figure 1.1. Regioisomeric coupling patterns in poly(alkylthiophene)s

Figure 1.2 shows some of the thiophene-based polymers and oligomers exhibiting p-channel semiconductivity. Poly(3-substituted thiophene)s are among the most studied polymeric materials for semiconductor applications. The oligothiophenes have rigid, rod-like molecules with extended π-conjugation along the molecular long axis and close molecular packing required for higher charge-carrier mobility. The drawbacks of using polymers for optoelectronic applications, however, are their low purity and difficulty in characterization inherent to their mass distribution.[7]

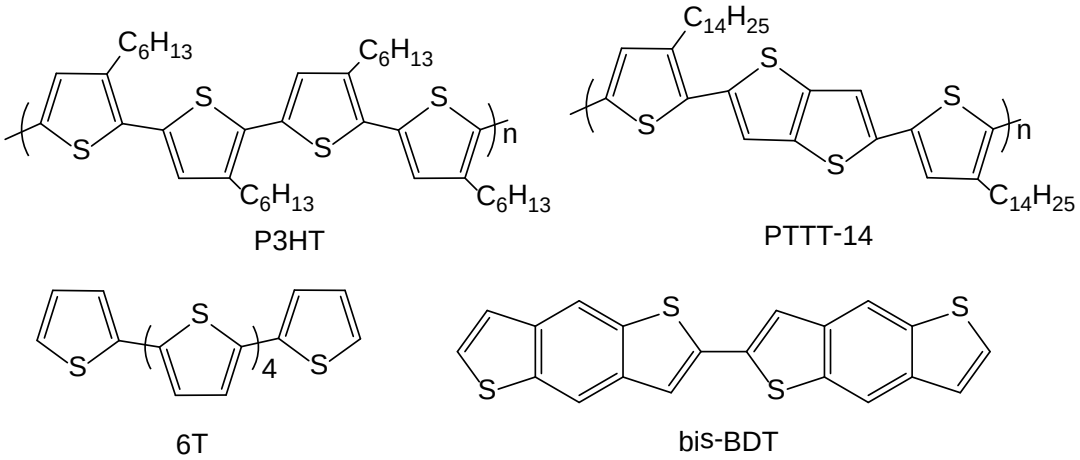

Figure 1.2. Chemical structures of some thiophene-based semiconducting polymers and oligomers

The small polycyclic aromatic hydrocarbons (oligoacenes) are interesting alternatives to polymeric semiconducting materials as they can be synthesized in high purity. Owing to their crystallinity, acene molecules often have the advantage that they order themselves very well in the solid state. The acenes possess high charge-carrier mobilities, low threshold voltages, and high on-to-off current ratios in OFETs, which are desirable qualities of semiconducting materials. However, the acenes molecules have poor solubility in common organic solvents, which hinder their solution processibility. Similarly, their instability in the presence of air and light leads to photodegradation, especially in the solution phase.[8,9]

Several strategies have been developed to fabricate pentacene and its derivatives in solution form. Müllen and coworkers reported the synthesis of soluble precursors, 6,13-dihydropentacene bridged at the 6,13 positions with 1,2,3,4-tetrachloro or 1,2,3,4-tetrabromocyclohexa-1,3-diene.[10,11] To solve the problem of multistep synthesis of the adduct and reduce the annealing

temperature, Alzali *et al.* synthesized soluble pentacene adducts by treating pentacene with N-sulfinylacetamide derivatives as dienophiles (Figure 1.3). After application of a thin film onto a suitable substrate, the bridging groups were removed thermally or photochemically in a retro-Diels-Alder reaction to give unsubstituted pentacene in a polycrystalline film.[12,13]

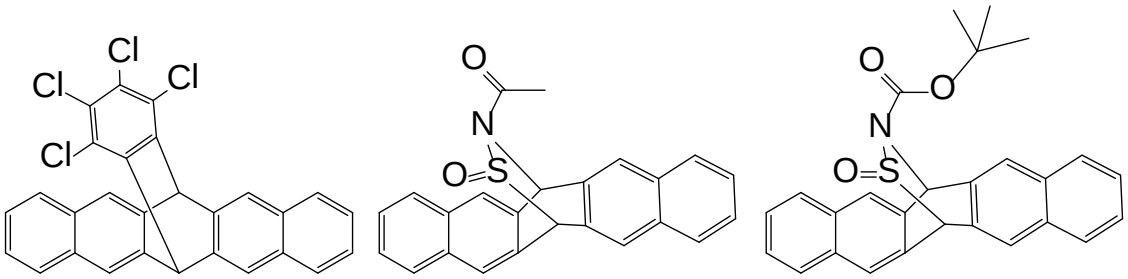

Figure 1.3. Soluble retro Diels-Alder pentacene precursors

Deposition of soluble precursors and their degradation on substrates produced film with high OFET mobility. However, these methods require annealing at around 200 °C. An alternative possibility for solubilization of pentacene was afforded by adding solubilizing side-groups. Bao and Wudl introduced methyl groups on terminal rings in order to tune the electronic properties as well as alter the solubility of pentacene.[14] After a careful calculation of the effect of size of side-groups on crystal packing of the acene molecules, Anthony *et al*. introduced trialkylsilylethynyl groups on one or more *peri* positions.[15] The size of the silylethynyl side group is pivotal for the electronic communication in the solid state and the stability of the acenes in solution. Moreover, sterically demanding substituents hinder the approach of dienophilic multiple bonds to the reactive central aromatic ring, preventing dimerization by

Diels-Alder cycloaddition. Aromatic annulation of the acene backbone is another way of modifying their properties. The Anthony group has optimized the method to extend the size of acene backbone all the way to nonacene (Figure 1.4).[16,17]

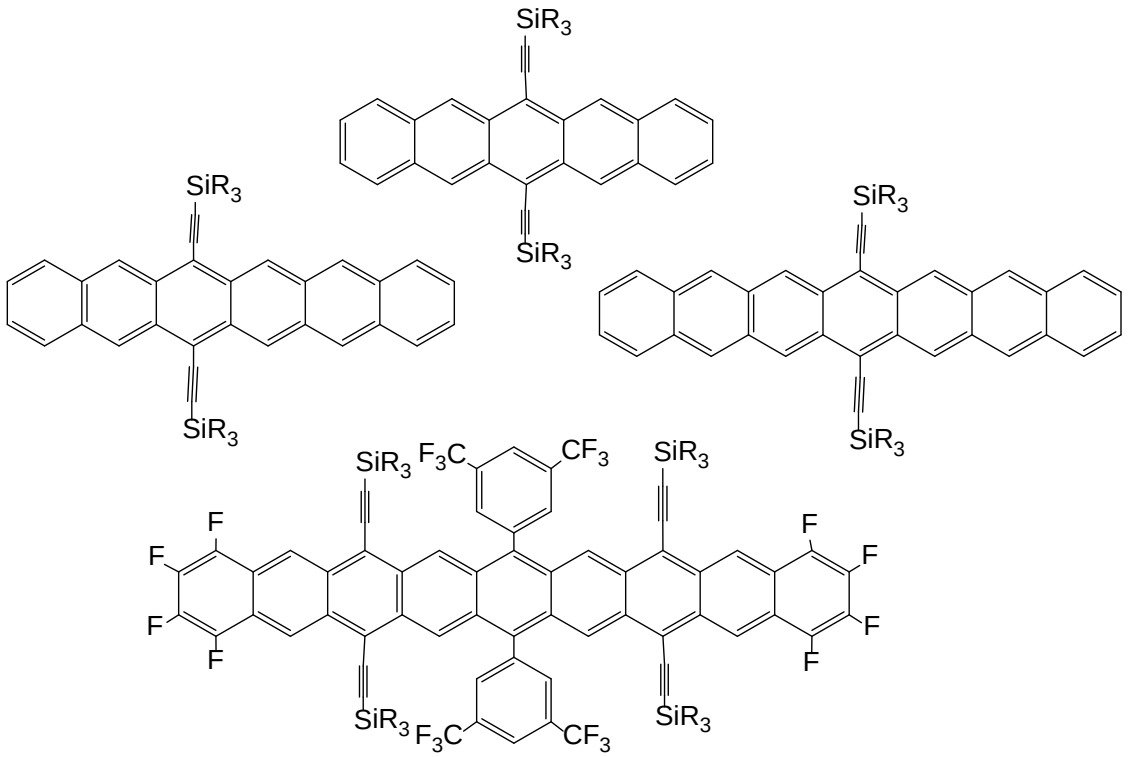

R = *i*-Pr, *i*-Bu, $SiMe_3$, *t*-Bu, Cyclopentyl

Figure 1.4. Some functionalized acene molecules

The size of the alkynyl side group plays a major role in the electronic communication of the molecules in solid state. Unsubstituted pentacene crystallizes in a herringbone packing motif, dominated by edge-to-face configuration of the molecule (Figure 1.5a). The functionalized side group, on the other hand, forces the acenes into a stacked face-to-face configuration. The Anthony group found that the electronic interaction of the pentacene molecules is greatest when the size of the substituents on the pentacene corresponds to the

about half the length of pentacene molecule (7 Å) (Figure 1.5b). The situation happens when triisopropylsilyl (7.5 Å) groups are used as substituents at the 6,13-positions of pentacene. Similarly, when the size of the substituents is slightly smaller than 7 Å (e.g., triethylsilyl, 6.6 Å), it adopts a one-dimensional columnar arrangement (Figure 1.5c). With substituents significantly larger than half the size of pentacene, a one-dimensional columnar arrangement is again found. [15,16,18]

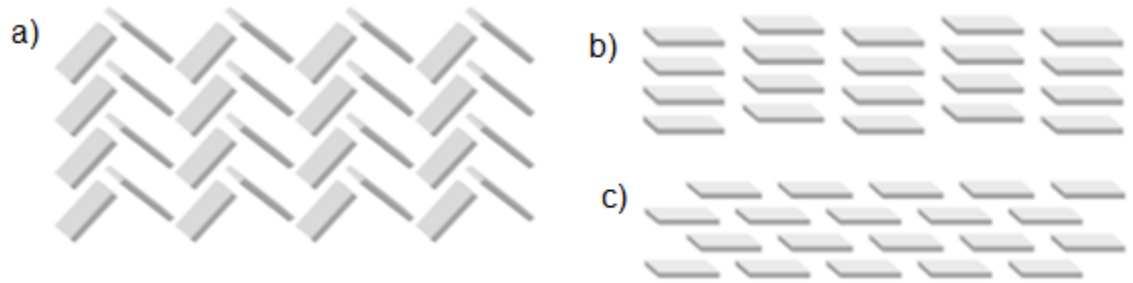

Figure 1.5. Arrangements of pentacenes in the solid state: **a)** herringbone arrangement in unsubstituted pentacene; **b)** one-dimensional columnar arrangement of alkynyl-substituted pentacene; **c)** two-dimensional brick-wall arrangement of silylalkynyl-substituted pentacene.[5]

Acenes have been modified by incorporating heteroatoms in their aromatic core to give linear fused (hetero)acenes. Katz and co-workers synthesized terminally alkyl-substituted anthradithiophene (ADT) in a multistep synthesis.[19] Similarly, the Anthony group synthesized ADT with its central aromatic ring substituted with a (trialkylsilyl)ethynyl group.[20] The same group has lately synthesized *syn* and *anti* isomers of ADT amides and separated them by fractional crystallization.[21] To control the regiochemistry of molecules, Geerts *et al*. recently designed a method to synthesize isomerically pure *anti*-ADT with

alkyl side chain attached to positions 2 and 8 of the ADT skeleton to fulfill solubility requirements (Figure1.6).[22] Isoelectronic with pentacene, substituted anthradithiophene (ADT) shows better stability towards photooxidation and higher charge-carrier mobility than similarly substituted pentacene.[23]

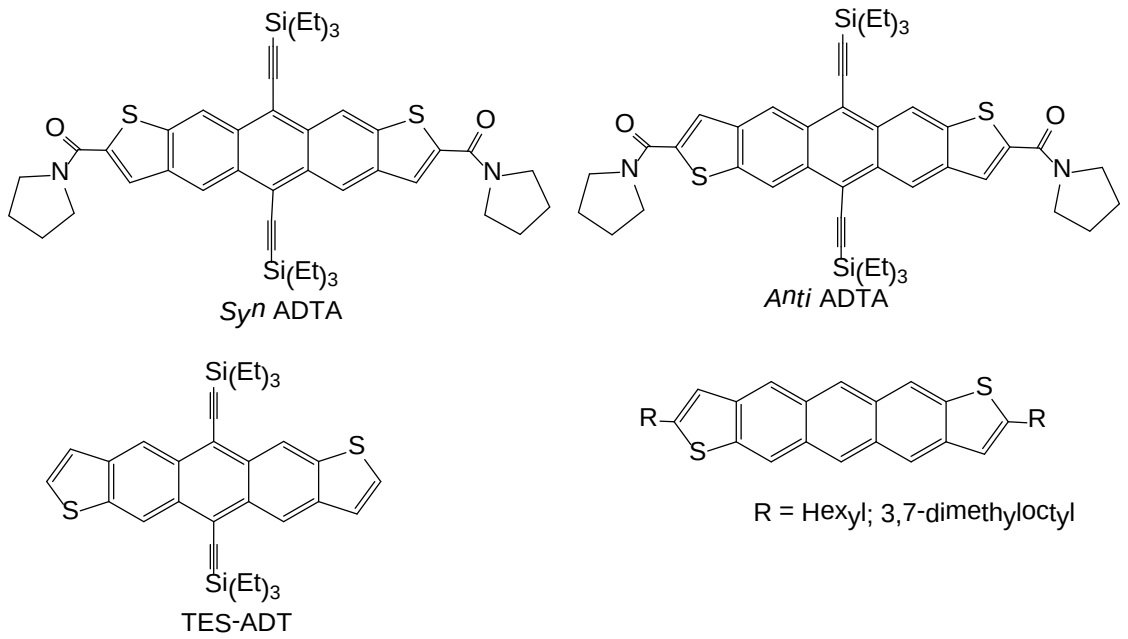

Figure 1.6. Some substituted anthradithiophenes

Existing at an interface of inorganic and traditional polymer chemistry, organometallic semiconducting materials may offer functional molecules that combine the physical and electronic properties of all-organic conducting materials with the physical, electronic, optical and catalytic properties inherent to organometallic complexes. Metallocenes can be attractive functional groups to incorporate on the main chain of the polymer because of their unique redox-active metal centers and the π-conjugated backbone to offer electron transfer. Electronic communication of metal centers with a polymeric backbone can be used for the design of novel electro-active organometallic materials.[24-30]

Organometallic conducting materials may display increased environmental stability due to the presence of transition metal centers in their molecules. The transition metal center may act as a 'switch' by changing its oxidation states, which enables these materials to be doped and undoped reversibly in different electronic environments.[31]

1.1.Organometallic Complexes of Fused-Ring Polyacenes

Organometallic sandwich and half-sandwich complexes with polycyclic aromatic acenes as ligands are not very common in semiconducting applications. However, fluorenyl and indenyl complexes of group 4 metals are extensively used in the regioregular catalysis of olefin polymerization. The most characteristic feature of these complexes is a facile change in bonding mode from $\eta^5 \rightarrow \eta^3 \rightarrow \eta^1$ (ring slippage) in the five-membered ring of indenyl or fluorenyl ligands (Figure 1.7). The haptotropic rearrangements of indenyl and fluorenyl ligands provide additional coordination sites at the metal center and thus increase their catalytic activity for olefin polymerization. Although fluorene and benz[*f*]indene are isomers, the fluorenyl complexes are less stable than indenyl complexes due to the involvement of the π-electrons of the central five-membered ring system in the aromaticity of fused six-membered rings.[32,33] Shortly after the discovery of ferrocene, some indenyl complexes were synthesized but fluorenyl complexes remained unexplored for a long time.

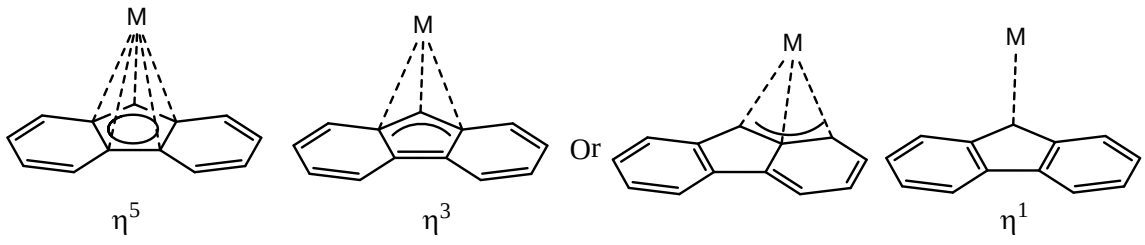

Figure 1.7. Haptotropic rearrangement of fluorenyl complexes

Fluorene can be regarded as a doubly benzannelated cyclopentadiene, which may be deprotonated at the 9 position to generate a substituted Cp ligand. Serious problems with fluorenyl complexes are their poor solubility and instability in donor solvents. In 1970 King and Efraty reported the synthesis of [Mn(η^5-fluorenyl)$(CO)_3$], the first transition metal η^5-fluorenyl complex in 11% yield by reacting fluorenylsodium with [$Mn(CO)_5Br$] in refluxing THF; its bonding modes was determined on the basis of NMR.[34] Decken *et al*. determined the crystal structures of [Mn(η^1-$C_{13}H_9$)$(CO)_5$] and [Mn(η^5-$C_{13}H_9$)$(CO)_3$], proving the intermediacy of a monohapto complex in the formation of a pentahapto one.[35] Even though Samuel and Setton synthesized the first group 4 bis(fluorenyl) complex, [Zr(η^5-$C_{13}H_9$)Cl_2] [36] in 1965, its structure was not determined for a decade.[37] The Gassman group synthesized [Ru(η^5-$C_{13}H_9$)(Cp*)] and compared the electronic effect of fluorenyl with cyclopentadienyl, indenyl and pentamethylcyclopentadienyl ligands.[38] Similarly, highly electron-rich 1,2,3,4,5,6,7,8-octamethylfluorene (Flu”) and 1,2,3,4,5,6,7,8,9-nonamethylfluorene (Flu*) gave mixed-ligand fluorenyl ruthenocenes.[39] To enhance the solubility and compare the electronic influence of an expanded aliphatic ring, the Millar group attached a octamethyloctahydrodibenzofluorenyl

(Oct) ligand to manganesetricarbonyl and made electronic comparisons between a sterically expanded ligand and its cyclopentadienyl analogues.[40] A fluorenyl sandwich complex of a rare earth metal, [Eu(thf)(η^5- η^5-$C_{13}H_9$)$_2$] has also been synthesized (Figure 1.8)[41]

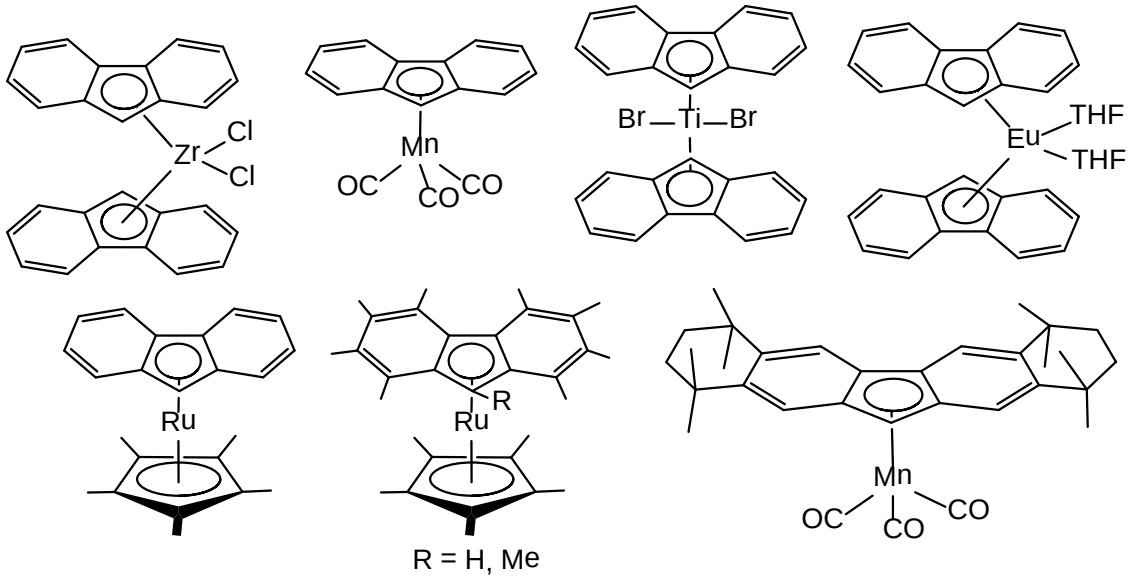

Figure 1.8. Some fluorenyl complexes of transition metals

In an attempt to synthesize a fluorenyl complex of iron, [Fe(η^5-C_5H_5)(η^5-$C_{13}H_9$)], Johnson and Treichel observed an unexpected ring-slippage where Fe atom was coordinated to a six-membered arene ring instead of a five-membered one to give a zwitterionic iron complex (Figure 1.9)[42] Similar results were obtained by the O'Hare group when metathesis of ferrocene was done with Flu*H in the presence of excess $AlCl_3$ and Al powder.[43] This is possibly due to weak coordination of π-extended Cp-type ligands that can lead to the ring slippage or metal shifting.

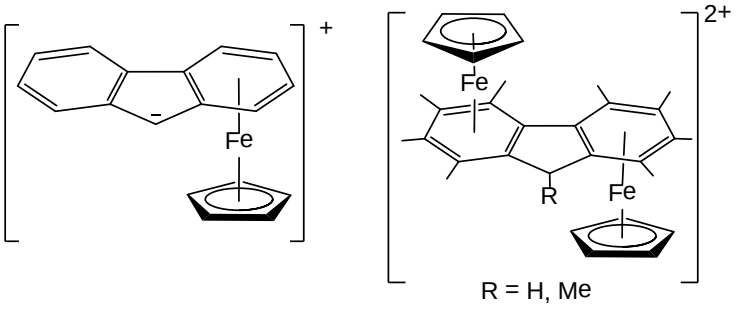

Figure 1.9. Ring slippage of metal center from η^5-Cp to η^6-arene

There are several examples of fluorenyl complexes of early transition metals containing a tether between two fluorenyl groups in '*ansa*' fashion (Figure 1.10) either with hydrocarbon[44] or silicon-containing chains[45,46] to enhance their stability as well as the steric rigidity needed for catalysis in regioregular olefin polymerization.[44,45] Millar and Bercaw synthesized mixed-sandwich *ansa* complexes of zirconium and hafnium using sterically expanded fluorene derivatives [$ZrMe_2C(Oct)Cl_2(C_5H_4)$] to see the influence of distal methyl substituents in syndiotactic polymerization of polypropylene.[47]

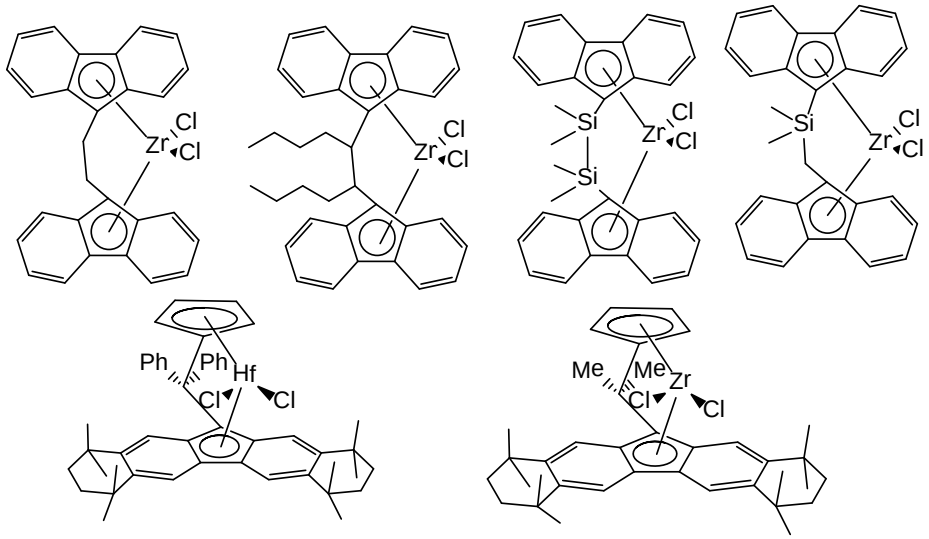

Figure 1.10. Fluorenyl complexes of zirconium tethered in ansa-fashion

Investigations of benz annulated cyclopentadienyl anions as ligands in organometallic chemistry have intensified in recent years. The Thiel group made a theoretical and experimental investigation to prove that the charge distribution in the Cp ring is much more uniform in dibenzo[*c,g*]fluorenyl (Dbf^-) anion than in fluorenyl anion.[48] This is due to localization of aromaticity in the five-membered and two of the four six-membered rings. The dbf^- ligand can stabilize a transition metal center almost as efficiently as cyclopentadienyl ligand. The same group synthesized sandwich and half-sandwich complexes of iron, manganese[50] and ruthenium using dibenzo[*c*,*g*]fluorenyl as a ligand. The chloro ligand in $[RuCl(PPh_3)_2(\eta^5\text{-Dbf})]$ has been abstracted by $AgSbF_6$ in the presence of acetonitrile to give an ionic complex.[51] Similarly, tetrabenzo[*a,c,g,i*]fluorenyl complexes of titanium have been synthesized (Figure 1.11).[49]

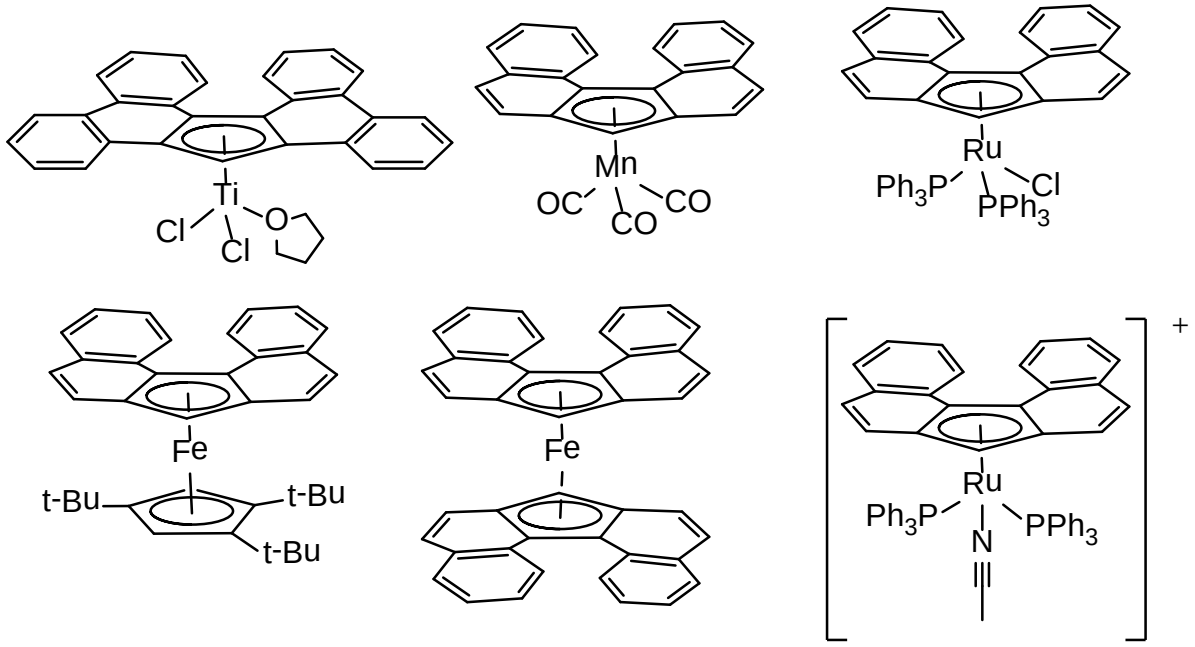

Figure 1.11. Dibenzo- and tetrabenzo-fluorenyl complexes of transition metals

Figure 1.12 shows some of the indenyl and benz[*f*]indenyl complexes of early and late transition metals. The use of benz[*f*]indene in place of cyclopentadienyl ligand has gained much attention because an annulated benzo ring might improve both stereo-control and a catalytic turnover.[50] Foster *et al.* synthesized catalyst precursors containing a substituted indenyl group as the ligand in a titanium complex that was activated by methylaluminoxane (MAO) to study the effect of indenyl substituents in catalysis of syndiospecific styrene polymerization.[51] Kim *et al.* prepared benz[*f*]indenyl zirconium complexes, and their catalytic activity was studied for the polymerization of ethene to high molecular weight linear polymers.[52] Roush *et al*. synthesized [$TiCl_3$benz[*e*]Ind] along with its 2-methyl and 1,2,3-trimethyl derivatives; however, their attempts to synthesize a benz[*f*]indenyl complex of titanium failed.[51]

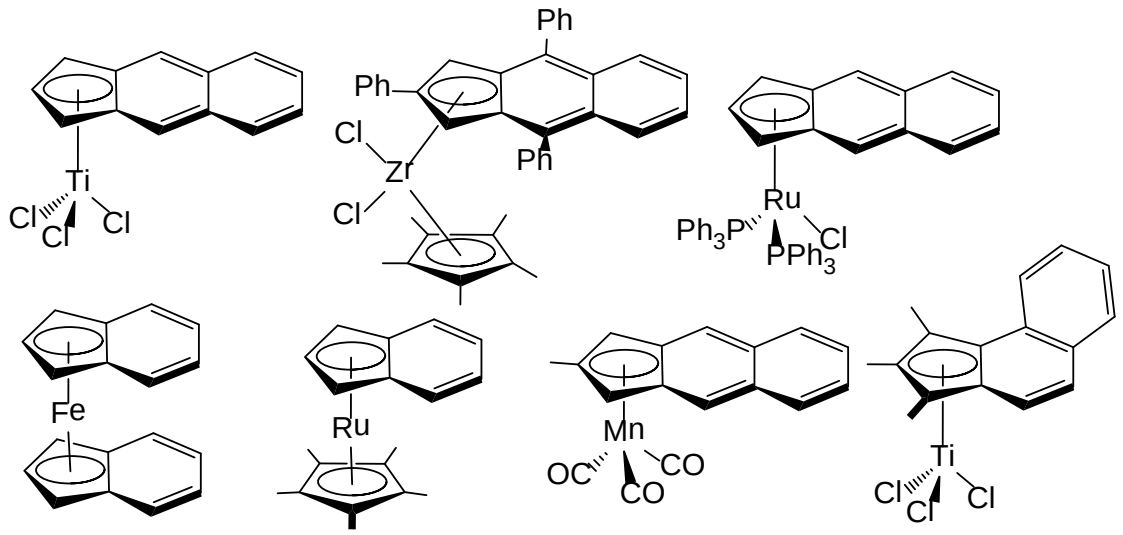

Figure 1.12. Indenyl and benz[*f*]indenyl complexes of transition metals.

Although bis(indenyl)iron (II) was successfully characterized,[53] there is no report of benz[*f*]indenyl and higher benz annulated complexes of iron. This might be due to the delocalization of the electronic charge over the aromatic backbone, which lessens the interaction of aromatic ligand with electron-rich iron center. However, analogous complexes of ruthenium[54] and manganese[55] have been isolated with different ancillary ligand environments. Even though almost all of the indenyl complexes mentioned above have been synthesized starting from indene or its derivatives, Tartar and Cuingnet prepared the methyl-substituted indenylmanganesetricarbonyl starting from substituted cymantrene.[55] Furuta *et al*. synthesized a double-decker ferrocene-type complex of a N-fused porphyrin, and its electronic state was compared with those of hypothetical π-extended ferrocene derivatives to evaluate their similarity.[56]

1.2. Metallocene-Fused Heterocycles

Our group has a long-term interest in the electronic properties of organometallic analogues of low-band-gap polymers and small molecules that incorporate η^5-cyclopentadienyl-fused heterocycle or polycyclic aromatic hydrocarbons as ligands (Figure 1.13). Selegue and Swarat prepared a chromium complex of benzo[3,4-*c*]thiophene, **(A),** from the reaction of benzo[3,4-*c*]thiophene with photochemically generated [Cr(thf)$(CO)_5$] at room temperature.[57] This first transition metal complex of benzo[3,4-c]thiophene was characterized with X-ray diffraction, showing that chromium is bound to the

benzo ring rather than the thiophene ring. The stability of the complex was found to be better than that of a free non-classical thiophene. Wallace *et al.* prepared pyridazine complexes of ruthenium, **(B)**, by employing two different methodologies. The first method involves the reaction of [Ru{η^5-$C_5H_3(CO_2Ph)_2$}(Cp*)] with hydrazine monohydrate; the second method involves the deprotonation of free cyclopenta[*d*]pyridazines[58] with thallium ethoxide followed by treatment with [Ru(μ_3-Cl)(Cp*)]$_4$ to give pyridazine complexes.[59] Similarly, 1,4-difurylcyclopenta[c]pyridazyl complexes of manganese and rhenium have been studied.[60] In quest of making η^5-cyclopenta[*c*]thienyl complexes, (e.g., **C)**, Snyder *et al.* followed two logical approaches. The first approach involves the complexation of preformed cyclopenta[*c*]thienyl anion to a metal center; the second approach entails the complexation of a suitable precursor ligand with a metal center followed by closure of a thiophene ring.[61] Tice expanded the work to prepare a number of cyclopenta[*c*]thienyl complexes of manganese including 4-chloro- and 4-bromothiapentanyl complexes and succeeded in coupling the 4-bromo complex with phenylboronic acid under Suzuki conditions.[62]

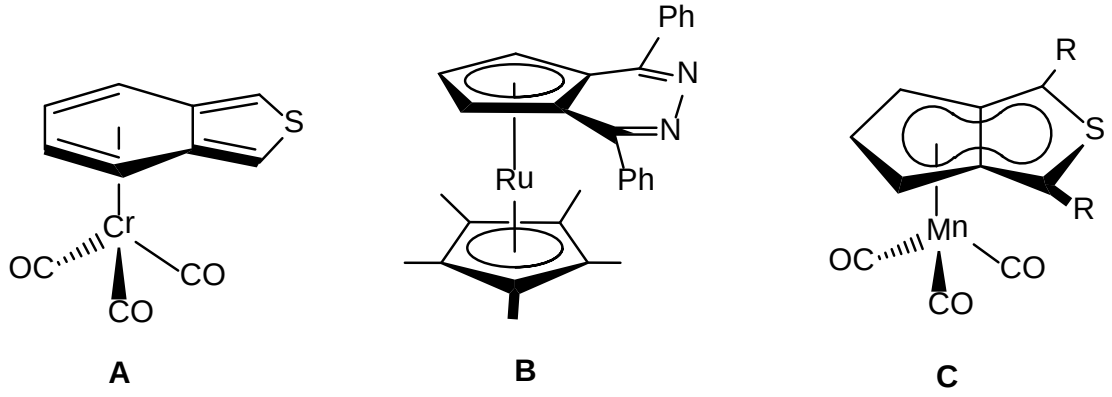

Figure 1.13. Some organometallic complexes prepared by the Selegue group: **C)** η^6-benzo[3,4-*c*]thiophene complex of chromium(0);[57] **D)** sandwich pyridazine complex of ruthenium(II);[59] **E)** η^5-cyclopenta[*c*]thienyl complexes of manganese(I).[61]

Chapter 2: The Synthesis, Characterization and Reactivities of 5,5-Fused Heterocyclic Complexes of Manganese and Ruthenium

2.1. Introduction

After the discovery of ferrocene[63] in 1951, the aromatic reaction chemistry of metallocenes was extensively developed. The heterocyclic derivatives of benzene like phthalic anhydride, thioanhydride and substituted phthalimides are versatile starting materials for various chemical transformations. For instance, phthalic anhydride is an important industrial chemical, especially for a large-scale production of plasticizers for plastics. Even though heterocycle-fused cyclopentadienylmetal complexes with heteroatom nitrogen,[64-69] sulfur[61,70] or oxygen[71-75] commonly reported in literatures; cyclic anhydride, thioanhydride or imide fused with cyclopentadienylmetal complexes are virtually rare. Richard[76] and Rousch[77] independently reported the isolation of ferrocene-1,2-dicarboxylic anhydride with some contradictory results in 1956 and 1974. We recently communicated the synthesis and characterization of 1',2',3',4',5'-pentamethylruthenocene-1,2-dicarboxylic anhydride *en route* to pentamethylruthenocene-fused quinones.[78] With the continuation of the same work, we are interested to explore the chemistry of nitrogen and sulfur containing heterocyclic derivatives from 1, 2-dicarboxylic acid bound to cyclopentadienyl metal complexes.

Herein, we report the synthesis and characterization of different heterocyclic derivatives (e.g. carboxylic anhydride, thioanhydride and p-toluoyl substituted

imides) of cyclopentadienyltricarbonylmanganese and pentamethylruthenocene (Scheme 2.1).

Scheme 2.1. Synthesis of heterocycle-fused cyclopentadienylmetal complexes

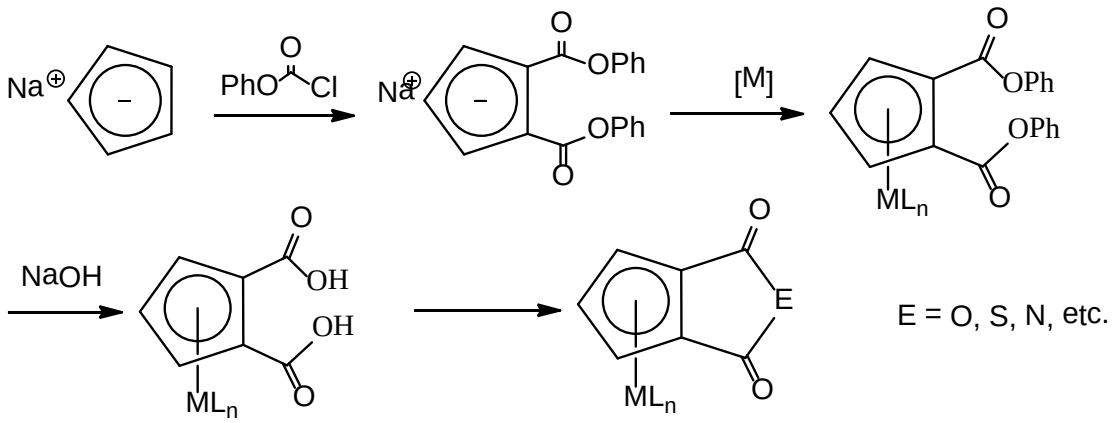

[M] = [Ru(μ_3-Cl)(Cp*)]$_4$; ML$_n$ = Ru(Cp*)
[MnBr(CO)$_5$]; ML$_n$ = Mn(CO)$_3$

2.2. Experimental

Reactions were carried out using standard Schlenk line techniques under nitrogen unless otherwise mentioned. Solvents were dried and distilled under nitrogen before use, including ethyl ether, benzene, tetrahydrofuran (THF), hexane and toluene from sodium benzophenone ketyl, dichloromethane and acetonitrile from calcium hydride, and acetic anhydride (Mallinckrodt) and trifluoroacetic anhydride (Aldrich) were freshly distilled from P_2O_5 before use. and distilled under nitrogen. $CDCl_3$, C_6D_6, DMSO-d_6 and acetone-d_6 (Cambridge Isotopes), [$Mn_2(CO)_{10}$], pentamethylcyclopentadiene and 18-crown-6 (Strem), $RuCl_3.3H_2O$ (Pressure Chemicals), phenyl chloroformate, oxalyl Chloride and *p*-toluidine (Acros), $LiAlH_4$, thionyl chloride, hexamethyldisilazide and lithium

triethylborohydride 1 M solution in THF (Aldrich), sodium hydroxide (Fischer), potassium hydroxide (EMD), and potassium fluoride and sodium (J. T. Baker) were used without further purification. The Organic phases were dried using anhydrous magnesium sulfate (Mallinckrodt). Flash chromatography was performed using 60-Å pore size, 230 x 400 mesh silica gel (Sorbent Technologies). Dicyclopentadiene (Acros) was cracked by heating in a mineral oil bath at 250 °C under nitrogen. [Na{1,2-$C_5H_3(CO_2Ph)_2$}] **1** was prepared by using a modified method[79] of Wallace and Selegue.[80] [$Mn(CO)_3${η^5-$C_5H_3(CO_2Ph)_2$-1,2}] **2b**,[79] 1,2-C_5H_3(COH-2-ClC_6H_4)(CO-2-ClC_6H_4) **7**,[81] [$MnBr(CO)_5$][82] and [Ru(μ_3-Cl)Cp*]$_4$[83] were prepared according to literature procedures.

^{1}H and ^{13}C NMR spectra were recorded on a Varian Gemini-400 spectrometer at ca. 22 °C unless mentioned otherwise and were referenced to residual solvent peaks. Infrared spectra were recorded on an ATI-Mattson Galaxy™ Series 5000 FTIR and ThermoFisher Scientific Corporation ATR spectrometers. Mass spectra were acquired by the University of Kentucky Mass Spectrometry Facility. Electron ionization (EI) mass spectra were recorded at 70 eV on a Thermo Finnigan PolarisQ (quadrupole ion trap). Samples were introduced via a heatable direct insertion probe. Melting points were taken on Thomas-Hoover capillary melting point apparatus and were uncorrected. X-ray diffraction data were collected at 90 K on either a Nonius KappaCCD diffractometer or a Bruker-Nonius X8 Proteum diffractometer. Crystal indexing and data processing were performed with either DENZO-SMN (KappaCCD)[84] or with Bruker APEX2 (X8 Proteum). The structures were solved and refined by

using SHELX-97.[85] Elemental analyses were performed at the University of Illinois Microanalysis Laboratory.

Synthesis of [Na{$C_5H_3(CO_2Ph)_2$}] (1). An oven-dried 200-mL Schlenk flask was cooled under nitrogen. The flask was equipped with a septum cap, magnetic stirrer and a glass stopcock. Sodium wire (3.09 g, 134 mmol) was collected in the reaction flask under argon. THF (80 mL) was added through a cannula and freshly cracked cyclopentadiene (8.66 g, 10.9 mL, 131 mmol) was added at 0 °C. The reaction mixture was stirred for 2.5 h at room temperature. To the clear solution of sodium cyclopentadienide, phenyl chloroformate (13.17 g, 10.58 mL, 86.95 mmol), dissolved in 30 mL of THF, was added through a dropping funnel at 0 °C. After stirring for 2 h at room temperature, the volatiles were removed under reduced pressure. The dark red solid was kept under vacuum at 80 °C for 4 h and then thoroughly washed with dry ethyl ether (3 x 60 mL) under nitrogen. The combined ethyl ether washings were concentrated *in vacuo*: the dark red, sticky, crude material was redissolved in a small amount of ethyl ether and precipitated by adding dry hexane. The precipitate was triturated for 2 h, filtered and dried to give **1** (7.16 g, 50.2%) as a light brown solid. **Mp:** 122–128 °C. **^{1}H NMR (400 MHz, DMSO-d_6, ppm):** δ 5.70 (t, 1H, ^{3}J = 3.3 Hz, CHC*H*CH), 6.67 (d, 2H, ^{3}J = 3.3 Hz, C*H*CHC*H*), 7.13–7.14 (m, 6H, Ar), 7.29–7.37 (m, 4H, Ph). **^{13}C{^{1}H} NMR (50 MHz, DMSO-d_6, ppm):** 109.7 (*C*HCH*C*H), 110.9 (CH*C*HCH), 115.1 (*ipso* Cp), 122.3 (*m*-Ph), 123.6 (*p*-Ph), 128.7 (*o*-Ph), 152.4 (*ipso*-Ph), 163.1 (CO). **IR(KBr, cm^{-1}):** 1705 (CO). Full characterization of **1a** was performed by Busetto *et al.*[79]

Synthesis of [Ru{η^5-$C_5H_3(CO_2Ph)_2$-1,2}(Cp*)] (2a). In a 200-mL Schlenk flask, [Ru(μ_3-Cl)Cp*]$_4$ (3.517 g, 3.234 mmol) was added to stirred solution of **1** (4.223 g, 12.87 mmol) in ca. 80 mL of THF. The solution was allowed to reflux for 24 h. The reaction mixture was cooled to room temperature, volatiles were removed *in vacuo* and CH_2Cl_2 (50 mL) was added. The suspension was filtered through a Celite pad and volatiles were removed *in vacuo*. The crude product was triturated with cold pentane and dried overnight *in vacuo* to give **2** (5.43 g, 77.6%) as a light yellow powder. Analytically pure product was obtained by recrystallization from a mixture of hexane and ethyl ether (3:1). **Mp:** 120–122 °C. **^{1}H NMR (400 MHz, acetone-d$_6$, ppm):** δ 1.92 (s, 15H, Cp*), 4.78 (t, 1H, ^{3}J = 2.6 Hz, CHC*H*CH), 5.13 (d, 2H, ^{3}J = 2.6 Hz, C*H*CHC*H*), 7.42–7.19 (m, 10H, Ph). **^{1}H NMR (200 MHz, CDCl$_3$, ppm):** δ 1.88 (s, 15H, Cp*), 4.61 (t, 1H, ^{3}J = 2.4 Hz, CHC*H*CH), 5.08 (d, 2H, ^{3}J = 2.4 Hz, C*H*CHC*H*), 7.15–7.35 (m, 10H, Ph). **^{13}C{^{1}H}NMR (50 MHz, $(CD_3)_2CO$, ppm):** δ 11.2 (Cp* Me), 77.7 (*C*HCH*C*H), 78.3 (CH*C*HCH), 80.0 (Cp* ring), 89.1 (*ipso*-Cp), 122.9 (*m*-Ph), 126.5 (*p*-Ph), 130.4 (*o*-Ph), 152.7 (*ipso*-Ph), 166.8 (CO). **IR (KBr, cm^{-1}):** 1725 (CO). **MS (EI):** m/z 542 (M^+). Analysis Calc. for: C, 64.31; H, 5.21. Found: C, 64.68; H, 5.35.

Synthesis of [Mn(CO)$_3${η^5-$C_5H_3(CO_2Ph)_2$-1,2}] (2b). In a 125-mL Schlenk flask, **1** (220 mg, 2.20 mmol) was added to a stirred solution of [MnBr(CO)$_5$] (518 mg, 1.90 mmol) in 50 mL of THF. The mixture was allowed to reflux for 5 h. The initially dark red color gradually changed to light yellow. The mixture was cooled to room temperature and volatiles were removed *in vacuo*. The product was extracted with dichloromethane, passed through a thin pad of Celite, and the

volatiles were removed *in vacuo*. The crude product was chromatographed on silica with ethyl ether as eluent. The light yellow band gave **2b** (712 mg, 87.1%) as a yellow solid. **Mp:** 110 °C (Lit.[79] 112 °C). **^{1}H NMR (400 MHz, acetone-d$_6$, ppm):** δ 5.28 (t, 1H, ^{3}J = 2.9 Hz, CHC*H*CH), 5.95 (d, 2H, ^{3}J = 2.9 Hz, C*H*CHC*H*), 7.49–7.20 (m, 10H, Ph). **^{13}C{^{1}H} NMR (50 MHz, acetone-d$_6$, ppm):** δ 83.2 (CH*C*HCH), 90.6 (*C*HCH*C*H), 91.7 (*CC*), 122.6, 127.3, 130.6, 151.8 (Ph), 163.5 (*C*OOPh), 223.6 (*C*O). **IR (KBr, cm^{-1}):** 2040, 1975, 1941 (CΞO), 1742 (C=O). Full characterization of the complex was performed by Busetto *et al.*[79]

Synthesis of 1,2-C$_5$H$_3$[C(OH)(OMe)](CO$_2$Me) (4). To a 250-mL three-necked round bottom flask, freshly cracked dicyclopentadiene (10.0 g, 12.5 mL, 151 mmol) was slowly added to a stirred solution of n-butyllithium (60.6 mL of 2.50 M, 151 mmol) in ethyl ether (100 mL). A white precipitate of cyclopentadienyllithium immediately formed. The white suspension was stirred at 0°C for 15 min. Methyl chloroformate (9.51 g, 7.80 mL, 101 mmol) was added dropwise using a dropping funnel. The reaction mixture was allowed to warm to room temperature and stirred overnight. The reaction mixture was hydrolyzed with 3 M hydrochloric acid (100 mL). The organic layer was collected and the aqueous layer was exacted with ethyl ether (3 x 50 mL). The ether extracts were combined and dried over $MgSO_4$. The volatiles were removed *in vacuo* to yield a yellow-orange oil of **4** (11.2 g, ca. 45.1% yield). The yield is approximate because of the impurity of the product. The impure product was used without purification in the subsequent reaction.

Synthesis of [Tl{1,2-$C_5H_3(CO_2Me)_2$}] (5). In a 250-mL Schlenk flask, TlOEt (4.40 g, 17.7 mmol) was added via syringe to a stirred solution of crude **4** (4.02 g) in 100 mL of THF. A yellow precipitate formed immediately. The suspension was allowed to stir for 2 h at room temperature and filtered through a fine porosity glass frit. The residue was washed with cold ethyl ether (20 mL) and dried under high vacuum overnight to give **5** (3.39 g, 40.0 %) as a white powder. **Mp:** 140–260 °C (dec). **^{1}H NMR (200 MHz, DMSO-d_6, ppm):** δ 3.50 (s, 6H, OMe), 5.54 (t, 1H, ^{3}J = 3.3 Hz, CHC*H*CH), 6.29 (d, 2H, ^{3}J = 3.3 Hz, C*H*CHC*H*). **^{13}C{^{1}H} NMR (50 MHz, DMSO-d_6, ppm):** δ 49.3 (OMe), 108.0 (CH*C*HCH), 112.5(*CC*), 118.5 (*C*HCH*C*H), 166.1 (CO). **IR (Nujol, cm^{-1}):** 1684 (COOMe). **MS (EI):** m/z 386 (M^+).

Synthesis of [Ru{η^5-$C_5H_3(CO_2Me)_2$-1,2}(Cp*)] (6a). In a 100-mL Schlenk flask, [Ru(μ_3-Cl)(Cp*)]$_4$ (538 mg, 0.49 mmol) was added to a stirred solution of **5** (763 mg, 1.97 mmol) in 40 mL of THF. The solution was stirred overnight at room temperature. The reddish brown suspension was passed through a thin pad of Celite and volatiles were removed *in vacuo*. The crude product was triturated with cold pentane to yield **6a** (231 mg, 29.0%) as a light yellow solid. Analytically pure product was obtained by slow evaporation of a concentrated ethyl ether solution in a stream of hexane-saturated nitrogen. **Mp:** 100–102 °C. **^{1}H NMR (200 MHz, $CDCl_3$, ppm):** δ 1.77 (s, 15H, Cp* Me), 3.74 (s, 6H, OCH_3) 4.46 (t, 1H, ^{3}J = 2.6 Hz, CHC*H*CH), 4.82 (d, 2H, ^{3}J = 2.6 Hz, C*H*CHC*H*). **^{13}C{^{1}H} NMR (50 MHz, $CDCl_3$, ppm):** δ 10.8 (Cp*CH_3) 51.6 (OCH_3), 73.7 (CC), 75.9 (CH*C*HCH), 78.7 (*C*HCH*C*H), 87.9 (Cp* ring), 168.5 (*C*O). **IR (Nujol, cm^{-1}):** 1731 (s), 1688

(m), 1453 (s). **MS (EI):** m/z 418 (M^+). The complex was characterized by an X-ray diffraction study.

Synthesis of 1,2-C_5H_3(COH-2-ClC_6H_4)(CO-2-ClC_6H_4) (7). To a 500-mL three-necked round bottom flask, freshly cracked cyclopentadiene (10.1 g, 12.5 mL, 155 mmol) was added dropwise to a stirred solution of n-butyllithium (66 mL of 2.5 M, 165 mmol) in 150 mL of ethyl ether. A white precipitate of cyclopentadienyllithium was immediately formed. The suspension was stirred at 0°C for 15 min. *o*-Chlorobenzoyl chloride (17.64 g, 100.8 mmol) was added to the reaction mixture. The mixture was allowed to warm to room temperature and stirred for 1 h. The reaction mixture was hydrolyzed with 3 M hydrochloric acid (100 mL). The organic layer was collected and the aqueous layer was exacted with ethyl ether (3 x 80 mL). The ether extracts were combined and dried over $MgSO_4$. The volatiles were removed *in vacuo* to give a yellow-brown semi-solid. Trituration with cold methanol and filtration gave **7** (4.84 g, 27.3%) as a yellow solid. **Mp:** 129–130 °C (Lit.[81] 146–147 °C). **^{1}H NMR (200 MHz, $CDCl_3$, ppm):** δ 6.36 (t, 1H, ^{3}J = 3.5 Hz, CHC*H*CH), 6.96 (d, 2H, ^{3}J = 3.5 Hz, C*H*CHC*H*), 7.35–7.51 (m, 10H, Ar), 17.94 (s, 1H, OH). Full characterization of the compound **7** was performed by Linn and Sharkey.[81]

Synthesis of [Tl{1,2-C_5H_3(CO-2-ClC_6H_4)$_2$}] (8). In a 125-mL Schlenk flask, TlOEt (727 mg, 2.92 mmol) was added via syringe to a stirred solution of **7** (1.00 g, 2.92 mmol) in 70 mL of THF. A yellow precipitate formed immediately. The suspension was allowed to stir for 2 h at room temperature and the volatiles were removed *in vacuo*. The crude product was washed with cold ethyl ether and

filtered to give **8** (1.42 g, 89%) as a light yellow solid. **Mp:** 245–255 °C (dec). **^{1}H NMR (200 MHz, DMSO-d$_6$ ppm):** δ 5.62 (t, 1H, ^{3}J = 3.6 Hz, CHC*H*CH), 6.11 (d, 2H, ^{3}J = 3.6 Hz, C*H*CHC*H*), 7.22–7.32 (m, 8H, Ar). **^{13}C{^{1}H} NMR (50 MHz, DMSO-d$_6$, ppm):** δ 111.3 (CH*C*HCH), 124.2 (*CC*), 125.7 (*C*HCH*C*H), 127.2, 128.3, 128.8, 129.0, 130.2, 144.3 (Ar), 185.4 (CO). **IR (Nujol, cm^{-1}):** 1557 (CO). **MS (EI):** m/z 546 (M$^+$). Analysis Calc. for $C_{19}H_{11}Cl_2O_2Tl$: C, 41.75; H, 2.03. Found: C, 39.56; H, 1.92.

Synthesis of [Ru{η^5-C$_5$H$_3$(CO-2-ClC$_6$H$_4$)$_2$-1,2}(Cp*)] (9a). In a 125-mL Schlenk flask, [Ru(μ$_3$-Cl)(Cp*)]$_4$ (380 mg, 0.69 mmol) was added to a stirred solution of **8** (497 mg, 0.91 mmol) in 40 mL of THF with minimum exposure to air. The reaction mixture was allowed to reflux for overnight, cooled to room temperature, and passed through a thin pad of Celite. The volatiles were removed *in vacuo*. The crude product was washed with ethyl ether and filtered. The volatiles were removed *in vacuo* to give **9a** (205 mg, 51.0%) as a light yellow solid. An analytically pure sample was obtained by recrystallization from hot hexane. **Mp:** 161 °C. **^{1}H NMR (200 MHz, CDCl$_3$, ppm):** δ 1.78 (s, 15H, Cp*) 4.57 (t, 1H, ^{3}J = 2.6 Hz, CHC*H*CH), 4.76 (d, 2H, ^{3}J = 2.6 Hz, C*H*CHC*H*), 7.13–7.43 (m, 8H, Ar). **^{13}C{^{1}H} NMR (50 MHz, CDCl$_3$, ppm):** δ 10.9 (*C*H$_3$ Cp*) 77.4 (CH*C*HCH), 81.1 (*C*HCH*C*H), 85.8 (*CC*), 88.2 (Cp* ring) 140 (*C*-CO) 132.0 (*C*-Cl), 126.2, 129.8, 130.1, 131.0 (Ar) 193.9 (*C*O). **IR (Nujol, cm^{-1}):** 1644.5 (CO). **MS (EI):** m/z 580 (M$^+$ + 2). Analysis Calc. for $C_{29}H_{26}Cl_2O_2Ru$: C, 60.21; H, 4.53. Found: C, 60.22, H, 4.52.

Synthesis of [Mn{η^5-C_5H_3(CO-2-ClC_6H_4)$_2$-1,2}(CO)$_3$] (9b). In a 200-mL Schlenk flask, [MnBr(CO)$_5$] (500 mg, 1.82 mmol) was added to a stirred solution of **8** (994 mg, 1.82 mmol) in 80 mL of benzene. The reaction mixture was allowed to reflux overnight, cooled to room temperature, and passed through a thin pad of Celite. Volatiles were removed *in vacuo*. The crude product was washed with ethyl ether and filtered. The volatiles were removed *in vacuo* and the crude product was recrystallized from hexane to give **9b** (366 mg, 42.0%) as a light yellow solid. **Mp:** 141-143 °C. **^{1}H NMR (200 MHz, C_6D_6, ppm):** δ 3.63 (t, 1H, ^{3}J = 2.9 Hz, CHC*H*CH), 4.58 (d, 2H, ^{3}J = 2.9 Hz, C*H*CHC*H*), 6.64–7.43 (m, 8H, Ar). Although peaks in the ^{1}H NMR spectrum of **9b** in $CDCl_3$ were broad such broadening was not observed in the ^{13}C NMR spectrum. **^{13}C{^{1}H} NMR (50 MHz, $CDCl_3$, ppm):** δ 79.5 (CH*C*HCH), 91.7 (*C*HCH*C*H), 98.7 (*CC*), 127.0, 130.4, 131.5, 132.5, 137.5 (Ar) 191.1 (*C*O) 221.9 (CΞO). **IR (Nujol mull, cm^{-1}):** 1663 (CO), 2034, 2045 (CΞO). **MS (EI):** m/z 481 (M^+ + 2). Analysis Calc. for $C_{22}H_{11}Cl_2O_5Mn$: C, 54.92; H, 2.30. Found: C, 54.90, H, 2.27.

Synthesis of [Ru{η^5-C_5H_3(CO_2H)$_2$-1,2}(Cp*)] (3a). Method A. To a solution of diester **2a** (2.20 g, 4.06 mmol) dissolved in dichloromethane (8 mL), NaOH (1.18 g, 29.57 mmol) dissolved in methanol (4 mL) was added. The resultant solution was refluxed for 12 h to form a light yellow suspension. The reaction mixture was cooled to room temperature and quenched with water (20 mL). The layers were separated; the aqueous phase was washed with dichloromethane (3 x 10 mL) and acidified to pH 2-3 with conc. HCl to give a light yellow precipitate. The precipitate was separated by filtration through a glass frit

of medium porosity. The residue was washed with water (50 mL) and hexane (30 mL) and dried *in vacuo* at 50 °C for 5 h to give **3a** (1.50 g, 95.0%) as a light yellow powder. Analytically pure product was obtained by slow evaporation of a concentrated dichloromethane solution in a stream of hexane-saturated nitrogen. **Mp:** 210–230 °C (dec) **^{1}H NMR (400 MHz, $(CD_3)_2CO$, ppm):** δ 1.81 (s, 15H, Cp*), 3.91 (br, 1H, COOH), 4.81 (t, 1H, ^{3}J = 2.7 Hz, CHC*H*CH), 5.07 (d, 2H, ^{3}J = 2.7 Hz, C*H*CHC*H*). **^{1}H NMR (400 MHz, DMSO-d_6, ppm):** δ 1.71 (s, 15H, Cp*), 3.39 (br, COO*H*), 4.80 (t, 1H, ^{3}J = 2.5 Hz, CHC*H*CH), 4.97 (d, 2H, ^{3}J = 2.5 Hz, C*H*CHC*H*). **^{13}C{^{1}H} NMR (50 MHz, $(CD_3)_2CO$, ppm):** δ 10.4 (Cp* CH_3), 78.8 (*C*HCH*C*H), 79.4 (CH*C*HCH), 81.2 (ring, Cp*), 88.6 (*CC*) 169.9 (*C*OOH). **^{13}C{^{1}H} NMR (50 MHz, DMSO-d_6, ppm):** δ 9.9 (Cp* CH_3), 75.1 (*ipso*, Cp), 77.7 (CH*C*HCH), 79.7 (*C*HCH*C*H), 87.1 (ring, Cp*), 171.0 (*C*OOH). **IR (KBr, cm^{-1}):** 3379 (OH), 1603 (CO). The complex was characterized by an X-ray diffraction study.

Method B. In a 125-mL Schlenk flask, KOH (134 mg, 1.92 mmol) was added to a stirred solution of **6** (150 mg, 0.38 mmol) in 3 mL of methanol. The reaction mixture was allowed to reflux for 4 h to give light yellow precipitate. The reaction mixture was cooled to room temperature and quenched with water (10 mL). Unreacted ester, if any, was extracted with ethyl ether (2 x 5 mL) and aqueous phase was acidified to pH = 2 with 6 M HCl. A light yellow precipitate was formed, which was filtered through a glass frit of medium porosity and dried under vacuum to give a light yellow powder of **3a** (133 mg, 89.0%). Analytically

pure product was obtained by slow crystallization from ethyl ether under nitrogen at room temperature.

Method C. A dry, 125-mL Schlenk flask equipped with magnetic stirrer and reflux condenser topped with nitrogen inlet was charged with potassium *tert*-butoxide (932 mg, 8.32 mmol) and freshly distilled dimethoxyethane (8 mL). Water (41 μL, 2.32 mmol) was added with stirring to produce a slurry, to which **9a** (200 mg, 0.416 mmol) was added. Dark red color developed immediately. As the reaction continued, the color changed from red to tan. After one hour of reflux, the reaction was cooled to room temperature and poured into cold water (10 mL). The resulting solution was extracted with ethyl ether (3 x 20 mL). Aqueous phase was acidified with concentrated hydrochloric acid. The product was extracted with ethyl ether, dried over $MgSO_4$ and volatiles were removed *in vacuo*. The crude product was triturated with cold pentane. The dark solid was dissolved in dichloromethane and filtered. The filtrate was evaporated to dryness. ^{1}H NMR of the resultant product showed exclusively [Ru(η^5-$C_5H_4CO_2H$)(Cp*)] (63 mg, 62%).

Synthesis of [Mn(CO)$_3${η^5-$C_5H_3(CO_2H)_2$-1,2}] (3b). Method A. In a 125-mL Schlenk flask, **2b** (200 mg, 0.460 mmol) was dissolved in a mixture of dichloromethane (6 mL) and methanol (0.6 mL). A methanolic solution of 2 M NaOH (1.2 mL, 2.4 mmol) was added dropwise so as to make final concentration of mixture in range of 0.1–0.2 M. The mixture was stirred at room temperature for 4 h until all ester was consumed to give a pale yellow precipitate. The reaction was quenched by adding water (20 mL). Resultant solution was extracted with dichloromethane (2 x 10 mL) and aqueous solution was acidified to pH = 2 with

conc. HCl. The solution was again extracted with ethyl ether (2 x 10 mL). Organic phase was dried *over* $MgSO_4$ and volatiles were removed *in vacuo*. The crude product was washed with hexane (3 x 10 mL) and dried under vacuum at 50 °C for 2 h to give **3b** (118 mg, 88.0%) as a dark yellow solid. Analytically pure product was obtained by slow evaporation of concentrated ethyl ether solution in a stream of nitrogen saturated with hexane. **Mp:** 162–164 °C. **^{1}H NMR (400 MHz, acetone-d$_6$, ppm):** δ 5.28 (br, 2H, C*H*CHC*H*), 5.91 (br, 1H, CHC*H*CH), 4.00–8.20 (br, COOH). **^{1}H NMR (400 MHz, DMSO-d$_6$, ppm):** δ 5.08 (t, 1H, CHC*H*CH), 5.61 (d, 2H, C*H*CHC*H*), 5.00–5.50 (br, COO*H*). **^{13}C{^{1}H} NMR (100 MHz, acetone-d$_6$, ppm):** δ 84.0 (CH*C*HCH), 94.8 (*C*HCH*C*H), 112.2 (*CC*), 164.4 (*C*OO*H*), 223.0 (*C*ΞO). **IR (KBr, cm^{-1}):** 3453 (COOH), 2038, 2040, 1958 (CΞO), 1706 (C=O). MS (EI): m/z 292 (M^+), 208 (M^+–3CO). The product was characterized by an X-ray diffraction study.

Method B. A dry, 125-mL Schlenk flask, equipped with magnetic stirrer and reflux condenser topped with nitrogen inlet, was charged with potassium *tert*-butoxide (1.472 g, 13.14 mmol) and freshly distilled dimethoxyethane (10 mL). Water (84 μL, 4.6 mmol) was added with stirring to produce a slurry, to which **9b** (250 mg, 0.657 mmol) was added. A dark red color developed immediately. The reaction mixture was allowed to reflux for 4 h, cooled to room temperature, and poured into cold water (10 mL). The layers were separated and the aqueous phase was extracted with ethyl ether (2 x 15 mL). Aqueous phase was acidified with concentrated hydrochloric acid to give light yellow turbidity. The product was extracted with ethyl ether (2 x 20 mL). The combined organic extracts were dried

over $MgSO_4$, filtered, and volatiles were removed *in vacuo*. The crude product was triturated with cold pentane. ^{1}H NMR of the product (71 mg, ca. 37%) shows the desired dicarboxylic acid **3b** and [$Mn(CO)_3(\eta^5$-$C_5H_4CO_2H)$] in a 2:1 ratio as an inseparable mixture.

Synthesis of [Ru{η^5-$C_5H_3(CO)_2O$-1,2}(Cp*)] (10a). Method A. In a 125-mL Schlenk flask, **3a** (1.00 g, 2.57 mmol) was added to freshly distilled acetic anhydride (30 mL). The solution was allowed to reflux for 45 min. The reaction mixture was cooled to room temperature. Volatiles were removed *in vacuo* and the product was isolated by chromatography on silica with ethyl ether:hexane (4:1) as eluent. The product was collected as the second fraction, a light yellow band. Volatiles were removed *in vacuo* to give **10a** (802 mg, 84.0%) as a light yellow powder. Analytically pure product was obtained by slow evaporation of a concentrated ethyl ether solution in a stream of hexane-saturated nitrogen. **Mp:** 198-202 °C. **^{1}H NMR (400 MHz, acetone-d$_6$, ppm):** δ 1.80 (s, 15H, Cp*), 5.03 (t, 1H, ^{3}J = 2.6 Hz, CHC*H*CH), 5.12 (d, 2H, ^{3}J = 2.6 Hz, C*H*CHC*H*). **^{13}C{^{1}H} NMR (50 MHz, acetone-d$_6$, ppm):** δ 10.4 (Cp* CH_3), 72.7 (ring, Cp*), 79.5 (*ipso*, Cp), 84.9 (CH*C*HCH), 89.9 (*C*HCH*C*H), 163.8 (CO). **IR (KBr, cm^{-1}):** 1820, 1765 (C=O). **MS (EI):** m/z 372 (M^+) 300 [M^+–$(CO)_2O$]. The complex was characterized by an X-ray diffraction study.

Method B. In a 50-mL Schlenk flask, **3a** (50 mg, 0.13 mmol) was added to stirred suspension of DCC (53 mg, 0.26 mmol) in dry acetone (5 mL). The reaction mixture was stirred for 1 h at room temperature. The volatiles were removed *in vacuo*. The crude mass was suspended in hot hexane and filtered.

The filtrate was evaporated to dryness to give **10a** (33 mg, 69%) as yellow solid. All physical and spectroscopic data were consistent with the previously prepared complex.

The residue was dissolved in ethyl ether and extracted with 1 M solution of $NaHCO_3$ (2 x 5 mL). The organic phase was collected and dried over $MgSO_4$. Removal of volatiles and analysis of the crude product with ^{1}H NMR showed a mixture of anhydride **10a** and N-acyl urea **15a** in a *ca.* 1:1 ratio. We were unable to obtain the analytically pure product but careful recrystallization of mixture from their ether solution with nitrogen-saturated hexane gave single crystal of N-acyl urea [Ru{η^5-C_5H_3(COOH)(CONCyCONHCy)-1,2}(Cp*)] **15a**. **^{1}H NMR (400 MHz, acetone-d$_6$, ppm):** δ 1.04-1.95 (m, 8H, CH_2, 1.24-1.35 (m, 8H, CH_2,), 1.63-1.68 (m, 4H, CH_2), 1.79 (s, 15H, Cp*), 3.46-3.50 (m, 2H, C*H*NH), 4.59 (t, 1H, ^{3}J = 2.8 Hz, CHC*H*CH), 4.81 (d, 2H, CHN*H*), 4.91 (ABC, 1H, Cp), 4.97 (ABC, 1H, Cp). **IR (ATR, cm^{-1}):** 3324 (m), 1715 (w), 1624 (s), 1573 (s). The aqueous phase was acidified with conc. HCl and the product was again extracted with ethyl ether (2 x 10 mL). The combined ether extracts were evaporated to dryness. The ^{1}H NMR analysis of the product showed the presence of only dicarboxylic acid **3a**.

Synthesis of [Mn(CO)$_3${η^5-C_5H_3(CO)$_2$O-1,2}] (10b). In a 100-mL Schlenk flask, trifluoroacetic anhydride (10 mL) was added to **3b** (200 mg, 0.68 mmol) and the mixture was refluxed for 3 h. The reaction mixture was cooled to room temperature and volatiles were removed *in vacuo*. The crude product was dissolved in benzene (15 mL) and filtered *via* cannula. The filtrate was evaporated to dryness to give **10b** (87 mg, 46%) as a deep yellow gum. The

product was sensitive to moist air. **^{1}H NMR (400 MHz, acetone-d$_6$, ppm):** δ 5.57 (t, 1H, ^{3}J = 2.4 Hz, CHC*H*CH), 5.90 (d, 2H, ^{3}J = 2.4 Hz, C*H*CHC*H*). **^{13}C{^{1}H} NMR (100 MHz, acetone-d$_6$, ppm):** δ 92.0 (*C*HCH*C*H), 92.6 (CH*C*HCH), 93.1(*CC*), 161.0 (*C*O), 222.1 (*C*ΞO). **IR (ATR cm^{-1}):** 2039, 1944 (CΞO), 1788, 1739 (C=O). **MS (EI):** m/z 273 (M$^+$).

Synthesis of [Ru{C$_5$H$_3$(CO)$_2$N-4-C$_6$H$_4$CH$_3$-1,2}(Cp*)] (11a). In a 100-mL Schlenk flask, p-toluidine (13 mg, 0.12 mmol) was added to stirred solution of [Ru{C$_5$H$_3$(CO)$_2$O-1,2}(Cp*)] (43 mg, 0.12 mmol) in THF (20 mL). The mixture was refluxed overnight at which time the starting materials were completely consumed. The reaction mixture was cooled to room temperature. Oxalyl chloride (20 µL, 0.24 mmol) and DMF (5 µL) were added to the reaction mixture and again refluxed for 5 h. The reaction mixture was cooled to room temperature and volatiles were removed *in vacuo*. The crude product was chromatographed on silica with ethyl acetate:hexane (1:5) as eluent to give a light yellow band. Removal of volatiles *in vacuo* and trituration with cold pentane gave **11a** (13 mg, 23%) as a pale yellow solid. **^{1}H NMR (400 MHz, CDCl$_3$, ppm):** δ 1.82 (s, 15H, Cp*), 2.34(s, 3H, C*H*$_3$), 4.68 (t, 1H, ^{3}J = 2.4 Hz, CHC*H*CH), 4.92 (d, 2H, ^{3}J = 2.4 Hz, C*H*CHC*H*), 7.50 (AA'BB', 2H, Ar), 7.68 (AA'BB', 2H, Ar). **^{13}C{^{1}H} NMR (100 MHz, CDCl$_3$, ppm):** δ 11.2 (Cp**C*H$_3$) 23.9 (*C*H$_3$), 68.4 (Cp**C*), 70.7 (*C*HCH*C*H), 80.8 (*CC*), 88.9 (CH*C*HCH), 126.6, 129.0, 131.1, 132.6 (Ar) 167.9 (*C*O). **IR (KBr, cm^{-1}):** 1629, 1654 (C=O). **MS (EI):** m/z 461 (M$^+$).

Synthesis of [Mn(CO)$_3${η^5-C$_5$H$_3$(CO)$_2$N-4-C$_6$H$_4$CH$_3$-1,2}] (11b). In a 100-mL Schlenk flask, trifluoroacetic acid (5 mL) was added to **1** (100 mg, 0.34 mmol) and the mixture was refluxed for 3 h. The reaction mixture was cooled to room temperature and volatiles were removed *in vacuo*. The crude product was dissolved in benzene (15 mL), *p*-toluidine (37 mg, 0.34 mmol) was added, and the reaction mixture was again stirred for 10 h at room temperature. Oxalyl chloride (1.36 mmol, 0.12 mL) and anhydrous DMF (10 µL) were added. The reaction mixture was refluxed for 2 h, cooled to room temperature, and the volatiles were removed *in vacuo*. The crude product was chromatographed on silica with ethyl ether:hexane (1:1) as eluent to give a light yellow band. Removal of volatiles *in vacuo* and trituration with cold pentane gave **11b** (52 mg, 42 %) as a light yellow solid. Analytically pure product was obtained by recrystallization from a saturated dichloromethane solution by partial evaporation in a slow stream of hexane-saturated nitrogen. **Mp:** 198-200 °C. **^{1}H NMR (400 MHz, acetone-d$_6$, ppm):** δ 2.37(s, 3H, C*H*$_3$), 5.38 (t, 1H, ^{3}J = 2.8 Hz, CHC*H*CH), 5.86 (d, 2H, ^{3}J = 2.8 Hz, C*H*CHC*H*), 7.19 (d, 2H, ^{3}J = 8.0 Hz, Ar), 7.31 (d, 2H, ^{3}J = 8.0 Hz, Ar). **^{13}C{^{1}H} NMR (100 MHz, acetone-d$_6$, ppm):** δ 21.7 (*C*H$_3$), 83.5 (*C*HCH*C*H), 88.0 (CH*C*HCH), 92.5 (*CC*), 120.5, 128.1, 130.4, 139.2 (Ar) 165.1 (*C*O), 224.7 (*C*ΞO). **IR (ATR, cm^{-1}):** 2028, 2046 (CΞO), 1725, 1714 (C=O). **MS (EI):** m/z 363 (M$^+$). The complex was characterized by an X-ray diffraction study.

Synthesis of [Ru{C$_5$H$_3$(COCl)$_2$-1,2}(Cp*)] (12a). In an oven-dried and cooled 125-mL Schlenk flask, **3a** (100 mg, 0.26 mmol) was dissolved in dry dichloromethane (40 mL). After stirring for 15 min at room temperature, oxalyl

chloride (0.13 g, 90.0 μL, 1.03 mmol) and DMF (5 μL) were added and the reaction mixture was stirred for 3 h at room temperature. Volatiles were removed *in vacuo* and the product was extracted into benzene under nitrogen. Volatiles were removed *in vacuo* to give **12a** (97 mg, 88%) as a light yellow powder. Analytically pure product was obtained by recrystallization from hexane. **Mp:** 165–180 °C (dec). **^{1}H NMR (400 MHz, $(CD_3)_2CO$, ppm):** δ 1.85 (s, 15H, Cp*), 5.12 (t, 1H, ^{3}J = 2.9 Hz, CHC*H*CH), 5.43 (d, 2H, ^{3}J = 2.9 Hz, C*H*CHC*H*). **^{13}C{^{1}H} NMR (50 MHz, $(CD_3)_2CO$, ppm):** δ 10.3 (Cp* *C*H_3), 80.2 (*CC*), 81.6 (Cp* ring), 86.5 (*C*HCH*C*H), 90.9 (CH*C*HCH), 162.7 (*C*O). **IR (CCl_4, cm^{-1}):** 1801 (CO). **MS (EI):** m/z 426 (M^+) 391 (M^+ - Cl).

Synthesis of [Mn(CO)$_3${η^5-C$_5$H$_3$(COCl)$_2$-1,2}] (12b). In a 100-mL Schlenk flask, oxalyl chloride (0.5 mL, 6.5 mmol) and a drop of DMF were added to a stirred suspension of **3b** (100 mg, 0.34 mmol) in benzene (15 mL). The reaction mixture was allowed to stir for 4 h at room temperature. The volatiles were removed *in vacuo*. The product was extracted with dry hexane under nitrogen and evaporated to dryness to give 1**2b** (73 mg, 65%) as an orange-yellow powder. Analytically pure product was obtained by slow cooling from a saturated solution of hexane at -10 °C for 3 days. **Mp:** 61–62 °C. **^{1}H NMR (400 MHz, acetone-d$_6$, ppm):** δ 5.41 (t, 1H, ^{3}J = 2.9 Hz, CHC*H*CH), 6.34 (d, 2H, ^{3}J = 2.9 Hz, C*H*CHC*H*). **^{1}H NMR (200 MHz, $CDCl_3$, ppm):** δ 4.89 (br, 1H, CHC*H*CH), 5.82 (br, 2H, C*H*CHC*H*). **^{1}H NMR (400 MHz, DMSO-d$_6$, ppm):** δ 5.06 (br, 1H, CHC*H*CH), 5.58 (br, 2H, C*H*CHC*H*). **^{13}C{^{1}H} NMR (100 MHz, acetone-d$_6$, ppm):** δ 82.8 (CH*C*HCH), 91.9 (*CC*), 98.2 (*C*HCH*C*H), 162.2 (*C*O), 221.4 (*C*ΞO). **IR**

(Nujol mull, cm^{-1}): 2049, 1984 (CΞO), 1796, 1782 (C=O). **IR (hexane, cm^{-1}):** 2051, 1987, 1979 (CΞO), 1798, 1781 (C=O). **MS (EI):** m/z 328 (M^+) 330 (M^+ + 2), 293 (M^+ - Cl). The complex was characterized by an X-ray diffraction study.

Synthesis of [Ru{$C_5H_3(CO)_2$S-1,2}(Cp*)] (13a). In a 100-mL Schlenk flask, oxalyl chloride (88 µL, 1.04 mmol) and DMF (10 µL) were added to a stirred suspension of **3a** (100 mg, 0.26 mmol) in benzene (20 mL). The reaction mixture was allowed to stir for 3 h at room temperature. The volatiles were removed *in vacuo*. Without further purification, dry potassium fluoride (148 mg, 2.56 mmol), 18-crown-6 ether (20 mg) and anhydrous methylene chloride (20 mL) were added to the flask. To the mixture, hexamethyldisilathiane (0.27 mL, 1.28 mmol) was added by syringe with stirring. After stirring the mixture for 10 h at room temperature, the volatiles were removed *in vacuo.* The crude product was chromatographed on silica with ethyl acetate:hexane (1:5) as eluent. The first fraction gave **13a** (75 mg, 75%) as a light yellow, crystalline solid. Analytically pure product was obtained by recrystallization from a saturated dichloromethane by partial evaporation in a slow stream of hexane-saturated nitrogen. **Mp:** 252-254 °C. **^{1}H NMR (400 MHz, $CDCl_3$, ppm):** δ 1.76 (s, 15H, Cp*), 4.85 (t, 1H, ^{3}J = 2.6 Hz, CHC*H*CH), 4.93 (d, 2H, ^{3}J = 2.6 Hz, C*H*CHC*H*). **^{13}C{^{1}H} NMR (100 MHz, $CDCl_3$, ppm):** δ 10.2 (Cp*CH_3), 72.0 (Cp**C*), 84.0 (*CC*), 88.3 (CH*C*HCH), 89.5 (*C*HCH*C*H), 187.3 (*C*O). **IR (ATR, cm^{-1}):** 1708, 1679 (CO), 1277 (CS) **MS (EI):** m/z 388 (M^+). The complex was characterized by an X-ray diffraction study.

Synthesis of [Mn(CO)$_3${η^5-C$_5$H$_3$(CO)$_2$S-1,2}] (13b). In a 100-mL Schlenk flask, oxalyl chloride (0.5 mL, 6.5 mmol) and DMF (10 µL) were added to a stirred suspension of **3b** (100 mg, 0.34 mmol) in benzene (15 mL). The reaction mixture was allowed to stir for 4 h at room temperature. The volatiles were removed *in vacuo*. Without further purification, dry potassium fluoride (80 mg, 2.74 mmol), 18-crown-6 ether (10 mg) and anhydrous methylene chloride (20 mL) were added to the flask. To the mixture, hexamethyldisilathiane (243 mg, 1.36 mmol) was added by syringe with stirring. The mixture was stirred for 6 h at room temperature and then filtered through a thin pad of silica. The volatiles were removed *in vacuo* and the crude product was triturated with cold pentane to give **13b** (66 mg, 66.5%) as a light orange solid. Analytically pure product was obtained by recrystallization from saturated dichloromethane solution by partial evaporation in a slow stream of hexane-saturated nitrogen. **Mp:** 99–101 °C. **^{1}H NMR (400 MHz, acetone-d$_6$, ppm):** δ 5.59 (t, 1H, ^{3}J = 2.8 Hz, CHC*H*CH), 5.91 (d, 2H, ^{3}J = 2.9 Hz, C*H*CHC*H*). **^{13}C{^{1}H} NMR (100 MHz, acetone-d$_6$, ppm):** δ 83.8 (*C*HCH*C*H), 91.4 (*C*HCH*C*H), 100.3 (*CC*), 186.1 (*C*O), 222.4 (*C*≡O). **IR (ATR, cm^{-1}):** 2035, 1950 (C≡O), 1720, 1689 (C=O). **MS (EI):** m/z 290 (M$^+$). The complex was characterized by an X-ray diffraction study.

Synthesis of [Ru{η^5-C$_5$H$_3$(CONHPh)$_2$-1,2}(Cp*)] (14a). To an oven-dried and cooled 125-mL Schlenk flask, oxalyl chloride (0.13 g, 0.09 ml, 1.03 mmol) and DMF (1 drop) were added to a stirred suspension of **3a** (100 mg, 0.257 mmol) in 5 mL of benzene. The reaction mixture was allowed to reflux for 1 h and cooled to room temperature. Volatiles were removed *in vacuo*. Light orange

powder of diacid chloride was redissolved in benzene (5 mL) without isolation and freshly distilled aniline (48 mg, 0.05 mL, 0.52 mmol) was added to it. The reaction mixture was stirred at room temperature for 1 h. Volatiles were removed *in vacuo*. The product was extracted into ethyl ether and washed with a saturated solution of sodium bicarbonate. The organic layer was dried *over* $MgSO_4$ and volatiles were removed *in vacuo*. The crude product was triturated with cold pentane to give **14a** (60 mg, 43%) as a light yellow crystalline solid. **Mp**: 280–300 °C (dec). **^{1}H NMR (200 MHz, $CDCl_3$, ppm):** δ 1.78 (s, 15H, Cp*), 4.57 (t, 1H, ^{3}J = 2.6 Hz, CHC*H*CH), 5.01 (d, 2H, ^{3}J = 2.6 Hz, C*H*CHC*H*), 7.07–7.13 (m, 2H, *p*-Ph), 7.29-7.37 (m, 4H, *m*-Ph), 7.62–7.67 (m, 4H, *o*-Ph), 9.83 (s, 2H, CON*H*). ^{13}C**{^{1}H} NMR (50 MHz, ($CDCl_3$, ppm):** δ 11.1 (Cp* CH_3), 76.1 (ring, Cp*), 78.2 (*C*HCH*C*H), 80.0 (*ipso*, Cp), 88.1 (CH*C*HCH), 120.3, 124.1, 129.2, 138.7 (Ph), 167.1(*C*ONH). **IR (KBr, thin film, cm^{-1}):** 3330, 2966, 2902, 2861, 1652, 1594, 1564, 1525. **MS (EI):** m/z 539 (M^+).

2.1. Results and Discussion

2.1.1. Synthesis. 1',2',3',4',5'-Pentamethylruthenocene-1,2-dicarboxylic acid **3a** and cymantrene-1,2-dicarboxylic acid **3b** were prepared as shown in Scheme 2.2. The first route involves the single-step reaction of sodium cyclopentadienide with phenyl chloroformate in a 3:2 ratio to isolate sodium salt of 1,2-dicarbophenoxycyclopentadiene [Na{$C_5H_3(CO_2Ph)_2$}] **1** (50%). The procedure combines the methods of Wallace and Selegue[59] and Busetto *et al.*[79] The reaction requires rigorously dry and air-free conditions; otherwise the light yellow powder of **1** turns to a dark, viscous mass. The carbophenoxy group exhibits 1,2-selectivity of addition to cyclopentadienyl anion than its carboalkoxy counterparts. Similar results were observed by Busetto in a two-step preparation of cyclopentadiene-1,2-diesters.[79] In contrast to the insolubility of carbomethoxycyclopentadienylsodium, 1,2-dicarbophenoxycyclopentadienylsodium is soluble in ether, probably due to significant covalency of cyclic sodium dienolate. Accordingly, the compound **1** was extracted with dry ethyl ether and precipitated by hexane to obtain the pure sodium salt.

Compound **1** was transmetalated with [Ru(μ_3-Cl)Cp*]$_4$ and [MnBr(CO)$_5$] to give [Ru{η^5-$C_5H_3(CO_2Ph)_2$-1,2}(Cp*)], **2a** and [Mn(CO)$_3${η^5-$C_5H_3(CO_2Ph)_2$-1,2}] **2b**[79] in good yields (**2a**, 78% and **2b**, 87%). This method bypasses the use of the toxic thallium reagent commonly used for transmetalation and reducing the number of synthetic steps.[59,61] The transmetalation reaction was much slower for

ruthenocene than for cymantrene. Crystals of ruthenium complex **2a** are air-stable for several months; however, the manganese complex **2b** darkens during storage in air.

Scheme 2.2. Synthesis of 1',2',3',4',5'-pentamethylruthenocene-1,2-dicarboxylic acid **3a**, cymantrene-1,2-dicarboxylic acid **3b** and their heterocyclic derivatives

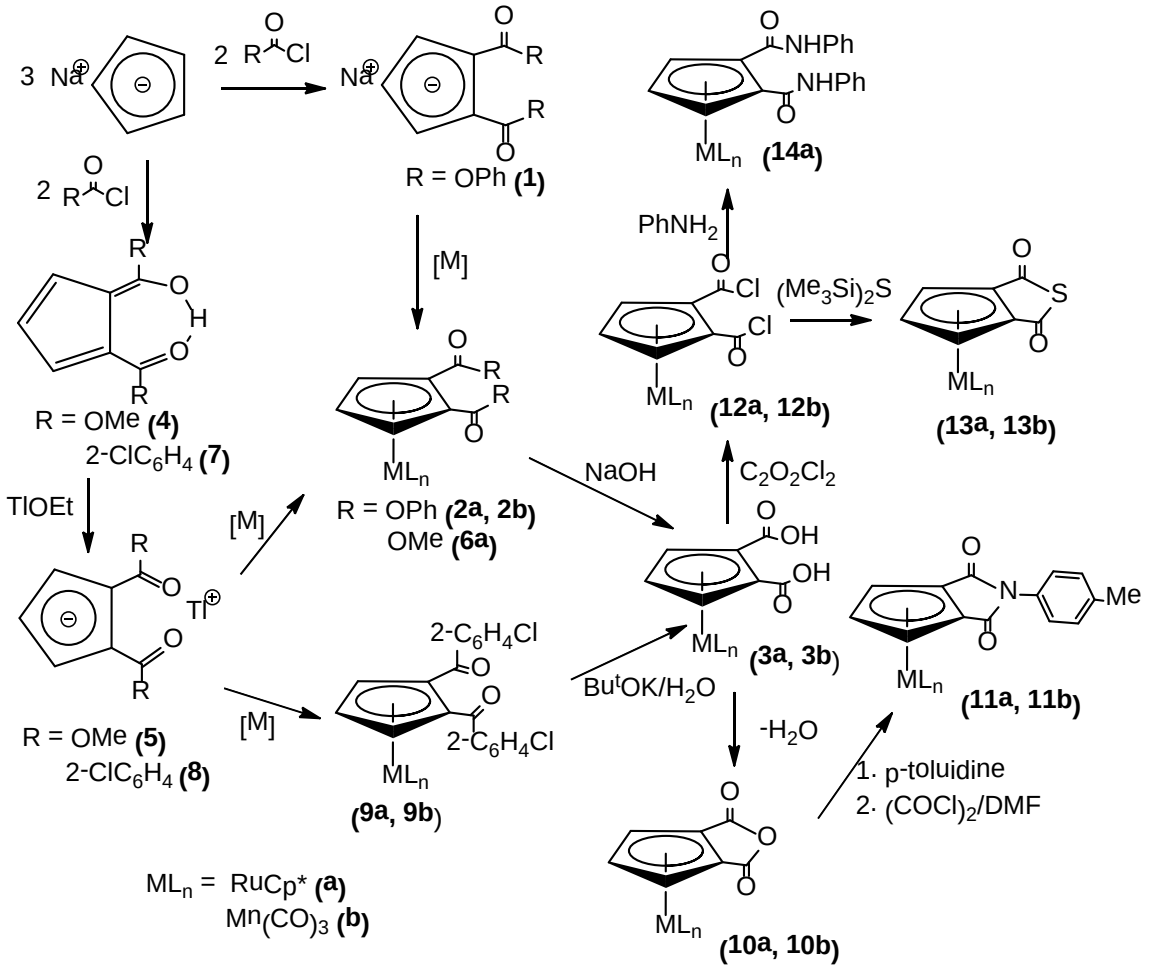

The second synthetic route involves the preparation of the carbomethoxyfulvene 1,2-C_5H_3[C(OH)(OMe)](CO_2Me) **4,** *via* the method used to prepare of 1,2-C_5H_3[C(OH)(OEt)](CO_2Et).[86] The poor selectivity of carbomethoxy groups at the 1,2-positions of cyclopentadiene resulted in the formation of

isomeric mixtures. Therefore, crude **4** was treated with excess TlOEt to obtain [Tl{1,2-$C_5H_3(CO_2Me)_2$}] **5** without purification. Since the enolic proton in the 1,2-disubstituted fulvene is a highly acidic, it selectively forms a thallium salt, leaving other impurities behind. Transmetalation was then carried out by stirring **5** with [Ru(μ_3-Cl)Cp*]$_4$ at room temperature in a 4:1 ratio to give [Ru{η^5-$C_5H_3(CO_2Me)_2$-1,2}(Cp*)] **6a** in moderate (29%) yield. Formation of insoluble thallium chloride indicates the completion of the reaction. An attempt to prepare [Mn{η^5-$C_5H_3(CO_2Me)_2$-1,2}$(CO)_3$] by reacting **5** with [MnBr$(CO)_5$] in benzene resulted in a dark, viscous material. Complete characterization of the product was impossible due to its low yield and the presence of paramagnetic impurities.

Saponification of **2a** and **6** was accomplished by using KOH in methanol by employing the modified procedure of Khurana[87] to give pentamethylruthenocene-1,2-dicarboxylic acid **3a** in 95% and 89%. Several attempts to saponify **2b** under similar conditions resulted in immediate decomposition to black solid. We theorize that the hydroxide ion displaces 1,2-$C_5H_3(CO_2Ph)_2$ from manganese under these conditions due to electron-withdrawing effects of esters. The saponification of **2b** was carried out by using NaOH in a mixture of dichloromethane and methanol at room temperature[88] to give dicarboxylic acid **3b** (88%). The diacid complexes **3a** and **3b**, the diacid complexes were purified by extraction with sodium bicarbonate solution to remove phenolic impurities.

The third attempted route involves the oxidative cleavage of 2-chlorobenzoylmetallocenes with potassium *tert*-butoxide and water in DME. It

requires the preparation of 1,2-C_5H_3(COH-2-ClC_6H_4)(CO-2-ClC_6H_4) **7**, its conversion to [Tl{1,2-C_5H_3(CO-2-ClC_6H_4)$_2$}] **8**, and transmetalation with ruthenium and manganese reagents by following our usual procedure.[59,62] The ruthenocene complex [Ru{η^5-C_5H_3(CO-2-ClC_6H_4)$_2$-1,2}(Cp*)] **9a** and cymantrene complex [Mn{η^5-C_5H_3(CO-2-ClC_6H_4)$_2$-1,2}(CO)$_3$] **9b** were isolated in 51% and 42% yield. The manganese complex **9b** decomposes in $CDCl_3$ to give a very broad ^{1}H NMR but gives a sharp spectrum in C_6D_6.

Scheme 2.3. Proposed mechanism of ketonic cleavage in 1,2-diacyl ketone complexes

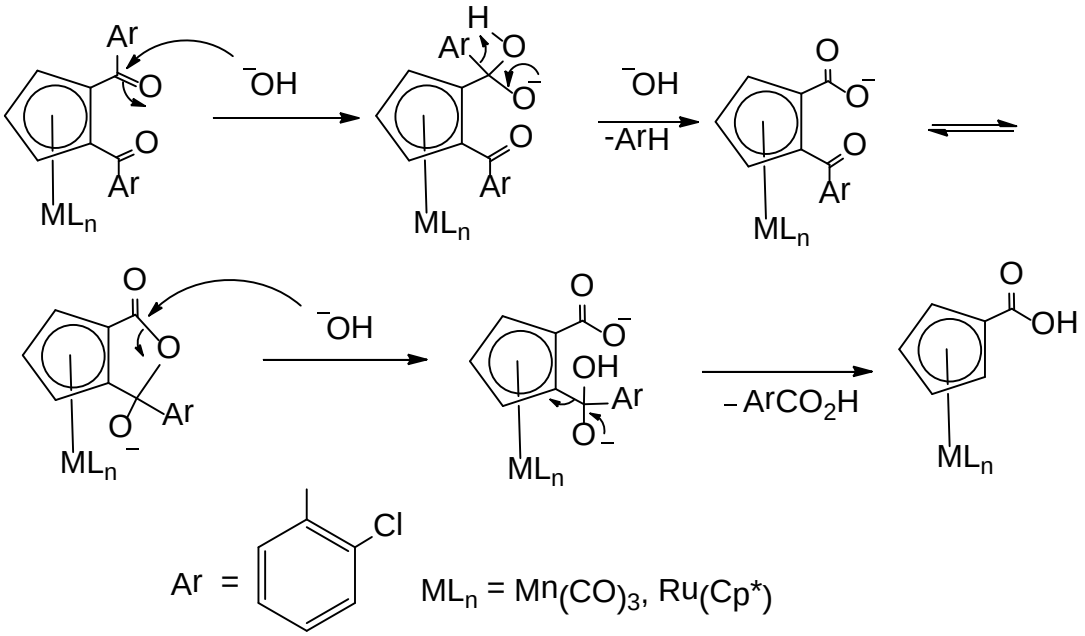

Following the procedure for the preparation of ferrocenecarboxylic acid in 74-83% from ferrocene *via* oxidative cleavage of (2-chlorobenzoyl)ferrocene,[89] we attempted a similar double cleavage reactions of **9a** and **9b.** The product was exclusively pentamethylruthenocenecarboxylic acid from **9a** and an inseparable

1:1 mixture of mono- and di-carboxylic acid from **9b**. On the basis of mechanistic studies of the Hodge group on oxidative cleavage of non-enolizable ketones,[90] we can propose the mechanism our results as shown in Scheme 2.3. We assume that after the first ketone cleavage, second cleavage takes at C-Cp bond rather than C-Ar bond. The presence of carboxylic group at 2-position of cyclopentadienylmetal complexes makes the complex moiety better leaving than the arene one.

1',2',3',4',5'-Pentamethylruthenocene-1,2-dicarboxylic anhydride **10a** (84%) was synthesized by dehydration of diacid **3a** in refluxing acetic anhydride. The product was purified by column chromatography and recrystallized from ethyl ether very easily. It was sufficiently stable to store for many days at room temperature in air. While N,N-dicyclohexylcarbodiimide (DCC) was used for the dehydration of **3a**, we isolated desired anhydride **10a** (69%) along with N-acyl urea [Ru{η^5-C_5H_3(COOH)(CONCyCONHCy)-1,2}(Cp*)] **15a** as a side-product (Scheme 2.4). The formation of side-product was indicated by the ABC pattern of substituted Cp in ^{1}H NMR. Similarly, bands at 3324 (cm-$^{-1}$), 1624 (cm^{-1}) and 1573 (cm^{-1}) on IR indicates the formation of N-acyl urea. Our attempt to separate **15a** from anhydride by extracting with $NaHCO_3$ was failed; however, careful recrystallization of the crude product gave its single crystals. The less acidic character of N-acyl urea might be due to its zwitterionic form in solution. A similar unusual structure has been reported on the reaction between *p*-bromobenzoic acid with DCC in the presence of DMAP by Wang *et al.*[91] The proposed mechanism of formation of N-acyl urea is depicted in Scheme 2.5. The O-

acylated product between dicarboxylic acid and DCC gets rearranged to N-acylated one.

Scheme 2.4. Synthesis of pentamethylruthenocene-1,2-dicarboxylic anhydride using DCC

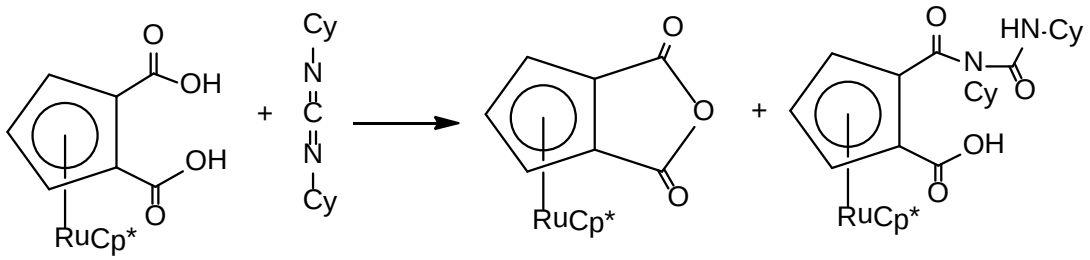

3a **10a** **15a**

Aside from somewhat contradictory reports of 1,2-ferrocenedicarboxylic anhydride by Rausch[77] and Richards,[76] **10a** is the first well characterized cyclic metallocene anhydride.[78] The cymantrene anhydride **5a** was prepared in 46% yield by dehydration of diacid **2a** in refluxing trifluoroacetic anhydride. Unlike the ruthenocene anhydride, the cymantrene anhydride was an air-sensitive gummy solid that decomposes under bench-top conditions. Analytically pure **5a** was obtained by extraction with scrupulously dry hexane under nitrogen.

We made several attempts to carry out Friedel-Crafts reactions between anhydride **10a** with hydroquinone and *p*-methoxyanisole in fused $AlCl_3$/NaCl[92] and with dibenzothiophene/$AlCl_3$ in CH_2Cl_2 at room temperature.[93] In all cases, we isolated intractable decomposition components along with small quantities of monocarboxylic acid produced as a result of the single Friedel-Crafts acylation.

Scheme 2.5. Proposed mechanism of N-acylation via four-membered cyclic tetrahedral intermediate[94]

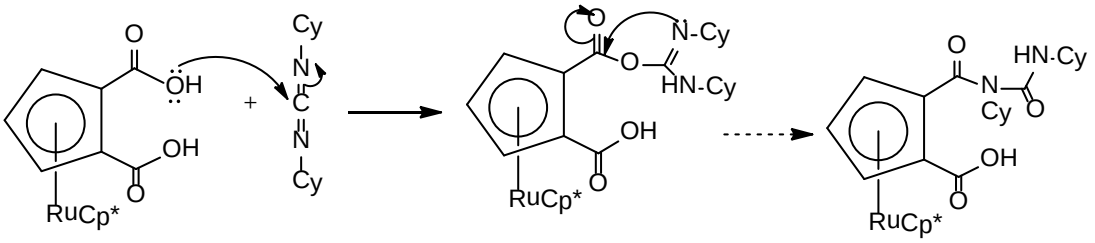

The *p*-tolylimides of pentamethylruthenocene **11a** and cymantrene **11b** were prepared from their anhydrides. Single-step conversion[95] of anhydrides **10a** and **10b** to a *p*-tolylimide failed, so the anhydrides were first treated with *p*-toluidine in THF to give the mixed acid-amide. Without isolation, ring closure was accomplished by converting the carboxylic acid to acyl chloride with oxalyl chloride/DMF resulting in **11a** (23%) and **11b** (42%). As usual, ruthenocene anhydride **11a** reacted more sluggishly with *p*-toluidine than its cymantrene counterpart **10b**, probably due to both more electron-rich character and steric crowdedness of the ruthenocene center.

Even though we were unable to obtain the desired cyclic imide, it became obvious that diacid chlorides $[Ru\{\eta^5\text{-}C_5H_3(CO_2Cl)_2\text{-}1,2\}(Cp^*)]$ **11a** and $[Mn(CO)_3\{\eta^5\text{-}C_5H_3(COCl)_2\text{-}1,2\}]$ **11b** are formed in the reaction of **3a** and **3b** on treatment with excess oxalyl chloride in the presence of catalytic amount of DMF. In fact, we successfully isolated **12a** and **12b** in 88% and 65% yields, respectively. Purification of the acid chlorides simply involves an extraction in dry hexane. Both complexes were stable under dry conditions. Cymantrene-1,2-

dicarboxylic acid chloride was crystallized from hexane at -10 °C and its molecular structure was determined.

Following a procedure used to convert 2,5-dibromothiophene-3,4-dicarboxylic acid to a cyclic imide,[96] we attempted to prepare a cyclic anilide of 1',2',3',4',5'-pentamethylruthenocene-1,2-dicarboxylic acid **3a** *via* its dichloride. Sequential treatment of **3a** with oxalyl chloride with one equivalent of aniline gave only diamide [Ru{η^5-$C_5H_3(CO_2NHPh)_2$-1,2}(Cp*)] **14a** (43%). Forcing conditions (200 °C) [97] simply resulted in the decomposition of starting complex.

The thioanhydride complexes of ruthenocene [Ru{$C_5H_3(CO)_2$S-1,2}(Cp*)] **13a** and cymantrene [$Mn(CO)_3${η^5-$C_5H_3(CO)_2$S-1,2}] **13b** were prepared by following the method optimized by Ando *et al*.[98] We prepared diacyl chloride from their corresponding diacids and without their isolation, hexamethyldisilathiane and dry potassium fluoride were added in a 4:8 ratio to obtain **13a** (75%) and **13b** (67%). A catalytic amount of 18-Crown-6 was used as phase transfer catalyst. The products were purified by chromatography on silica and crystallized by partial evaporation of a dichloromethane solution in a slow stream of hexane-saturated nitrogen. The ruthenocenethioanhydride was air-stable over a long period of time but the cymantrene thioanhydride decomposes slowly in air.

2.1.2. Spectroscopy. All new compounds were fully characterized by spectroscopic methods including ^{1}H and ^{13}C NMR, IR and mass spectroscopy. Previously synthesized compounds **1** and **2b** were characterized by comparison of their ^{1}H NMR and ^{13}C NMR spectra with those reported by Busetto *et al*.[79]

A direct comparison in chemical shifts of proton resonance is not possible due to difference in NMR solvents for different compounds. However, a correlation can be made between chemical shift and the changing electronic environment in the molecule. Tables 2.1 and 2.2 show the chemical shifts of some of the distinguishable protons and carbons of ruthenium complexes **2a**-**14a** and manganese complexes **2b**-**13b**. The proton and carbon resonances of sodium 1,2-dicarbophenoxycyclopentadienide **1** (δ_H 5.70, 6.67; δ_C 109.7, 110.9, 115.1) move upfield (δ_H 4.78, 5.13; δ_C 77.7, 78.3, 89.1) when the ligand is bound to ruthenium in **2a**. The ^{1}H NMR singlet of pentamethylcyclopentadienyl in **2a-17a** lies between 1.76 to 1.92 ppm depending mainly on the solvent. The ^{1}H NMR resonances of cyclopentadienyl ligand of ruthenium complexes **2a-14a** and manganese complexes **2b-11b** display a characteristic 2:1 doublet: triplet pattern indicating symmetrical distribution.

The inner (triplet) protons resonances (CHC*H*CH) of ruthenocene complexes **2a-14a** generally range from δ 4.46 to 5.12 while the outer (doublet) proton resonances (C*H*CHC*H*) range from δ 5.28 to 6.34. For manganese complexes **2b-11b** the triplets range from δ 5.28-5.91 and doublets range from δ 5.28 to 6.67. Comparison of chemical shifts in ^{1}H and ^{13}C NMR of ruthenium and manganese complexes with similar functional groups has revealed that resonances in Cp region of ruthenium complexes are at higher field than analogous resonances of the manganese complexes. This might be due to the higher electron-releasing effect of pentamethylcyclopentadienyl ligand (Cp*) than that of carbonyl ligands. The carbonyl ligands tend to make manganese center

electron-deficient due to their tendency to accept electrons from the metal center by backbonding. In addition, higher number of electrons in d-orbitals of ruthenium causes higher local ring-current than manganese. ^{13}C NMR of Cp *ipso* carbons are very weak due to their long relaxation times.

^{13}C NMR resonances of carbonyl carbon of 5,5-fused system showed similar chemical shifts for same functionality. In typical, the anhydride complexes display upfield (δ 163.8, **10a**; 161.0, **10b**) shift than the thioanhydride complexes (δ 187.3, **13a**; 186.1, **13b**) with an intermediate shifts in tolyl imides (δ 167.9, **11a**; 165.1, **11b**). These values lie within the normal range of analogous phthalic acid derivatives. The effect of different metals on the carbonyl peak resonances is less obvious but shifts due to ruthenium are slightly deshielded than manganese. The metal carbonyl signals of the cymantrene complexes are in typical range varying from 221 to 224 ppm which is typical range for 1,2-disubstituted metal complexes.[61]

Table 2.1. Selected ^{1}H and ^{13}C NMR data (ppm) for **1**–**13a**

	δ_H			δ_C						
	Cp*	CHC*H* CH	C*H*CH C*H*	Cp* ring	Cp* Me	*C*HCH *C*H	CH*C* HCH	*CC*	*C*O	Solvent
1	-	5.70	6.67	-	-	109.7	110.9	115.1	163.1	b
2a	1.92	4.78	5.13	80	11.2	77.7	78.3	89.1	166.8	a
3a	1.81	4.81	5.07	81.2	10.4	78.8	79.4	88.6	169.9	a
5	-	5.54	6.29	-	-	118.5	108	113	166.1	b
6a	1.77	4.46	4.82	87.9	10.8	78.7	75.9	73.7	168.5	c
8	-	5.62	6.11	-	-	125.7	111.3	124.2	185.4	b
9a	1.78	4.57	4.76	88.2	10.9	88.1	77.4	85.8	193.9	c
10a	1.80	5.03	5.12	72.7	10.4	89.9	84.9	79.5	163.8	a
11a	1.82	4.68	4.92	68.4	11.2	70.7	88.9	80.8	167.9	c
12a	1.85	5.12	5.43	81.6	10.3	86.5	90.9	80.2	162.7	a
13a	1.76	4.85	4.93	72.0	10.2	89.5	88.3	84.0	187.3	c

Sovents: a = acetone-d_6; b = DMSO-d_6; c = $CDCl_3$

Table 2.2. Selected ^{1}H and ^{13}C NMR data (ppm) for **1**, **2b**, **3b**, **8**, and **10b**–**13b**

	δ_H			δ_C				
	CHC*H*CH	C*H*CHC*H*	*C*HCH*C*H	CH*C*HCH	*CC*	*C*O	Mn(*C*O)	Solvent
1	5.70	6.67	109.7	110.9	115.1	163.1	-	b
2b	5.28	5.95	90.6	83.2	91.7	163.5	223.6	a
3b	5.91	5.28	94.8	84.0	112.2	164.4	223.0	a
8	5.62	6.11	125.7	111.3	124.2	185.4	-	b
10b	5.57	5.90	92.0	92.6	93.1	161.0	222.1	a
11b	5.38	5.86	83.5	88.0	92.5	165.1	224.7	a
12b	5.41	6.34	98.2	82.8	91.9	162.2	221.4	a
13b	5.59	5.91	91.4	83.8	100.3	186.1	222.4	a

Sovents: a = acetone-d_6; b = DMSO-d_6; c = $CDCl_3$

With the exception of anhydrides and diacyl chlorides, the IR stretches of the organic carbonyls are at higher frequency for manganese complexes **2b**-**13b** than for analogous ruthenium complexes **2a**-**13a** reflecting the greater donation of electron density from electron-rich pentamethylruthenocene center (Table 2.3). The cyclic derivatives of 1,2-dicarboxylic acids of pentamethylruthenocene and cymantrene typically show two bands due to symmetric and antisymmetric stretching of two carbonyl groups. The metal carbonyl groups in cymantrene complexes **2b-11b** show characteristics stretching in normal region varying from 1940 to 2050 cm^{-1}. The mass spectra of all compounds show characteristic peaks corresponding to molecular ions. The M+2 peaks of **12a** and **12b** have half the intensity of their molecular ion peaks, showing isotopic distribution of two chlorine atoms.

Table 2.3. Selected IR absorption frequencies of ruthenium and manganese complexes

Compound	C=O (cm^{-1})	CΞO (cm^{-1})	Phase
2a	1725	-	KBr
2b	1742	1941, 1975, 2040	KBr
3a	1603	-	KBr
3b	1706	1958, 2038, 2040	KBr
10a	1820	-	KBr
10b	1739, 1788	2039, 1944	ATR
11a	1629, 1654	-	KBr
11b	1714, 1725	2028, 2046	ATR
12a	1801	-	CCl_4
12b	1782, 1796	2049, 1984	Nujol
13a	1679, 1708	-	ATR
13b	1689, 1720	2035, 1950	ATR

2.1.3. Structure. The structures of ruthenocene complexes [Ru{η^5-$C_5H_3(CO_2Me)_2$-1,2}(Cp*)] **6**, [Ru{η^5-$C_5H_3(CO_2H)_2$-1,2}(Cp*)] **3a**, [Ru{η^5-$C_5H_3(CO)_2O$-1,2}(Cp*)] **10a**, [Ru{η^5-$C_5H_3(CO)_2S$-1,2}(Cp*)] **13a**, [Ru{η^5-C_5H_3(COOH)(CONCyCONHCy)-1,2}(Cp*)] **15a** and cymantrene complexes [$Mn(CO)_3${ η^5-$C_5H_3(CO_2H)_2$-1,2}] **3b**, and [$Mn(CO)_3${ η^5-$C_5H_3(CO)_2N$-4-$C_6H_4CH_3$-1,2}] **11b**, [$Mn(CO)_3${ η^5-$C_5H_3(COCl)_2$-1,2}] **12b** and [$Mn(CO)_3${ η^5-$C_5H_3(CO)_2S$-1,2}] **13b** were determined by X-ray crystallographic methods. All the crystals except **11b** were grown by slow evaporation of a concentrated ethyl ether solution in a stream of hexane-saturated nitrogen at room temperature, while **11b** was grown from its saturated solution in hexane by cooling to -10 °C. These crystals were mounted on glass fibers with polyisobutene oil. Hydrogen atoms were placed in geometrically calculated positions. Thermal ellipsoid plots with

numbering schemes are shown in Figures 2.1-2.9. The crystal structure and refinement data for compounds **6a, 3a, 10a, 3b** and **11b** can be found in Tables 2.4-2.7. Similarly, bond distance and bond length can be found in Tables 2.8-2.16.

The ruthenium complexes **6a, 3a, 10a** and **15a** display typical ruthenocene geometries where cyclopentadienyl ligands are η^5- bonded to the metal centers. The angles between centroids of two Cp and Ru in **6a**, **3a**, **10a** and **13a** are nearly linear. For example, centroid-Ru-centroid angle in **10a** is 177.31°. The average bond distances of ruthenium to the centroids of Cp and Cp* are: **3a** [1.820(3) Å; 1.804(3) Å], **6a** [1.820(2) Å; 1.801(2) Å], **10a** [1.819(3) Å; 1.802(3) Å] and **13a** [1.814(3) Å; 1.803(3)], **15a** [1.814; 1.798 Å]. This established that ruthenium center was not spaced evenly between electron-releasing and electron-withdrawing cyclopentadienyl ligands. The proximities of Cp* towards metal center by ca. 0.02 Å might be due to the higher electron-releasing effect of methyl substituent. The same structural effect was observed for 1,2,3,4,5-pentamethylruthenocene.[99]

One common feature of **3a, 6a** and **10a** is that the *ipso* carbon atoms (C1 and C5) in Cp are slightly nearer to ruthenium center, displaying their stronger interaction towards metal than the remaining three carbon atoms (C2, C3 and C4). The average distortion is 0.033(3) Å, 0.022(3) Å, 0.029(3) Å and 0.025 (3) Å in **3a**, **6a**, **10a** and **13a** respectively. This type of asymmetry in the bonding pattern of carbon atoms was observed by Gassman *et al.* in their study of (η^5-pentamethylcyclopentadienyl) (η^5-acetylcyclopentadienyl) ruthenium (II).[38] One

possibility of the asymmetric bonding pattern can be due to the better electronic interaction of electron-rich metal center with electron-deficient carbons of the Cp next to the electron-withdrawing carboxylic acid derivatives.

In cyclic anhydride **10a,** two molecules in the asymmetric unit are in an antiparallel orientation. One of the molecules is almost fully eclipsed while the other is fully staggered, which implies a very low barrier to rotation of Cp ligands with respect to Ru. In **3a** and **15a** molecules acquire a gauche conformation while in **6a** and **13a** they are almost eclipsed.

The cymantrene complexes, **3b**, **11b**, **12b** and **13b** possess a typical pseudooctahedral or piano-stool geometry in which Cp ligand occupies three coordination sites and OC-Mn-CO angles are close to 90°. The C-C bond length of the Cp ring in 5,5-fused system is quite regular and ranges 1.399 (4)-1.434(4) Å. However, the C1-C2 bond length in open-chain complexes **3b** 1.456(2) Å and **12b** 1.455(2) Å are slightly longer. Irregularities in bonding of Cp carbons are observed in ruthenium complexes **3a** and **13a** in the similar order of analogous complexes of manganese. This might be due to the fulvenoid character of the Cp ligand caused by the electron-withdrawing effects of carboxylic functionality.[100] The average distance from the Cp centroid to Mn ranges from 1.764 Å (**12b**) to 1.769 (**3b** and **13b**). The *ipso* carbon atoms (C1 and C2) of the cyclopentadienyl ligand are closer to Mn than the rest of the carbon atoms (C3, C4 and C5). The distortions in **3b**, **11b, 12b** and **13b** are 0.029(17) Å, 0.029(3) Å, 0.038(13) Å, and [0.033(3) Å, respectively.

In **6a**, the carbon atoms of the ester methyl groups are positioned on the same side of ruthenium center with C9 -0.148 Å, C7 -0.188 Å with respect to least-squares plane of Cp. The twist angles of plane containing C1-C6-O1-Cl1 and C2-C7-O2-Cl2 with respect to Cp plane in **12b** are 10.69° and -29.48° respectively. The deviation from their co-planarity might be due to the steric interaction between two O-atoms. Similarly, Chlorine and oxygen atoms in **12b** are located on opposite sides of the Cp least-squares plane with Cl1 0.110 Å and Cl2 -0.529 Å, O1 -0.329 Å and O2 0.711 Å.

The heterocyclic five-membered rings in all metallocenes were essentially coplanar with Cp. The folding angles between these two planes are: 2.71°and 4.96° (**10a**), 4.06° (**13a**) 1.59° (**11b**), 1.26° and 1.24° (**13b**). The folding in ruthenium complexes is higher than manganese ones probably due to steric interaction of Cp* ligands. Similarly, the average C-heteroatom-C angles of the 5,5-fused heterocyclic complexes are: **10a** [111.5(2)°], **13a** [93.96(14)°], **11b** [113.5(2)°] and **13b** [94.13(11)°]. The angles at heteroatoms are in normal range of phthalic anhydride,[101] phthalimide[102] and thiophthalic anhydride.[103] The *p*-tolyl group in **11b** is oriented at an angle of 70.44° with respect to heterocycle-fused cyclopentadienyl, probably to avoid the steric interaction of the arene *ortho* hydrogens with the carbonyl oxygens.

The 1',2',3',4',5'-pentamethylruthenocene-1,2-dicarboxylic acid **3a** and cymantrene-1,2-dicarboxylic acid **3b** structures exhibit both inter- and intramolecular H-bonding through the intermediate water and methanol molecules in **3a** but without any small molecules in **3b**. The two carboxylic acid

moieties lie on the cyclopentadienyl plane with interplanar angle 3.2-4.4° (**2a**) and 2.58-2.82° (**2b**), held together by a network of intra- and intermolecular H-bonds with carboxylate O-H-O distances ranging from 2.532(4) to 2.592(4) Å in **2a** and 2.517(2) Å to 2.608(2) Å in **2b**. The molecular structure of **15a** also shows the intramolecular H-bond between O-H of carboxylic acid with carbonyl oxygen of amide making a seven-member ring with donor-acceptor distance of 2.503 (3) Å. Similarly, the N-H of the secondary amide makes network of intermolecular H-bonding with carbonyl oxygen with donor acceptor distance of 2.822(3) Å.

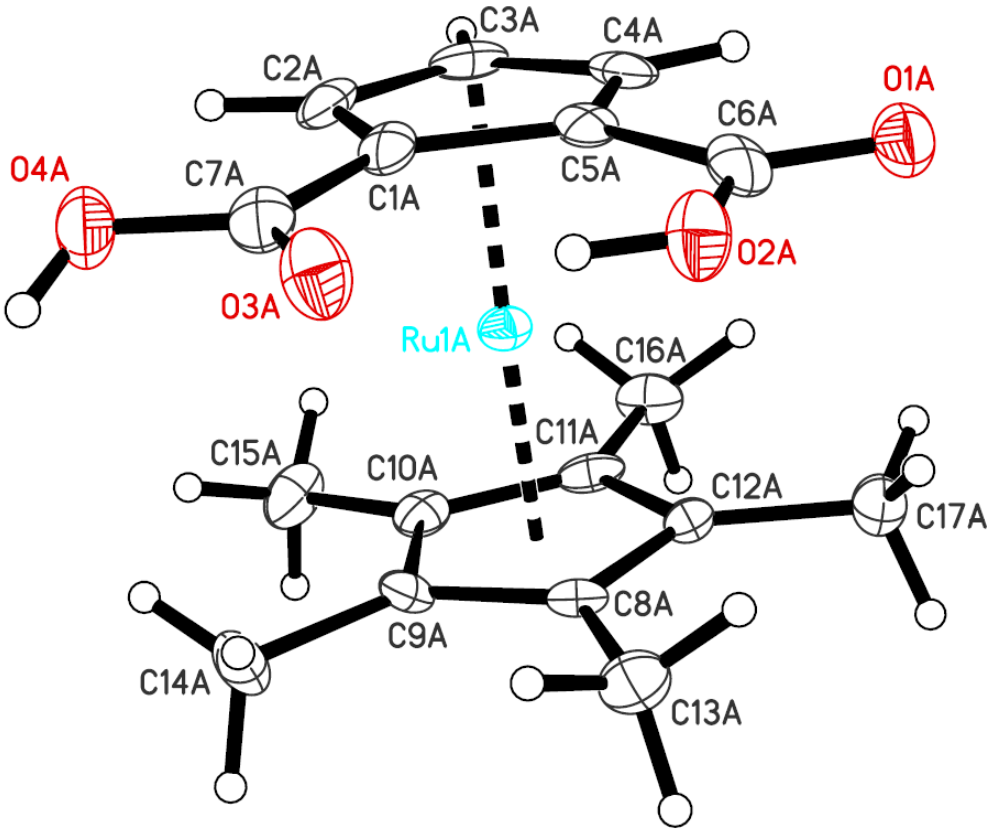

Figure 2.1. Molecular structure of [Ru{η^5-$C_5H_3(CO_2H)_2$-1,2}(Cp*)] **3a**

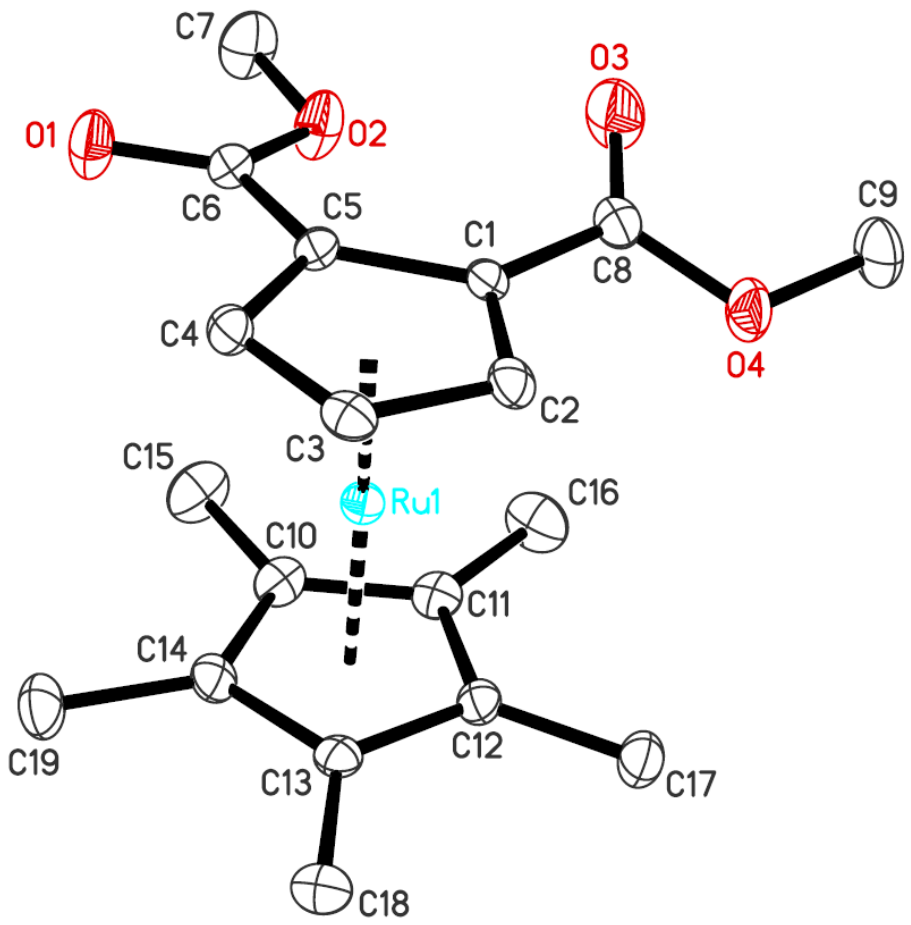

Figure 2.2. Molecular structure of [Ru{η^5-$C_5H_3(CO_2Me)_2$-1,2}(Cp*)] **6a**

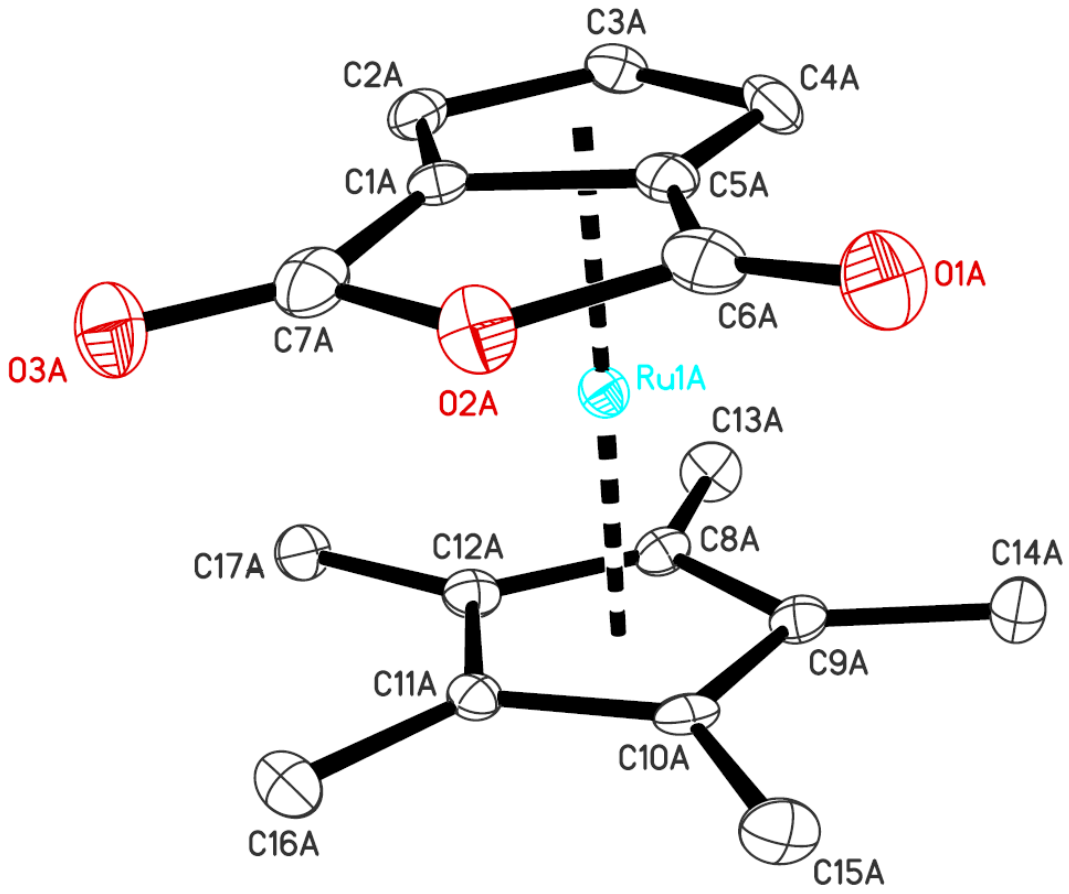

Figure 2.3. Molecular structure of [Ru{$C_5H_3(CO)_2O$-1,2}(Cp*)] **10a**

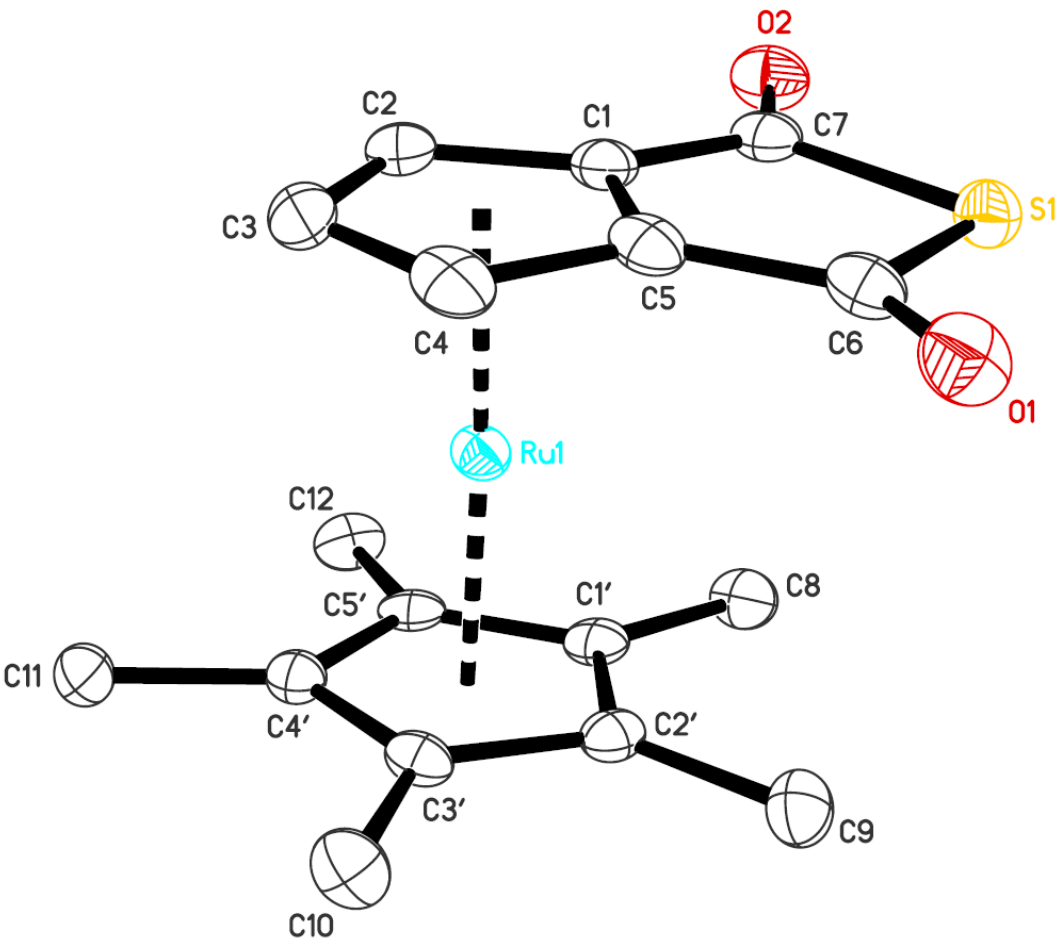

Figure 2.4. Molecular structure of [Ru{$C_5H_3(CO)_2$S-1,2}(Cp*)] **13a**

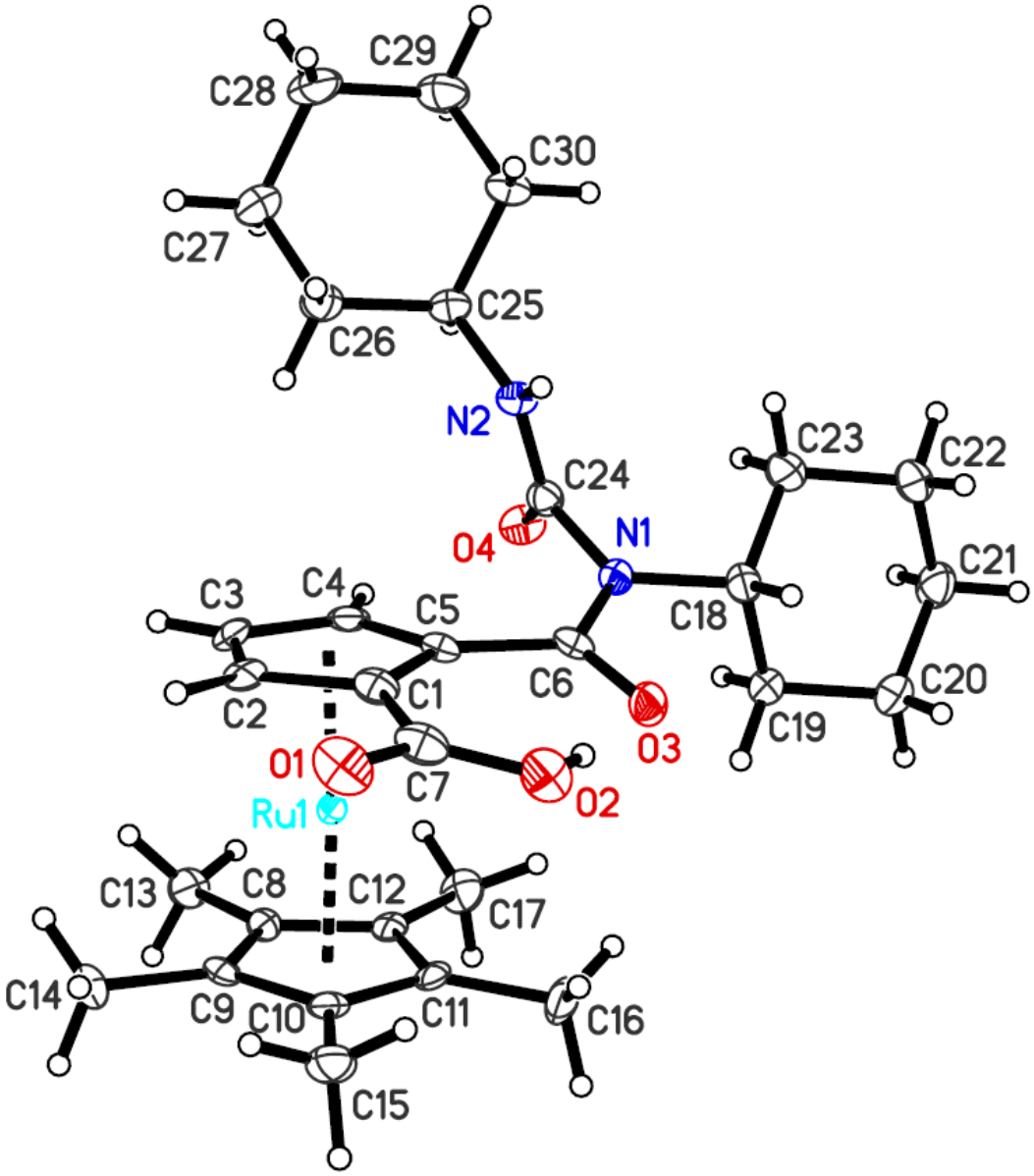

Figure 2.5. Molecular structure of [Ru{η^5-C_5H_3(COOH)(CONCyCONHCy)-1,2}(Cp*)] **15a**

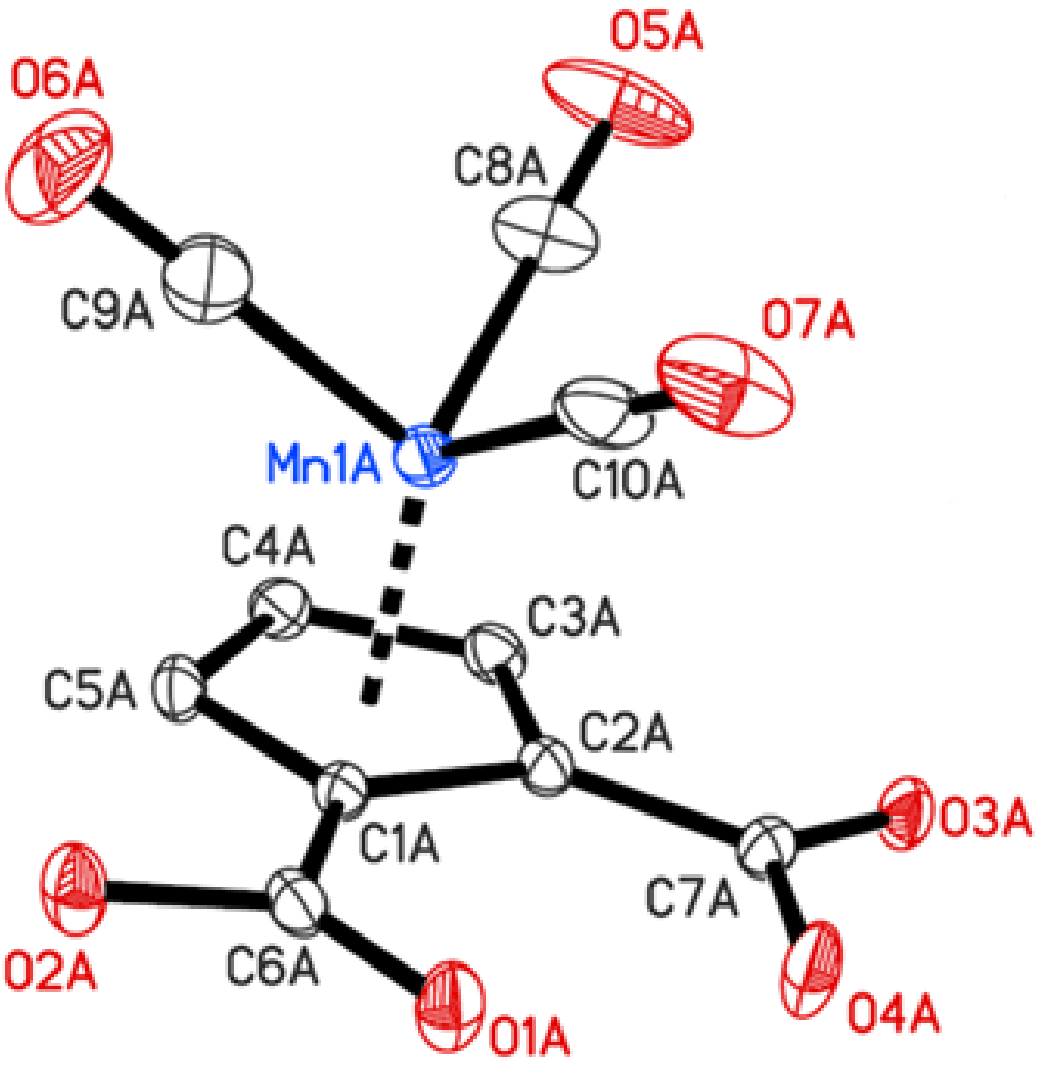

Figure 2.6. Molecular structure of $[Mn(CO)_3\{\eta^5\text{-}C_5H_3(CO_2H)_2\text{-}1,2\}]$ **3b**

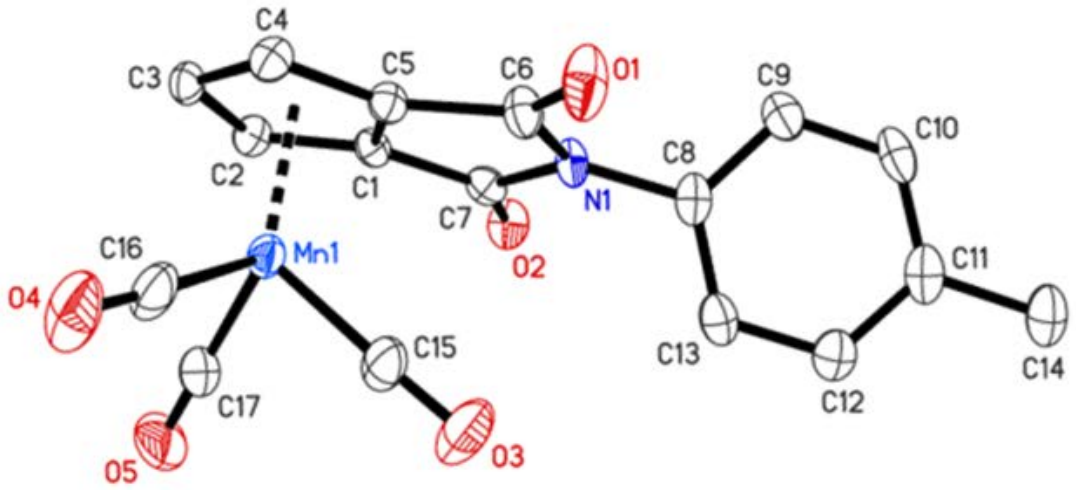

Figure 2.7. Molecular structure of $[Mn(CO)_3\{\eta^5\text{-}C_5H_3(CO)_2N\text{-}4\text{-}C_6H_4CH_3\text{-}1,2\}]$ **11b**

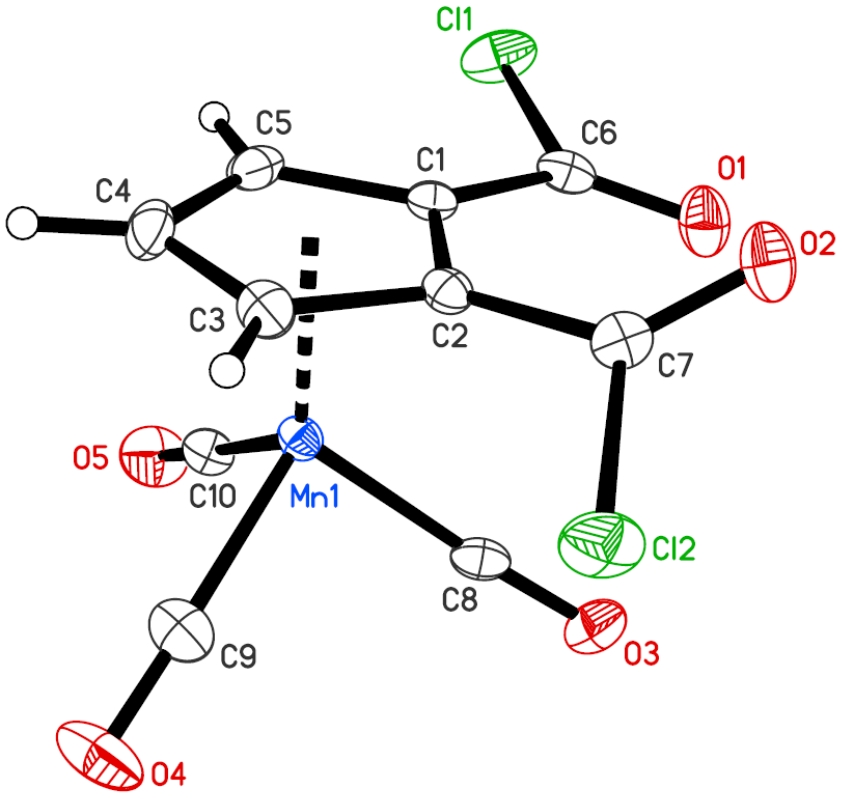

Figure 2.8. Molecular structure of $[Mn(CO)_3\{\eta^5\text{-}C_5H_3(CO_2Cl)_2\text{-}1,2\}]$ **12b**

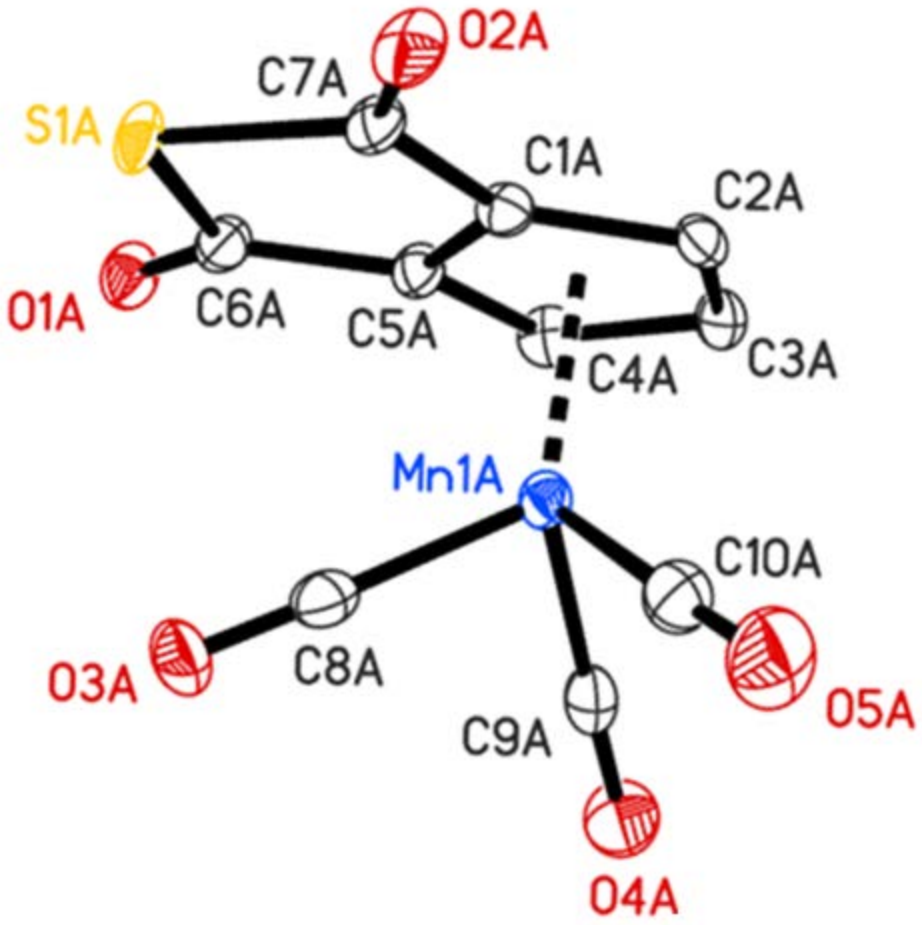

Figure 2.9. Molecular structure of $[Mn(CO)_3\{\eta^5\text{-}C_5H_3(CO)_2S\}]$ **13b**

Table 2.4. Crystal Data and Structure Refinement for Compounds **3a** and **6a**

	3a	**6a**
Formula	$C_{17.36}H_{21.44}O_{4.36}Ru$	$C_{19}H_{24}O_4Ru$
Formula wt (amu)	400.98	417.45
T, K	90.0(2)	90.0(2)
Wavelength (Å)	1.54178	0.71073
Crystal system, space group	Orthorhombic, $P2_12_12_1$	Monoclinic, $P2_1/n$
a, Å	14.3634(7)	13.8414(2)
b, Å	14.8024(8)	9.4165(1)
c, Å	15.3413(8)	14.9224(2)
α,(deg)	90	90
β, (deg)	90	115.2629(7)
γ, (deg)	90	90
V, $Å^3$	3261.8(3)	1758.93(4)
Z, d_{calc}, Mg/m^3	8, 1.633	4, 1.576
Absorption coef μ (mm^{-1})	7.947	0.910
F(000)	1636.1	856
Crystal size (mm^3)	0.15 x 0.12 x 0.08	0.12 x 0.10 x 0.08
θ range (deg)	4.15 to 68.62	1.00 to 27.48
Limiting indices	$-17 \le h \le 17$, $-17 \le k \le 17$, $-18 \le l \le 18$	$-17 \le h \le 16$, $0 \le k \le 12$, $0 \le l \le 19$
Reflections collected/unique	74431/5989, [$R_{(int)}$ = 0.0366]	28746/4015, [$R_{(int)}$ = 0.040]
Absorption correction	Semi-empirical from equivalents	Semi-empirical from equivalents
Max. and min. transmission	0.530 and 0.260	0.931 and 0.899
Refinement method	Full-matrix least-squares on F^2	Full-matrix least-squares on F^2
Data/restraints/parameters	5939 / 0 / 433	4015 / 0 / 224
Goodness-of-fit on F^2	1.178	1.133
Final R indices [$I>2\sigma(I)$]	R_1 = 0.0228, wR_2 = 0.0606	R_1 = 0.0270, wR_2 = 0.0634
R indices (all data)	R_1 = 0.0230, wR_2 = 0.0607	R_1 = 0.0325, wR_2 = 0.0659
Largest diff. peak and hole e•$Å^{-3}$	0.861 and -0.430	1.328 and -0.931

Table 2.5. Crystal Data and Structure Refinement for Compounds **10a** and **15a**

	10a	**15a**
Formula	$C_{17}H_{18}O_3Ru$	$C_{30}H_{42}N_2O_4Ru$
Formula wt (amu)	371.38	595.73
T, K	90.0(2)	90.0(2)
Wavelength Å	0.71073	1.54178
Crystal system, space group	Monoclinic, $P2_1/c$	Monoclinic, $P2_1/n$
Z, d_{calc}, Mg/m^3	8, 1.676	4, 1.425
a, Å	9.2355(18)	8.2131(2)
b, Å	25.569(5)	13.2136(3)
c, Å	12.611(3)	25.5973(7)
α,(deg)	90	90
β, (deg)	98.75(3)	91.342(2)
γ, (deg)	90	90
V, $Å^3$	2943.4(10)	2777.18(12)
Absorption coef μ (mm^{-1})	1.072	4.866
F(000)	1504	1248
Crystal size (mm^3)	0.20 x 0.15 x 0.12	0.125 x 0.0053 x 0.00033
θ range for data collection (deg)	1.59 to 27.49	3.45 to 68.48
Limiting indices	$-11 \le h \le 11$	$-8 \le h \le 9$
	$-33 \le k \le 33$	$-15 \le k \le 15$
	$-16 \le l \le 16$	$-30 \le l \le 30$
Reflections collected/unique	44065/6736, [$R_{(int)}$ = 0.0499	39897/5092 [$R_{(int)}$ = 0.0716]
Absorption correction	Semi-empirical from equivalents	Semi-empirical from equivalents
Max. and min. transmission	0.882 and 0.782	0.984 and 0.772
Refinement method	Full-matrix least-squares on F^2	Full-matrix least-squares on F^2
Data/restraints/parameters	6736 /0/389	5092 /0/341
Goodness-of-fit on F^2	1.052	1.029
Final R indices [$I>2\sigma(I)$]	R_1 = 0.0319, wR_2 = 0.0726	R_1 = 0.0313, wR_2 = 0.0655
R indices (all data)	R_1 = 0.0507, wR_2 = 0.0811	R_1 = 0.0447, wR_2 = 0.0705
Largest diff. peak and hole, $e \bullet Å^{-3}$	1.256 and -0.771	0.420 and -0.604

Table 2.6. Crystal Data and Structure Refinement for Compounds **3b**, **11b** and **12b**

	3b	**11b**	**12b**
Formula	$C_{10}H_5O_7Mn$	$C_{17}H_{10}MnNO_5$	$C_{10}H_3Cl_2O_5Mn$
Formula wt (amu)	292.08	363.20	328.96
T, K	90.0(2)	90.0(2)	90.0(2)
Wavelength (Å)	0.7107	0.7107 Å	0.7107 Å
Crystal system, space group	Monoclinic, *P2₁/c*	Orthorhombic, *Pbca*	Triclinic, *P-1*
a, Å	7.5419(15)	15.5245(3)	6.9962(1)
b, Å	11.743(2)	15.4893(3)	7.2154(1)
c, Å	24.501(5)	12.7932(3)	12.8685(3)
α,(deg)	90	90	88.6308(9)
β, (deg)	92.13(3)	90	87.9181(9)
γ, (deg)	90	90	67.0535(9)
Volume, $Å^3$	2168.5(7)	3076.30(11)	597.775(18)
Z, d_{calc}, Mg/m^3	8, 1.789	8, 1.568	2, 1.828
Absorption coef μ (mm^{-1})	1.242	0.885	1.558
F(000)	1168	1472	324
Crystal size (mm^3)	0.22 x 0.20 x 0.10	0.25 x 0.22 x 0.08	0.18 x 0.15 x 0.12
2θ range (deg)	1.92 to 27.448	2.45 to 27.48	1.58 to 27.49
Limiting indices	$-9 \le h \le 9$	$-20 \le h \le 20$	$-9 \le h \le 9$
	$-15 \le k \le 15$	$-20 \le k \le 20$	$-9 \le k \le 9$
	$-31 \le l \le 31$	$-16 \le l \le 16$	$-16 \le l \le 16$
Reflections collected/unique	44633/4959 [R_{int} = 0.0393]	6636/3523, [R_{int} = 0.0505]	13267/2733, [R_{int} = 0.0159]
Absorption correction	Semi-empirical from equivalents	Semi-empirical from equivalents	Semi-empirical from equivalents
Max. and min. transmission	0.886 and 0.772	0.933 and 0.809	0.835 and 0.767
Refinement method	Full-matrix least-squares on F^2	Full-matrix least-squares F^2	Full-matrix least-squares on F^2
Data/restraints/parameters	4959 / 0 / 329	3523 / 0 / 218	2733 / 0 / 163
Goodness-of-fit on F^2	1.094	1.010	1.062
Final R indices [I>2σ(I)]	R_1 = 0.0291, wR_2 = 0.0709	R_1 = 0.0494, wR_2 = 0.1172	R_1 = 0.0224, wR_2 = 0.0541
R indices (all data)	R_1 = 0.0377, wR_2 = 0.0757	R_1 = 0.0964, wR_2 = 0.1371	R_1 = 0.0251, wR_2 = 0.0554
Largest diff. peak and hole e•$Å^{-3}$	0.413 and -0.306	1.167 and -0.366	0.379 and -0.388

Table 2.7. Crystal data and structure refinement for **13a** and **13b**

Compound	**13a**	**13b**
Empirical formula	$C_{17}H_{18}O_2RuS$	$C_{10}H_3$ MnO_5S
Formula weight	387.44	290.12
T(K)	90.0(2)	90.0(2)
Wavelength (Å)	1.54178	1.54178
Crystal system, space group	Monoclinic, *P* $2_1/c$	Monoclinic, *I 2/a*
a (Å)	7.2286(2)	23.629(5)
b (Å)	15.6173(4)	7.7330(15)
c (Å)	14.5631(3)	24.340(5)
α (°)	90	90
β (°)	111.750(1)	111.39(3)
γ (°)	90	90
Volume, $Å^3$	1527.01(7)	4141.2(14)
Z, calculated density	4, 1.685	16, 1.861
Absorption coefficient μ (mm^{-1})	9.592	12.360
F(000)	784	2304
Crystal size (mm^3)	0.12 x 0.01 x 0.01	0.16 x 0.10 x 0.03
θ range for data collection (°)	4.32 to 68.37	3.90 to 68.59
Limiting indices	-8≤ h≤6, -18≤k≤18, -17≤l≤16	-23≤h≤28, -9≤k≤9, -28≤l≤29
Reflections collected/unique	24164/2797 [$R_{(int)}$ = 0.0890	39565/3795 [$R_{(int)}$ = 0.0676]
Absorption correction	Semi-empirical from equivalents	Semi-empirical from equivalents
Max. and min. transmission	0.753 and 0.502	0.708 and 0.403
Refinement method	Full-matrix least-squares on F^2	Full-matrix least-squares on F^2
Data/restraints/parameters	2797 / 0 / 195	3795 / 0 / 307
Goodness-of-fit on F^2	1.059	1.026
Final R indices [I>2σ(I)]	R_1 = 0.0323, wR_2 = 0.0895	R_1 = 0.0309, wR_2 = 0.0774
R indices (all data)	R_1 = 0.0342, wR_2 = 0.0910	R_1 = 0.0384, wR_2 = 0.0819
Largest diff. peak and hole ($eÅ^{-3}$)	0.876 and -0.655	0.479 and -0.319

Table 2.8. Bond Distances [Å] and Angles [°] for **3a**

Ru1A-C5A	2.165(3)
Ru1A-C12A	2.167(3)
Ru1A-C1A	2.174(3)
Ru1A-C11A	2.175(3)
Ru1A-C8A	2.177(3)
Ru1A-C10A	2.187(3)
Ru1A-C9A	2.187(3)
Ru1A-C4A	2.187(4)
Ru1A-C2A	2.208(3)
Ru1A-C3A	2.211(3)
O1A-C6A	1.230(4)
O2A-C6A	1.304(4)
O3A-C7A	1.248(5)
O4A-C7A	1.297(4)
C1A-C2A	1.428(5)
C1A-C7A	1.455(5)
C1A-C5A	1.462(5)
C2A-C3A	1.410(5)
C3A-C4A	1.412(5)
C4A-C5A	1.433(5)
C5A-C6A	1.478(5)
C8A-C9A	1.430(5)
C8A-C12A	1.445(5)
C8A-C13A	1.499(5)
C9A-C10A	1.443(5)
C9A-C14A	1.487(5)
C10A-C11A	1.455(5)
C10A-C15A	1.482(5)
C11A-C12A	1.420(5)
C11A-C16A	1.491(5)
C12A-C17A	1.504(5)
Ru1B-C1B	2.154(3)
Ru1B-C10B	2.168(3)
Ru1B-C12B	2.172(3)
Ru1B-C8B	2.176(3)
Ru1B-C5B	2.180(3)
Ru1B-C11B	2.186(3)
Ru1B-C9B	2.193(3)
Ru1B-C2B	2.194(3)
Ru1B-C4B	2.207(3)

Ru1B-C3B	2.212(3)
O1B-C6B	1.246(5)
O2B-C6B	1.297(4)
O3B-C7B	1.248(4)
O4B-C7B	1.282(5)
C1B-C2B	1.435(5)
C1B-C5B	1.451(5)
C1B-C7B	1.476(5)
C2B-C3B	1.423(5)
C3B-C4B	1.411(5)
C4B-C5B	1.432(5)
C5B-C6B	1.462(5)
C8B-C12B	1.433(4)
C8B-C9B	1.456(5)
C8B-C13B	1.491(5)
C9B-C10B	1.438(5)
C9B-C14B	1.482(5)
C10B-C11B	1.424(5)
C10B-C15B	1.507(5)
C11B-C12B	1.424(4)
C11B-C16B	1.491(4)
C12B-C17B	1.504(4)
O1M-C1M	1.363(7)
C5A-Ru1A-C12A	116.92(13)
C5A-Ru1A-C1A	39.37(12)
C12A-Ru1A-C1A	148.21(12)
C5A-Ru1A-C11A	143.61(14)
C12A-Ru1A-C11A	38.17(13)
C1A-Ru1A-C11A	173.58(13)
C5A-Ru1A-C8A	115.11(12)
C12A-Ru1A-C8A	38.85(12)
C1A-Ru1A-C8A	120.83(13)
C11A-Ru1A-C8A	64.53(13)
C5A-Ru1A-C10A	177.26(13)
C12A-Ru1A-C10A	64.60(12)
C1A-Ru1A-C10A	138.21(13)
C11A-Ru1A-C10A	38.98(13)
C8A-Ru1A-C10A	64.43(12)
C5A-Ru1A-C9A	139.45(12)

Table 2.8 continued

C12A-Ru1A-C9A	64.61(12)
C1A-Ru1A-C9A	116.75(12)
C11A-Ru1A-C9A	64.76(13)
C8A-Ru1A-C9A	38.26(12)
C10A-Ru1A-C9A	38.53(13)
C5A-Ru1A-C4A	38.43(13)
C12A-Ru1A-C4A	111.84(13)
C1A-Ru1A-C4A	64.39(13)
C11A-Ru1A-C4A	114.66(13)
C8A-Ru1A-C4A	137.04(13)
C10A-Ru1A-C4A	143.78(13)
C9A-Ru1A-C4A	175.30(14)
C5A-Ru1A-C2A	64.13(12)
C12A-Ru1A-C2A	170.98(13)
C1A-Ru1A-C2A	38.02(12)
C11A-Ru1A-C2A	135.58(13)
C8A-Ru1A-C2A	149.93(13)
C10A-Ru1A-C2A	114.76(13)
C9A-Ru1A-C2A	121.09(12)
C4A-Ru1A-C2A	62.86(13)
C5A-Ru1A-C3A	63.76(12)
C12A-Ru1A-C3A	134.17(13)
C1A-Ru1A-C3A	63.54(13)
C11A-Ru1A-C3A	111.56(13)
C8A-Ru1A-C3A	172.51(13)
C10A-Ru1A-C3A	117.07(12)
C9A-Ru1A-C3A	147.25(13)
C4A-Ru1A-C3A	37.44(14)
C2A-Ru1A-C3A	37.22(14)
C2A-C1A-C7A	123.1(3)
C2A-C1A-C5A	106.9(3)
C7A-C1A-C5A	129.9(3)
C2A-C1A-Ru1A	72.3(2)
C7A-C1A-Ru1A	120.0(2)
C5A-C1A-Ru1A	70.0(2)
C3A-C2A-C1A	108.9(3)
C3A-C2A-Ru1A	71.53(18)
C1A-C2A-Ru1A	69.7(2)
C2A-C3A-C4A	108.6(3)
C2A-C3A-Ru1A	71.25(18)
C4A-C3A-Ru1A	70.36(19)
C3A-C4A-C5A	108.7(3)
C3A-C4A-Ru1A	72.20(19)

C5A-C4A-Ru1A	69.9(2)
C4A-C5A-C1A	106.8(3)
C4A-C5A-C6A	122.4(3)
C1A-C5A-C6A	130.7(3)
C4A-C5A-Ru1A	71.6(2)
C1A-C5A-Ru1A	70.6(2)
C6A-C5A-Ru1A	119.2(2)
O1A-C6A-O2A	120.6(3)
O1A-C6A-C5A	120.0(3)
O2A-C6A-C5A	119.4(3)
O3A-C7A-O4A	121.8(3)
O3A-C7A-C1A	123.4(3)
O4A-C7A-C1A	114.8(3)
C9A-C8A-C12A	108.0(3)
C9A-C8A-C13A	126.3(3)
C12A-C8A-C13A	125.7(3)
C9A-C8A-Ru1A	71.25(18)
C12A-C8A-Ru1A	70.20(17)
C13A-C8A-Ru1A	125.1(2)
C8A-C9A-C10A	108.1(3)
C8A-C9A-C14A	126.3(3)
C10A-C9A-C14A	125.6(3)
C8A-C9A-Ru1A	70.49(18)
C10A-C9A-Ru1A	70.72(18)
C14A-C9A-Ru1A	125.7(2)
C9A-C10A-C11A	107.4(3)
C9A-C10A-C15A	126.3(3)
C11A-C10A-C15A	126.2(3)
C9A-C10A-Ru1A	70.75(18)
C11A-C10A-Ru1A	70.07(18)
C15A-C10A-Ru1A	127.9(2)
C12A-C11A-C10A	108.0(3)
C12A-C11A-C16A	126.3(3)
C10A-C11A-C16A	125.7(3)
C12A-C11A-Ru1A	70.61(18)
C10A-C11A-Ru1A	70.95(18)
C16A-C11A-Ru1A	123.9(2)
C11A-C12A-C8A	108.4(3)
C11A-C12A-C17A	126.6(3)
C8A-C12A-C17A	124.9(3)
C11A-C12A-Ru1A	71.22(18)
C8A-C12A-Ru1A	70.95(17)

Table 2.8 continued

C17A-C12A-Ru1A	125.2(2)
C1B-Ru1B-C10B	131.64(13)
C1B-Ru1B-C12B	153.61(13)
C10B-Ru1B-C12B	63.82(13)
C1B-Ru1B-C8B	121.87(13)
C10B-Ru1B-C8B	64.46(12)
C12B-Ru1B-C8B	38.50(12)
C1B-Ru1B-C5B	39.13(12)
C10B-Ru1B-C5B	169.84(13)
C12B-Ru1B-C5B	122.61(13)
C8B-Ru1B-C5B	114.82(13)
C1B-Ru1B-C11B	167.14(12)
C10B-Ru1B-C11B	38.17(13)
C12B-Ru1B-C11B	38.13(12)
C8B-Ru1B-C11B	64.49(12)
C5B-Ru1B-C11B	151.75(13)
C1B-Ru1B-C9B	112.42(13)
C10B-Ru1B-C9B	38.49(13)
C12B-Ru1B-C9B	64.55(12)
C8B-Ru1B-C9B	38.93(13)
C5B-Ru1B-C9B	134.42(13)
C11B-Ru1B-C9B	64.55(12)
C1B-Ru1B-C2B	38.54(14)
C10B-Ru1B-C2B	111.09(13)
C12B-Ru1B-C2B	167.21(13)
C8B-Ru1B-C2B	152.01(13)
C5B-Ru1B-C2B	64.35(13)
C11B-Ru1B-C2B	130.60(13)
C9B-Ru1B-C2B	119.64(14)
C1B-Ru1B-C4B	64.01(12)
C10B-Ru1B-C4B	149.53(14)
C12B-Ru1B-C4B	114.96(13)
C8B-Ru1B-C4B	135.47(13)
C5B-Ru1B-C4B	38.10(13)
C11B-Ru1B-C4B	120.68(13)
C9B-Ru1B-C4B	171.75(14)
C2B-Ru1B-C4B	62.81(12)
C1B-Ru1B-C3B	64.10(13)
C10B-Ru1B-C3B	118.81(13)
C12B-Ru1B-C3B	132.69(13)
C8B-Ru1B-C3B	169.92(14)
C5B-Ru1B-C3B	63.82(13)
C11B-Ru1B-C3B	111.53(12)

C9B-Ru1B-C3B	149.36(14)
C2B-Ru1B-C3B	37.68(14)
C4B-Ru1B-C3B	37.25(13)
C2B-C1B-C5B	107.6(3)
C2B-C1B-C7B	122.8(3)
C5B-C1B-C7B	129.5(3)
C2B-C1B-Ru1B	72.2(2)
C5B-C1B-Ru1B	71.4(2)
C7B-C1B-Ru1B	119.1(2)
C3B-C2B-C1B	108.3(3)
C3B-C2B-Ru1B	71.84(19)
C1B-C2B-Ru1B	69.2(2)
C4B-C3B-C2B	108.1(3)
C4B-C3B-Ru1B	71.20(19)
C2B-C3B-Ru1B	70.49(19)
C3B-C4B-C5B	109.5(3)
C3B-C4B-Ru1B	71.55(19)
C5B-C4B-Ru1B	69.9(2)
C4B-C5B-C1B	106.6(3)
C4B-C5B-C6B	123.3(3)
C1B-C5B-C6B	130.0(3)
C4B-C5B-Ru1B	72.0(2)
C1B-C5B-Ru1B	69.5(2)
C6B-C5B-Ru1B	119.7(2)
O1B-C6B-O2B	122.9(3)
O1B-C6B-C5B	122.9(3)
O2B-C6B-C5B	114.2(3)
O3B-C7B-O4B	120.5(3)
O3B-C7B-C1B	118.8(3)
O4B-C7B-C1B	120.7(3)
C12B-C8B-C9B	107.6(3)
C12B-C8B-C13B	126.2(3)
C9B-C8B-C13B	126.2(3)
C12B-C8B-Ru1B	70.60(17)
C9B-C8B-Ru1B	71.17(18)
C13B-C8B-Ru1B	126.5(2)
C10B-C9B-C8B	106.4(3)
C10B-C9B-C14B	127.8(4)
C8B-C9B-C14B	125.8(3)
C10B-C9B-Ru1B	69.83(19)
C8B-C9B-Ru1B	69.90(17)
C14B-C9B-Ru1B	125.9(2)

Table 2.8 continued

C11B-C10B-C9B	109.6(3)
C11B-C10B-C15B	125.7(3)
C9B-C10B-C15B	124.6(3)
C11B-C10B-Ru1B	71.57(19)
C9B-C10B-Ru1B	71.7(2)
C15B-C10B-Ru1B	125.4(2)
C12B-C11B-C10B	107.4(3)
C12B-C11B-C16B	126.9(3)
C10B-C11B-C16B	125.7(3)

C12B-C11B-Ru1B	70.42(17)
C10B-C11B-Ru1B	70.26(18)
C16B-C11B-Ru1B	126.5(2)
C11B-C12B-C8B	109.1(3)
C11B-C12B-C17B	126.3(3)
C8B-C12B-C17B	124.5(3)
C11B-C12B-Ru1B	71.45(17)
C8B-C12B-Ru1B	70.90(17)
C17B-C12B-Ru1B	126.8(2)

Table 2.9. Bond Distances (Å) and Angles [°] for **6a**

Ru1-C12	2.168(2)
Ru1-C13	2.169(2)
Ru1-C11	2.173(2)
Ru1-C1	2.1731(19)
Ru1-C10	2.179(2)
Ru1-C5	2.181(2)
Ru1-C14	2.185(2)
Ru1-C2	2.1904(19)
Ru1-C4	2.198(2)
Ru1-C3	2.211(2)
O1-C6	1.213(3)
O2-C6	1.323(3)
O2-C7	1.447(3)
O3-C8	1.198(3)
O4-C8	1.354(3)
O4-C9	1.446(3)
C1-C2	1.439(3)
C1-C5	1.454(3)
C1-C8	1.477(3)
C2-C3	1.421(3)
C3-C4	1.418(3)
C4-C5	1.433(3)
C5-C6	1.483(3)
C10-C14	1.429(3)
C10-C11	1.430(3)
C10-C15	1.503(3)
C11-C12	1.438(3)
C11-C16	1.490(3)
C12-C13	1.435(3)
C12-C17	1.498(3)
C13-C14	1.432(3)
C13-C18	1.502(3)
C14-C19	1.506(3)
C12-Ru1-C13	38.65(7)
C12-Ru1-C11	38.69(8)
C13-Ru1-C11	64.67(8)
C12-Ru1-C1	122.63(8)
C13-Ru1-C1	155.45(8)
C11-Ru1-C1	111.47(8)
C12-Ru1-C10	64.41(8)
C13-Ru1-C10	64.31(8)
C11-Ru1-C10	38.37(8)

C1-Ru1-C10	129.11(8)
C12-Ru1-C5	156.25(8)
C13-Ru1-C5	164.00(8)
C11-Ru1-C5	123.69(8)
C1-Ru1-C5	39.03(7)
C10-Ru1-C5	112.59(8)
C12-Ru1-C14	64.42(8)
C13-Ru1-C14	38.41(8)
C11-Ru1-C14	64.32(8)
C1-Ru1-C14	164.50(8)
C10-Ru1-C14	38.23(8)
C5-Ru1-C14	129.24(8)
C12-Ru1-C2	111.47(8)
C13-Ru1-C2	123.06(8)
C11-Ru1-C2	128.71(8)
C1-Ru1-C2	38.51(7)
C10-Ru1-C2	164.15(8)
C5-Ru1-C2	64.44(8)
C14-Ru1-C2	155.96(8)
C12-Ru1-C4	163.45(8)
C13-Ru1-C4	129.13(8)
C11-Ru1-C4	157.12(8)
C1-Ru1-C4	64.12(7)
C10-Ru1-C4	125.11(8)
C5-Ru1-C4	38.21(7)
C14-Ru1-C4	113.39(8)
C2-Ru1-C4	63.21(8)
C12-Ru1-C3	128.57(8)
C13-Ru1-C3	112.30(8)
C11-Ru1-C3	163.46(8)
C1-Ru1-C3	63.91(7)
C10-Ru1-C3	157.01(8)
C5-Ru1-C3	63.84(8)
C14-Ru1-C3	124.46(8)
C2-Ru1-C3	37.66(7)
C4-Ru1-C3	37.52(8)
C6-O2-C7	116.00(18)
C8-O4-C9	114.51(18)
C2-C1-C5	107.30(17)
C2-C1-C8	122.86(18)
C5-C1-C8	129.76(18)
C2-C1-Ru1	71.40(11)

Table 2.9 continued

C5-C1-Ru1	70.77(11)
C8-C1-Ru1	125.61(14)
C3-C2-C1	108.48(18)
C3-C2-Ru1	71.97(11)
C1-C2-Ru1	70.10(11)
C4-C3-C2	108.21(18)
C4-C3-Ru1	70.72(12)
C2-C3-Ru1	70.38(11)
C3-C4-C5	109.08(17)
C3-C4-Ru1	71.76(12)
C5-C4-Ru1	70.26(11)
C4-C5-C1	106.92(17)
C4-C5-C6	120.90(18)
C1-C5-C6	132.12(19)
C4-C5-Ru1	71.53(11)
C1-C5-Ru1	70.20(11)
C6-C5-Ru1	121.31(14)
O1-C6-O2	124.0(2)
O1-C6-C5	122.38(19)
O2-C6-C5	113.58(18)
O3-C8-O4	122.0(2)
O3-C8-C1	127.3(2)
O4-C8-C1	110.54(17)
C14-C10-C11	108.43(18)
C14-C10-C15	125.6(2)
C11-C10-C15	126.0(2)
C14-C10-Ru1	71.10(11)

C11-C10-Ru1	70.59(11)
C15-C10-Ru1	125.25(16)
C10-C11-C12	107.75(18)
C10-C11-C16	126.3(2)
C12-C11-C16	126.0(2)
C10-C11-Ru1	71.04(11)
C12-C11-Ru1	70.49(11)
C16-C11-Ru1	124.94(15)
C13-C12-C11	107.85(17)
C13-C12-C17	126.49(19)
C11-C12-C17	125.54(19)
C13-C12-Ru1	70.71(11)
C11-C12-Ru1	70.82(11)
C17-C12-Ru1	126.98(15)
C14-C13-C12	108.02(18)
C14-C13-C18	125.71(19)
C12-C13-C18	126.20(19)
C14-C13-Ru1	71.37(12)
C12-C13-Ru1	70.64(11)
C18-C13-Ru1	126.04(15)
C10-C14-C13	107.95(18)
C10-C14-C19	125.8(2)
C13-C14-C19	126.2(2)
C10-C14-Ru1	70.66(12)
C13-C14-Ru1	70.22(11)
C19-C14-Ru1	127.69(15)

Table 2.10. Bond Distance (Å) and Angle [°] of **10a**

Ru1A-C1A	2.162(3)
Ru1A-C8A	2.169(3)
Ru1A-C12A	2.170(3)
Ru1A-C9A	2.178(3)
Ru1A-C5A	2.178(3)
Ru1A-C10A	2.179(3)
Ru1A-C11A	2.183(3)
Ru1A-C2A	2.187(3)
Ru1A-C3A	2.201(3)
Ru1A-C4A	2.211(3)
O1A-C6A	1.193(3)
O2A-C6A	1.408(4)
O2A-C7A	1.419(3)
O3A-C7A	1.190(3)
C1A-C2A	1.422(4)
C1A-C5A	1.433(4)
C1A-C7A	1.466(4)
C2A-C3A	1.429(4)
C3A-C4A	1.432(4)
C4A-C5A	1.424(4)
C5A-C6A	1.464(4)
C8A-C12A	1.432(4)
C8A-C9A	1.435(4)
C8A-C13A	1.496(4)
C9A-C10A	1.443(4)
C9A-C14A	1.498(4)
C10A-C11A	1.436(4)
C10A-C15A	1.497(4)
C11A-C12A	1.436(4)
C11A-C16A	1.496(4)
C12A-C17A	1.501(4)
Ru1B-C5B	2.167(3)
Ru1B-C9B	2.168(3)
Ru1B-C8B	2.171(3)
Ru1B-C1B	2.172(3)
Ru1B-C12B	2.183(3)
Ru1B-C11B	2.183(3)
Ru1B-C10B	2.189(3)
Ru1B-C4B	2.198(3)
Ru1B-C3B	2.198(3)
Ru1B-C2B	2.200(3)
O1B-C6B	1.193(3)

O2B-C7B	1.407(3)
O2B-C6B	1.415(3)
O3B-C7B	1.195(3)
C1B-C2B	1.421(4)
C1B-C5B	1.435(4)
C1B-C7B	1.462(4)
C2B-C3B	1.427(4)
C3B-C4B	1.430(4)
C4B-C5B	1.429(4)
C5B-C6B	1.461(4)
C8B-C12B	1.429(4)
C8B-C9B	1.435(4)
C8B-C13B	1.502(4)
C9B-C10B	1.436(4)
C9B-C14B	1.502(4)
C10B-C11B	1.439(4)
C10B-C15B	1.499(4)
C11B-C12B	1.439(4)
C11B-C16B	1.493(4)
C12B-C17B	1.499(4)
C1A-Ru1A-C8A	160.26(10)
C1A-Ru1A-C12A	126.63(10)
C8A-Ru1A-C12A	38.53(10)
C1A-Ru1A-C9A	160.24(10)
C8A-Ru1A-C9A	38.54(10)
C12A-Ru1A-C9A	64.70(10)
C1A-Ru1A-C5A	38.57(10)
C8A-Ru1A-C5A	158.24(10)
C12A-Ru1A-C5A	162.99(10)
C9A-Ru1A-C5A	126.61(10)
C1A-Ru1A-C10A	126.67(10)
C8A-Ru1A-C10A	64.45(10)
C12A-Ru1A-C10A	64.50(10)
C9A-Ru1A-C10A	38.69(10)
C5A-Ru1A-C10A	114.95(10)
C1A-Ru1A-C11A	112.64(11)
C8A-Ru1A-C11A	64.46(10)
C12A-Ru1A-C11A	38.54(10)
C9A-Ru1A-C11A	64.68(10)
C5A-Ru1A-C11A	130.00(10)
C10A-Ru1A-C11A	38.44(10)

Table 2.10 continued

C1A-Ru1A-C2A	38.17(10)
C8A-Ru1A-C2A	125.21(10)
C12A-Ru1A-C2A	109.39(10)
C9A-Ru1A-C2A	160.55(10)
C5A-Ru1A-C2A	64.23(10)
C10A-Ru1A-C2A	157.95(10)
C11A-Ru1A-C2A	123.37(10)
C1A-Ru1A-C3A	63.17(11)
C8A-Ru1A-C3A	110.83(11)
C12A-Ru1A-C3A	122.69(11)
C9A-Ru1A-C3A	127.66(10)
C5A-Ru1A-C3A	63.03(11)
C10A-Ru1A-C3A	163.53(10)
C11A-Ru1A-C3A	156.04(10)
C2A-Ru1A-C3A	38.02(10)
C1A-Ru1A-C4A	64.02(11)
C8A-Ru1A-C4A	124.09(10)
C12A-Ru1A-C4A	156.00(10)
C9A-Ru1A-C4A	112.91(11)
C5A-Ru1A-C4A	37.87(10)
C10A-Ru1A-C4A	130.02(10)
C11A-Ru1A-C4A	164.66(10)
C2A-Ru1A-C4A	64.29(11)
C3A-Ru1A-C4A	37.87(10)
C6A-O2A-C7A	111.3(2)
C2A-C1A-C5A	108.7(2)
C2A-C1A-C7A	143.7(3)
C5A-C1A-C7A	107.4(2)
C2A-C1A-Ru1A	71.87(15)
C5A-C1A-Ru1A	71.33(15)
C7A-C1A-Ru1A	116.91(19)
C1A-C2A-C3A	106.5(2)
C1A-C2A-Ru1A	69.96(15)
C3A-C2A-Ru1A	71.54(16)
C2A-C3A-C4A	109.7(2)
C2A-C3A-Ru1A	70.45(15)
C4A-C3A-Ru1A	71.41(16)
C5A-C4A-C3A	106.6(2)
C5A-C4A-Ru1A	69.84(15)
C3A-C4A-Ru1A	70.72(15)
C4A-C5A-C1A	108.4(2)
C4A-C5A-C6A	143.2(3)
C1A-C5A-C6A	108.3(2)

C4A-C5A-Ru1A	72.29(15)
C1A-C5A-Ru1A	70.10(15)
C6A-C5A-Ru1A	120.77(19)
O1A-C6A-O2A	120.2(3)
O1A-C6A-C5A	133.5(3)
O2A-C6A-C5A	106.4(2)
O3A-C7A-O2A	120.1(3)
O3A-C7A-C1A	133.4(3)
O2A-C7A-C1A	106.5(2)
C12A-C8A-C9A	108.5(2)
C12A-C8A-C13A	125.6(2)
C9A-C8A-C13A	125.7(2)
C12A-C8A-Ru1A	70.75(15)
C9A-C8A-Ru1A	71.05(15)
C13A-C8A-Ru1A	127.53(19)
C8A-C9A-C10A	107.4(2)
C8A-C9A-C14A	126.4(2)
C10A-C9A-C14A	126.2(2)
C8A-C9A-Ru1A	70.42(15)
C10A-C9A-Ru1A	70.69(15)
C14A-C9A-Ru1A	126.29(19)
C11A-C10A-C9A	108.3(2)
C11A-C10A-C15A	126.1(2)
C9A-C10A-C15A	125.6(2)
C11A-C10A-Ru1A	70.94(15)
C9A-C10A-Ru1A	70.62(15)
C15A-C10A-Ru1A	126.13(19)
C10A-C11A-C12A	107.8(2)
C10A-C11A-C16A	125.5(2)
C12A-C11A-C16A	126.7(2)
C10A-C11A-Ru1A	70.62(15)
C12A-C11A-Ru1A	70.24(15)
C16A-C11A-Ru1A	125.64(19)
C8A-C12A-C11A	108.1(2)
C8A-C12A-C17A	125.6(2)
C11A-C12A-C17A	126.3(2)
C8A-C12A-Ru1A	70.72(15)
C11A-C12A-Ru1A	71.23(15)
C17A-C12A-Ru1A	125.45(19)
C5B-Ru1B-C9B	137.68(11)
C5B-Ru1B-C8B	174.85(10)
C9B-Ru1B-C8B	38.62(10)

Table 2.10 continued

C5B-Ru1B-C1B	38.63(10)
C9B-Ru1B-C1B	176.11(10)
C8B-Ru1B-C1B	144.93(10)
C5B-Ru1B-C12B	146.62(10)
C9B-Ru1B-C12B	64.33(10)
C8B-Ru1B-C12B	38.31(10)
C1B-Ru1B-C12B	119.43(10)
C5B-Ru1B-C11B	118.47(11)
C9B-Ru1B-C11B	64.58(10)
C8B-Ru1B-C11B	64.54(10)
C1B-Ru1B-C11B	117.48(11)
C12B-Ru1B-C11B	38.48(10)
C5B-Ru1B-C10B	114.91(11)
C9B-Ru1B-C10B	38.49(10)
C8B-Ru1B-C10B	64.44(10)
C1B-Ru1B-C10B	141.05(10)
C12B-Ru1B-C10B	64.19(10)
C11B-Ru1B-C10B	38.44(10)
C5B-Ru1B-C4B	38.20(10)
C9B-Ru1B-C4B	111.93(11)
C8B-Ru1B-C4B	136.88(10)
C1B-Ru1B-C4B	64.37(11)
C12B-Ru1B-C4B	175.19(10)
C11B-Ru1B-C4B	143.76(11)
C10B-Ru1B-C4B	115.10(10)
C5B-Ru1B-C3B	63.00(11)
C9B-Ru1B-C3B	115.12(11)
C8B-Ru1B-C3B	114.08(11)
C1B-Ru1B-C3B	62.93(11)
C12B-Ru1B-C3B	139.78(11)
C11B-Ru1B-C3B	178.26(10)
C10B-Ru1B-C3B	142.35(10)
C4B-Ru1B-C3B	37.97(10)
C5B-Ru1B-C2B	64.13(11)
C9B-Ru1B-C2B	142.49(10)
C8B-Ru1B-C2B	116.56(11)
C1B-Ru1B-C2B	37.94(10)
C12B-Ru1B-C2B	116.32(10)
C11B-Ru1B-C2B	141.40(10)
C10B-Ru1B-C2B	178.95(10)
C4B-Ru1B-C2B	64.48(11)
C3B-Ru1B-C2B	37.86(10)
C7B-O2B-C6B	111.5(2)

C2B-C1B-C5B	108.5(2)
C2B-C1B-C7B	143.0(3)
C5B-C1B-C7B	108.1(2)
C2B-C1B-Ru1B	72.07(15)
C5B-C1B-Ru1B	70.50(15)
C7B-C1B-Ru1B	116.07(19)
C1B-C2B-C3B	106.4(2)
C1B-C2B-Ru1B	69.98(16)
C3B-C2B-Ru1B	71.02(16)
C2B-C3B-C4B	110.4(2)
C2B-C3B-Ru1B	71.12(16)
C4B-C3B-Ru1B	71.01(16)
C5B-C4B-C3B	105.9(2)
C5B-C4B-Ru1B	69.73(16)
C3B-C4B-Ru1B	71.02(16)
C4B-C5B-C1B	108.8(2)
C4B-C5B-C6B	143.2(3)
C1B-C5B-C6B	107.7(2)
C4B-C5B-Ru1B	72.07(16)
C1B-C5B-Ru1B	70.87(15)
C6B-C5B-Ru1B	116.1(2)
O1B-C6B-O2B	120.4(3)
O1B-C6B-C5B	133.2(3)
O2B-C6B-C5B	106.4(2)
O3B-C7B-O2B	120.4(2)
O3B-C7B-C1B	133.2(3)
O2B-C7B-C1B	106.3(2)
C12B-C8B-C9B	108.0(2)
C12B-C8B-C13B	126.1(3)
C9B-C8B-C13B	125.8(2)
C12B-C8B-Ru1B	71.31(15)
C9B-C8B-Ru1B	70.57(15)
C13B-C8B-Ru1B	126.3(2)
C8B-C9B-C10B	108.1(2)
C8B-C9B-C14B	125.7(3)
C10B-C9B-C14B	126.2(3)
C8B-C9B-Ru1B	70.82(15)
C10B-C9B-Ru1B	71.55(15)
C14B-C9B-Ru1B	123.3(2)
C9B-C10B-C11B	107.9(2)
C9B-C10B-C15B	126.8(2)
C11B-C10B-C15B	125.3(2)

Table 2.10 continued

C9B-C10B-Ru1B	69.96(15)
C11B-C10B-Ru1B	70.58(15)
C15B-C10B-Ru1B	126.42(19)
C12B-C11B-C10B	107.6(2)
C12B-C11B-C16B	126.8(2)
C10B-C11B-C16B	125.5(2)
C12B-C11B-Ru1B	70.76(15)
C10B-C11B-Ru1B	70.98(15)

C16B-C11B-Ru1B	126.5(2)
C8B-C12B-C11B	108.3(2)
C8B-C12B-C17B	127.1(3)
C11B-C12B-C17B	124.5(2)
C8B-C12B-Ru1B	70.38(15)
C11B-C12B-Ru1B	70.77(15)
C17B-C12B-Ru1B	126.41(19)

Table 2.11. Bond lengths [Å] and angles [°] for **13a**

Ru1-C3'	2.160(3)
Ru1-C5	2.167(3)
Ru1-C4'	2.168(3)
Ru1-C1	2.171(3)
Ru1-C2'	2.182(3)
Ru1-C5'	2.185(3)
Ru1-C1'	2.187(3)
Ru1-C4	2.188(3)
Ru1-C3	2.197(3)
Ru1-C2	2.199(3)
S1-C6	1.822(3)
S1-C7	1.830(3)
O1-C6	1.204(4)
O2-C7	1.207(4)
C1-C2	1.432(4)
C1-C5	1.435(4)
C1-C7	1.454(4)
C2-C3	1.427(5)
C3-C4	1.433(5)
C4-C5	1.431(5)
C5-C6	1.455(4)
C1'-C5'	1.424(4)
C1'-C2'	1.441(4)
C1'-C8	1.497(4)
C2'-C3'	1.430(4)
C2'-C9	1.494(4)
C3'-C4'	1.434(4)
C3'-C10	1.498(4)
C4'-C5'	1.438(4)
C4'-C11	1.499(4)
C5'-C12	1.492(4)
C3'-Ru1-C5	127.08(11)
C3'-Ru1-C4'	38.70(11)
C5-Ru1-C4'	160.75(11)
C3'-Ru1-C1	164.29(11)
C5-Ru1-C1	38.63(11)

C4'-Ru1-C1	156.97(11)
C3'-Ru1-C2'	38.46(11)
C5-Ru1-C2'	113.02(11)
C4'-Ru1-C2'	64.52(10)
C1-Ru1-C2'	131.83(10)
C3'-Ru1-C5'	64.46(10)
C5-Ru1-C5'	159.74(12)
C4'-Ru1-C5'	38.59(11)
C1-Ru1-C5'	126.79(11)
C2'-Ru1-C5'	64.10(11)
C3'-Ru1-C1'	64.50(11)
C5-Ru1-C1'	126.78(11)
C4'-Ru1-C1'	64.41(11)
C1-Ru1-C1'	116.23(11)
C2'-Ru1-C1'	38.52(11)
C5'-Ru1-C1'	38.01(11)
C3'-Ru1-C4	108.34(12)
C5-Ru1-C4	38.36(12)
C4'-Ru1-C4	124.91(12)
C1-Ru1-C4	64.42(12)
C2'-Ru1-C4	122.10(12)
C5'-Ru1-C4	161.25(12)
C1'-Ru1-C4	156.99(11)
C3'-Ru1-C3	120.52(11)
C5-Ru1-C3	63.50(12)
C4'-Ru1-C3	109.56(11)
C1-Ru1-C3	63.34(11)
C2'-Ru1-C3	153.81(12)
C5'-Ru1-C3	128.55(11)
C1'-Ru1-C3	164.74(12)
C4-Ru1-C3	38.14(12)
C3'-Ru1-C2	153.53(11)
C5-Ru1-C2	64.38(12)
C4'-Ru1-C2	122.37(10)
C1-Ru1-C2	38.24(11)

Table 2.11 continued

C2'-Ru1-C2	167.25(11)
C5'-Ru1-C2	113.59(11)
C1'-Ru1-C2	131.79(11)
C4-Ru1-C2	64.45(12)
C3-Ru1-C2	37.88(12)
C6-S1-C7	93.96(14)
C2-C1-C5	108.5(3)
C2-C1-C7	136.5(3)
C5-C1-C7	114.9(3)
C2-C1-Ru1	71.92(17)
C5-C1-Ru1	70.52(16)
C7-C1-Ru1	119.5(2)
C3-C2-C1	106.7(3)
C3-C2-Ru1	70.98(17)
C1-C2-Ru1	69.84(16)
C2-C3-C4	109.8(3)
C2-C3-Ru1	71.14(16)
C4-C3-Ru1	70.60(17)
C5-C4-C3	106.6(3)
C5-C4-Ru1	70.02(17)
C3-C4-Ru1	71.25(18)
C4-C5-C1	108.4(3)
C4-C5-C6	136.1(3)
C1-C5-C6	115.3(3)
C4-C5-Ru1	71.62(17)
C1-C5-Ru1	70.85(16)
C6-C5-Ru1	118.8(2)
O1-C6-C5	129.8(3)
O1-C6-S1	122.3(2)
C5-C6-S1	107.9(2)
O2-C7-C1	130.1(3)
O2-C7-S1	122.0(2)

C1-C7-S1	107.9(2)
C5'-C1'-C2'	108.0(3)
C5'-C1'-C8	125.9(3)
C2'-C1'-C8	126.1(3)
C5'-C1'-Ru1	70.90(15)
C2'-C1'-Ru1	70.54(16)
C8-C1'-Ru1	125.78(19)
C3'-C2'-C1'	107.8(3)
C3'-C2'-C9	125.6(3)
C1'-C2'-C9	126.6(3)
C3'-C2'-Ru1	69.94(16)
C1'-C2'-Ru1	70.95(16)
C9-C2'-Ru1	125.5(2)
C2'-C3'-C4'	108.3(2)
C2'-C3'-C10	126.3(3)
C4'-C3'-C10	125.3(3)
C2'-C3'-Ru1	71.60(15)
C4'-C3'-Ru1	70.97(16)
C10-C3'-Ru1	125.1(2)
C3'-C4'-C5'	107.5(2)
C3'-C4'-C11	125.6(3)
C5'-C4'-C11	126.8(3)
C3'-C4'-Ru1	70.34(15)
C5'-C4'-Ru1	71.33(16)
C11-C4'-Ru1	125.05(19)
C1'-C5'-C4'	108.4(3)
C1'-C5'-C12	125.5(3)
C4'-C5'-C12	125.9(3)
C1'-C5'-Ru1	71.09(15)
C4'-C5'-Ru1	70.09(16)
C12-C5'-Ru1	128.43(19)

Table 2.12. Bond lengths [Å] and angles [°] for **15a**

Ru1-C1	2.163(3)
Ru1-C9	2.168(3)
Ru1-C5	2.169(3)
Ru1-C8	2.170(3)
Ru1-C12	2.173(3)
Ru1-C11	2.179(3)
Ru1-C4	2.183(3)
Ru1-C10	2.185(3)
Ru1-C2	2.197(3)
Ru1-C3	2.211(3)
N1-C6	1.348(4)
N1-C24	1.460(4)
N1-C18	1.487(4)
N2-C24	1.328(4)
N2-C25	1.462(4)
O1-C7	1.220(4)
O2-C7	1.315(4)
O3-C6	1.254(4)
O4-C24	1.212(4)
C1-C2	1.428(4)
C1-C5	1.469(4)
C1-C7	1.482(4)
C2-C3	1.411(4)
C3-C4	1.418(4)
C4-C5	1.434(4)
C5-C6	1.481(4)
C8-C12	1.431(4)
C8-C9	1.439(4)
C8-C13	1.490(4)
C9-C10	1.443(4)
C9-C14	1.492(4)
C10-C11	1.442(4)
C10-C15	1.485(4)
C11-C12	1.435(4)
C11-C16	1.489(4)
C12-C17	1.495(4)
C18-C23	1.522(4)

C18-C19	1.526(4)
C19-C20	1.526(4)
C20-C21	1.513(5)
C21-C22	1.516(5)
C22-C23	1.533(4)
C25-C30	1.522(4)
C25-C26	1.526(4)
C26-C27	1.531(4)
C27-C28	1.513(5)
C28-C29	1.522(5)
C29-C30	1.520(5)
C1-Ru1-C9	134.69(11)
C1-Ru1-C5	39.65(11)
C9-Ru1-C5	174.20(11)
C1-Ru1-C8	171.32(11)
C9-Ru1-C8	38.74(11)
C5-Ru1-C8	147.05(11)
C1-Ru1-C12	149.69(11)
C9-Ru1-C12	64.79(11)
C5-Ru1-C12	119.57(11)
C8-Ru1-C12	38.48(10)
C1-Ru1-C11	120.34(11)
C9-Ru1-C11	64.54(10)
C5-Ru1-C11	116.02(11)
C8-Ru1-C11	64.35(10)
C12-Ru1-C11	38.51(11)
C1-Ru1-C4	64.81(11)
C9-Ru1-C4	144.94(11)
C5-Ru1-C4	38.49(11)
C8-Ru1-C4	117.30(11)
C12-Ru1-C4	114.45(11)
C11-Ru1-C4	138.53(11)
C1-Ru1-C10	113.66(11)
C9-Ru1-C10	38.71(11)
C5-Ru1-C10	138.07(11)
C8-Ru1-C10	64.79(10)

Table 2.12 continued

C12-Ru1-C10	64.86(11)
C11-Ru1-C10	38.58(11)
C4-Ru1-C10	176.12(11)
C1-Ru1-C2	38.23(11)
C9-Ru1-C2	111.95(11)
C5-Ru1-C2	64.33(11)
C8-Ru1-C2	133.98(11)
C12-Ru1-C2	171.31(11)
C11-Ru1-C2	148.74(12)
C4-Ru1-C2	63.07(11)
C10-Ru1-C2	118.22(11)
C1-Ru1-C3	64.00(11)
C9-Ru1-C3	116.11(11)
C5-Ru1-C3	64.02(11)
C8-Ru1-C3	111.99(11)
C12-Ru1-C3	135.58(11)
C11-Ru1-C3	173.87(11)
C4-Ru1-C3	37.64(11)
C10-Ru1-C3	145.56(11)
C2-Ru1-C3	37.34(12)
C6-N1-C24	124.4(2)
C6-N1-C18	118.6(2)
C24-N1-C18	117.0(2)
C24-N2-C25	123.5(2)
C2-C1-C5	106.7(3)
C2-C1-C7	120.1(3)
C5-C1-C7	132.9(3)
C2-C1-Ru1	72.16(16)
C5-C1-Ru1	70.40(15)
C7-C1-Ru1	117.9(2)
C3-C2-C1	109.5(3)
C3-C2-Ru1	71.91(16)
C1-C2-Ru1	69.61(15)
C2-C3-C4	108.1(3)
C2-C3-Ru1	70.76(16)
C4-C3-Ru1	70.09(16)
C3-C4-C5	109.0(3)

C3-C4-Ru1	72.27(16)
C5-C4-Ru1	70.23(15)
C4-C5-C1	106.7(2)
C4-C5-C6	127.6(3)
C1-C5-C6	125.7(3)
C4-C5-Ru1	71.28(15)
C1-C5-Ru1	69.95(15)
C6-C5-Ru1	123.1(2)
O3-C6-N1	119.3(3)
O3-C6-C5	120.8(3)
N1-C6-C5	119.8(3)
O1-C7-O2	120.7(3)
O1-C7-C1	119.9(3)
O2-C7-C1	119.4(3)
C12-C8-C9	108.3(2)
C12-C8-C13	126.5(3)
C9-C8-C13	125.2(3)
C12-C8-Ru1	70.87(15)
C9-C8-Ru1	70.56(15)
C13-C8-Ru1	126.1(2)
C8-C9-C10	108.2(2)
C8-C9-C14	125.3(3)
C10-C9-C14	126.5(3)
C8-C9-Ru1	70.70(15)
C10-C9-Ru1	71.29(16)
C14-C9-Ru1	124.9(2)
C11-C10-C9	107.1(2)
C11-C10-C15	125.9(3)
C9-C10-C15	127.0(3)
C11-C10-Ru1	70.48(16)
C9-C10-Ru1	70.01(15)
C15-C10-Ru1	124.8(2)
C12-C11-C10	108.6(2)
C12-C11-C16	126.2(3)
C10-C11-C16	125.1(3)
C12-C11-Ru1	70.52(15)

Table 2.12 continued

C10-C11-Ru1	70.94(15)
C16-C11-Ru1	126.7(2)
C8-C12-C11	107.8(2)
C8-C12-C17	126.0(3)
C11-C12-C17	126.2(3)
C8-C12-Ru1	70.65(15)
C11-C12-Ru1	70.97(15)
C17-C12-Ru1	125.6(2)
N1-C18-C23	112.0(2)
N1-C18-C19	110.9(2)
C23-C18-C19	111.1(3)
C18-C19-C20	110.3(3)
C21-C20-C19	111.6(3)
C20-C21-C22	111.5(3)

C21-C22-C23	112.1(3)
C18-C23-C22	110.3(3)
O4-C24-N2	127.6(3)
O4-C24-N1	120.3(3)
N2-C24-N1	112.1(2)
N2-C25-C30	109.6(2)
N2-C25-C26	111.8(2)
C30-C25-C26	110.7(3)
C25-C26-C27	110.4(3)
C28-C27-C26	111.8(3)
C27-C28-C29	111.4(3)
C30-C29-C28	111.5(3)
C29-C30-C25	111.4(3)

Table 2.13. Bond lengths [Å] and Angles [°] for **3b**

Mn1A-C8A	1.804(2)
Mn1A-C9A	1.809(2)
Mn1A-C10A	1.811(2)
Mn1A-C1A	2.1200(18)
Mn1A-C2A	2.1281(18)
Mn1A-C3A	2.1490(19)
Mn1A-C5A	2.1514(18)
Mn1A-C4A	2.1715(19)
C1A-C5A	1.422(2)
C1A-C2A	1.456(2)
C1A-C6A	1.471(2)
O1A-C6A	1.230(2)
O2A-C6A	1.310(2)
C2A-C3A	1.417(2)
C2A-C7A	1.485(2)
C3A-C4A	1.412(2)
O3A-C7A	1.224(2)
O4A-C7A	1.312(2)
C4A-C5A	1.412(2)
O5A-C8A	1.143(3)
O6A-C9A	1.144(3)
O7A-C10A	1.138(3)
Mn1B-C10B	1.808(2)
Mn1B-C8B	1.8083(19)
Mn1B-C9B	1.817(2)
Mn1B-C2B	2.1178(17)
Mn1B-C1B	2.1354(17)
Mn1B-C3B	2.1387(18)
Mn1B-C5B	2.1488(17)
Mn1B-C4B	2.1678(18)
O1B-C6B	1.222(2)
C1B-C5B	1.428(2)
C1B-C2B	1.450(2)
C1B-C6B	1.485(2)
O2B-C6B	1.314(2)
C2B-C3B	1.418(2)

C2B-C7B	1.481(2)
O3B-C7B	1.225(2)
C3B-C4B	1.421(2)
O4B-C7B	1.316(2)
C4B-C5B	1.409(2)
O5B-C8B	1.144(2)
O6B-C9B	1.144(2)
O7B-C10B	1.146(3)
C8A-Mn1A-C9A	91.08(11)
C8A-Mn1A-C10A	91.62(10)
C9A-Mn1A-C10A	91.60(11)
C8A-Mn1A-C1A	156.31(9)
C9A-Mn1A-C1A	109.84(9)
C10A-Mn1A-C1A	98.55(8)
C8A-Mn1A-C2A	118.01(9)
C9A-Mn1A-C2A	149.86(9)
C10A-Mn1A-C2A	95.04(8)
C1A-Mn1A-C2A	40.09(6)
C8A-Mn1A-C3A	91.31(8)
C9A-Mn1A-C3A	142.42(9)
C10A-Mn1A-C3A	125.81(9)
C1A-Mn1A-C3A	65.40(7)
C2A-Mn1A-C3A	38.70(7)
C8A-Mn1A-C5A	135.45(9)
C9A-Mn1A-C5A	88.60(9)
C10A-Mn1A-C5A	132.93(8)
C1A-Mn1A-C5A	38.89(7)
C2A-Mn1A-C5A	65.58(7)
C3A-Mn1A-C5A	64.25(7)
C8A-Mn1A-C4A	99.88(8)
C9A-Mn1A-C4A	104.69(9)
C10A-Mn1A-C4A	159.75(8)
C1A-Mn1A-C4A	64.88(7)
C2A-Mn1A-C4A	64.86(7)
C3A-Mn1A-C4A	38.13(7)

Table 2.13 continued

C5A-Mn1A-C4A	38.14(7)
C5A-C1A-C2A	107.25(15)
C5A-C1A-C6A	123.98(16)
C2A-C1A-C6A	128.74(15)
C5A-C1A-Mn1A	71.74(10)
C2A-C1A-Mn1A	70.25(10)
C6A-C1A-Mn1A	122.00(13)
C3A-C2A-C1A	106.76(15)
C3A-C2A-C7A	122.57(16)
C1A-C2A-C7A	130.62(16)
C3A-C2A-Mn1A	71.45(10)
C1A-C2A-Mn1A	69.66(10)
C7A-C2A-Mn1A	125.78(13)
C4A-C3A-C2A	109.21(16)
C4A-C3A-Mn1A	71.80(11)
C2A-C3A-Mn1A	69.85(11)
C3A-C4A-C5A	108.14(16)
C3A-C4A-Mn1A	70.07(10)
C5A-C4A-Mn1A	70.16(10)
C4A-C5A-C1A	108.63(16)
C4A-C5A-Mn1A	71.70(10)
C1A-C5A-Mn1A	69.36(10)
O1A-C6A-O2A	122.81(17)
O1A-C6A-C1A	123.70(16)
O2A-C6A-C1A	113.49(15)
O3A-C7A-O4A	119.75(16)
O3A-C7A-C2A	121.39(16)
O4A-C7A-C2A	118.84(16)
O5A-C8A-Mn1A	179.2(2)
O6A-C9A-Mn1A	178.4(2)
O7A-C10A-Mn1A	179.5(2)
C10B-Mn1B-C8B	94.05(9)
C10B-Mn1B-C9B	92.37(9)
C8B-Mn1B-C9B	91.07(9)
C10B-Mn1B-C2B	90.90(8)
C8B-Mn1B-C2B	122.51(8)
C9B-Mn1B-C2B	145.93(8)

C10B-Mn1B-C1B	103.53(8)
C8B-Mn1B-C1B	154.15(7)
C9B-Mn1B-C1B	106.76(8)
C2B-Mn1B-C1B	39.88(6)
C10B-Mn1B-C3B	115.71(8)
C8B-Mn1B-C3B	89.65(8)
C9B-Mn1B-C3B	151.79(8)
C2B-Mn1B-C3B	38.91(6)
C1B-Mn1B-C3B	65.76(7)
C10B-Mn1B-C5B	141.37(8)
C8B-Mn1B-C5B	124.19(8)
C9B-Mn1B-C5B	92.21(8)
C2B-Mn1B-C5B	65.35(7)
C1B-Mn1B-C5B	38.93(6)
C3B-Mn1B-C5B	64.54(7)
C10B-Mn1B-C4B	153.79(8)
C8B-Mn1B-C4B	90.95(8)
C9B-Mn1B-C4B	113.27(8)
C2B-Mn1B-C4B	64.98(7)
C1B-Mn1B-C4B	65.06(7)
C3B-Mn1B-C4B	38.52(7)
C5B-Mn1B-C4B	38.10(6)
C5B-C1B-C2B	106.31(14)
C5B-C1B-C6B	121.83(15)
C2B-C1B-C6B	131.64(15)
C5B-C1B-Mn1B	71.04(10)
C2B-C1B-Mn1B	69.41(9)
C6B-C1B-Mn1B	128.35(12)
C3B-C2B-C1B	107.97(15)
C3B-C2B-C7B	123.93(15)
C1B-C2B-C7B	128.07(15)
C3B-C2B-Mn1B	71.34(10)
C1B-C2B-Mn1B	70.71(10)
C7B-C2B-Mn1B	122.02(12)
C2B-C3B-C4B	108.40(15)
C2B-C3B-Mn1B	69.75(10)

Table 2.13 continued

C4B-C3B-Mn1B	71.85(10)
C5B-C4B-C3B	107.98(15)
C5B-C4B-Mn1B	70.22(10)
C3B-C4B-Mn1B	69.63(10)
C4B-C5B-C1B	109.33(15)
C4B-C5B-Mn1B	71.68(10)
C1B-C5B-Mn1B	70.03(10)
O1B-C6B-O2B	119.16(16)

O1B-C6B-C1B	121.74(16)
O2B-C6B-C1B	119.02(15)
O3B-C7B-O4B	123.21(16)
O3B-C7B-C2B	123.61(15)
O4B-C7B-C2B	113.18(15)
O5B-C8B-Mn1B	176.55(17)
O6B-C9B-Mn1B	179.54(19)
O7B-C10B-Mn1B	176.30(17)

Table 2.14. Bond lengths [Å] and Angles [°] for **11b**

Mn1-C15	1.797(3)
Mn1-C16	1.799(4)
Mn1-C17	1.799(4)
Mn1-C5	2.113(3)
Mn1-C1	2.126(3)
Mn1-C3	2.146(3)
Mn1-C2	2.146(3)
Mn1-C4	2.153(3)
N1-C6	1.412(4)
N1-C7	1.419(3)
N1-C8	1.437(3)
O1-C6	1.202(3)
O2-C7	1.210(3)
C1-C2	1.415(4)
C1-C5	1.420(4)
C1-C7	1.476(4)
C2-C3	1.402(4)
C3-C4	1.434(4)
C4-C5	1.399(4)
C5-C6	1.491(4)
C8-C13	1.381(4)
C8-C9	1.388(4)
C9-C10	1.383(4)
C10-C11	1.389(4)
C11-C12	1.388(4)
C11-C14	1.509(4)
C12-C13	1.393(4)
C15-O3	1.146(3)
C16-O4	1.154(4)
C17-O5	1.150(4)
C15-Mn1-C16	92.78(14)
C15-Mn1-C17	91.48(16)
C16-Mn1-C17	91.56(15)
C15-Mn1-C5	93.12(13)
C16-Mn1-C5	120.76(14)
C17-Mn1-C5	147.03(13)
C15-Mn1-C1	100.51(12)

C16-Mn1-C1	155.88(14)
C17-Mn1-C1	107.96(13)
C5-Mn1-C1	39.15(10)
C15-Mn1-C3	157.20(13)
C16-Mn1-C3	96.48(13)
C17-Mn1-C3	108.98(13)
C5-Mn1-C3	64.27(11)
C1-Mn1-C3	64.28(11)
C15-Mn1-C2	136.23(12)
C16-Mn1-C2	130.93(12)
C17-Mn1-C2	89.70(13)
C5-Mn1-C2	64.96(11)
C1-Mn1-C2	38.69(10)
C3-Mn1-C2	38.14(10)
C15-Mn1-C4	120.38(13)
C16-Mn1-C4	90.84(14)
C17-Mn1-C4	147.88(13)
C5-Mn1-C4	38.27(10)
C1-Mn1-C4	65.08(11)
C3-Mn1-C4	38.97(11)
C2-Mn1-C4	65.10(11)
C6-N1-C7	113.5(2)
C6-N1-C8	122.9(2)
C7-N1-C8	123.1(2)
C2-C1-C5	107.5(2)
C2-C1-C7	143.4(3)
C5-C1-C7	109.1(2)
C2-C1-Mn1	71.41(16)
C5-C1-Mn1	69.91(16)
C7-C1-Mn1	122.69(19)
C3-C2-C1	107.5(2)
C3-C2-Mn1	70.92(16)
C1-C2-Mn1	69.90(15)
C2-C3-C4	109.3(2)
C2-C3-Mn1	70.93(16)
C4-C3-Mn1	70.80(16)

Table 2.14 continued

C5-C4-C3	106.2(2)
C5-C4-Mn1	69.29(16)
C3-C4-Mn1	70.23(16)
C4-C5-C1	109.5(2)
C4-C5-C6	142.3(3)
C1-C5-C6	108.1(2)
C4-C5-Mn1	72.44(16)
C1-C5-Mn1	70.94(15)
C6-C5-Mn1	123.1(2)
O1-C6-N1	124.8(3)
O1-C6-C5	130.5(3)
N1-C6-C5	104.7(2)
O2-C7-N1	124.3(3)
O2-C7-C1	131.1(3)

N1-C7-C1	104.6(2)
C13-C8-C9	120.5(3)
C13-C8-N1	118.5(3)
C9-C8-N1	121.0(3)
C10-C9-C8	119.1(3)
C9-C10-C11	121.9(3)
C12-C11-C10	117.8(3)
C12-C11-C14	120.2(3)
C10-C11-C14	121.9(3)
C11-C12-C13	121.4(3)
C8-C13-C12	119.3(3)
O3-C15-Mn1	177.5(3)
O4-C16-Mn1	177.8(3)
O5-C17-Mn1	179.1(3)

Table 2.15. Bond lengths [Å] and Angles [°] for **12b**

Mn1-C9	1.8085(16)
Mn1-C10	1.8107(16)
Mn1-C8	1.8117(15)
Mn1-C2	2.1119(13)
Mn1-C1	2.1220(13)
Mn1-C3	2.1445(14)
Mn1-C5	2.1508(14)
Mn1-C4	2.1717(15)
C1-C5	1.425(2)
C1-C2	1.4551(19)
C1-C6	1.471(2)
C2-C3	1.419(2)
C2-C7	1.475(2)
C3-C4	1.412(2)
C4-C5	1.412(2)
C6-O1	1.1808(19)
C6-Cl1	1.7864(14)
C7-O2	1.1879(18)
C7-Cl2	1.7790(15)
C8-O3	1.1431(18)
C9-O4	1.1453(19)
C10-O5	1.1414(19)
C9-Mn1-C10	90.64(7)
C9-Mn1-C8	92.94(7)
C10-Mn1-C8	92.87(7)
C9-Mn1-C2	117.72(6)
C10-Mn1-C2	150.53(6)
C8-Mn1-C2	93.43(6)
C9-Mn1-C1	156.46(6)
C10-Mn1-C1	110.45(6)
C8-Mn1-C1	96.19(6)
C2-Mn1-C1	40.20(5)
C9-Mn1-C3	91.21(6)
C10-Mn1-C3	141.81(6)
C8-Mn1-C3	125.11(6)
C2-Mn1-C3	38.95(5)
C1-Mn1-C3	65.83(5)
C9-Mn1-C5	136.27(7)
C10-Mn1-C5	88.76(6)
C8-Mn1-C5	130.76(6)

C2-Mn1-C5	65.61(5)
C1-Mn1-C5	38.96(5)
C3-Mn1-C5	64.45(6)
C9-Mn1-C4	100.57(7)
C10-Mn1-C4	104.22(6)
C8-Mn1-C4	157.95(6)
C2-Mn1-C4	64.88(6)
C1-Mn1-C4	65.01(6)
C3-Mn1-C4	38.17(6)
C5-Mn1-C4	38.13(6)
C5-C1-C2	106.62(12)
C5-C1-C6	126.62(13)
C2-C1-C6	126.52(12)
C5-C1-Mn1	71.61(8)
C2-C1-Mn1	69.52(7)
C6-C1-Mn1	119.54(9)
C3-C2-C1	107.53(12)
C3-C2-C7	124.58(13)
C1-C2-C7	127.43(12)
C3-C2-Mn1	71.77(8)
C1-C2-Mn1	70.27(7)
C7-C2-Mn1	129.37(10)
C4-C3-C2	108.57(13)
C4-C3-Mn1	71.96(8)
C2-C3-Mn1	69.29(8)
C3-C4-C5	108.42(13)
C3-C4-Mn1	69.87(8)
C5-C4-Mn1	70.13(8)
C4-C5-C1	108.86(13)
C4-C5-Mn1	71.74(8)
C1-C5-Mn1	69.43(8)
O1-C6-C1	127.83(13)
O1-C6-Cl1	119.65(11)
C1-C6-Cl1	112.51(10)
O2-C7-C2	126.32(13)
O2-C7-Cl2	120.22(11)
C2-C7-Cl2	113.40(10)
O3-C8-Mn1	176.57(13)
O4-C9-Mn1	178.65(16)
O5-C10-Mn1	178.35(14)

Table 2.16. Bond lengths [Å] andbond angles [°] for **13**

Mn1A-C10A	1.805(3)
Mn1A-C9A	1.807(3)
Mn1A-C8A	1.811(3)
Mn1A-C5A	2.116(2)
Mn1A-C1A	2.124(2)
Mn1A-C2A	2.154(2)
Mn1A-C4A	2.155(3)
Mn1A-C3A	2.159(2)
S1A-C6A	1.815(3)
S1A-C7A	1.824(2)
O1A-C6A	1.197(3)
C1A-C5A	1.413(3)
C1A-C2A	1.419(3)
C1A-C7A	1.469(3)
O2A-C7A	1.199(3)
C2A-C3A	1.413(3)
O3A-C8A	1.138(3)
C3A-C4A	1.434(4)
O4A-C9A	1.137(3)
C4A-C5A	1.413(3)
C5A-C6A	1.472(3)
O5A-C10A	1.142(3)
Mn1B-C8B	1.811(3)
Mn1B-C9B	1.811(3)
Mn1B-C10B	1.817(3)
Mn1B-C5B	2.123(2)
Mn1B-C1B	2.127(2)
Mn1B-C4B	2.154(2)
Mn1B-C2B	2.155(2)
Mn1B-C3B	2.159(2)
S1B-C6B	1.816(2)
S1B-C7B	1.826(2)
O1B-C6B	1.200(3)
C1B-C2B	1.418(3)
C1B-C5B	1.425(3)
C1B-C7B	1.472(3)
O2B-C7B	1.196(3)

C2B-C3B	1.423(3)
O3B-C8B	1.140(3)
C3B-C4B	1.420(4)
O4B-C9B	1.143(3)
C4B-C5B	1.419(3)
O5B-C10B	1.138(3)
C5B-C6B	1.466(3)
C10A-Mn1A-C9A	90.98(12)
C10A-Mn1A-C8A	92.20(12)
C9A-Mn1A-C8A	91.01(12)
C10A-Mn1A-C5A	145.84(11)
C9A-Mn1A-C5A	122.59(11)
C8A-Mn1A-C5A	93.22(10)
C10A-Mn1A-C1A	107.01(11)
C9A-Mn1A-C1A	157.30(11)
C8A-Mn1A-C1A	101.74(10)
C5A-Mn1A-C1A	38.94(9)
C10A-Mn1A-C2A	88.79(11)
C9A-Mn1A-C2A	131.29(11)
C8A-Mn1A-C2A	137.68(10)
C5A-Mn1A-C2A	65.10(9)
C1A-Mn1A-C2A	38.74(9)
C10A-Mn1A-C4A	147.63(11)
C9A-Mn1A-C4A	92.27(11)
C8A-Mn1A-C4A	119.92(11)
C5A-Mn1A-C4A	38.64(9)
C1A-Mn1A-C4A	65.11(9)
C2A-Mn1A-C4A	65.29(10)
C10A-Mn1A-C3A	108.85(11)
C9A-Mn1A-C3A	97.38(11)
C8A-Mn1A-C3A	157.09(10)
C5A-Mn1A-C3A	64.31(9)
C1A-Mn1A-C3A	64.14(9)
C2A-Mn1A-C3A	38.24(9)
C4A-Mn1A-C3A	38.82(9)
C6A-S1A-C7A	94.13(11)

Table 2.16 continued

C5A-C1A-C2A	108.4(2)
C5A-C1A-C7A	114.9(2)
C2A-C1A-C7A	136.6(2)
C5A-C1A-Mn1A	70.22(13)
C2A-C1A-Mn1A	71.77(13)
C7A-C1A-Mn1A	123.96(16)
C3A-C2A-C1A	106.9(2)
C3A-C2A-Mn1A	71.08(13)
C1A-C2A-Mn1A	69.49(13)
C2A-C3A-C4A	109.5(2)
C2A-C3A-Mn1A	70.68(13)
C4A-C3A-Mn1A	70.43(13)
C5A-C4A-C3A	106.1(2)
C5A-C4A-Mn1A	69.19(13)
C3A-C4A-Mn1A	70.75(13)
C1A-C5A-C4A	109.1(2)
C1A-C5A-C6A	115.4(2)
C4A-C5A-C6A	135.5(2)
C1A-C5A-Mn1A	70.84(13)
C4A-C5A-Mn1A	72.18(13)
C6A-C5A-Mn1A	124.29(16)
O1A-C6A-C5A	129.4(2)
O1A-C6A-S1A	122.86(19)
C5A-C6A-S1A	107.72(17)
O2A-C7A-C1A	129.5(2)
O2A-C7A-S1A	122.66(19)
C1A-C7A-S1A	107.81(17)
O3A-C8A-Mn1A	177.8(2)
O4A-C9A-Mn1A	178.8(2)
O5A-C10A-Mn1A	178.4(3)
C8B-Mn1B-C9B	92.11(11)
C8B-Mn1B-C10B	89.81(11)
C9B-Mn1B-C10B	90.20(11)
C8B-Mn1B-C5B	97.23(10)
C9B-Mn1B-C5B	116.26(10)
C10B-Mn1B-C5B	152.17(10)
C8B-Mn1B-C1B	99.40(10)

C9B-Mn1B-C1B	153.77(10)
C10B-Mn1B-C1B	113.16(10)
C5B-Mn1B-C1B	39.17(9)
C8B-Mn1B-C4B	127.85(10)
C9B-Mn1B-C4B	89.15(10)
C10B-Mn1B-C4B	142.34(10)
C5B-Mn1B-C4B	38.75(9)
C1B-Mn1B-C4B	65.18(9)
C8B-Mn1B-C2B	132.20(10)
C9B-Mn1B-C2B	135.69(10)
C10B-Mn1B-C2B	90.22(10)
C5B-Mn1B-C2B	65.20(9)
C1B-Mn1B-C2B	38.67(9)
C4B-Mn1B-C2B	65.09(9)
C8B-Mn1B-C3B	161.29(10)
C9B-Mn1B-C3B	99.27(10)
C10B-Mn1B-C3B	104.86(10)
C5B-Mn1B-C3B	64.42(9)
C1B-Mn1B-C3B	64.38(9)
C4B-Mn1B-C3B	38.44(9)
C2B-Mn1B-C3B	38.51(9)
C6B-S1B-C7B	94.22(11)
C2B-C1B-C5B	108.4(2)
C2B-C1B-C7B	136.7(2)
C5B-C1B-C7B	114.8(2)
C2B-C1B-Mn1B	71.76(13)
C5B-C1B-Mn1B	70.28(13)
C7B-C1B-Mn1B	125.82(16)
C1B-C2B-C3B	107.0(2)
C1B-C2B-Mn1B	69.57(12)
C3B-C2B-Mn1B	70.89(13)
C4B-C3B-C2B	109.3(2)
C4B-C3B-Mn1B	70.58(13)
C2B-C3B-Mn1B	70.60(13)
C5B-C4B-C3B	107.0(2)
C5B-C4B-Mn1B	69.45(13)

Table 2.16 continued

C3B-C4B-Mn1B	70.98(14)		O1B-C6B-S1B	123.01(19)
C4B-C5B-C1B	108.3(2)		C5B-C6B-S1B	107.91(16)
C4B-C5B-C6B	136.4(2)		O2B-C7B-C1B	129.5(2)
C1B-C5B-C6B	115.3(2)		O2B-C7B-S1B	122.82(18)
C4B-C5B-Mn1B	71.79(13)		C1B-C7B-S1B	107.60(17)
C1B-C5B-Mn1B	70.55(13)		O3B-C8B-Mn1B	178.8(2)
C6B-C5B-Mn1B	123.56(15)		O4B-C9B-Mn1B	177.2(2)
O1B-C6B-C5B	129.1(2)		O5B-C10B-Mn1B	178.6(2)

2.3. Summary

Out of different attempts of synthesizing 1,2-dicarboxylic acid complexes of pentamethylruthenocene and cymantrene, the 1,2-dicarbophenoxycyclopentadienide sodium **1** was proved to be an ideal entry. This is due to better selectivity of carbophenoxy groups at 1,2-positions of cyclopentadienyl anion than carboalkoxy groups. The sodium salt **1** was isolable and gave excellent results for transmetallation with $[Ru(\mu_3\text{-}Cl)(Cp^*)]_4$[83] and $[MnBr(CO)_5]$[82] to give 1,2-dicarbophenoxycyclopentadienylpentamethylruthenocene (**2a**, 78%) and 1,2-dicarbophenoxycymantrene (**2b**, 87%). This method bypasses the use of toxic thallium reagents generally used for the complexation and also reduces the number of synthetic steps.

Pentamethylruthenocene-1,2-dicarboxylic acid **3a** (95%) and cymantrene-1,2-dicarboxylic acid **3b** (88%) were synthesized by saponification of **2a** and **2b** under basic conditions. Both dicarboxylic acids exhibit a network of inter- and

intra-molecular H-bonding with co-planarity of COOH group with Cp in their molecular structures. The carboxylic acid are used to synthesize cyclopentadienyl-fused 1,2-dicarboxylic anhydride of ruthenium **10a** (84%) and manganese **10b** (46%). The complex **10a** is be crystalline capable to withstand aqueous work-up while the **10b** was low-melting solid showing sensitivity towards bench-top conditions. The molecular structure of **10a** showed co-planarity on 5,5-fused ligand.

Both anhydride complexes were used to convert *p*-tolylimide *via* two-step reactions. The first step involves the nucleophilic ring opening with amine and then conversion of carboxylic acid to acyl chloride for the ring closure. The intermediate acid-amides were used for ring closure without their isolation to give ruthenocene (**11a**, 23%) and cymantrene (**11b**, 42%) complexes.

Similarly, dicarboxylic acid complexes were converted to diacyl chlorides with oxalyl chloride/DMF to give **12a** (88%) and **12b** (50%) and molecular structure of **12b** was analyzed with an X-ray crystallography. The diacyl chlorides were used to prepare thioanhydride (**13a**, 75% and **13b**, 66%) in the presence of hexamethyldisilathiane by following literature procedure.[98] The molecular structures of both complexes showed the co-planarity of thioanhydride moiety with Cp ring.

In general, we established a facile method of synthesizing cyclopentadienyl-fused carboxylic anhydride, thioanhydride and *p*-tolylimide of both electron-rich pentamethylcyclopentadienylruthenium and electron-deficient

manganesetricarbonyl starting from readily available starting materials. The general stability of the ruthenium complexes was found to be higher than analogous manganese complexes.

Chapter 3: Synthesis and Characterization of 1,2-Diacylcyclopentadienyl p-Cymene Complexes of Ruthenium(II)

3.1. Introduction

Cationic sandwich complexes of ruthenium play an important role in modern organometallic chemistry. The temporary complexation of $[Ru(\eta^5\text{-}C_5H_5)]^+$ unit to an arene has been widely used in synthetic organic chemistry for the activation of arenes towards nucleophilic substitution.[104-110] The $[Ru(Cp)(\eta^6\text{-arene})]^+$ complexes have been designed for the desulfurization of petroleum feedstock due to higher affinity of heterocyclic aromatics towards ruthenium than carbocyclic aromatics.[109,111]

Scheme 3.1. Synthesis of 1,2-diacylmetallocene complexes

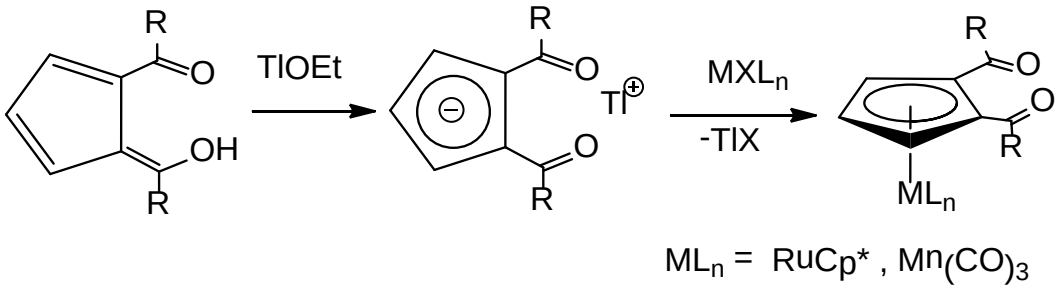

As cationic cyclopentadienylmetal complexes are deactivated towards Friedel-Crafts acylation, monoacyl and diacyl cyclopentadiene precursors are used to design mono- or diacylcyclopentadienylmetal complexes. By following a similar strategy, cationic acylcyclopentadienyl arene complexes of ruthenium have been synthesized *via* an intermediacy of thallium reagent.[112-115] Similarly, our group has synthesized 1,2-diacyl neutral sandwich[59] complexes of ruthenium

and half-sandwich[62] complexes of manganese starting from 1,2-diacylcyclopentadiene[81] by the intermediacy of thallium reagent[116] (Scheme 3.1). We want to extend the same methodology to design 1,2-diacylcyclopentadienyl-p-cymene complexes of ruthenium(II), which are viable precursors of heterocycle-fused cationic sandwich complexes.

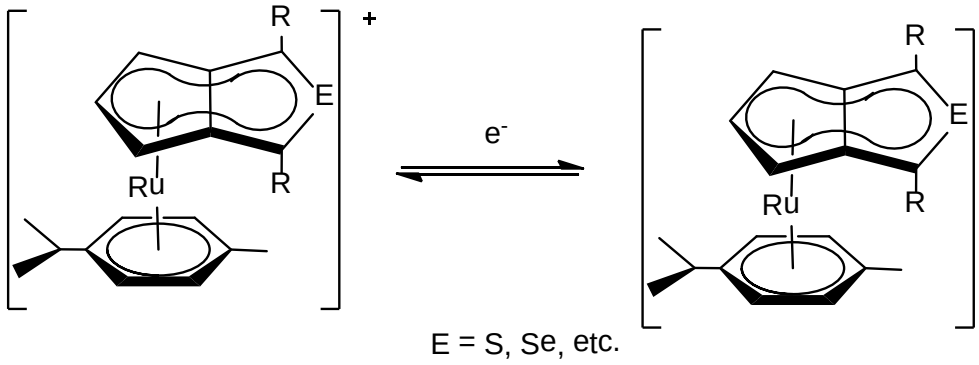

Figure 3.1. Targeted n-doped heterocycle-fused sandwich complexes of ruthenium(II).

The π-bound transition metal complexes of heterocycle-fused cyclopentadienyl ligand might be more stable than corresponding arene complexes due to better donation of negatively charged Cp than neutral arene ligand to the metal center. Given the stability of the complexes and feasibility of the functional group transformations; the current project entails the synthesis of cationic 1,2-diacylcyclopentadienyl ruthenium p-cymene complexes and their subsequent ring closure to thiophenes or selenophenes. As heterocycles-fused cationic complexes can accept electrons, the resultant cationic complexes of Cp-fused heterocycles can find their position in “n-doped” organic semiconducting applications (Figure 3.1). This might give some additional features upon “all organic” semiconducting materials due to the presence of metal center.

Herein, we report the synthesis and characterization of precursor cationic complexes *en route* to possible cationic complexes of ruthenium(II) bound to cyclopenta[*c*]thienyl ligand by employing the conditions reported by Snyder et al.[61] and Tice and Selegue.[62]

3.2. Experimental

Chapter 2 lists the general conditions for all experiments. TlOEt, *n*-BuLi, P_4S_{10} (Acros), Tl_2SO_4 and α-phellandrene (Aldrich) were used as received. $[Ru(\eta^6\text{-cymene})(\mu\text{-Cl})Cl]_2$[117] was prepared according to literature method. 1,2-$C_5H_3(CBu^tOH)(COBu^t)$ **1a**,[80] $Tl\{1,2\text{-}C_5H_3(CO\text{-}4\text{-}Tol)_2\}]$ **21b**,[62] $Tl\{1,2\text{-}C_5H_3(CO\text{-}4\text{-}Cl\text{-}C_6H_4)_2\}]$ **22b**[62] were prepared by modified method employed by Wallace and Snyder.[61] *p*-Iodobenzoyl chloride was prepared from *p*-iodobenzoic acid and oxalyl chloride. Elemental analyses were performed at the University of Illinois Microanalysis Laboratory.

Synthesis of 1,2-$C_5H_3(CBu^tOH)(COBu^t)$ (1a). To a 500-mL three-necked round- bottom flask, freshly cracked cyclopentadiene (25.2 g, 31.4 mL, 388 mmol) was slowly added to a stirred solution of *n*-BuLi (161 mL, 2.5 M in hexane, 400 mmol) in ethyl ether (150 mL). A white precipitate of cyclopentadienyllithium immediately formed. The white suspension was stirred at 0 °C for 15 min. Pivaloyl chloride (29.4 g, 30.0 mL, 243 mmol) was added dropwise and a bright yellow color formed immediately. The yellow suspension was allowed to warm to room temperature and stirred for 2 h. The reaction mixture was hydrolyzed with 3% hydrochloric acid (50 mL). The organic layer was collected and the aqueous

layer was exacted with ethyl ether (3 x 50 mL). The ether extracts were combined and dried over $MgSO_4$. The volatiles were removed *in vacuo* to give an orange semi-solid. The crude product was chromatographed on silica with hexane:ethyl ether (3:2) as eluent. The first fraction of column was crystallized from methanol to give **1a** (7.65 g, 29.4%) as a yellow orange crystals. All spectroscopic data were consistent with those reported previously.[80]

Synthesis of 1,2-C_5H_3(C-4-TolOH)(CO-4-Tol) (1b). In a 250-mL Schlenk flask, assembled with a magnetic stirrer, rubber septum and glass stopcock, sodium wire (2.80 g, 122 mmol) was collected under nitrogen and then freshly dried THF (100 mL) was added by syringe. Freshly cracked dicyclopentadiene (8.03 g, 10.2 mL, 122 mmol) was slowly added to the flask at 0 °C. The reaction mixture was allowed to warm to room temperature and stirred for 3.5 h, at which time the sodium wire was completely consumed. The mixture was again cooled to 0 °C and *p*-toluoyl chloride (10.8 mL, 154.6 mmol) was added dropwise. The reaction mixture was allowed to warm to room temperature and stirred for 2 h and hydrolyzed with 3% hydrochloric acid (60 mL). The organic layer was collected and the aqueous layer was exacted with ethyl ether (3 x 60 mL). The ether extracts were combined and dried over $MgSO_4$. The volatiles were removed *in vacuo* to give an orange semi-solid. The crude product was purified by trituration with cold methanol and filtered to give **1b** (6.83 g, 55.7%) as a yellow-orange solid. **Mp:** 139-140 °C (Lit.[61] 141-143 °C). All spectroscopic data were consistent with those reported previously.[61]

Synthesis of 1,2-C_5H_3(C-4-Cl-C_6H_4-OH)(CO-4-Cl-C_6H_4) (1c). In a 250-mL Schlenk flask assembled with a magnetic stirrer, rubber septum and glass stopcock, sodium wire (2.05 g, 89.1 mmol) was collected under nitrogen and then freshly dried THF (80 mL) was added by syringe. Freshly cracked dicyclopentadiene (5.88 g, 7.50 mL, 89.1 mmol) was slowly added to the flask. The reaction mixture was allowed to stir for 3 h at room temperature, at which time the sodium wire was completely consumed. The reaction mixture was cooled to 0 °C and 4-chlorobenzoyl chloride (7.6 mL, 59.4 mmol) was added dropwise. The reaction mixture was allowed to warm to room temperature and stirred for 2 h and then hydrolyzed with 3% hydrochloric acid (50 mL). The organic layer was collected and the aqueous layer was exacted with ethyl ether (3 x 50 mL). The ether extracts were combined and dried over $MgSO_4$. The volatiles were removed *in vacuo* to give a dark brown semi-solid. The crude product was dissolved in minimum ethyl ether, layered with hexane, and then cooled overnight at -10 °C to give **1c** (6.67 g, 65.5%) as dark brown crystals. **Mp**: 60-62 °C. All spectroscopic data were consistent with those reported previously.[80]

Synthesis of 1,2-C_5H_3(COH-4-IC_6H_4)(CO-4-IC_6H_4) (1d). Synthesis of **1d** was previously performed by Little and Koestler[118] without full characterization. Their procedure was used with some modifications. To a 250-mL two-necked round-bottom flask, freshly cracked cyclopentadiene (2.77 g, 3.46 mL, 42.0 mmol) was added dropwise to sodium wire (0.94 g, 40.8 mmol) in ethyl ether (70 mL). A white precipitate of cyclopentadienylsodium was formed. The suspension

was stirred at room temperature for 2 h. To the reaction mixture, *p*-iodobenzoyl chloride (6.24 g, 23.7 mmol) dissolved in ether (15 mL) was added dropwise at 0 °C. The reaction mixture was allowed to warm to room temperature and stir for 1 h and then hydrolyzed with 3 M hydrochloric acid (100 mL). The organic layer was collected and the aqueous layer was exacted with ethyl ether (3 x 50 mL). The ether extracts were combined and dried over $MgSO_4$. The volatiles were removed *in vacuo* to give a yellow-brown semi-solid. Trituration with cold pentane and drying gave **1d** (4.45 g, 71.6%) as a deep-yellow solid. Analytically pure product was obtained by recrystallization from acetone. **Mp:** 145–150 °C. **^{1}H NMR (200 MHz, $CDCl_3$, ppm):** δ 6.49 (t, 1H, ^{3}J = 4 Hz, CHC*H*CH), 7.22 (d, 2H, ^{3}J = 4 Hz, C*H*CHC*H*), 7.50 (dt, 4H, ^{3}J = 8.4 Hz, ^{4}J = 2.1 Hz, Ar), 7.847.85 (dt, 4H, ^{3}J = 8.4 Hz, ^{4}J = 2.1 Hz, Ar), 18.34 (s, 1H, OH). **^{13}C{^{1}H} NMR (50 MHz, $CDCl_3$, ppm):** δ 98.8 (CH*C*HCH), 123.8 (*C*HCH*C*H), 124.6 (*CC*), 131.5, 137.2, 137.8, 141.9 (Ar), 184.6 (*C*O). **IR (Nujol mull, cm^{-1}):** 1579 (CO). Analysis Calc. for $C_{19}H_{12}O_2I_2$: C, 43.38; H, 2.30. Found: C, 44.56; H, 1.83.

Synthesis of [Tl{1,2-C_5H_3(COBu^t)$_2$}] (2a). In a 200-mL Schlenk flask, Tl_2SO_4 (1.07 g, 2.12 mmol) was added to a stirred solution of **1a** (1.00 g, 4.27 mmol) in ethyl ether (50 mL). Aqueous KOH (50, 3 M) was added and the suspension was allowed to stir for 2 h at room temperature. The reaction mixture was filtered through a medium porosity glass frit and washed with deionized water until the filtrate was neutral. The residue was washed with ethyl ether (20 mL) and dried under vacuum overnight to give **2a** (941 mg, 50.8%) as a bright yellow solid. **Mp:** 175–185 °C (decompose). **^{1}H NMR (200 MHz, $CDCl_3$ ppm):** δ

1.25 (s, 18H, Bu^t), 5.87 (t, 1H, ^3J = 3.3 Hz, CHC*H*CH), 6.26 (d, 2H, ^3J = 3.3 Hz, C*H*CHC*H*). **$^{13}C\{^1H\}$ NMR (50 MHz, $CDCl_3$, ppm):** δ 29.5 $C(CH_3)_3$, 42.7 $C(CH_3)$, 108.4 (CHCHCH) 110.4 (CHCHCH) 126.5 (*CC*), 206.5 (*C*O). **IR (KBr, cm^{-1}):** 1576 (C=O). **MS (EI):** m/z 438.1 (M^+).

Synthesis of [Tl{1,2-C_5H_3(CO-*p*-Tol)$_2$}] (2b). In a 250-mL round-bottom flask, Tl_2SO_4 (624 mg, 1.24 mmol) and aqueous KOH (40 mL, 3 M) were added to a stirred solution of **1b** (750 mg, 2.48 mmol) in ethyl ether (100 mL). The suspension was stirred vigorously for 4 h at room temperature by then a yellow precipitate was formed. The precipitate was separated by filtration, washed with water (50 mL) followed by ethyl ether (20 mL) and dried under high vacuum overnight to give **2b** (772 mg, 61.8%) as a bright yellow solid. **Mp:** 195–205 °C (dec). All spectroscopic and physical data were consistent with those reported previously.[61]

Synthesis of [Tl{1,2-C_5H_3(CO-4-Cl-C_6H_4)$_2$}] (2c). In a 250-mL round-bottom flask, Tl_2SO_4 (1.42 g, 5.64 mmol) and aqueous KOH (50 mL, 3 M) were added to a stirred solution of **1b** (750 mg, 2.48 mmol) in ethyl ether (60 mL). The suspension was stirred vigorously for 3 h at room temperature. The yellow precipitate was separated by filtration, washed with water (50 mL) followed by ethyl ether (20 mL). The residue was dried under high vacuum overnight to give **2b** (1.43 g, 46.5%) as a yellow solid. **Mp:** 180–200 °C (dec). All spectroscopic and physical data were consistent with those reported previously.[61]

Synthesis of [Tl{1,2-C_5H_3(CO-4-IC_6H_4)$_2$}] (2d). In a 250-mL round-bottom flask, Tl_2SO_4 (1.44 g, 2.85 mmol) and aqueous KOH (50 mL, 3 M) were added to a stirred solution of **1d** (3.12 g, 5.94 mmol) in ethanol (100 mL). The suspension was stirred overnight at room temperature. The reddish-brown precipitate was separated by filtration and washed with water (50 mL) and ethyl ether (20 mL). The residue was dried under high vacuum overnight to give **2d** (2.75g, 63.6%) as a deep-yellow solid. **Mp:** 200–230 °C (dec). **^{1}H NMR (200 MHz, DMSO-d_6 ppm):** δ 5.68 (t, 1H, ^{3}J = 3.6 Hz, CHC*H*CH), 6.23 (d, 2H, ^{3}J = 3.6, C*H*CHC*H*), 7.37 (d, 4H, ^{3}J = 8.0 Hz, Ar), 7.61 (d, 4H, ^{3}J = 8.0 Hz, Ar).**^{13}C{^{1}H} NMR (50 MHz, DMSO-d_6, ppm):** δ 96.1 (CH*C*HCH)110.5(*CC*), 123.2(*C*HCH*C*H), 124.7,130.8,135.8, 142.7 (Ar), 187.4 (*C*O).**IR (KBr,cm^{-1}):** 1650 (CO). **MS (EI):** m/z 729 (M^+), 525 (M^+-Tl). Analysis Calc. for $C_{19}H_{11}I_2O_2Tl$: C, 31.28; H, 1.52. Found: C, 32.95; H, 1.9.

Synthesis of [Ru{η^5-1,2-C_5H_3(COBu^t)$_2$}(η^6-p-cymene)][PF_6] (3a). In a 200-mL Schlenk flask, **21a** (689 mg, 1.13 mmol) was added to a stirred solution of [Ru(η^6-cymene)(μ-Cl)Cl]$_2$ in acetonitrile (70 mL). The reaction mixture was allowed to stir for 24 h at room temperature. The reaction mixture was filtered through a thin pad of Celite. Methanol (7 mL) and NH_4PF_6 (747 mg, 4.58 mmol) were added and the solution was stirred at room temperature for 2 h. Water (15 mL) was added and resulting solution was extracted with dichloromethane (3 x 15 mL). The combined organic layer was dried over $MgSO_4$ and volatiles were removed *in vacuo.* Trituration with cold pentane gave **3a** (281 mg, 39.9%) as a reddish-yellow solid. Analytically pure product was obtained by slow evaporation

of a concentrated ethyl ether solution in a stream of hexane-saturated nitrogen. **Mp:** 125–127 °C. **^{1}H NMR (200 MHz, acetone-d$_6$, ppm):** δ 1.21 [s, 18H,C(C*H*$_3$)$_3$], 1.28 (d, 6H ^{3}J = 6.9 Hz, *i*-Pr methyls), 2.21 (s, 3H, C*H*$_3$), 2.82 (sept, 1H, ^{3}J = 6.9 Hz, *i*-Pr methane), 5.69 (t, 1H, ^{3}J = 2.6 Hz, CHC*H*CH), 6.05 (d, 2H, ^{3}J = 2.6 Hz, C*H*CHC*H*), 6.39-6.49 (m, 4H, Ar). **^{13}C{^{1}H} NMR (50 MHz, acetone- d$_6$, ppm):** δ 18.7 (Ar*C*H$_3$), 23.3 (i-Pr methyls), 27.4 (Bu^t Me), 32.7 (methine*)*, 45.4 (*C*(CH$_3$)$_3$, 80.8 (*C*HCH*C*H), 83 (CH*C*HCH), 87.0 (Ar), 90.6 (Ar), 99.5 (*CC*), 105.4 (Ar), 114.8 (Ar), 205.2 (*C*O). **IR (Nujol mull, cm^{-1}):** 1710, (C=O), 833 (PF$_6$). The complex was characterized by an X-ray diffraction study.

Synthesis of [Ru{η^5-1,2-C$_5$H$_3$(CO-4-tol)$_2$}(η^6-*p*-cymene)][PF$_6$] (3b). In a 125-mL Schlenk flask, **2b**[61] (762 mg, 1.51 mmol) was added to a stirred solution of [Ru(η^6-cymene)(μ-Cl)Cl]$_2$ (461 mg, 0.75 mmol) in 50 mL of acetonitrile. The reaction mixture was allowed to stir for 24 h at room temperature and then filtered through a thin pad of Celite. Methanol (10 mL) and NH$_4$PF$_6$ (480 mg, 2.94 mmol) were added and the solution was stirred at room temperature for 3 h. Water (15 mL) was added and resulting solution was extracted with dichloromethane (3 x 10 mL). The combined organic layer was dried over MgSO$_4$ and volatiles were removed *in vacuo.* Trituration with cold pentane gave **3b** (430 mg, 83.9%) as a light-brown solid. Analytically pure product was obtained by recrystallization from hexane:dichloromethane (3:1). **Mp:** 122–125 °C. **^{1}H NMR (200 MHz, CD$_2$Cl$_2$, ppm):** δ 1.20 (d, 6H ^{3}J = 6.8 Hz, *i*-Pr methyls), 2.22 (s, 3H, p-cymene C*H*$_3$), 2.38 (s, 6H, PhC*H*$_3$), 2.71 (sept, 1H, ^{3}J = 6.8 Hz, *i*-Pr methine), 5.70 (t, 1H, ^{3}J = 2.5 Hz, CHC*H*CH), 5.74 (d, 2H, ^{3}J = 2.5 Hz, C*H*CHC*H*), 6.11-

6.19 (m, 4H, p-cymene, Ar), 7.26 (dt, 4H, ^3J = 8.4 Hz, ^4J = 1.7 Hz, Ar), 7.66 (dt, 4H, ^3J = 8.4 Hz, ^4J = 1.8 Hz, Ar). **$^{13}C\{^1H\}$ NMR (100 MHz, CD_2Cl_2, ppm):** δ 19.2 (*i*-Pr methine), 22.0 (Ar Me) 23.4 (*i*-Pr methyls), 32.2 (Tolyl *C*H_3), 82.1 (CH*C*HCH), 83.0 (*C*HCH*C*H), 87.5 , 90.2, 104.6, 114.0 (p-cymene Ar), 99.9 (*ipso* Cp), 129.5, 130.2, 133.8, 146.5 (p-*Ar* CH_3), 189.8 (*C*O). **IR (Nujol mull, cm^{-1}):** 1698 (CO), 832 (PF_6). Analysis Calc. for $C_{31}H_{31}F_6O_2PRu$: C, 54.63; H, 4.58. Found: C, 53.23; H, 4.17.

Synthesis of [Ru{η^5-1,2-C_5H_3(CO-4-ClC_6H_4)$_2$}(η^6-p-cymene)][PF_6] (3c). In a 125-mL Schlenk flask, **2c**[61] (357 mg, 0.65 mmol) was added to a stirred solution of [Ru(η^6-cymene)(μ-Cl)Cl]$_2$ (200 mg, 0.33 mmol) in acetonitrile (15 mL). The reaction mixture was allowed to stir for 24 h at room temperature and filtered through a thin pad of Celite. Methanol (5 mL) and NH_4PF_6 (200 mg, 1.22 mmol) were added and the solution was stirred at room temperature for 3 h. Water (15 mL) was added and resulting solution was extracted with dichloromethane (3 x 10 mL). The combined organic layer was dried over $MgSO_4$ and volatiles were removed *in vacuo.* Trituration with cold ethyl ether gave **3c** (281 mg, 72.0%) as a dark-brown solid. Analytically pure product was obtained by slow crystallization from dichloromethane by layering with hexane at -10 °C. **Mp:** 110–114 °C. **^1H NMR (200 MHz, acetone-d_6, ppm):** δ 1.26 (d, 6H, ^3J = 6.8 Hz, *i*-Pr Methyls), 2.29 (s, 3H, *p*-cymene C*H*$_3$), 2.79 (sept, 1H, ^3J = 6.8 Hz, *i*-Pr methine), 5.94 (t, 1H, ^3J = 2.8 Hz, CHC*H*CH), 6.21 (d, 2H, ^3J = 2.8 Hz, C*H*CHC*H*), 6.38-6.51 (m, 4H, p-cymene, Ar), 7.54 (dt, 4H, ^3J = 8.8 Hz, ^4J = 1.6 Hz, Ar), 7.95 (dt, 4H, ^3J = 8.8 Hz, ^4J = 1.6 Hz, Ar). **$^{13}C\{^1H\}$ NMR (100 MHz, acetone-d_6, ppm):** δ 18.9 (*i*-Pr

methine), 23.3 (*i*-Pr methyls), 32.6 (Ar CH_3), 83.1 (CH*C*HCH), 84.1 (*C*HCH*C*H), 87.9 , 90.9, 105.5, 114.8 (p-cymene Ar), 99.2 (*ipso* Cp), 130.1, 131.7, 135.9, 140.8 (p-*Ar* Cl), 190.1 (*C*O). **IR (Nujol mull, cm^{-1}):** 1693 (CO), 832 (PF_6). Analysis Calc. for $C_{29}H_{25}F_6Cl_2O_2PRu$: C, 46.16; H, 3.34. Found: C, 46.84; H, 3.24.

Synthesis of [Ru{η^5-1,2-C_5H_3(CO-4-IC_6H_4)$_2$}(η^6-p-cymene)][PF_6] (3d). In a 200-mL Schlenk flask, **2d** (405 mg, 0.55 mmol) was added to a stirred solution of [Ru(η^6-cymene)(μ-Cl)Cl]$_2$ (225 mg, 0.40 mmol) in acetonitrile (40 mL). The reaction mixture was allowed to stir for 24 h at room temperature. The reaction mixture was filtered through a thin pad of Celite and washed with acetonitrile (5 mL). Methanol (5 mL) and NH_4PF_6 (245 mg, 1.50 mmol) were added and the solution was stirred at room temperature for 3 h. Water (15 mL) was added and resulting solution was extracted with dichloromethane (3 x 15 mL). The combined organic layer was dried over $MgSO_4$ and the volatiles were removed *in vacuo.* Trituration with cold pentane gave **3d** (345 mg, 69.4%) as a dark-brown solid. **Mp:** 112-113 °C. **^{1}H NMR (200 MHz, acetone- d_6, ppm):** δ 1.26 (d, 6H ^{3}J = 6.9 Hz, ^{i}Pr methyls, 2.29 (s, 3H, CH_3), 2.80 (sept, 1H, ^{3}J = 6.9 Hz, ^{i}Pr methine), 5.92 (t, 1H, ^{3}J = 2.5 Hz, CHC*H*CH), 6.19 (d, 2H, ^{3}J = 2.5 Hz, C*H*CHC*H*), 6.38-6.49 (m, 4H, p-cymene, Ar), 7.68 (dt, 4H, ^{3}J = 8.4 Hz, ^{4}J = 1.8 Hz, Ar), 7.92 (dt, 4H, ^{3}J = 8.4 Hz, ^{4}J = 1.8 Hz, Ar). **^{1}H NMR (200 MHz, $CDCl_3$, ppm):** δ 1.18(d, 6H, ^{3}J = 6.6 Hz, ^{i}Pr methyls, 2.19 (s, 3H, CH_3), 2.71 (sept, 1H, ^{3}J = 6.6 Hz, *i*-Pr methine, 5.81 (line merges with *p*-cymene aromatic, 3 H, CHC*H*CH and Ar), 6.16 (lines merge with *p*-cymene aromatic 4 H, C*H*CHC*H* and Ar), 7.46 (d, 4H, ^{3}J = 8.0, Ar), 7.46

(d, 4H, ^3J = 8.0 Hz, Ar). **$^{13}C\{^1H\}$ NMR (50 MHz, $CDCl_3$, ppm):** δ 19.1 (*i*-Pr methine), 23.3 (*i*-Pr methyls), 31.9 (Ph*C*H_3), 79.0 (CH*C*HCH), 83.2 (*C*HCH*C*H), 87.4 , 90.0, 104.6, 114.6 (*p*-cymene Ar), 98.6 (*ipso* Cp), 103.4, 130.3, 135.0, 138.8 (*p*-IPh), 189.7 (*C*O). **IR (Nujol mull, cm^{-1}):** 1655, 836 (PF_6). Analysis Calc. for $C_{29}H_{25}F_6I_2O_2PRu$: C, 38.47; H, 2.78. Found: C, 38.23; H, 2.34.

Attempted Synthesis of [Ru{η^5-1,2-C_5H_3(CO-4-tol)$_2$S(η^6-*p*-cymene)}][PF_6] (4b): In a 125-mL Schlenk flask, **3b** (100 mg, 0.146 mmol) was added to a stirred suspension of P_4S_{10} (500 mg, 1.03 mmol) and $NaHCO_3$ (100 mg, 1.18 mmol) in dichloromethane (40 mL). The reaction mixture was allowed to stir for 2 h at room temperature. The color changed from pale yellow to deep purple. The reaction mixture was then filtered through a thick pad of alumina and the solvent was evaporated to its 1/3rd. Ethyl ether was added dropwise to give a precipitate which was separated by filtration and dried overnight to give purple powder (100 mg). ^1H NMR of the product showed a loss of p-cymene ligand. The attempts of further analysis by separating the fractions failed.

3.3. Results and Discussion

3.3.1. Synthesis. 1,2-Diacylcyclopentadienes (**1a**-**d**) are easily prepared by the treatment of a suspension of sodium or lithium cyclopentadienide with acyl chloride in a 3:2 ratio.[59,61,81,86,116,119-121] These compounds exist as intramolecularly H-bonded 2-acyl-6-hydroxyfulvenes and are fairly strong acids (Figure 3.2).

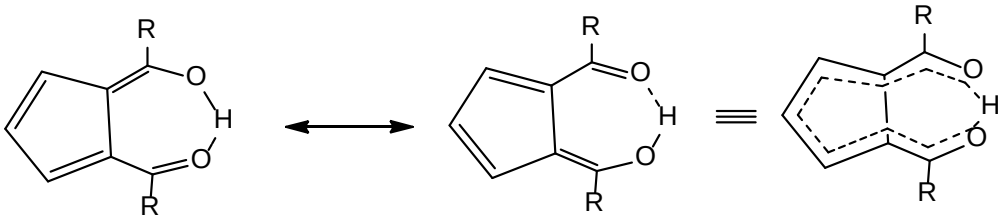

Figure 3.2. Resonance structures of 2-acyl-6-hydroxyfulvenes[121]

Wallace and Selegue previously prepared *tert*-butyl fulvene **1a** in 13% yield.[80] We improved the yield to 29% by slight modification in work-up procedure. Similarly Tice and Selegue prepared *p*-tolyl **(1b)**, *p*-chlorophenyl **(1c)**[62] to obtain in 54% and 45% respectively by using *n*-BuLi as a base. We modified the method by using sodium as deprotonating agent of cyclopentadiene to obtain **1b** (55.7%) and **1c** (65.5%). We extended the procedure to prepare *p*-iodophenyl **(1d)** fulvene in 71.6% yield.

Rather than deprotonating fulvenes **1a**-**d** with TlOEt,[59,61,62,116] we developed a more convenient method using inexpensive, readily available thallium sulfate in the presence of 3 M KOH to obtain the thallium salts [Tl{1,2-$C_5H_3(COBu^t)_2$}] **2a**, [Tl{1,2-C_5H_3(CO-4-Tol)$_2$}] **2b**, [Tl{1,2-C_5H_3(CO-4-$ClC_6H_4)_2$}] **2c** and C_5H_3(CO-4-$IC_6H_4)_2$}] **2d** in 51-85% yield. The light yellow thallium salts were found to be stable in air indefinitely.

Scheme 3.2. Synthesis of 1,2-diacylcyclopentadienylp-cymene complexes of ruthenium(II)

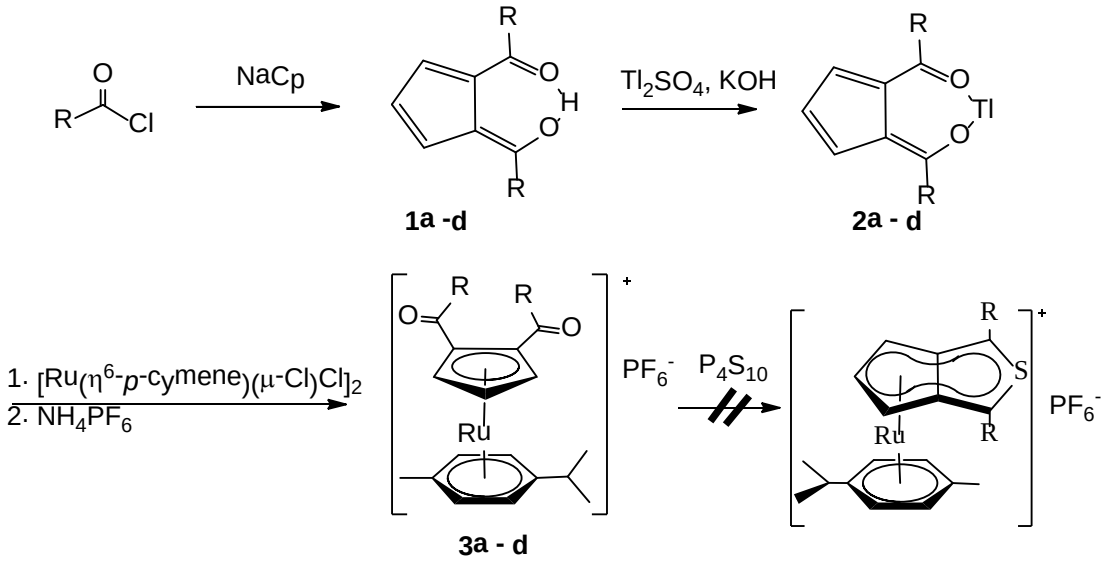

R = Bu^t (**a**), 4-Me-C_6H_5 (**b**), 4-Cl-C_6H_5 (**c**),4-I-C_6H_5 (**d**)

The thallium salts **2a-d** were treated with $[Ru(\eta^6\text{-p-cymene})(\mu\text{-Cl})Cl]_2$[117] in a 2:1 ratio at room temperature in acetonitrile varying from 24 to 36 h. The completion of the reaction at the transmetallation step was monitored by the formation of insoluble byproducts of thallium, which can be easily removed by simple filtration through Celite. The chloride ion can be easily metathesized with NH_4PF_6 in methanol to obtain the cationic ruthenium cyclopentadienyl arene complexes **3a-d** in 39-83% yield.[86] Further purification of the complexes was generally carried out by trituration with cold pentane, ethyl ether or by slow crystallization from a mixture of dichloromethane and hexane. Our attempts of converting 1,4-diketone complex **3b** to thiophene-fused cyclopentadienyl-p-cymene cationic complex adopting the method employed by Snyder *et al*[61] failed.

3.3.2. Spectroscopy. All new compounds were fully characterized by spectroscopic methods including ^{1}H and ^{13}C NMR, IR and high-resolution mass spectroscopy. The compounds **1a-c** and **2a-c** were characterized by comparison of their ^{1}H NMR spectra with previous reports.[62,86] The Cp resonances in the ^{1}H NMR spectra of fulvenes **1a-d** displayed a characteristic doublet and triplet integrating in a 2:1 ratio showing the symmetry of the molecule. Their enolic form is evidenced by the resonance of bridging acidic proton at 16-20 ppm in ^{1}H NMR and carbonyl absorbance in significantly lower energy (e. g., 1607 cm^{-1} for **1b**, 1579 cm^{-1} for **1d**) than regular aromatic ketones. ^{1}H NMR spectra of the thallium salts **2a-d** were similar to those of corresponding fulvenes with slightly up-field resonances, possibly due to the higher electronic density in cyclopentadienyl anion. The formation of the thallium salt was evidenced by loss of the hydroxyl proton. The thallium derivatives consistently analyze low in carbon. This is possibly due to contamination by NMR silent Tl_2O and TlOH. These salts are very insoluble in common organic solvents and decompose below their sublimation temperature, making the preparation of analytically pure samples difficult.

The transmetallation of thallium salt with *p*-cymene ruthenium chloride gave additional peaks of doublet (δ 1.20-1.28 ppm), singlet (δ 2.21- 2.29 ppm) and septet (δ 2.38-2.82 ppm) in complexes **3a-d** (Table 3.1). These are due to isopropyl methyls, CH_3 and isopropyl methine protons, respectively in *p*-cymene ligand. The coupling constant between isopropyl methyls and isopropyl methine was about 7.0 Hz. Similarly, the inner (CHC*H*CH) and the outer (C*H*CHC*H*)

protons of the cyclopentadienyl ligand appear as triplet and doublet showing a plane of symmetry in the Cp ligand. The chemical shift ranges from 5.69 to 5.94 ppm for outer and from 5.74 to 6.21 ppm to inner protons respectively. The arene protons *p*-cymene resonance ranges from 5.81 to 6.51 ppm (spin system AA'BB') showing complexation. Similarly, the carbon resonances of the arene ligand vary from 87 to 114 ppm. These values are in the similar ranges of *p*-cymene complexes reported by Fischer *et al*.[122] Those complexes exhibited a characteristic peak in ^{13}C NMR ranging from 189.7 to 205.2 ppm. A strong IR stretching of ketonic groups ranges from 1655 cm^{-1} to 1710 cm^{-1}. A medium absorbance from 832 cm^{-1} to 836 cm^{-1} is characteristic of P-F stretching of counter anion. Mass spectra of **3a** showed a peak at m/z 468 which is characteristics of (M^+ - PF_6). However, the mass analysis of **3b-d** in electron impact (EI) mode could not be detected any cationic peak of the complex. This might be due to the involatility of the complex salt.

Table 3.1. Selected NMR and IR (Nujol) Data of **3a-d**

	δ_H (ppm)						δ_C (ppm)	ν (cm^{-1})		
	CH(C*H*$_3$)$_2$	p-Cym C*H*$_3$	C*H* (CH$_3$)$_2$	CHC *H*CH	C*H*C HC*H*	p-cym Ar-H	*C*O	CO	PF_6	Solvent
3a	1.28	2.21	2.82	5.69	6.05	6.39-6.49	205.2	1710	833	a
3b	1.20	2.22	2.71	5.70	5.74	6.11-6.19	189.8	1698	832	b
3c	1.26	2.29	2.79	5.94	6.21	6.38-6.51	190.1	1693	832	a
3d	1.26	2.29	2.80	5.92	6.19	6.38-6.49	-	1655	836	a
3d	1.18	2.19	2.71	5.81	6.16	5.81-6.16	189.7	1655	836	c

Solvents: a = $(CD_3)_2CO$; b = CD_2Cl_2; c = $CDCl_3$

3.3.3. Structure. The crystals of **3a** suitable for X-ray crystal structure determination were obtained by slow diffusion of hexane on the solution in dichloromethane under nitrogen. A thermal ellipsoid plot of the molecular structure of [Ru{η^5-1,2-$C_5H_3(COBu^t)_2$}(η^6-p-cymene)][PF_6] **(3a)** is shown in Figure 3.3 with atom numbering scheme. The crystal structure and refinement data for compound **3a** can be found in Table 4.2. Selected bond distances and angles are given in Table 3.2. In the cationic part of the complex salt ruthenium atom is embedded in a mixed sandwich comprising the η^6-bound *p*-cymene and η^5-bound Cp fragment derived from thallium salt while the counter anion, PF_6 displays a typical octahedral geometry.

An average ruthenium–carbon bond length with respect to the Cp ring was 2.179(4) Å. Similarly, the metal-carbon bond length with respect to Ar ring was 2.214(4). The distances from the centroids of Cp and Ar ligands to Ru were 1.809(4) Å and 1.710(4) respectively. These values are consisted with the Ru-Cp distance reported in literatures for cationic complexes.[115] The centroid-Ru-centroid angle was 175.08°. The average distance of C1 and C2 from Ru center is higher by 0.01 Å in comparison to the average distance of C3-C5. This might be due to inductive effect of carbonyl group. The shortest distance of Ru-C4, 2.164(4) Å among Cp ring carbons and longest distances of Ru-C16, 2.262 (4) Å among arene carbons indicated the steric interactions between *tert*-butyl group and isopropyl groups of opposite rings. One oxygen atom is positioned towards the ruthenium center while another is slightly away from ruthenium with O1 0.042 Å and O2 -0.874 Å with respect to Cp least-square plane. Similarly, C7 and C12

atoms are displaced 0.172 Å and 1.527 Å with respect to the least-squares plane of Cp. The angle between two rings of the complex was 6.13°. This indicated the steric interaction between side chains of two rings. To the best of our knowledge, this is the first reported crystal structure of 1,2-diacyl ruthenium cationic complex.

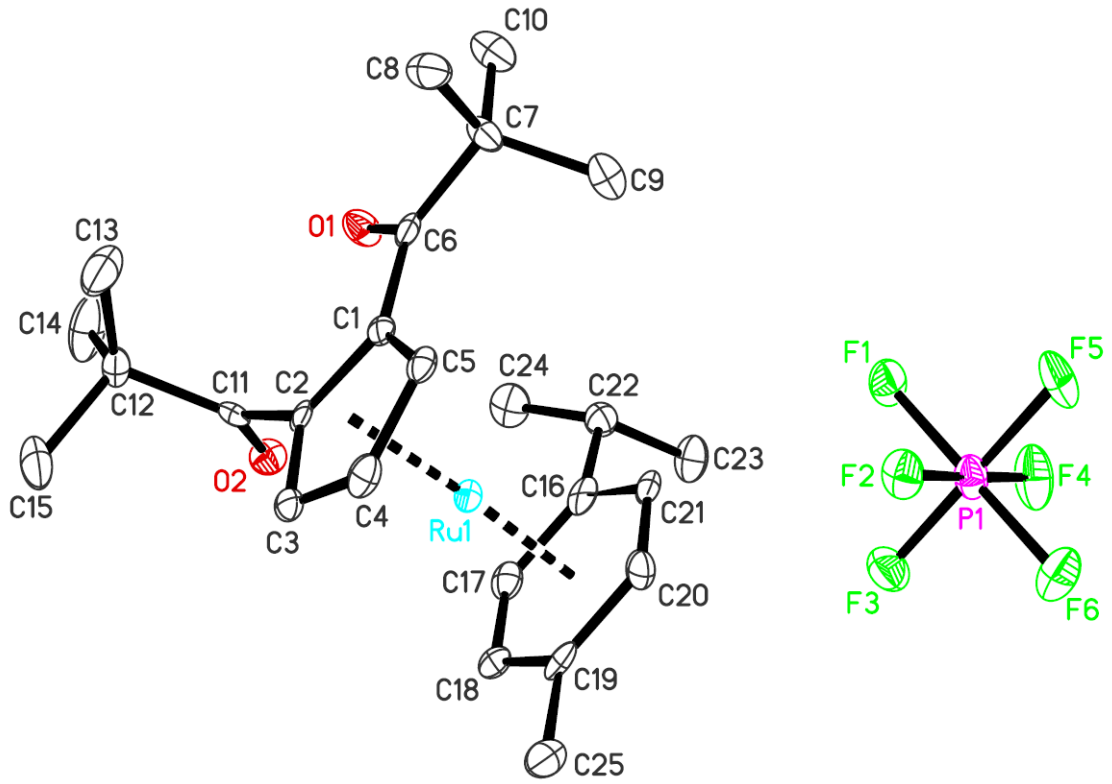

Figure 3.3. Molecular structure of [Ru{η^5-1,2-C_5H_3(COBut)$_2$}(η^6-p-cymene)][PF_6] (**3a**)

Table 3.2. Crystal Data and Structure Refinement for Compound **3a**

Formula	$C_{25}H_{35}F_6O_2PRu$	Monochromator	Graphite
Formula wt (amu)	613.57	Absorption coef μ (mm^{-1})	0.727
T, K	90.0(2)	Diffractometer	Nonius KappaCCD diffractometer
Crystal system	Orthorhombic	2θ range (deg)	1.71 to 27.49
Space group	*Pna2₁*	Limiting indices	$-13 \leq h \leq 13$
Z	4		$-30 \leq k \leq 30$
a, Å	10.4848(2)		$-13 \leq l \leq 13$
b, Å	23.8423(5)	Reflections collected	24539
c, Å	10.4241(2)	Independent reflections	5947 (R_{int} = 0.0632)
α,(deg)	90	Absorption correction	Semi-empirical from equivalents
β, (deg)	90	Refinement method	SHELXL-97
γ, (deg)	90	Refinement method	Full-matrix least-squares on F^2
V, $Å^3$	2605.83(9)	Data/restraints/parameters	5947 / 1 / 325
d_{calc}, Mg/m^3	1.564	Goodness-of-fit on F^2	1.043
F(000)	1256	Final R indices [$I>2\sigma(I)$]	R_1 = 0.0376, wR_2 = 0.0693
Crystal size (mm^3)	0.30 x 0.12 x 0.10	R indices (all data)	R_1 = 0.0632, wR_2 = 0.0778
Radiation	Mo Kα (λ = 0.71073 Å)	Largest diff. peak and hole	1.560 e•$Å^{-3}$ and -0.511 e•$Å^{-3}$

Table 3.3. Bond angle [°] and bond distance [Å] of compound **3a**

Ru1-C4	2.164(4)
Ru1-C5	2.178(3)
Ru1-C3	2.184(4)
Ru1-C2	2.186(4)
Ru1-C1	2.187(3)
Ru1-C18	2.196(3)
Ru1-C17	2.211(4)
Ru1-C19	2.210(3)
Ru1-C20	2.211(4)
Ru1-C21	2.218(4)
Ru1-C16	2.262(4)
O1-C6	1.225(4)
O2-C11	1.215(5)
C1-C2	1.440(5)
C1-C5	1.448(5)
C1-C6	1.497(5)
C2-C3	1.429(5)
C2-C11	1.518(5)
C3-C4	1.407(5)
C4-C5	1.421(5)
C6-C7	1.525(5)
C7-C10	1.531(6)
C7-C9	1.536(6)
C7-C8	1.545(5)
C11-C12	1.535(5)
C12-C13	1.522(6)
C12-C14	1.528(6)
C12-C15	1.534(6)
C16-C17	1.417(5)
C16-C21	1.424(5)
C16-C22	1.524(6)
C17-C18	1.402(5)
C18-C19	1.419(5)
C19-C20	1.408(6)
C19-C25	1.494(6)
C20-C21	1.411(5)
C22-C24	1.508(6)
C22-C23	1.526(6)
P1-F3	1.591(3)
P1-F4	1.599(3)
P1-F6	1.602(2)
P1-F2	1.608(3)

P1-F5	1.610(3)
P1-F1	1.615(2)
C4-Ru1-C5	38.20(14)
C4-Ru1-C3	37.77(14)
C5-Ru1-C3	63.74(14)
C4-Ru1-C2	63.66(14)
C5-Ru1-C2	63.98(14)
C3-Ru1-C2	38.17(14)
C4-Ru1-C1	64.49(14)
C5-Ru1-C1	38.74(13)
C3-Ru1-C1	64.40(14)
C2-Ru1-C1	38.46(14)
C4-Ru1-C18	119.81(15)
C5-Ru1-C18	156.60(14)
C3-Ru1-C18	103.56(15)
C2-Ru1-C18	119.23(14)
C1-Ru1-C18	155.84(14)
C4-Ru1-C17	151.82(15)
C5-Ru1-C17	166.07(14)
C3-Ru1-C17	119.25(15)
C2-Ru1-C17	109.16(14)
C1-Ru1-C17	128.34(14)
C18-Ru1-C17	37.10(13)
C4-Ru1-C19	102.06(15)
C5-Ru1-C19	125.46(13)
C3-Ru1-C19	110.74(17)
C2-Ru1-C19	144.91(17)
C1-Ru1-C19	164.18(14)
C18-Ru1-C19	37.57(13)
C17-Ru1-C19	67.45(14)
C4-Ru1-C20	109.00(15)
C5-Ru1-C20	108.18(14)
C3-Ru1-C20	137.66(15)
C2-Ru1-C20	171.86(15)
C1-Ru1-C20	136.44(14)
C18-Ru1-C20	66.90(14)
C17-Ru1-C20	78.97(15)
C19-Ru1-C20	37.12(16)
C4-Ru1-C21	135.44(14)
C5-Ru1-C21	111.66(14)
C3-Ru1-C21	173.07(15)
C2-Ru1-C21	145.96(14)

Table 3.3 continued

C1-Ru1-C21	115.76(14)
C18-Ru1-C21	78.82(14)
C17-Ru1-C21	66.54(14)
C19-Ru1-C21	67.11(16)
C20-Ru1-C21	37.15(14)
C4-Ru1-C16	171.00(15)
C5-Ru1-C16	134.06(14)
C3-Ru1-C16	149.89(15)
C2-Ru1-C16	119.70(14)
C1-Ru1-C16	112.31(14)
C18-Ru1-C16	66.82(14)
C17-Ru1-C16	36.92(14)
C19-Ru1-C16	79.65(15)
C20-Ru1-C16	67.00(15)
C21-Ru1-C16	37.03(14)
C2-C1-C5	106.4(3)
C2-C1-C6	122.6(3)
C5-C1-C6	131.0(3)
C2-C1-Ru1	70.74(19)
C5-C1-Ru1	70.28(19)
C6-C1-Ru1	126.1(3)
C3-C2-C1	108.6(3)
C3-C2-C11	123.1(3)
C1-C2-C11	128.1(3)
C3-C2-Ru1	70.9(2)
C1-C2-Ru1	70.8(2)
C11-C2-Ru1	128.2(3)
C4-C3-C2	108.0(4)
C4-C3-Ru1	70.3(2)
C2-C3-Ru1	71.0(2)
C3-C4-C5	109.0(3)
C3-C4-Ru1	71.9(2)
C5-C4-Ru1	71.4(2)
C4-C5-C1	108.1(3)
C4-C5-Ru1	70.4(2)
C1-C5-Ru1	70.98(19)
O1-C6-C1	116.5(3)
O1-C6-C7	122.4(3)
C1-C6-C7	121.0(3)
C6-C7-C10	109.3(3)
C6-C7-C9	111.9(3)
C10-C7-C9	108.0(3)
C6-C7-C8	107.9(3)

C10-C7-C8	109.3(3)
C9-C7-C8	110.4(3)
O2-C11-C2	121.4(3)
O2-C11-C12	121.9(4)
C2-C11-C12	116.4(3)
C13-C12-C14	110.1(4)
C13-C12-C15	108.5(4)
C14-C12-C15	109.4(4)
C13-C12-C11	112.3(3)
C14-C12-C11	109.9(3)
C15-C12-C11	106.6(3)
C17-C16-C21	117.6(4)
C17-C16-C22	123.0(4)
C21-C16-C22	119.4(4)
C17-C16-Ru1	69.6(2)
C21-C16-Ru1	69.8(2)
C22-C16-Ru1	134.1(3)
C18-C17-C16	121.1(4)
C18-C17-Ru1	70.9(2)
C16-C17-Ru1	73.5(2)
C17-C18-C19	121.0(4)
C17-C18-Ru1	72.0(2)
C19-C18-Ru1	71.77(19)
C20-C19-C18	118.5(4)
C20-C19-C25	121.6(3)
C18-C19-C25	119.9(4)
C20-C19-Ru1	71.5(2)
C18-C19-Ru1	70.66(19)
C25-C19-Ru1	129.1(3)
C19-C20-C21	120.6(4)
C19-C20-Ru1	71.4(2)
C21-C20-Ru1	71.7(2)
C20-C21-C16	121.2(4)
C20-C21-Ru1	71.2(2)
C16-C21-Ru1	73.2(2)
C16-C22-C23	108.2(3)
F3-P1-F4	90.39(15)
F3-P1-F6	90.59(14)
F4-P1-F6	90.63(15)
F3-P1-F2	90.37(14)
F4-P1-F2	178.98(18)
F6-P1-F2	90.05(14)
F3-P1-F5	179.87(18)

Table 3.3 continued

F4-P1-F5	89.74(15)		F4-P1-F1	89.97(15)
F6-P1-F5	89.42(15)		F6-P1-F1	179.15(15)
F2-P1-F5	89.50(13)		F2-P1-F1	89.35(15)
F3-P1-F1	90.00(14)		F5-P1-F1	89.98(15)

3.4. Summary

An easy route to [Ru{η^5-1,2-$C_5H_3(COR)_2$}(η^6-p-cymene)] [PF_6] with various substituents starting from commonly available starting materials is described. The 1,2-diacylcyclopentadienes **1a-d** (29-71%) were synthesized by treating cyclopentadienide sodium with acyl chlorides in a 3:2 ratio.[61] The fulvenes were thalliated in the presence of 3 M aqueous KOH and Tl_2SO_4 to thallium reagents **2a-2d** (51-85%). The thallium salts **2a-d** were treated with [Ru(η^6-p-cymene)(μ-Cl)Cl]$_2$[117] in a 2:1 ratio at room temperature in acetonitrile varying from 24 to 36 h followed by ion exchange with NH_4PF_6 to give cationic ruthenium complexes **3a-d** in 39-83% yield with PF_6 as counter anion. The molecular structure of complex **3a** was studied. Our attempts so far to cyclize the γ-diketone complexes with sulfur and selenium failed.

Chapter 4: Synthesis, Characterization, and Reactivity of Some Metallocene-Fused Acene-Quinone Complexes

Introduction

Our group work involves the synthesis of 1,2-diacyl- and 1,2-diester-cyclopentadienyl complexes of manganese[61] and ruthenium.[59,78] We realized to extend the methodology to synthesize 1,2-diformyl or 1,2-dicarboxylic acids of cymantrene and pentamethylruthenocene. The 1,2-diformylcyclopentadienyl metal complexes can be used as an starting material for acene-quinone forming reactions via aldol condensation. Similarly, Cp-bound 1,2-diacyl chloride or anhydrides can be an ideal entry point to design Cp-capped quinone complexes of manganese and ruthenium *via* a Friedel-Crafts acylation.

Our immediate goal is to develop efficient methodologies to synthesize quinone complexes (**A**) with carbonyl groups at different positions of polycyclic backbone starting from 1,2-disubstituted cyclopentadienyl metal complexes (Figure 4.1). Once we establish the chemistry of Cp-bound quinone complexes, aromatization of the ligand can extend the π-conjugation to give unique metallocene-fused polyacene complexes (**B**). Similarly, release of polycyclic backbone from metal center gives cyclopentadiene-capped acene quinone. The functionalization of the resultant quinone with (trialkylsilyl)ethynyl group gives unique carbocyclic frameworks (**C**). The bis(cyclopentadiene)-fused substituted anthracene should be structurally and electronically close to anthradithiophene synthesized by the Anthony group.[20]

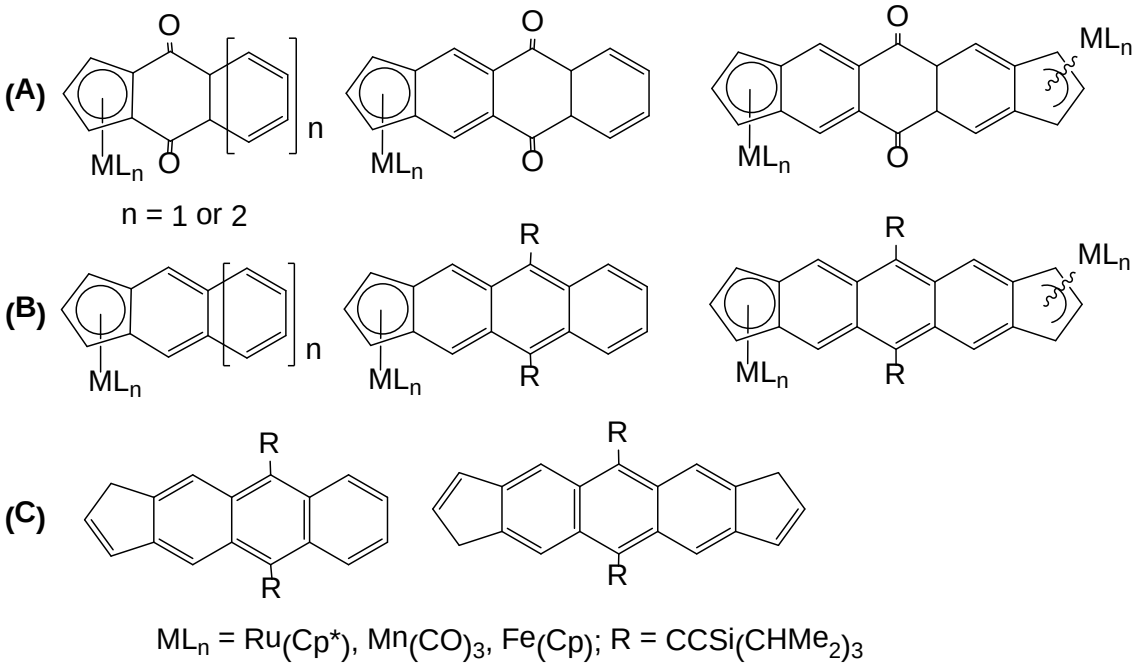

Figure 4.1. The desired acene precursors, metallocene acenes and free acenes

Incorporation of a redox-active metal center on the acene backbone can alter the physical and electrochemical properties of the organic acenes. The metal center can act as a switch, allowing the acene molecules to be reversibly doped and undoped at different electronic environments. Ruthenocene, ferrocene and cymantrene are well known cyclopentadienyl metal complexes with coordinatively saturated metal centers. The selection of the pentamethylcyclopentadienyl (Cp*) ligand in ruthenocene complex offers a better electron-donation to the metal center and hence increases the stability. The methyl groups also increase the solubility of the resultant complex and provide stereoselectivity towards different reagents. Similarly, carbonyl ligands make the manganese center electron-deficient due to the ability of carbonyl ligands to accept electrons by back-bonding. To study the comparative electronic

influences of metal and ancillary ligand bound to them, we work with electron-rich pentamethylruthenocene, electron-deficient manganesetricarbonyl and intermediate cyclopentadienyl iron.

4.1. Friedel-Crafts Acylation

A major route to polycyclic aromatic hydrocarbons is the double Friedel-Crafts acylation of an aromatic substrate with a phthalic anhydride.[123-125] The cyclopentadienyl ligand of metal complexes like ferrocene, ruthenocene and cymantrene are well known nucleophiles for Friedel-Crafts acylation due to its high electronic densities. However, double acylation of metallocene with organic anhydrides fails because of the deactivation of cyclopentadienyl ring after the first acylation, preventing the second acylation.[126] To come up with the similar results, we decided to switch the functionalities between two substrates where cyclopentadienyl (Cp)-bound 1,2-diacyl chlorides or dicarboxylic anhydrides metal complexes can be treated with organic or organometallic aromatics in the presence of aluminum chloride to give desired quinones (Scheme 4.1).

Scheme 4.1. Proposed synthetic scheme of organometallic acene complexes

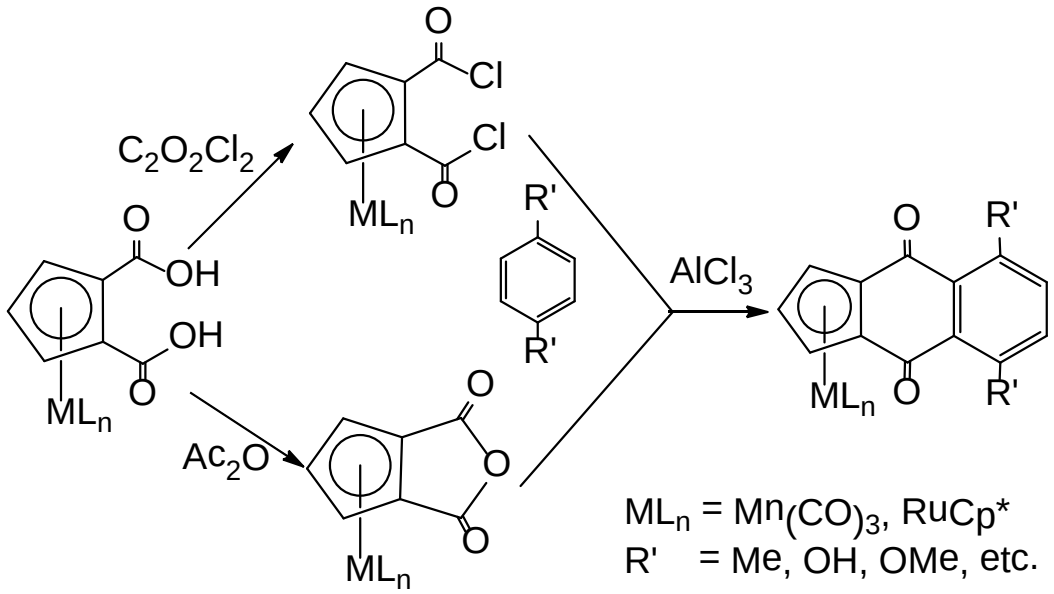

Herein, we report the detail synthesis and characterization of Cp-fused quinone complexes of ruthenium and manganese *en route* to targeted organometallic acenes.

4.1.1. Experimental

Chapter 2 lists general conditions for all experiments. Cyclic voltammetry (CV) was recorded with a BASi-Epsilon apparatus. A three-electrode cell with a platinum disk working electrode, a platinum wire counter electrode, and an Ag/AgCl reference electrode were employed in conjunction with a potentiostat interfaced to a personal computer. *o*-Xylene (99%), *p*-dimethoxybenzene (99%), oxalyl chloride, ferrocene (Acros), lithium triethylborohydride, $LiAlH_4$, $AlCl_3$ (99.8%), N,N-dimethylformamide (99.8%), cyclohexane-1,4-dione, lithium aluminum hydride (1 M solution in THF) (Aldrich), manganese(IV)oxide

precipitated active and diisobutylaluminum hydride (Acros) were used without further purification. Naphthalene- and anthracene-1,4-diol were obtained by reducing naphthalene-1,4-dione[127] (Aldrich) and anthracene-1,4-dione[128] (Aesar) with sodium dithionite (J. T. Baker). [Ru{η^5-$C_5H_3(CO_2Ph)_2$-1,2}(Cp*)] (**2a**), [Ru{η^5-$C_5H_3(CO_2H)_2$-1,2}(Cp*)][78] (**3a**) and [$Mn(CO)_3${η^5-$C_5H_3(CO_2Ph)_2$-1,2}][79] (**2b**) were synthesized according to the procedure in Chapter 2.

Synthesis of [Ru{η^5-$C_5H_3(CO)_2C_6H_4$-1,2}(Cp*)] (3a). To an oven-dried and cooled 125-mL Schlenk flask, **1** (50 mg, 0.13 mmol) was dissolved in ca. 10 mL of dry benzene. After stirring for 15 min at room temperature, oxalyl chloride (64 mg, 44 µL, 0.51 mmol) and DMF (5 µL) were added. The mixture was stirred for 3 h. The resultant yellow solution was evaporated completely under high vacuum at 40 °C. Without further purification of diacid chloride, dry benzene (10 ml) was added through a syringe, followed by anhydrous aluminum chloride (70 mg, 0.52 mmol). The reaction mixture was refluxed for 1.5 h. The reaction mixture was quenched with 2 M solution of NaOH (5 mL) and the product was extracted with ethyl ether (2 x 10 mL). Combined ether extracts were dried over $MgSO_4$, filtered, and volatiles were removed *in vacuo.* The product was isolated as an orange-red band from chromatography on silica with ethyl ether as eluent to give **3a** (32 mg, 58%) as a red powder. Analytically pure product was obtained by crystallization from hexane by cooling at -5 °C for 3 days. **Mp**: 278–280 °C. **^{1}H NMR (400 MHz, $CDCl_3$, ppm):** δ 1.49 (s, 15H, Cp*), 4.91 (t, 1H, ^3J = 2.6 Hz, CHC*H*CH), 5.24 (d, 2H, ^3J = 2.6 Hz, C*H*CHC*H*), 7.58–7.60 (m, 2H, Ar), 8.09–8.11 (m, 2H, Ar). **^{13}C{^{1}H} NMR (100 MHz, $CDCl_3$, ppm):** δ 10.1(Cp* *C*H_3), 75.4

(*C*HCH*C*H), 80.5 (CH*C*HCH), 82.7 (*CC*, Cp), 89.1 (ring, Cp*), 126.4 (4*C*, 5*C*, Ar), 132.9 (3*C*, 6*C*), 134.4 (*CC*, Ar), 184.8 (*C*O). **IR (ATR, cm^{-1}):** 1650 (C=O), 1590 (C=C). **MS (EI):** m/z 432 (M^+). The complex was characterized by an X-ray diffraction study.

Synthesis of [Ru{η^5-$C_5H_3(CO)_2C_6H_3CH_3$-1,2}(Cp*)] (3b). To an oven-dried and cooled 200-mL Schlenk flask, **1** (1.00 g, 2.57 mmol) was dissolved in ca. 80 mL of dry benzene. After stirring for 15 min at room temperature, oxalyl chloride (1.30 g, 0.88 mL, 10.3 mmol) and DMF (25 µL) were added. The reaction mixture was stirred for 3 h. Evolution of gases was observed during stirring. The resultant yellow solution was evaporated completely under high vacuum. Without further purification of diacid chloride, dry toluene (20 mL) was added through a cannula, followed by anhydrous aluminum chloride (680 mg, 5.14 mmol). The resultant mixture was stirred for 4 h at room temperature. The reaction mixture was quenched with 2 M solution of NaOH (10 mL) and the product was extracted with ethyl ether (3 x 20 mL). Combined ether extracts were dried over $MgSO_4$, filtered, and volatiles were removed *in vacuo.* The crude product was purified by chromatography on silica with ethyl ether:hexane (4:1) as eluent. Removal of volatiles gave **3b** (808 mg, 71.0%) as a bright yellow solid. Analytically pure product was obtained by slow diffusion of dry hexane saturated with nitrogen through the solution in ethyl ether. **Mp**: 265-267 °C. **^{1}H NMR (400 MHz, $CDCl_3$, ppm):** δ 1.51 (s, 15H, Cp*), 2.43 (s, 3H, Ph*C*H_3), 4.89 (t, 1H, ^3J = 2.6 Hz, CHC*H*CH), 5.23 (d, 2H, ^3J = 2.6 Hz, C*H*CHC*H*), 7.38 (dd, 1H, ^3J = 7.6 Hz, ^4J = 1.2 Hz, Ph), 7.90 (d, 1H, ^3J = 1.2 Hz, Ph), 7.99 (d, 1H, ^3J = 7.6 Hz, Ph).

$^{13}C\{^1H\}$ **NMR (100 MHz, $CDCl_3$, ppm):** δ 10.1 (Cp* CH_3), 21.9 (Ph*C*H_3), 75.2 (C1), 75.3 (C3), 80.3 (C2), 82.7 (C9a), 82.8 (C3a), 88.9 (Cp* ring), 126.6 (C8a), 126.8 (C4a), 132.6 (C8), 133.6 (C5), 134.8 (C7), 143.6 (C6), 184.8 (C4), 185.1 (C9) (Figure 4.2).

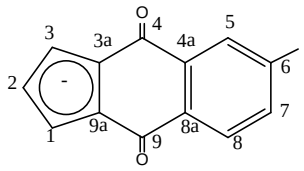

Figure 4.2. Numbering scheme in benz[*f*]indenyl ligands

IR (KBr, thin film, cm^{-1}): 1656 (CO), 1598 (CC). **MS (EI):** m/z 446 (M^+). Analysis Calc. for $C_{24}H_{24}O_2Ru$: C, 64.70; H, 5.43. Found: C, 63.37, H, 5.65. The complex was characterized with an X-ray diffraction studies.

Synthesis of [Ru{η^5-$C_5H_3(CO)_2C_6H_2(CH_3)_2$-1,2}(Cp*)] (3c, 3d). To an oven-dried and cooled 125-mL Schlenk flask, **1** (100 mg, 0.26 mmol) was dissolved in ca. 40 mL of dry benzene. After stirring for 15 min at room temperature, oxalyl chloride (130 mg, 0.08 mL, 1.28 mmol) and DMF (5 µL) were added. The reaction mixture was stirred for 3 h at room temperature. Evolution of gases was observed during stirring. The resultant yellow solution was evaporated completely under high vacuum. To the bright yellow powder of diacid chloride, *o*-xylene (20 mL) followed by anhydrous aluminum chloride (68.0 mg, 0.51 mmol) were added. The reaction mixture was stirred for 4 h at room temperature and quenched with 2 M aqueous NaOH (10 mL) and extracted with ethyl ether (3 x 10 mL). The combined ether extracts were dried over $MgSO_4$, filtered and volatiles

were removed *in vacuo*. The product was isolated by chromatography on silica with ethyl ether:hexane (4:1) as eluent to give a yellow powder (64 mg, 55%). Analysis by ^{1}H NMR of the product showed the formation of two isomeric products **3c** and **3d** in a 1:1 ratio. Attempts to separate the isomers by column chromatography and recrystallization failed. **^{1}H NMR (400 MHz, $CDCl_3$, ppm): 3c.** δ 1.52 (s, 15H, Cp*), 2.38 (s, 3H, PhCH_3), 2.68 (s, 3H, PhCH_3), 4.87 (t, 1H, ^{3}J = 2.4 Hz, CHC*H*CH), 5.16 (dd, 1H, ^{3}J = 2.4 Hz, ^{4}J = 1.2 Hz, C*H*CHCH), 5.18 (dd, 1H, ^{3}J = 2.4 Hz, ^{4}J = 1.2 Hz, CHC*H*CH), 7.36 (d, 1H, ^{3}J = 7.6 Hz, Ph), 7.97 (d, 1H, ^{3}J = 7.6 Hz, Ph). **3d.** δ 1.51 (s, 15H, Cp*), 2.34 (s, 6H, Ph (CH_3)$_2$), 4.82 (t, 1H, ^{3}J = 2.4 Hz, CHC*H*CH), 5.21 (d, 2H, ^{3}J = 2.4 Hz, C*H*CHC*H*), 7.84 (s, 2H, Ph).

Synthesis of [Ru{η^5-$C_5H_3(CO)_2C_6H_4(OMe)_2$-1,2}(Cp*)] (3e). To an oven-dried and cooled 125-mL Schlenk flask, **1** (50 mg, 0.13 mmol) was dissolved in dry benzene (10 mL). After stirring for 15 min at room temperature, oxalyl chloride (64 mg, 44 µL, 0.51 mmol) and DMF (5 µL) were added. The reaction mixture was stirred for 3 h. The resultant yellow solution was evaporated completely under high vacuum at 40 °C. Without further purification of diacid chloride, dry dichloromethane (20 mL) was added through a syringe, followed by 1,4-dimethoxybenzene (20 mg, 0.14 mmol) and anhydrous aluminum chloride (70 mg, 0.52 mmol). The reaction mixture was refluxed for 2 h. The reaction was quenched with 2 M solution of NaOH (5 mL) and the product was extracted with ethyl ether (2 x 10 mL). Combined ether extracts were dried over $MgSO_4$, filtered, and volatiles were removed *in vacuo.* The crude product was chromatographed on silica with ethyl ether as eluent. The ^{1}H NMR analysis of the first band showed

the formation of mono acylated product (7 mg, 11%) as a yellow powder. The second band was collected and solvents were evaporated to give **3e** (26 mg, 41.3%) as an orange solid. **Mp**: 276–278 °C. **^{1}H NMR (400 MHz, $CDCl_3$, ppm):** δ 1.57 (s, 15H, Cp*), 3.89 (s, 6H, OCH_3), 4.73 (t, 1H, ^3J = 2.6 Hz, CHC*H*CH), 5.01 (d, 2H, ^3J = 2.6 Hz, C*H*CHC*H*), 7.20 (s, 2H, Ar). **$^{13}C\{^1H\}$ NMR (100 MHz, $CDCl_3$, ppm):** δ10.5 (Cp* *C*H_3), 57.8 (O*C*H_3), 74.4 (*C*HCH*C*H), 79.5 (CH*C*HCH), 83.7 (*CC*, Cp) 88.7 (ring, Cp*), 120.8 (*C*H, Ar), 125.3 (*CC*, Ar), 155 (*C*-OCH_3), 185.4 (C=O). **IR (ATR, cm^{-1}):** 1646 (C=O), 1564 (C=C). **MS (EI):** m/z 492 (M^+), 477 (M^+ - CH_3).

Synthesis of [Ru{η^5-$C_5H_3(CO)_2C_5H_3$(Fc)-1,2}(Cp*)] (4). To an oven-dried and cooled 125-mL Schlenk flask, **1** (50 mg, 0.13 mmol) was dissolved in dry benzene (10 mL). After stirring for 15 min at room temperature, oxalyl chloride (64 mg, 44 µL, 0.51 mmol) and DMF (5 µL) were added. The mixture was stirred for 3 h at room temperature. The resultant yellow solution was evaporated completely under high vacuum at 40 °C. Without further purification of diacid chloride was dry dichloromethane (5 ml) and ferrocene (20 mg, 0.14 mmol) and anhydrous aluminum chloride (70 mg, 0.52 mmol) were added at once. The reaction mixture was stirred for 2 h at room temperature, quenched with 2 M aqueous NaOH (5 mL), and the product was extracted with ethyl ether (2 x 10 mL). Combined ether extracts were dried over $MgSO_4$, filtered, and volatiles were removed *in vacuo.* The crude product was chromatographed on alumina with dichloromethane:hexane (3:1) as eluent. A red band was found to contain the desired product **4** (26 mg, 36%) as a red solid. **Mp**: 220–222 °C. **^{1}H NMR (400**

MHz, $CDCl_3$, ppm): δ 1.56 (s, 15H, Cp*), 4.23 (s, 5H, Cp unsubstituted), 4.79 (t, 1H, ^3J = 2.8 Hz, RuCHC*H*CH), 4.84 (t, 1H, ^3J = 2.8 Hz, FeCHC*H*CH), 5.11 (d, 2H, ^3J = 2.8 Hz, RuC*H*CHC*H*), 5.16 (d, 2H, ^3J = 2.8 Hz, FeC*H*CHC*H*). **$^{13}C\{^1H\}$ NMR (100 MHz, $CDCl_3$, ppm):** δ 10.4 (Cp* *C*H_3), 70.7 (Fe*C*HCH*C*H), 72.7(FeCH*C*HCH), 74.2 (Fe*CC*), 74.7 (Ru*C*HCH*C*H), 77.4 (Cp unsubstituted), 79.6 (RuCH*C*HCH) 84.9 (Ru*CC*), 88.5 (ring, Cp*), 190.7 (C=O). **IR (ATR, cm^{-1}):** 1643 (C=O). **MS (EI):** m/z 540 (M^+). **^1H NMR (400 MHz, CF_3COOD, ppm):** δ 1.52 (s, 15H, Cp*), 4.49 (s, 5H, Cp), 5.38 (t, 1H, ^3J = 2.8 Hz, RuCHC*H*CH), 5.65 (t, 1H, ^3J = 2.8 Hz, FeCHC*H*CH), 5.68 (d, 2H, ^3J = 2.8 Hz, RuC*H*CHC*H*), 5.75 (d, 2H, ^3J = 2.8 Hz, FeC*H*CHC*H*). **$^{13}C\{^1H\}$ NMR (100 MHz, CF_3COOD, ppm):** δ 9.8 (Cp* *C*H_3), 77.1 (Fe*C*HCH*C*H), 78.2 (Cp unsubstituted), 79.4 (FeCH*C*HCH), 80.2 (Fe*CC*), 83.5 (Ru*C*HCH*C*H), 86.2 (RuCH*C*HCH) 89.1 (Ru*CC*), 96.0 (ring, Cp*), 197.6 (C=O).The solution is evaporated to dryness and triturated with pentane to obtain dark solid and ^1H NMR was taken in $CDCl_3$. **^1H NMR (400 MHz, $CDCl_3$, ppm):** 1.55 (s, 15H, Cp*), 4.27 (s, 5H, Cp), 4.87 (br, 1H, RuCHC*H*CH), 4.95 (br, 1H, FeCHC*H*CH), 5.18 (br, 2H, RuC*H*CHC*H*), 5.24 (br, 1H, FeCHC*H*CH). **IR (ATR, cm^{-1}):** 3388 (br, OH), 1651 (CO).

Synthesis of [Ru{η^5-$C_5H_3(CHOH)_2C_6H_3CH_3$-1,2}(Cp*)] (5). To an oven-dried and cooled 125-mL Schlenk flask, **3b** (100 mg, 0.22 mmol) was dissolved in 10 mL of THF. The mixture was cooled to 0 °C and $LiAlH_4$ (42 mg, 1.1 mmol) was added. The color of the solution slowly faded from orange to almost colorless. The reaction mixture was stirred for 2 h at room temperature and quenched with water (30 mL). The layers were separated and the aqueous

phase was extracted with ethyl ether (3 x 10 mL). The combined organic extracts were dried over $MgSO_4$, filtered and volatiles were removed *in vacuo*. Trituration with cold pentane gave **5** (68 mg, 67.8%) as a light yellow powder. **Mp**: 160-162 ˚C **^{1}H NMR (400 MHz, $CDCl_3$, ppm):** δ 1.67 (s, 15H, Cp*), 2.37 (s, 3H, PhC*H*$_3$), 4.18 (t, 1H, ^{3}J = 2.4 Hz, CHC*H*CH), 4.10 (d, 2H, ^{3}J = 2.4 Hz, C*H*CHC*H*), 5.09 (d, 2H, ^{2}J = 12 Hz, C*H*OH), 7.18 (d, 1H, ^{3}J = 8 Hz, Ph), 7.50 (s, 1H, Ph), 7.56 (d, 1H, ^{3}J = 8 Hz, Ph), OH peaks were invisible in proton NMR. ^{13}C**{^{1}H} NMR (100 MHz, $CDCl_3$, ppm):** δ 12.3 (Cp* CH_3), 21.4 (Ph*C*H$_3$), 64.1, 64.2 (*C*H$_2$OH), 69.8 (*C*HCH*C*H), 74.0 (CH*C*HCH), 86.1 (Cp* ring), 94.3, 94.5 (*CC*), 126.6, 127.1, 128.1 (Ar, substituted), 135.2, 136.9, 137.9 (Ar, unsubstituted). **IR (KBr, thin film, cm^{-1}):** 3473 (br, OH).

Synthesis of [Ru{η^5-C_5H_3(COCHOH)$C_6H_3CH_3$-1,2}(Cp*)] (6). To a suspension of 29% ammonium hydroxide (5 mL), zinc powder (250 mg, 3.82 mmol), and copper sulfate (7 mg, 0.028 mmol), **3b** (30.0 mg, 0.067 mmol) in toluene (5 mL), was added. The mixture was heated at 50-60 °C for 5 h in a sealed tube. TLC analysis of the product shows the almost similar R_f value as the starting material with slightly different color. The reaction mixture was cooled to room temperature and the product was extracted with ethyl ether (2 x 20 mL). The organic phase was dried over $MgSO_4$, and the volatiles were removed *in vacuo*. The crude product was triturated with cold pentane to give **6** (21 mg, 69%) as a yellow powder. Analytically pure product was obtained by slow evaporation of concentrated ethyl ether solution in a stream of nitrogen saturated with hexane. **Mp:** melting point was not noticeable as material sublimes before

melting. **^{1}H NMR (400 MHz, $CDCl_3$, ppm):** δ 1.57 (s, 15H, Cp*), 2.41 (s, 3H, Ph*C*H_3), 4.52 (t, 1H, ^{3}J = 2.4 Hz, CHC*H*CH), 4.83–4.84 (m, 1H, C*H*CHC*H*), 4.90–4.91 (m, 1H), 5.19(d, 2H, ^{2}J = 12 Hz, C*H*OH), 7.19 (d, 2H, ^{3}J = 8.0 Hz, Ph), 7.53 (s, 2H, Ph), 8.02 (d, 2H, ^{3}J = 8 Hz, Ph). The OH proton was exchanged with water present in $CDCl_3$ broadening its peak. **^{13}C{^{1}H} NMR (50 MHz, $CDCl_3$, ppm):** δ 11.0 (Cp* CH_3), 21.9 (Ph*C*H_3), 63.7 (*C*HOH), 71.6, 73.5 (*C*HCH*C*H), 76.6 (CH*C*HCH), 87.2 (Cp*, ring), 97.2, 101.4 (*ipso* Cp), 126.4 128.5, 128.8 (Ph unsubstituted), 132.9, 142.7, 143.7 (Ph substituted), 184.7 (CO). **IR (KBr, cm^{-1}):** 3413 (OH), 1629 (CO). **MS (EI):** m/z 448 (M^+), 430 (M^+-H_2O). The X-ray diffraction of the crystal structure was solved, confirming the proposed molecular structure, but full refinement was not possible because of its structural disorder (Figure 4.3).

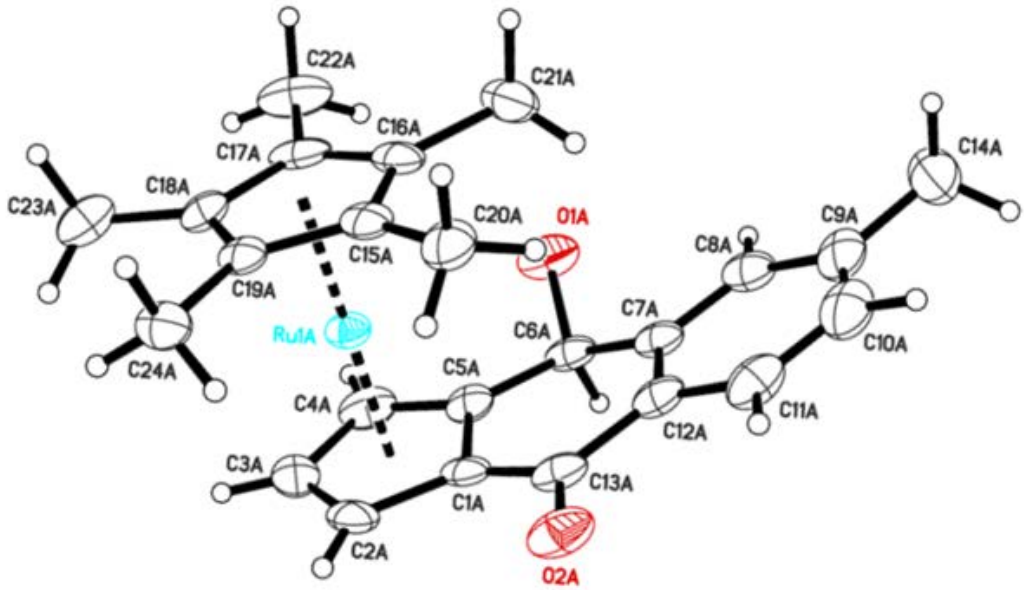

Figure 4.3. Disordered molecular structure of [Ru{η^5-C_5H_3(COCHOH)$C_6H_3CH_3$-1,2}(Cp*)] **(6)**

Synthesis of [Ru{η^5-$C_5H_3(CO)_2C_6H_4(OH)_2$-1,2}(Cp*)] (7). To an oven-dried and cooled 125-mL Schlenk flask, **3e** (50 mg, 0.10 mmol) was dissolved in dry dichloromethane (10 mL) and anhydrous $AlCl_3$ (50 mg, 0.41 mmol) was added in it. The reaction mixture was stirred at room temperature for 2 h, quenched with water (20 mL), and layered with dichloromethane. The aqueous phase was found to be deep purple, which changed to pink on acidification with conc. HCl (3 mL). The product was extracted with dichloromethane (2 X 10 mL), dried over $MgSO_4$, filtered, and volatiles were removed *in vacuo.* The crude product was chromatographed on silica with ethyl ether as eluent. Evaporation of solvents to dryness gave **7** (38 mg, 81%) as a pink solid. **Mp**: 238–240 °C. **^{1}H NMR (400 MHz, $CDCl_3$, ppm):** δ 1.55 (s, 15H, Cp*), 4.98 (t, 1H, ^{3}J = 2.6 Hz, CHC*H*CH), 5.27 (d, 2H, ^{3}J = 2.6 Hz, C*H*CHC*H*), 7.09 (s, 2H, Ar), 12.93 (s, 2H, OH). **^{13}C{^{1}H} NMR (100 MHz, $CDCl_3$, ppm):** δ 10.0 (Cp* *C*H_3), 75.5 (*C*HCH*C*H), 81.4 (CH*C*HCH), 81.9 (*CC*, Cp), 88.5 (ring, Cp*), 114.3 (*CC*, Ar), 127.6 (*C*H, Ar), 156.5 (*C*-OH), 190.0 (C=O). **IR (ATR, cm^{-1}):** 3500–2500 (br, OH), 1595 (C=O). **MS (EI):** m/z 492 (M^+), 477 (M^+ - CH_3).

4.1.2. Results and Discussion

4.1.2.1 Synthesis. The quinone complexes, **3a-e** and **4** were synthesized in two-step reactions starting from 1',2',3',4',5'-pentamethylruthenocene-1,2-dicarboxylic acids without isolation of the intermediate product.[78] The first step involves the generation of pentamethylruthenocene-1,2-diacyl chloride **2** by treatment of dicarboxylic acid, **1**

with oxalyl chloride in the presence of catalytic amount of DMF by following the modified procedure of Zhang *et al*.[96] The second step involves the removal of volatiles from the reaction mixture and treatment of diacyl chlorides with benzene, toluene, *o*-xylene, *p*-dimethoxybenzene, and ferrocene (Scheme 4.2) in the presence of aluminum chloride to give "acenequionone" complexes, **3a–e** (42–58%) and **7** (36%) respectively. The second step of the reaction requires a rigorously dry reaction conditions. The acylation of benzene, toluene and *o*-xylene were done *neat* while for *p*-dimethoxybenzene and ferrocene, dichloromethane was used as a solvent. Whereas toluene gives a single product (**3b**), ^{1}H NMR shows that *o*-xylene gives two inseparable isomers (**3c–d**) in a 1:1 ratio, implying that the arene undergoes electrophilic substitution first *para* to an activating substituent, followed by an indiscriminate second acylation (Scheme 4.3).

The reduction of the quinone **3b** using $LiAlH_4$ in THF at room temperature gave diol **5** in 68% isolated yield. Appearance of a doublet (δ 5.09 ppm, J = 12 Hz) in ^{1}H NMR and a broad band centered at 3473 cm^{-1} on IR indicates the formation of alcohol. The ^{1}H and ^{13}C NMR of the product reveals the formation of only one isomer, most probably the *endo* diol, caused by the *exo* attack of hydride to avoid the steric interaction of bulky Cp* ligand. Our attempt to dehydroxylate **5** using Sn^{2+}/HCl[20] gave a mixture of intractable products. In another attempt of reduction of quinone **3b**, we used zinc and ammonium hydroxide[129] in toluene as a cosolvent. The reduction of quinone **3b** stops at mono-keto-alcohol even with sealed-tube heating at 60-70 °C for 5 h, giving **6** in

69% yield. The product shows similar R_f value of starting quinone in TLC with lighter color. The crystallographic analysis of the product shows the position of OH group *endo* with respect to Ru center (Figure 4.3).

Scheme 4.2. Synthesis of acene-quinone complexes of ruthenium and their derivatives

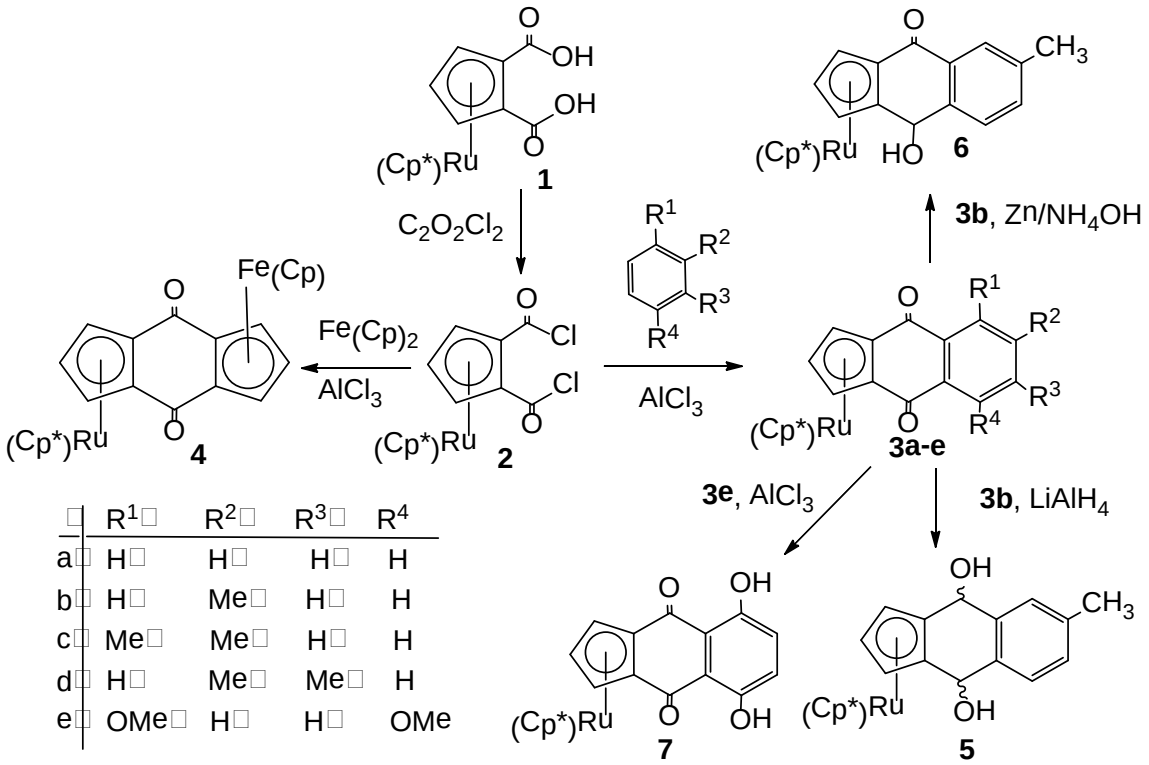

	R^1	R^2	R^3	R^4
a	H	H	H	H
b	H	Me	H	H
c	Me	Me	H	H
d	H	Me	Me	H
e	OMe	H	H	OMe

In an attempt to homologate dimethoxyquinone **3e** by use of pentamethylruthenium-1,2-diacyl chloride in the presence of aluminum chloride, we obtained demethylated quinone **7** in 81% yield. We rationalize the results of demethylation of quinone on the basis of strong chelation of O-atoms of ketone and methoxy group with Al^{3+} ion forming a stable six-membered ring. Our assumption was corroborated by very good solubility of the resultant complex in

water. The isolation of the complex **7** was possible only by maintaining the pH of aqueous solution in a range of 1-2. The disappearance of the methyl singlet and appearance of the hydrogen-bonded phenolic singlet at 12.93 ppm in ^{1}H-NMR indicated the demethylation of quinone **3e**.

Scheme 4.3. Mechanism showing selectivity of *o*-xylene for double acylation

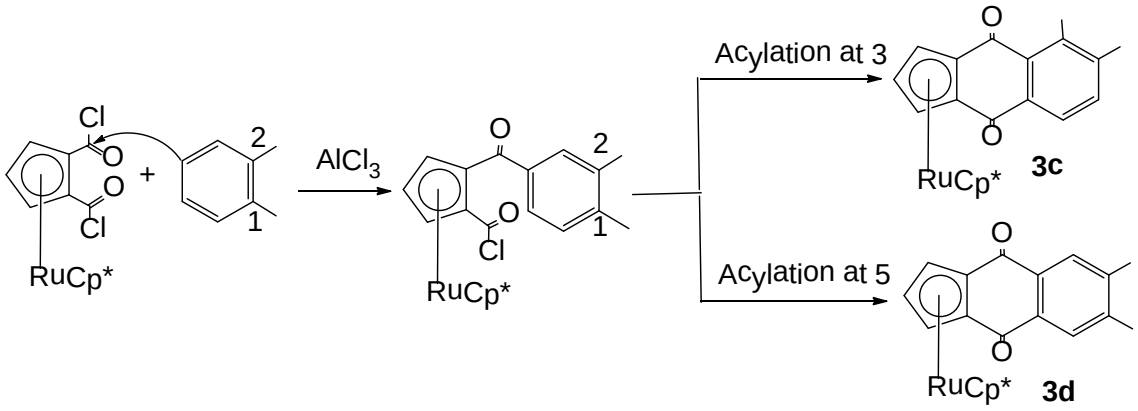

To examine the basic nature of the carbonyl oxygen atom alpha to both pentamethylruthenocene and ferrocene moieties, we dissolved quinone complex **4** in deuterated trifluoroacetic acid and observed the shifts of proton and carbon resonances in NMR conditions. The complex gives deep blue color while dissolved in deuterated trifluoroacetic acid. The color change was accompanied by downfield shifts in ^{1}H and ^{13}C resonances of the complex. The quinone-fused cyclopentadienyl resonances were found to be shifted to downfield up to 0.81 ppm (in $CDCl_3$) in comparison to the resonance before acidification. Similarly, the quinone-fused Cp carbon resonances were found to be shifted up to 8.8 ppm to downfield. To see if this is due to the solvent effect, the volatiles were removed *in vacuo* and the resultant dark-blue solid was redissolved in $CDCl_3$, we found shifts up to 0.11 ppm to downfield. The shifts was, however, not significant in case of

proton and carbon resonances of unsubstituted Cp of ferrocene and Cp* of ruthenocene moieties. The similar result was observed by Sato *et. al.* on binuclear ruthenium complexes.[130] The results of downfield shifts of proton and carbon resonances can be explained on the basis of delocalization of positive charge, generated during acidification, to different centers as shown in Scheme 4.4. Retaining of diamagnetism even after acidification reveals that the positive charge is localized on the carbonyl carbon rather than metal center. The observation is also supported by the presence of C=O (1651 cm^{-1}) and O-D (3388 cm^{-1}) bands in IR spectra of acidified product.

Scheme 4.4. Resonating structures of bimetallic quinone complex after acidification

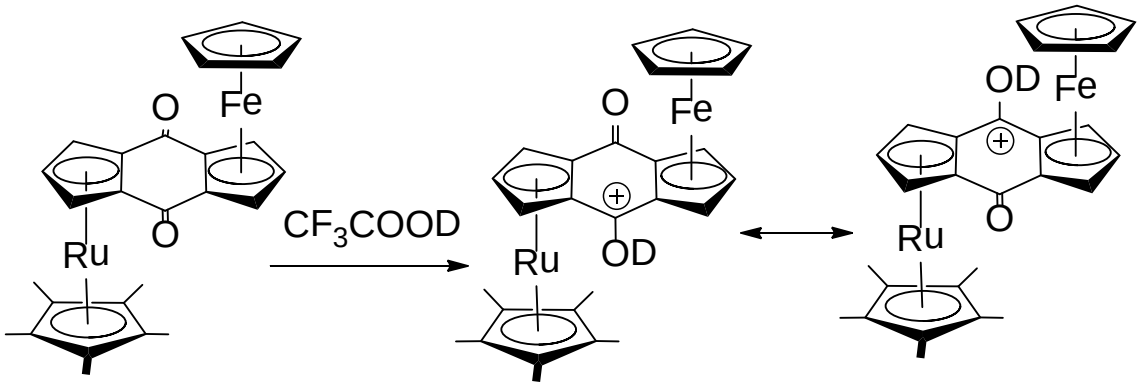

4.1.2.2. Spectroscopy. All new complexes were characterized with ^{1}H and ^{13}C NMR, IR and mass spectroscopy. The selected ^{1}H and ^{13}C NMR resonances and IR of complexes **3a-7** are shown in Table 4.1. All quinones and their derivatives display a sharp singlet ranging from δ 1.49 to 1.67 ppm integrating 15H in the ^{1}H NMR and 10.0 to 11.0 ppm in ^{13}C NMR showing the complexation of Cp*. Similarly, ring carbons of Cp* ligand appear in range of 87.2

to 89.1 which is in close range of the halosubstituted pentamethylruthenocene.[131] The carbon resonances of quinone-fused Cp was assigned by comparing the chemical shift values of complex **3b** in which carbon at 1,2- and 3,5-positions of Cp exhibit slightly different resonances and hence are distinguishable in ^{13}C NMR. The chemical shifts of proton and carbon resonances of hetero-nuclear complex, **4** display that peaks corresponding to quinone-fused Cp of ruthenocene appear to lower ppm than the analogous signals of ferrocene revealing the better electron-donation of pentamethylcyclopentadienylruthenium than cyclopentadienyliron.

Table 4.1. Selected ^{1}H NMR and ^{13}C NMR (ppm) data in $CDCl_3$ and IR data of complexes **3a-7**

	δ_H			δ_C						IR (cm^{-1})
	Cp*	CHC *H*CH	C*H*C HC*H*	Cp*$_{ring}$	Cp*$_{Me}$	*C*HC H*C*H	CH*C* HCH	*CC*	*C*O	CO
3a	1.49	4.91	5.24	89.1	10.1	75.4	80.5	82.7	184.8	1650
3b	1.51	4.89	5.23	88.9	10.1	75.2 75.3	80.3	82.7 82.8	184.8 185.1	1656
3e	1.57	4.73	5.01	88.7	10.5	74.4	79.5	83.7	185.4	1656
4	1.56	4.79	5.11	88.5	10.4	74.7	79.6	84.9	190.7	1643
5	1.67	4.18	4.10	86.1	12.3	69.8	74.0	94.3	-	-
6	1.57	4.52	4.83 4.90	87.2	11.0	71.6 73.5	76.6	97.2 101.4	184.7	1629
7	1.55	4.98	5.27	88.5	10.0	75.5	81.4	81.9	-	-

The quinone-fused Cp shows a triplet (δ 4.18-4.98 ppm) and a doublet (δ 5.01-5.24 ppm) resonance in a 1:2 ratio in ^{1}H NMR with coupling constant of ca. 2.8 Hz. The 3,5-Cp protons of **3b** appear as doublet in ^{1}H NMR but ^{13}C NMR shows the two different resonances showing dissymmetry of the ligand. Similar

dissymmetry has been observed in complex **6** as well. The Cp carbon resonance for the quinones **3a**–**e** and their derivatives **4**–**7** consist of a set of three resonances attributed to inner position (74.0–81.4 ppm, CH*C*HCH), the outer positions (69.8–75.5 ppm, *C*HCH*C*H), and the quaternary positions (81.9–101.4 ppm, *CC*). The ketone carbons display resonances between 184.7 and 190.7 ppm, typical of organic carbonyls. The IR stretching of the carbonyl group is of all complexes ranges generally less than 9,10 anthraquinone (e.g. 1660 cm^{-1}). This is due to electron-releasing effect of the metallocene to carbonyl carbon.[132,133] More importantly, the ketone group doubly activated with metallocene in **6** stretches at very low energy (e.g.1629 cm^{-1}). The mass spectra of all complexes show stable molecular ion peak.

4.1.3.3. Electrochemistry. Cyclic voltammetry of [Ru{η^5-$C_5H_3(CO)_2C_6H_4$-1,2}(Cp*)] **3a**, [Ru{η^5-$C_5H_3(CO)_2C_6H_3CH_3$-1,2}(Cp*)] **3b** and [Ru{η^5-$C_5H_3(CO)_2C_5H_3$(Fc)-1,2}(Cp*)] **4** was carried out at room temperature under nitrogen at 25-50 mV s^{-1} in a 0.1 M (Bu_4NPF_6/CH_2Cl_2) solution as the supporting electrolyte. The voltammograms for complexes **3a**, **3b** and **4** are exhibited in Figures 4.4-4.6 with peak numbers to show the direction of scan. The electrochemical data are summarized in Table 4.2-4.3. The half-wave potentials of each oxidation ($E^0_{1/2,ox}$) and reduction ($E^0_{1/2,red}$) wave were calculated by averaging the corresponding anodic (E_{pa}) and cathodic (E_{pc}) peak potentials. The mononuclear ruthenium quinone complexes, **3a** and **3b** show irreversible wave towards oxidation at 1174-1251 mV. The non-reversible features in the CV of ruthenocene capped quinone may suggest that oxidation of the molecule is

followed by a chemical reaction. Similarly, the hetero-binuclear complex, **4** showed two quasi-reversible waves towards oxidation showing the redox activity of two metal centers.

Diaz and Mueller-Westerhoff established from the studies of electrochemistry of [1.1]metallocenophanes that hetero binuclear iron/ruthenium system exhibits ferrocene-centered reversible one-electron oxidation at lower potential and a ruthenocene- centered irreversible two-electron oxidation at higher potential.[134] The heterometallic complex exhibit a large separation between $0/1^+$ and $1^+/2^+$ redox wave suggesting substantial delocalization of charge. By comparison with nature of wave and peak potential of complex **3a** and **3b**, we can assign the peak 1 and 4 to the oxidation of ferrocenyl moiety and peak 2 and 3 to the oxidation of ruthenocenyl moiety of complex **4** (Figure 4.6). The electrochemical data reveals that the ferrocenyl moiety gave quasi-reversible redox potential ($E_{1/2}$ = 952 mV), indicated by the i_{pa}/i_{pc} ratio of 0.79. Similarly, ruthenocenyl moiety display another quasi-reversible redox potential ($E_{1/2}$ = 1242 mV), indicated by the i_{pa}/i_{pc} ratio of 1.98. The peak separation ($\Delta E = E_{pa}–E_{pc}$) for ferrocenyl and ruthenocenyl moiety are 190 mV and 163 mV respectively. The oxidation potential of ruthenocenyl moiety in complex **4** is found to be higher than that of complex **3a** and **3b** which might be due to the electronic interaction of mixed-valance states of intramolecular electron transfer process.

Unlike anthraquinone and 2-methylanthraquinone,[135] reduction of complexes **3a** and **3b** show only one reversible wave with half reduction potential centered at -1415 mV and -1403 mV, respectively showing one electron

reduction. However, there is a small broadening at the beginning of reduction of both quinone complexes. The higher negative value of metallocene-fused quinone complexes in comparison to anthraquinone (-911 mV) might be due to the electron releasing effect of pentamethylruthenocene moiety. The ratio of current (i_{pa}/i_{pc}) in both complexes is found to be very close to unity indicating the reversibility of the process. The difference in anodic and cathodic peak in **3a** and **3b** was found to be 133 mV and 111 mV respectively. The complex gives irreversible wave with anodic peak centered at 1649 mV. The differential pulse voltammetry of the complex gave a broad peak centered at -1764 mV. The higher negative value of reduction of quinone might be due to the electron-releasing effects of metallocene moieties on both sides of the carbonyl groups.

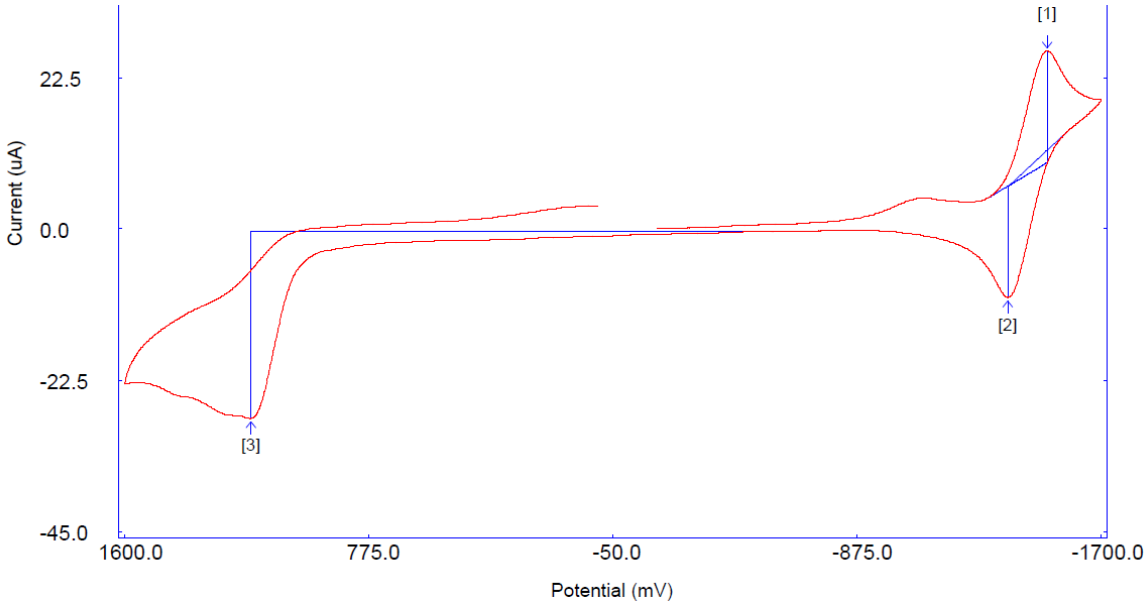

Figure 4.4. Cyclic voltammogram of [Ru{η^5-$C_5H_3(CO)_2C_6H_4$-1,2}(Cp*)] (3a) vs. Ag/Ag+ in 0.1 M Bu_4NPF_6/CH_2Cl_2 at scan rate of 50 mV/sec

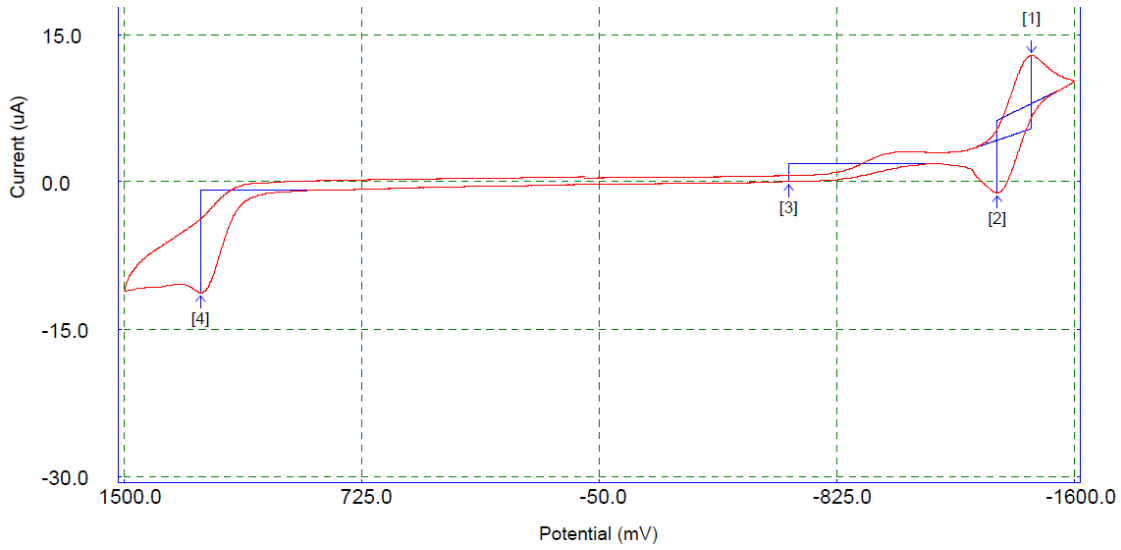

Figure 4.5. Cyclic voltammogram of [Ru{η^5-$C_5H_3(CO)_2C_6H_3CH_3$-1,2}(Cp*)] **(3b)** *vs.* Ag/Ag^+ in 0.1 M Bu_4NPF_6/CH_2Cl_2 at scan rate of 25 mV/sec

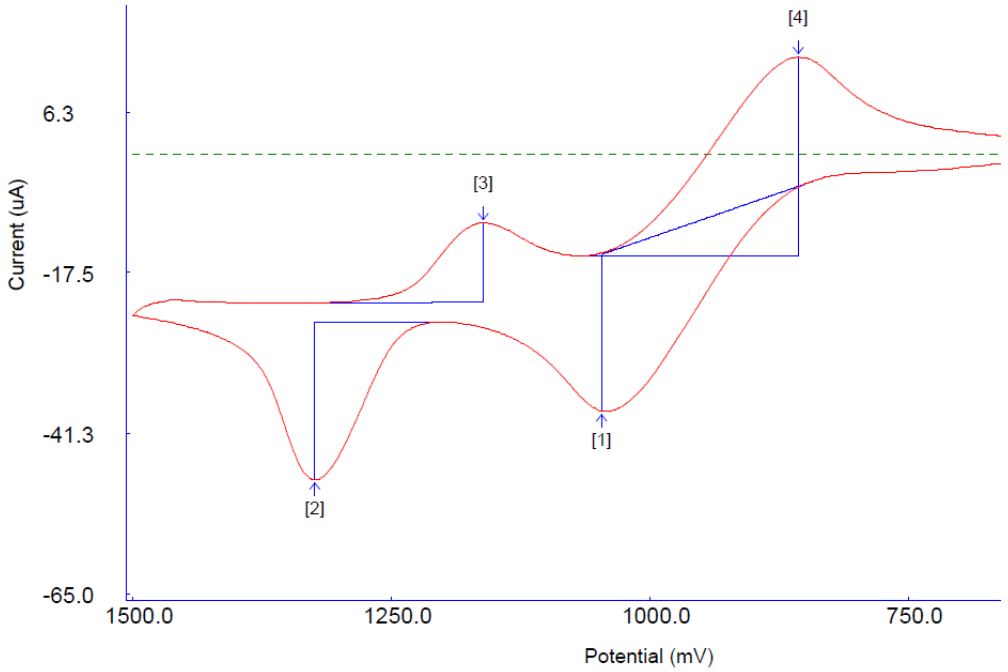

Figure 4.6. Cyclic voltammogram of [Ru{η^5-$C_5H_3(CO)_2C_5H_3$(Fc)-1,2}(Cp*)] **(4)** *vs.* Ag/Ag^+ in 0.1 M Bu_4NPF_6/CH_2Cl_2 at scan rate of 50 mV/sec

Table 4.2. Electrochemical data of complexes **3a**, **3b** and **4** showing oxidation

Comp		E_{pa}	E_{pc}	$E^0_{1/2, Ox}$	i_{pa}	i_{pc}	i_{pa}/ i_{pc}
3a	Ru(II)/Ru(III)	1174	-	-	27.84	-	-
3b	Ru(II)/Ru(III)	1251	-	-	10.43	-	-
4	Fe(II)/Fe(III)	1047	857	952	23.45	29.43	0.79
	Ru(II)/Ru(III)	1324	1161	1242	23.29	11.74	1.98

Table 4.3. Electrochemical data of complexes **3a**, **3b** and **4** showing reduction

Comp	E_{pa}	E_{pc}	ΔE	$E^0_{1/2, Red}$	i_{pa}	i_{pc}	i_{pa}/ i_{pc}
3a	-1385	-1518	133	-1415	16.44	16.68	0.98
3b	-1348	-1459	111	-1403	7.35	7.39	0.99
4	-1649	-		-	-	14.65	-

4.1.3.4. Structure. The structures of [Ru{η^5-$C_5H_3(CO)_2C_6H_4$-1,2}(Cp*)] (**3a**), [Ru{η^5-$C_5H_3(CO)_2C_6H_3CH_3$-1,2}(Cp*)] (**3b**), and [Ru{η^5-$C_5H_3(CO)_2C_5H_3$(Fc)-1,2}(Cp*)] (**4**) were determined by X-ray crystallographic methods. The crystals for which data were collected were typical of the others in the batch, which had been grown by slow evaporation from solvent at room temperature. These crystals were mounted on glass fibers with Paratone N oil. Data were collected at 90 K on a Nonius KappaCCD diffractometer. The main programs used were DENZO-SMN to obtain cell parameters and for data reduction, SCALEPACK for absorption correction,[136] SHELXS-86 for structure solution, and SHELXS-97 for refinement. Hydrogen atoms were placed in geometrically calculated positions. Plots of [Ru{η^5-$C_5H_3(CO)_2C_6H_4$-1,2}(Cp*)] (**3a**), [Ru{η^5-$C_5H_3(CO)_2C_6H_3CH_3$-

1,2}(Cp*)] (**3b**), and [Ru{η^5-$C_5H_3(CO)_2C_5H_3$(Fc)-1,2}(Cp*)] (**4**) are shown in Figures 4.7, 4.8, and 4.9. The crystal structure of the complex **3b** showed whole-molecule disorder with duplication of structural parameters. Crystal structure and refinement data for compounds **3a**, **3b** and **4** can be found on Table 4.4. Bond distances and angles for **3a**, **3b**, and **4** can be found in Tables 4.5–4.7.

The pentamethylruthenocene moiety in all complexes and ferrocene moiety in **4** exhibit a typical metallocene geometry with both Cp and Cp* ligands coordinated with the metal center with pentahapto(η^5-coordination). The distances of centroids of quinone-fused Cp and Cp* with ruthenium center are as follows: [**3a**, 1.817 Å, 1.804 Å; **3b**, 1.834, 1.797 Å; **4**, 1.795 Å, 1.824 Å]. Similarly, the distances of iron from the centroids of quinone-fused Cp and free Cp are 1.690 Å and 1.857 Å respectively. In mononuclear quinone complexes, **3a** and **3b**, the positive inductive effects of pentamethylcyclopentadienyl and negative inductive effects of three carbonyls can be the responsible factors for those bonding variations. However, the distance of centroids from the metal in hetero-binuclear quinone, **4** exhibits the opposite effects due to the unusual bonding mode of metal center with *ipso* carbons of two metal centers with quinone-fused Cp. In all three complexes Ru center inclines towards the *ipso* carbons, the difference in average distance of *ipso* carbons from that of remaining three carbons of quinone-fused Cp ranges from 0.026 Å in **3a** to 0.084 Å in **4**. This type of asymmetry in the bonding pattern of carbon atoms was observed by Gassman *et al.* in their study of (η^5- pentamethylcyclopentadienyl) (η^5-acetylcyclopentadienyl) ruthenium (II).[38] The iron center, on the other hand, in **4** shows opposite effect

with negative distortion of 0.079 Å. The angle between overall bending of quinone ligand at *ipso* carbons towards Ru center in **3a** and **3b** are 6.56° and 7.17° respectively.

One possibility of the asymmetric bonding pattern can be due to the delocalization of electrons from Cp ring to carbonyl carbon making fulvenoid structure of cyclopentadienyl ring as supported by the result of facile protonation of ketonic oxygen on anti-[1.1](2,18)(6,14)ruthenocenophan-1,13 dione by deuterated trifluoroacetic acid.[130] The evidence is further supported by the shorter bond distance of carbonyl carbon from ruthenocene moiety than from that of arene side. For instance, the average difference between in bond length in **3a** and **3b** was found to be 0.043 Å and 0.048 Å respectively. The difference in bond length in **4**, on the other hand, is not significant. This might be due to the effect of metallocene moieties on both sides of the carbonyl group in complex **4**. The low IR absorption frequency of C=O bond (1650 cm^{-1} in **3a**, 1646 cm^{-1} in **3b** and 1643 in **4**) of metallocene-fused quinone complexes in comparison to 9,10-anthraquinone (1660 cm^{-1}) also supports the fact of facile delocalization of Cp electrons to carbonyl carbon.

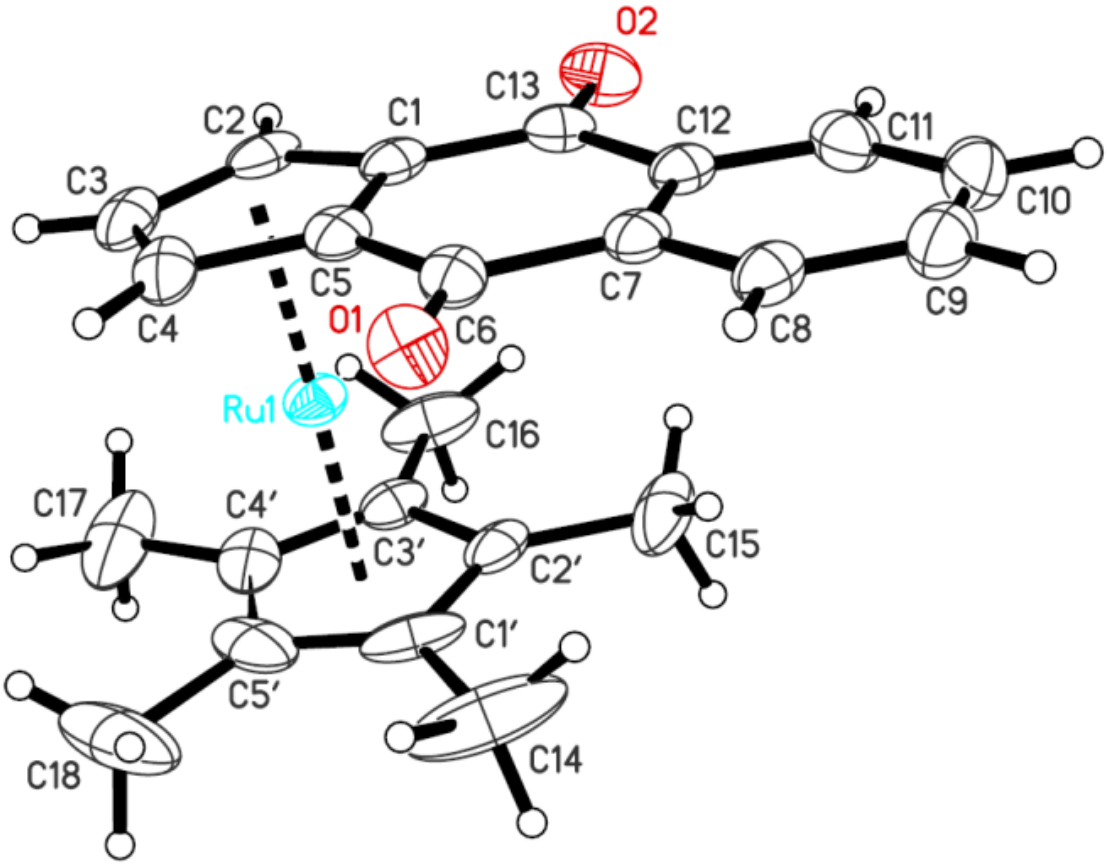

Figure 4.7. Molecular structure of [Ru{η^5-$C_5H_3(CO)_2C_6H_4$-1,2}(Cp*)] **(3a)**

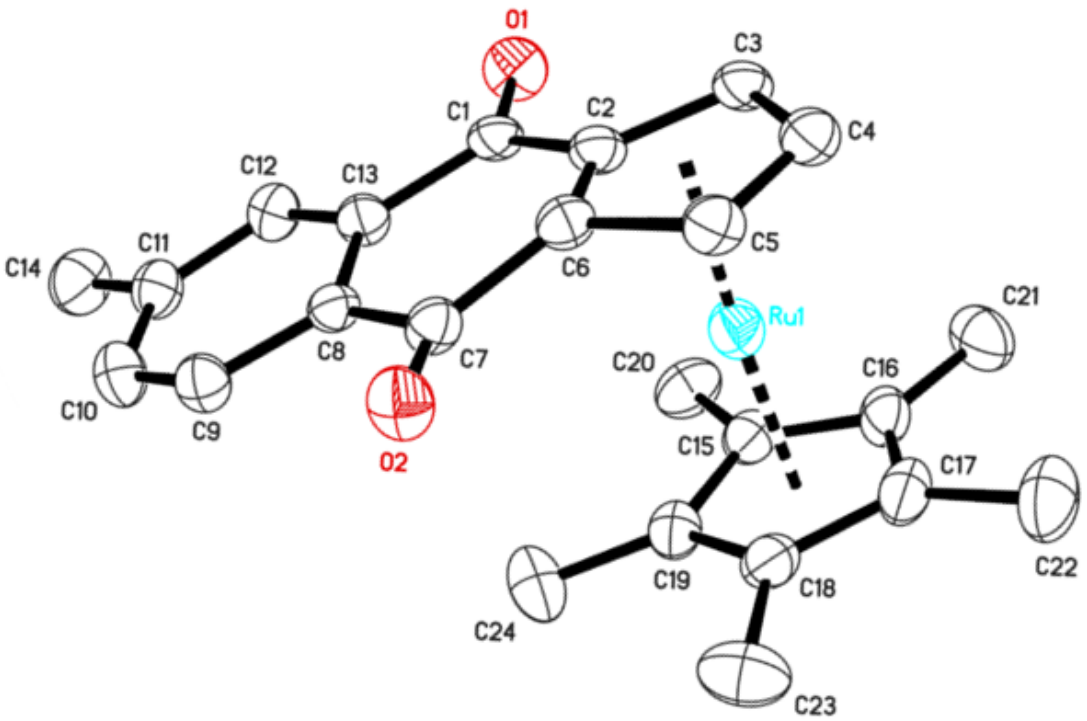

Figure 4.8. Molecular structure of [Ru{η^5-$C_5H_3(CO)_2C_6H_3CH_3$-1,2}(Cp*)] **(3b)**

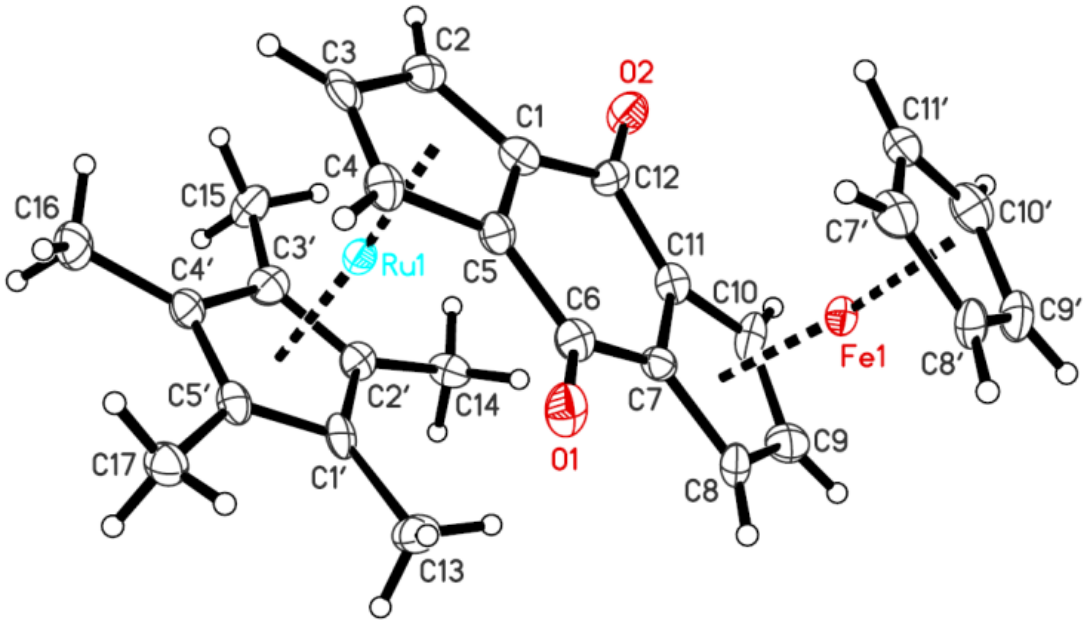

Figure 4.9. Molecular structure of [Ru{η5-C5H3(CO)2C5H3(Fc)-1,2}(Cp*)] **(4)**

Table 4.4. Crystal data and structure refinement for **3a**, **3b** and **6**

	3a	**3b**	**6**
Formula	$C_{23}H_{23.68}O_{2.84}Ru$	$C_{24.50}H_{25}O_{2.50}$ Ru	$C_{27}H_{26}FeO_2$ Ru
Formula wt (amu)	446.61	460.52	539.4
T, K	90.0(2)	90.0(2)	90.0(2)
Wavelength (Å)	0.71073	1.54178	1.54178
Crystal system, space group	Triclinic, *P-1*	Triclinic, *P-1*	Monoclinic, *P21*
a, Å	7.5391(15)	7.5341(3)	7.3554(3)
b, Å	8.2538(17)	8.3195(3)	11.1759(5)
c, Å	16.266(3)	17.1059(6)	12.9896(5)
α,(deg)	87.43(3)	89.140(2)	90
β, (deg)	86.56(3)	87.921(2)	92.167(2)
γ, (deg)	69.75(3)	68.982(2)	90
V, $Å^3$	947.6(3)	1000.20(6)	1067.02(8)
Z, d_{calc}, Mg/m^3	2, 1.565	2, 1.529	2, 1.679
Absorption coef μ (mm^{-1})	0.847	6.494	11.350
F(000)	457	472	548
Crystal size (mm^3)	0.20 x 0.13 x 0.03	0.08 x 0.08 x 0.03	0.16 x 0.10 x 0.08
2θ range (deg)	1.25 to 27.48	2.58 to 69.30	3.40 to 68.37
Limiting indices	$-9 \le h \le 9$, $-10 \le k \le 10$, $-21 \le l \le 21$	$-9 \le h \le 9$, $-9 \le k \le 9$, $0 \le l \le 20$	$-8 \le h \le 8$, $0 \le k \le 13$, $0 \le l \le 15$
Reflections collected / unique	23149 / 4348 [R(int) = 0.0368]	3595 / 3595 [R(int) = 0.0000]	17341 / 1965 [R(int) = 0.0740]
Absorption correction	Semi-empirical from equivalents	Semi-empirical from equivalents	Semi-empirical from equivalents
Max. and min. transmission	0.975 and 0.724	0.830 and 0.625	0.467 and 0.223
Refinement method	Full-matrix least-squares on F^2	Full-matrix least-squares on F^2	Full-matrix least-squares on F^2
Data/restraints/parameters	4348 / 0 / 260	3595 / 248 / 375	1965 / 421 / 286
Goodness-of-fit on F^2	1.040	1.356	1.101
Final R indices [I>2sigma(I)]	R_1 = 0.0340, wR_2 = 0.0794	R_1 = 0.0719, wR_2 = 0.1920	R_1 = 0.0665, wR_2 = 0.1958
R indices (all data)	R_1 = 0.0442, wR_2 = 0.0842	R_1 = 0.0751, wR_2 = 0.1936	R_1 = 0.0667, wR_2 = 0.1960
Largest diff. peak and hole, $e.A^{-3}$	1.496 and -0.828	1.146 and -1.796	1.186 and -2.479

Table 4.5. Bond lengths [Å] and angles [°] for **3a**

Ru1-C3'	2.161(3)
Ru1-C4'	2.164(3)
Ru1-C1	2.164(3)
Ru1-C2'	2.180(3)
Ru1-C5	2.180(3)
Ru1-C5'	2.182(3)
Ru1-C1'	2.184(3)
Ru1-C2	2.189(3)
Ru1-C3	2.202(3)
Ru1-C4	2.204(3)
O1-C6	1.225(3)
O2-C13	1.223(3)
C1-C2	1.435(4)
C1-C5	1.443(4)
C1-C13	1.464(4)
C2-C3	1.426(4)
C3-C4	1.420(4)
C4-C5	1.436(4)
C5-C6	1.457(4)
C6-C7	1.500(4)
C7-C8	1.401(4)
C7-C12	1.406(4)
C8-C9	1.379(4)
C9-C10	1.380(5)
C10-C11	1.390(4)
C11-C12	1.389(4)
C12-C13	1.508(4)
C1'-C5'	1.426(5)
C1'-C2'	1.437(5)
C1'-C14	1.494(5)
C2'-C3'	1.424(4)
C2'-C15	1.491(5)
C3'-C4'	1.426(4)
C3'-C16	1.502(4)
C4'-C5'	1.423(5)
C4'-C17	1.503(5)
C5'-C18	1.504(5)
C3'-Ru1-C4'	38.51(12)
C3'-Ru1-C1	120.33(11)
C4'-Ru1-C1	149.83(13)
C3'-Ru1-C2'	38.29(11)

C4'-Ru1-C2'	64.39(11)
C1-Ru1-C2'	113.94(11)
C3'-Ru1-C5	153.99(11)
C4'-Ru1-C5	167.48(11)
C1-Ru1-C5	38.81(10)
C2'-Ru1-C5	124.79(11)
C3'-Ru1-C5'	64.04(12)
C4'-Ru1-C5'	38.22(14)
C1-Ru1-C5'	171.30(13)
C2'-Ru1-C5'	64.15(12)
C5-Ru1-C5'	134.32(12)
C3'-Ru1-C1'	64.08(11)
C4'-Ru1-C1'	64.11(13)
C1-Ru1-C1'	135.07(13)
C2'-Ru1-C1'	38.45(13)
C5-Ru1-C1'	116.65(11)
C5'-Ru1-C1'	38.13(15)
C3'-Ru1-C2	109.65(11)
C4'-Ru1-C2	117.50(12)
C1-Ru1-C2	38.49(10)
C2'-Ru1-C2	130.92(12)
C5-Ru1-C2	64.46(10)
C5'-Ru1-C2	149.44(14)
C1'-Ru1-C2	168.80(13)
C3'-Ru1-C3	128.78(11)
C4'-Ru1-C3	109.78(11)
C1-Ru1-C3	63.65(11)
C2'-Ru1-C3	165.34(11)
C5-Ru1-C3	63.45(11)
C5'-Ru1-C3	120.51(13)
C1'-Ru1-C3	153.28(14)
C2-Ru1-C3	37.90(12)
C3'-Ru1-C4	164.62(11)
C4'-Ru1-C4	130.00(11)
C1-Ru1-C4	64.29(11)
C2'-Ru1-C4	156.34(11)
C5-Ru1-C4	38.24(10)
C5'-Ru1-C4	113.69(12)
C1'-Ru1-C4	124.57(12)
C2-Ru1-C4	63.89(12)

Table 4.5 continued

C3-Ru1-C4	37.60(11)
C2-C1-C5	108.1(3)
C2-C1-C13	129.0(3)
C5-C1-C13	122.4(2)
C2-C1-Ru1	71.70(15)
C5-C1-Ru1	71.19(15)
C13-C1-Ru1	116.46(18)
C3-C2-C1	107.2(3)
C3-C2-Ru1	71.54(17)
C1-C2-Ru1	69.81(15)
C4-C3-C2	109.5(3)
C4-C3-Ru1	71.26(16)
C2-C3-Ru1	70.56(16)
C3-C4-C5	107.6(3)
C3-C4-Ru1	71.14(16)
C5-C4-Ru1	69.98(15)
C4-C5-C1	107.6(2)
C4-C5-C6	129.5(3)
C1-C5-C6	122.5(2)
C4-C5-Ru1	71.78(15)
C1-C5-Ru1	69.99(15)
C6-C5-Ru1	118.49(18)
O1-C6-C5	123.7(3)
O1-C6-C7	121.0(3)
C5-C6-C7	115.3(2)
C8-C7-C12	119.3(3)
C8-C7-C6	118.1(3)
C12-C7-C6	122.6(2)
C9-C8-C7	120.4(3)
C8-C9-C10	120.3(3)
C9-C10-C11	120.1(3)
C12-C11-C10	120.6(3)
C11-C12-C7	119.3(3)
C11-C12-C13	118.8(3)
C7-C12-C13	121.9(2)

O2-C13-C1	123.6(3)
O2-C13-C12	121.2(3)
C1-C13-C12	115.2(2)
C5'-C1'-C2'	108.0(3)
C5'-C1'-C14	127.6(4)
C2'-C1'-C14	124.4(4)
C5'-C1'-Ru1	70.87(18)
C2'-C1'-Ru1	70.62(16)
C14-C1'-Ru1	125.7(2)
C3'-C2'-C1'	107.4(3)
C3'-C2'-C15	125.5(3)
C1'-C2'-C15	127.1(3)
C3'-C2'-Ru1	70.15(16)
C1'-C2'-Ru1	70.93(17)
C15-C2'-Ru1	126.4(2)
C2'-C3'-C4'	108.6(3)
C2'-C3'-C16	126.0(3)
C4'-C3'-C16	125.4(3)
C2'-C3'-Ru1	71.56(16)
C4'-C3'-Ru1	70.85(16)
C16-C3'-Ru1	124.9(2)
C5'-C4'-C3'	107.8(3)
C5'-C4'-C17	126.9(4)
C3'-C4'-C17	125.2(4)
C5'-C4'-Ru1	71.58(17)
C3'-C4'-Ru1	70.64(16)
C17-C4'-Ru1	123.7(2)
C4'-C5'-C1'	108.2(3)
C4'-C5'-C18	126.0(4)
C1'-C5'-C18	125.7(4)
C4'-C5'-Ru1	70.20(17)
C1'-C5'-Ru1	71.00(17)
C18-C5'-Ru1	126.6(2)

Table 4.6. Bond lengths [Å] and Angles [°] for **3b**

Ru1-C5'	2.07(10)
Ru1-C18'	2.07(6)
Ru1-C3'	2.14(14)
Ru1-C17'	2.12(5)
Ru1-C16	2.14(3)
Ru1-C15	2.15(5)
Ru1-C6	2.14(7)
Ru1-C19'	2.2(2)
Ru1-C4'	2.195(15)
Ru1-C2	2.14(10)
Ru1-C19	2.18(15)
Ru1-C6'	2.24(14)
O1-C1	1.240(19)
O2-C7	1.168(18)
C1-C2	1.46(3)
C1-C13	1.508(18)
C2-C6	1.448(15)
C2-C3	1.46(3)
C3-C4	1.47(6)
C4-C5	1.36(6)
C5-C6	1.44(3)
C6-C7	1.47(3)
C7-C8	1.518(18)
C8-C13	1.403(16)
C8-C9	1.405(19)
C9-C10	1.354(19)
C10-C11	1.41(2)
C11-C12	1.38(2)
C11-C14	1.494(18)
C12-C13	1.41(2)
O1'-C1'	1.23(2)
O2'-C7'	1.18(2)
C1'-C2'	1.47(3)
C1'-C13'	1.51(2)
C2'-C6'	1.450(17)
C2'-C3'	1.47(3)
C3'-C4'	1.48(7)
C4'-C5'	1.35(7)
C5'-C6'	1.44(3)
C6'-C7'	1.47(3)
C7'-C8'	1.52(2)

C8'-C13'	1.395(19)
C8'-C9'	1.41(2)
C9'-C10'	1.36(2)
C10'-C11'	1.41(3)
C11'-C12'	1.38(2)
C11'-C14'	1.48(2)
C12'-C13'	1.42(2)
C15-C19	1.430(14)
C15-C16	1.443(16)
C15-C20	1.513(16)
C16-C17	1.393(19)
C16-C21	1.530(18)
C17-C18	1.442(18)
C17-C22	1.515(16)
C18-C19	1.441(14)
C18-C23	1.506(17)
C19-C24	1.495(14)
C15'-C19'	1.428(17)
C15'-C16'	1.444(19)
C15'-C20'	1.516(19)
C16'-C17'	1.39(2)
C16'-C21'	1.53(2)
C17'-C18'	1.44(2)
C17'-C22'	1.521(19)
C18'-C19'	1.441(16)
C18'-C23'	1.50(2)
C19'-C24'	1.495(18)
C1S-O1S	1.60(5)
C5'-Ru1-C18'	158.0(13)
C5'-Ru1-C3'	67(3)
C18'-Ru1-C3'	111(3)
C5'-Ru1-C17'	121.6(18)
C18'-Ru1-C17'	40.2(9)
C3'-Ru1-C17'	126(2)
C5'-Ru1-C16	113(2)
C18'-Ru1-C16	55.7(12)
C3'-Ru1-C16	147.4(17)
C17'-Ru1-C16	23.9(9)
C5'-Ru1-C15	125(2)
C18'-Ru1-C15	61.0(15)

Table 4.6 continued

C3'-Ru1-C15	166.2(18)
C17'-Ru1-C15	56.4(13)
C16-Ru1-C15	39.3(7)
C5'-Ru1-C6	68(2)
C18'-Ru1-C6	123.7(15)
C3'-Ru1-C6	33.0(17)
C17'-Ru1-C6	156.1(10)
C16-Ru1-C6	179.2(14)
C15-Ru1-C6	140.0(12)
C5'-Ru1-C19'	159(2)
C18'-Ru1-C19'	40(3)
C3'-Ru1-C19'	127(3)
C17'-Ru1-C19'	66(4)
C16-Ru1-C19'	65(4)
C15-Ru1-C19'	39(3)
C6-Ru1-C19'	115(4)
C5'-Ru1-C4'	37(2)
C18'-Ru1-C4'	128(2)
C3'-Ru1-C4'	40(2)
C17'-Ru1-C4'	111.9(12)
C16-Ru1-C4'	120.3(15)
C15-Ru1-C4'	154(2)
C6-Ru1-C4'	60.5(18)
C19'-Ru1-C4'	164(3)
C5'-Ru1-C2	42.3(15)
C18'-Ru1-C2	158.1(10)
C3'-Ru1-C2	63(3)
C17'-Ru1-C2	161.0(11)
C16-Ru1-C2	140.8(14)
C15-Ru1-C2	120(2)
C6-Ru1-C2	39.5(12)
C19'-Ru1-C2	125(4)
C4'-Ru1-C2	62(2)
C5'-Ru1-C19	157.2(18)
C18'-Ru1-C19	41(2)
C3'-Ru1-C19	128(3)
C17'-Ru1-C19	67(3)
C16-Ru1-C19	65(3)
C15-Ru1-C19	38.6(17)
C6-Ru1-C19	114(3)
C19'-Ru1-C19	1(4)
C4'-Ru1-C19	165(3)
C2-Ru1-C19	124(3)

C5'-Ru1-C6'	39(2)
C18'-Ru1-C6'	162.3(11)
C3'-Ru1-C6'	66(3)
C17'-Ru1-C6'	156.2(14)
C16-Ru1-C6'	136(2)
C15-Ru1-C6'	118(3)
C6-Ru1-C6'	44(2)
C19'-Ru1-C6'	127(4)
C4'-Ru1-C6'	62(3)
C2-Ru1-C6'	5(2)
C19-Ru1-C6'	126(3)
O1-C1-C2	125.0(17)
O1-C1-C13	119.9(15)
C2-C1-C13	114.9(13)
C6-C2-C3	108(3)
C6-C2-C1	125(2)
C3-C2-C1	127(2)
C6-C2-Ru1	70(4)
C3-C2-Ru1	76(4)
C1-C2-Ru1	117(6)
C4-C3-C2	104(3)
C4-C3-Ru1	68(2)
C2-C3-Ru1	66(4)
C5-C4-C3	110.9(12)
C5-C4-Ru1	73(4)
C3-C4-Ru1	74(2)
C4-C5-C6	109(3)
C4-C5-Ru1	71(3)
C6-C5-Ru1	68(4)
C5-C6-C2	107(2)
C5-C6-C7	131(2)
C2-C6-C7	121(2)
C5-C6-Ru1	73(4)
C2-C6-Ru1	70(5)
C7-C6-Ru1	116(4)
O2-C7-C6	123.5(16)
O2-C7-C8	122.9(15)
C6-C7-C8	113.6(12)
C13-C8-C9	117.0(14)
C13-C8-C7	125.2(14)
C9-C8-C7	117.6(13)
C10-C9-C8	122.7(14)

Table 4.6 continued

C9-C10-C11	120.3(13)
C12-C11-C10	118.8(13)
C12-C11-C14	119.5(14)
C10-C11-C14	121.8(14)
C11-C12-C13	120.3(14)
C8-C13-C12	120.7(15)
C8-C13-C1	120.3(15)
C12-C13-C1	118.9(13)
O1'-C1'-C2'	126(2)
O1'-C1'-C13'	119.1(19)
C2'-C1'-C13'	114.4(17)
C6'-C2'-C3'	109(3)
C6'-C2'-C1'	124(3)
C3'-C2'-C1'	126(3)
C6'-C2'-Ru1	72(7)
C3'-C2'-Ru1	68(6)
C1'-C2'-Ru1	117(7)
C2'-C3'-C4'	103(3)
C2'-C3'-Ru1	73(6)
C4'-C3'-Ru1	72(5)
C5'-C4'-C3'	110.5(18)
C5'-C4'-Ru1	67(4)
C3'-C4'-Ru1	68(6)
C4'-C5'-C6'	109(3)
C4'-C5'-Ru1	76(4)
C6'-C5'-Ru1	77(7)
C5'-C6'-C2'	106(3)
C5'-C6'-C7'	131(4)
C2'-C6'-C7'	122(3)
C5'-C6'-Ru1	64(6)
C2'-C6'-Ru1	70(6)
C7'-C6'-Ru1	122(9)
O2'-C7'-C6'	124(2)
O2'-C7'-C8'	123(2)
C6'-C7'-C8'	112.7(18)
C13'-C8'-C9'	118.8(19)
C13'-C8'-C7'	125.4(19)
C9'-C8'-C7'	115.6(18)
C10'-C9'-C8'	121.6(18)
C9'-C10'-C11'	119.0(18)
C12'-C11'-C10'	121.0(17)
C12'-C11'-C14'	118.6(18)
C10'-C11'-C14'	120.3(17)

C11'-C12'-C13'	119.0(17)
C8'-C13'-C12'	120.2(18)
C8'-C13'-C1'	121.1(19)
C12'-C13'-C1'	118.6(17)
C19-C15-C16	107.5(11)
C19-C15-C20	123.6(12)
C16-C15-C20	128.9(13)
C19-C15-Ru1	72(7)
C16-C15-Ru1	70(2)
C20-C15-Ru1	124(4)
C17-C16-C15	108.5(11)
C17-C16-C21	131.3(15)
C15-C16-C21	119.8(15)
C17-C16-Ru1	73.7(18)
C15-C16-Ru1	71(3)
C21-C16-Ru1	126(2)
C16-C17-C18	108.9(10)
C16-C17-C22	126.9(15)
C18-C17-C22	124.1(16)
C16-C17-Ru1	68.9(19)
C18-C17-Ru1	71.1(18)
C22-C17-Ru1	123(2)
C19-C18-C17	107.1(11)
C19-C18-C23	127.0(13)
C17-C18-C23	125.7(13)
C19-C18-Ru1	70(6)
C17-C18-Ru1	70.8(17)
C23-C18-Ru1	129(2)
C15-C19-C18	107.9(10)
C15-C19-C24	126.9(14)
C18-C19-C24	125.1(13)
C15-C19-Ru1	70(5)
C18-C19-Ru1	72(5)
C24-C19-Ru1	127(10)
C19'-C15'-C16'	107.9(13)
C19'-C15'-C20'	123.6(17)
C16'-C15'-C20'	128.5(17)
C19'-C15'-Ru1	66(10)
C16'-C15'-Ru1	71(4)
C20'-C15'-Ru1	126(6)
C17'-C16'-C15'	108.4(13)
C17'-C16'-C21'	130(2)
C15'-C16'-C21'	1**21**(2)

Table 4.6 continued

C17'-C16'-Ru1	66(3)
C15'-C16'-Ru1	72(4)
C21'-C16'-Ru1	125(4)
C16'-C17'-C18'	108.9(13)
C16'-C17'-C22'	129(2)
C18'-C17'-C22'	122(2)
C16'-C17'-Ru1	77(3)
C18'-C17'-Ru1	68(3)
C22'-C17'-Ru1	124(3)
C19'-C18'-C17'	107.3(13)
C19'-C18'-C23'	127.0(18)

C17'-C18'-C23'	125.6(17)
C19'-C18'-Ru1	73(10)
C17'-C18'-Ru1	72(3)
C23'-C18'-Ru1	123(4)
C15'-C19'-C18'	107.5(14)
C15'-C19'-C24'	128(2)
C18'-C19'-C24'	125(2)
C15'-C19'-Ru1	76(8)
C18'-C19'-Ru1	67(8)
C24'-C19'-Ru1	127(10)

Table 4.7. Bond lengths [Å] and Angles [°] for **4**

Ru1-C5	2.077(16)
Ru1-C1	2.156(17)
Ru1-C3'	2.171(16)
Ru1-C2'	2.181(15)
Ru1-C1'	2.181(16)
Ru1-C4	2.187(15)
Ru1-C5'	2.188(15)
Ru1-C3	2.206(17)
Ru1-C2	2.206(15)
Ru1-C4'	2.236(15)
Fe1-C9'	1.932(17)
Fe1-C10'	1.967(17)
Fe1-C8'	1.983(16)
Fe1-C9	2.024(15)
Fe1-C7'	2.040(15)
Fe1-C11'	2.040(17)
Fe1-C8	2.054(16)
Fe1-C10	2.070(16)
Fe1-C7	2.122(15)
Fe1-C11	2.140(17)
O1-C6	1.252(19)
O2-C12	1.233(19)
C1-C2	1.43(2)
C1-C12	1.45(2)
C1-C5	1.46(2)
C2-C3	1.39(2)
C3-C4	1.40(2)
C4-C5	1.46(2)
C5-C6	1.46(2)
C6-C7	1.47(2)
C7-C8	1.44(2)
C7-C11	1.46(2)
C8-C9	1.42(2)
C9-C10	1.42(2)
C10-C11	1.43(2)
C11-C12	1.44(2)
C1'-C5'	1.42(2)
C1'-C2'	1.45(2)
C1'-C13	1.48(3)
C2'-C3'	1.41(2)
C2'-C14	1.48(2)

C3'-C4'	1.41(2)
C3'-C15	1.56(2)
C4'-C5'	1.46(2)
C4'-C16	1.50(2)
C5'-C17	1.48(2)
C7'-C11'	1.41(2)
C7'-C8'	1.43(2)
C8'-C9'	1.40(2)
C9'-C10'	1.45(3)
C10'-C11'	1.40(2)
C5-Ru1-C1	40.3(6)
C5-Ru1-C3'	164.5(6)
C1-Ru1-C3'	128.9(6)
C5-Ru1-C2'	129.6(6)
C1-Ru1-C2'	115.4(6)
C3'-Ru1-C2'	37.9(6)
C5-Ru1-C1'	112.3(6)
C1-Ru1-C1'	129.0(7)
C3'-Ru1-C1'	64.1(6)
C2'-Ru1-C1'	38.9(6)
C5-Ru1-C4	39.9(6)
C1-Ru1-C4	65.8(6)
C3'-Ru1-C4	155.0(6)
C2'-Ru1-C4	163.3(6)
C1'-Ru1-C4	126.3(6)
C5-Ru1-C5'	123.5(6)
C1-Ru1-C5'	160.7(7)
C3'-Ru1-C5'	63.9(6)
C2'-Ru1-C5'	64.2(6)
C1'-Ru1-C5'	37.9(6)
C4-Ru1-C5'	108.8(6)
C5-Ru1-C3	64.2(6)
C1-Ru1-C3	63.5(6)
C3'-Ru1-C3	125.0(6)
C2'-Ru1-C3	159.5(6)
C1'-Ru1-C3	158.6(6)
C4-Ru1-C3	37.1(6)
C5'-Ru1-C3	124.3(6)
C5-Ru1-C2	64.8(6)
C1-Ru1-C2	38.2(6)
C3'-Ru1-C2	114.0(6)

Table 4.7 continued

C2'-Ru1-C2	129.2(6)
C1'-Ru1-C2	163.7(6)
C4-Ru1-C2	62.9(6)
C5'-Ru1-C2	157.7(6)
C3-Ru1-C2	36.6(6)
C5-Ru1-C4'	156.7(6)
C1-Ru1-C4'	160.5(6)
C3'-Ru1-C4'	37.2(6)
C2'-Ru1-C4'	63.0(6)
C1'-Ru1-C4'	63.4(6)
C4-Ru1-C4'	122.0(6)
C5'-Ru1-C4'	38.4(6)
C3-Ru1-C4'	110.7(6)
C2-Ru1-C4'	125.9(6)
C9'-Fe1-C10'	43.7(8)
C9'-Fe1-C8'	41.9(7)
C10'-Fe1-C8'	71.7(7)
C9'-Fe1-C9	110.8(7)
C10'-Fe1-C9	122.8(7)
C8'-Fe1-C9	128.3(7)
C9'-Fe1-C7'	70.4(7)
C10'-Fe1-C7'	70.1(7)
C8'-Fe1-C7'	41.6(7)
C9-Fe1-C7'	163.5(7)
C9'-Fe1-C11'	69.9(7)
C10'-Fe1-C11'	40.7(7)
C8'-Fe1-C11'	69.2(7)
C9-Fe1-C11'	156.0(6)
C7'-Fe1-C11'	40.5(6)
C9'-Fe1-C8	124.8(7)
C10'-Fe1-C8	160.9(7)
C8'-Fe1-C8	109.9(7)
C9-Fe1-C8	40.7(7)
C7'-Fe1-C8	124.4(7)
C11'-Fe1-C8	158.3(7)
C9'-Fe1-C10	125.5(7)
C10'-Fe1-C10	104.8(7)
C8'-Fe1-C10	164.6(7)
C9-Fe1-C10	40.5(7)
C7'-Fe1-C10	152.4(7)
C11'-Fe1-C10	118.4(7)
C8-Fe1-C10	68.4(7)
C9'-Fe1-C7	160.2(7)

C10'-Fe1-C7	154.8(7)
C8'-Fe1-C7	122.6(6)
C9-Fe1-C7	67.1(6)
C7'-Fe1-C7	105.8(6)
C11'-Fe1-C7	120.5(7)
C8-Fe1-C7	40.4(6)
C10-Fe1-C7	66.8(6)
C9'-Fe1-C11	159.2(7)
C10'-Fe1-C11	118.3(7)
C8'-Fe1-C11	155.4(7)
C9-Fe1-C11	67.5(7)
C7'-Fe1-C11	117.5(7)
C11'-Fe1-C11	103.0(7)
C8-Fe1-C11	68.4(7)
C10-Fe1-C11	39.6(6)
C7-Fe1-C11	40.1(5)
C2-C1-C12	130.1(15)
C2-C1-C5	105.6(14)
C12-C1-C5	123.8(15)
C2-C1-Ru1	72.8(9)
C12-C1-Ru1	118.3(12)
C5-C1-Ru1	67.0(9)
C3-C2-C1	109.3(14)
C3-C2-Ru1	71.7(9)
C1-C2-Ru1	69.0(9)
C2-C3-C4	111.0(16)
C2-C3-Ru1	71.7(10)
C4-C3-Ru1	70.7(9)
C3-C4-C5	106.0(14)
C3-C4-Ru1	72.2(9)
C5-C4-Ru1	66.0(8)
C4-C5-C1	107.9(14)
C4-C5-C6	130.0(14)
C1-C5-C6	122.0(15)
C4-C5-Ru1	74.1(9)
C1-C5-Ru1	72.8(9)
C6-C5-Ru1	117.6(11)
O1-C6-C5	122.9(15)
O1-C6-C7	123.6(15)
C5-C6-C7	113.5(13)
C8-C7-C11	108.6(14)
C8-C7-C6	128.3(14)
C11-C7-C6	123.1(14)

Table 4.7 continued

C8-C7-Fe1	67.2(9)
C11-C7-Fe1	70.6(9)
C6-C7-Fe1	127.9(11)
C9-C8-C7	106.6(15)
C9-C8-Fe1	68.5(9)
C7-C8-Fe1	72.3(9)
C10-C9-C8	109.7(15)
C10-C9-Fe1	71.5(9)
C8-C9-Fe1	70.8(9)
C9-C10-C11	109.0(15)
C9-C10-Fe1	68.0(9)
C11-C10-Fe1	72.9(10)
C10-C11-C12	131.2(14)
C10-C11-C7	106.1(15)
C12-C11-C7	122.7(14)
C10-C11-Fe1	67.6(9)
C12-C11-Fe1	129.1(11)
C7-C11-Fe1	69.3(9)
O2-C12-C11	123.3(14)
O2-C12-C1	122.7(15)
C11-C12-C1	114.0(13)
C5'-C1'-C2'	107.9(15)
C5'-C1'-C13	124.3(14)
C2'-C1'-C13	127.8(15)
C5'-C1'-Ru1	71.3(9)
C2'-C1'-Ru1	70.5(9)
C13-C1'-Ru1	123.5(12)
C3'-C2'-C1'	107.3(14)
C3'-C2'-C14	128.5(15)
C1'-C2'-C14	124.2(15)
C3'-C2'-Ru1	70.7(9)
C1'-C2'-Ru1	70.6(8)
C14-C2'-Ru1	124.9(12)
C4'-C3'-C2'	109.7(15)

C4'-C3'-C15	125.0(16)
C2'-C3'-C15	124.6(15)
C4'-C3'-Ru1	73.9(9)
C2'-C3'-Ru1	71.4(9)
C15-C3'-Ru1	129.1(12)
C3'-C4'-C5'	107.3(15)
C3'-C4'-C16	125.3(15)
C5'-C4'-C16	127.3(15)
C3'-C4'-Ru1	68.9(9)
C5'-C4'-Ru1	69.0(9)
C16-C4'-Ru1	125.4(11)
C1'-C5'-C4'	107.6(13)
C1'-C5'-C17	128.3(16)
C4'-C5'-C17	123.6(16)
C1'-C5'-Ru1	70.8(9)
C4'-C5'-Ru1	72.6(8)
C17-C5'-Ru1	128.2(11)
C11'-C7'-C8'	106.9(14)
C11'-C7'-Fe1	69.8(9)
C8'-C7'-Fe1	67.1(9)
C9'-C8'-C7'	108.1(15)
C9'-C8'-Fe1	67.1(9)
C7'-C8'-Fe1	71.3(9)
C8'-C9'-C10'	108.5(15)
C8'-C9'-Fe1	71.0(10)
C10'-C9'-Fe1	69.5(10)
C11'-C10'-C9'	106.2(15)
C11'-C10'-Fe1	72.5(10)
C9'-C10'-Fe1	66.8(9)
C10'-C11'-C7'	110.2(15)
C10'-C11'-Fe1	66.8(10)
C7'-C11'-Fe1	69.7(9)

4.1.4. Summary

The pentamethylruthenocene-capped quinone complexes were obtained by single-step Friedel-Crafts acylation reaction between *in situ* generated pentamethylruthenocene-1,2-diacyl chloride **2** with benzene (**3a**, 58%), toluene (**3b**, 71%), *o*-xylene (**3c** and **3d**, 55%), *p*-methoxybenzene (**3e**, 41%) and ferrocene (**4**, 36%) in the presence of anhydrous $AlCl_3$.[78] The pentamethylruthenocene-1,2-diacyl chloride **2** was synthesized by the reaction of pentamethylruthenocene-1,2-dicarboxylic acid **1** with oxalyl chloride in the presence of catalytic amount of DMF. The acylation of benzene, toluene and *o*-xylene was done in neat while in case of *p*-methoxyanisole and ferrocene, reaction was carried out in dichloromethane. Although toluene gave single product, *o*-xylene gave two quinone isomers in a 1:1 ratio showing indiscrimination of second acylation.

The quinone **3b** was reduced to dihydroxy complex **5** (68%) as a single isomer, probably the *endo* diol, however, our attempt to dehydroxylate complex **5** using Sn^{2+}/HCl failed. In another attempt of reduction of **3b** using Zn/NH_4OH, we isolated pentamethylruthenocenyl hydroxyanthrone **6** (69%) with hydroxyl group oriented to *endo* with respect to Ru center. The quinone **3e** undergoes a facile demethylation in the presence of $AlCl_3$ to give dihydroxyquinone **7** (81%), which is characterized with its H-bonded acidic protons with resonance at 12.93 ppm in ^{1}H NMR.

While mononuclear quinone **3a** and **3b** exhibit co-planarity of quinone with Cp, the binuclear quinone **5** shows an unusual bonding mode of its two metal centers with respect to quinone backbone in their molecule structures. In complex **5**, The Ru-center inclines towards carbonyl carbon in comparison to Fe, possibly due to the interaction between electron-rich Cp*Ru in comparison to CpFe. The bimetallic complex also exhibits facile protonation of carbonyl group showing the electron releasing effect of two metallocene moieties. The quinone complexes **3a** and **3b** exhibit irreversible oxidation but reversible single-electron reduction while bimetallic complex **4** exhibits two-electron pseudoreversible oxidation due to iron and ruthenium and irreversible reduction due to quinone in their cyclic Voltammetry studies.

4.2. Aldol Condensation

The four-fold aldol condensation between a 1,2-dialdehyde and a 1,4-cyclohexanedione [20,137-140] and the two-fold aldol condensation between a 1,2-dialdehyde and 1,4-dihydroxynaphthalene[16,141-143] have been used extensively in synthesizing quinone precursors of acenes. Our goal is to extend those synthetic procedures to give mono-nuclear and bi-nuclear quinone complexes in the organometallic arena.

Scheme 4.5. Proposed synthetic schemes of organometallic quinone complexes

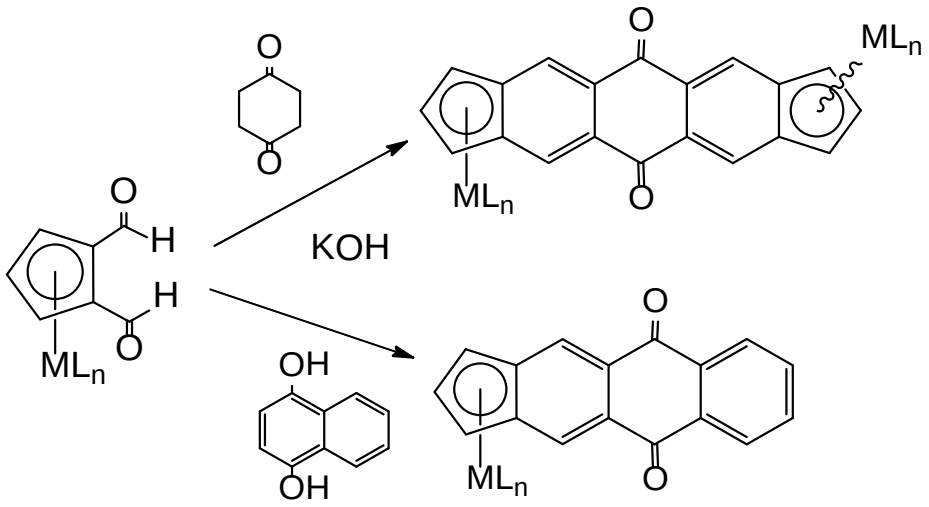

ML$_n$ = Mn$(CO)_3$, RuCp*

While the synthetic procedure of ferrocene-1,2-dialdehyde is well documented,[144-146] other organometallic sandwich and half-sandwich complexes need 1,2-diformylcyclopentadiene (6-hydroxy-2-formylfulvene) to introduce the formyl functionality. The conventional route of making 1,2-diacylcyclopentadiene[81] cannot be extended to 1,2-diformylcyclopentadiene because of the extreme lability of formyl chloride. In order to overcome the difficulties, we designed a new synthetic route, which involves the synthesis of 1,2-dicarbophenoxy ester of cymantrene and pentamethylruthenocene, their reduction to diol, and then oxidation to dialdehyde. The diformyl complexes can be treated as starting materials for two-fold and four-fold aldol condensation to give mono-nuclear and bi-nuclear quinone complexes respectively (Scheme 4.5). The quinone complexes we designed in this way have carbonyl group at γ-position with respect to cyclopentadienyl ligand.

Herein, we report the detail synthesis and characterization of Cp-fused quinone complexes of ruthenium and manganese by aldol reaction.

4.2.1. Experimental

Synthesis of [Ru{η^5-$C_5H_3(CH_2OH)_2$-1,2}(Cp*)] (8a): In a 200-mL Schlenk flask, $LiAlH_4$ (4.2 mL of 1 M in THF, 4.2 mmol) was added dropwise to a stirred solution of **2a** (1.50 g, 2.77 mmol) in THF (100 mL) at 0 °C. The reaction mixture was allowed to stir overnight at room temperature. The initial dark brown color of the solution slowly turned to a light yellow. Volatiles were removed *in vacuo* and the crude product was dissolved in ethyl ether (40 mL). The phenolic impurities were removed in by extraction with a 10% solution of NaOH (2 x 20 mL). The organic phase was dried over $MgSO_4$, filtered, and volatiles were removed *in vacuo.* The crude product was triturated with cold pentane to give **8a** (950 mg, 95%) as a light yellow powder. Analytically pure product was obtained by slow crystallization from ethyl ether under nitrogen at room temperature. **Mp**: 147 °C **^{1}H NMR (400 MHz, $CDCl_3$, ppm):** δ 1.86 (s, 15H, Cp*), 2.14 (br, 2H, OH), 4.01 (d, 2H, ^2J = 12.5 Hz, C$H_A$$H_B$), 4.13 (t, 1H, ^3J = 2.4 Hz, CHC*H*CH) 4.16 (d, 2H, ^2J = 12.5 Hz, $CH_A$$H_B$), 4.23 (d, 2H, ^3J = 2.4 Hz, C*H*CHC*H*). **^{13}C{^{1}H} NMR (100 MHz, $CDCl_3$, ppm):** δ 12.2 (*C*H_3, Cp*), 58.9 (*C*H_2OH), 73.3 (CH*C*HCH), 74.8 (*C*HCH*C*H), 85.9 (Cp* ring), 88.7 (*ipso*). (**IR (KBr, cm^{-1}):** 3292 (br, OH). **MS (EI):** m/z 362 (M^+). The complex was characterized with an X-ray diffraction study.

Synthesis of [Mn{η^5-$C_5H_3(CH_2OH)_2$-1,2}$(CO)_3$] (8b): In a 125-mL Schlenk flask, DIBAL-H (6.9 mL of 1 M solution in hexane, 6.9 mmol) was added

dropwise to a stirred solution of **2b** (700 mg, 1.58 mmol) in anhydrous dichloromethane (15 mL) at -78 °C. The reaction mixture was allowed to stir for 30 min. The temperature is raised to -70 °C and saturated solution of NH_4Cl (5 mL) was added to give a gelatinous mass. The reaction mixture was filtered through Celite and washed with dichloromethane until the filtrate was colored. The filtrate was collected and layers were separated. The organic phase was dried over $MgSO_4$, filtered and volatiles were removed *in vacuo.* The crude product was triturated with cold pentane to give **8b** (238 mg, 58%) as light yellow powder. **Mp**: 58-59 °C **^{1}H NMR (400 MHz, $CDCl_3$, ppm):** δ 3.08 (br, 2H, CH_2O*H*), 4.27 (br, 2H, CH_2), 4.40 (br, 2H, CH_2), 4.58 (br, 1H, CHC*H*CH), 4.76 (br, 2H, C*H*CHC*H*). **^{1}H NMR (400 MHz, acetone-d_6, ppm):** δ 4.28-4.44 (m, 6H, CH_2O*H*), 4.75 (t, 1H, 3J = 2.8 Hz, CHC*H*CH), 4.97 (d, 2H, ^{3}J = 2.8 Hz, C*H*CHC*H*). **^{13}C{^{1}H} NMR (100 MHz, $CDCl_3$, ppm):** δ 57.9 (*C*H_2OH), 78.7 (CH*C*HCH), 83.2 (*C*HCH*C*H), 84.9 (*ipso*), 224.4 (M-*C*≡O). **^{13}C{^{1}H} NMR (100 MHz, acetone-d_6, ppm):** δ 57.5 (*C*H_2OH), 80.1 (CH*C*HCH), 84.2 (*C*HCH*C*H), 105.2 (*CC*), 226.3 (M-*C*≡O). (**IR (KBr, cm^{-1}):** 1920, 2017 (C≡O), 3343 (br, OH). Full characterization of the complex was done by Herberhold and Biersack.[147]

Synthesis of [Ru{η^5-$C_5H_3(CHO)_2$-1,2}(Cp*)] (9a): In a 125-mL Schlenk flask, excess MnO_2 (3.50 g, 88% precipitated active) was added to stirred solution of **8a** (358 mg, 0.99 mmol) in 20 mL of chloroform. The suspension was refluxed for 8 h. The reaction mixture was passed through thin pad of silica and washed with ethyl ether until the filtrate was colorless. Volatiles were removed *in vacuo* to give **9a** (184 mg, 52%) as a bright yellow solid. Analytically pure product

was obtained by recrystallization from hot hexane. **Mp:** 195–210 °C. **^{1}H NMR (400 MHz, $CDCl_3$, ppm):** δ 1.79 (s, 15H, Cp*), 4.78 (t, 1H, ^{3}J = 2.7 Hz, CHC*H*CH), 4.99 (d, 2H, ^{3}J = 2.7 Hz, C*H*CHC*H*) 9.81 (s, 2H, CHO). **^{13}C{^{1}H} NMR (100 MHz, $CDCl_3$, ppm):** δ 11.4 (*C*H_3, Cp*), 78.5(Cp* ring), 80.2 (CH*C*HCH), 89.6 (*C*HCH*C*H), 84.3 (*ipso*), 190.1 (CHO). **IR (KBr, cm^{-1}):** 1674 (CHO). **MS (EI):** m/z 358 (M^+). Full characterization of the complex was performed by Wallace and Selegue.[80]

Synthesis of [Mn{η^5-C_5H_3(CHO)$_2$-1,2}(CO)$_3$] (9b): In a 125-mL Schlenk flask, activated MnO_2 (669 mg, 7.70 mmol) was added to stirred solution of **8b** (115 mg, 0.442 mmol) in 20 mL of dichloromethane. The suspension was stirred for 12 h at room temperature. The reaction mixture was passed through thin pad of silica and washed with dichloromethane until the filtrate was colorless. The filtrate was collected and volatiles were removed *in vacuo* to give gummy solid. Final purification was done by chromatography on silica with dichloromethane as eluent to collect first fraction. Removal of volatiles *in vacuo* gave **9b** (82 mg, 73%) as a bright yellow solid. An analytically pure product was obtained by recrystallization through hot hexane. **Mp:** 98–99 °C. **^{1}H NMR (400 MHz, $CDCl_3$, ppm):** δ 4.93 (br, 1H, CHC*H*CH), 5.64 (br, 2H, C*H*CHC*H*), 10.04 (s, 2H, CHO). **^{13}C{^{1}H} NMR (100 MHz, $CDCl_3$, ppm):** δ 82.3 (CH*C*HCH), 90.7 (*C*HCH*C*H), 93.8 (*ipso*), 188.1 (*C*HO), 227.9 (M-*C*≡O). **IR (KBr, cm^{-1}):** 1684 (C=O), 1944, 2031 (C≡O). **MS (EI):** m/z 260 (M^+).

Synthesis of [Ru(η^5-1,2-C_5H_3CHCO)(Cp*)]$_2$ (10a): In a 50-mL Schlenk flask, cyclohexane-1,4-dione (4.5 mg, 0.04 mmol) was added to the stirred solution of **9a** (25 mg, 0.07 mmol) in ethanol (2 mL). To the reaction mixture, 20% of KOH (0.1 mL) was added. The reaction mixture was stirred at room temperature for overnight. The reaction mixture was cooled with liquid nitrogen and filtered at cold through frit of medium porosity. The residue was washed with water followed by cold ethyl ether and dried under vacuum to give **10a** (18 mg, 68%) as a dark solid. The ^{1}H NMR analysis of the product showed of *syn* and *anti* isomers in a 1:2 ratio. **^{1}H NMR (400 MHz, $CDCl_3$, ppm):** *Syn* isomer. δ 1.59 (s, 30H, Cp*), 4.80 (t, 2H, ^{3}J = 2.4 Hz, CHC*H*CH), 5.06 (d, 4H, ^{3}J = 2.4 Hz, C*H*CHC*H*), 8.40 (s, 4H, Ar). *Anti* isomer. δ 1.58 (s, 30H, Cp*), 4.80 (t, 2H, ^{3}J = 2.4 Hz, CHC*H*CH), 5.08 (d, 4H, ^{3}J = 2.4 Hz, C*H*CHC*H*), 8.42 (s, 4H, Ar). The assignment was made on the basis of integration ratio of protons.

Synthesis of [Mn(η^5-1,2-C_5H_3CHCO)(CO)$_3$]$_2$ (10b): In a 50-mL Schlenk flask, cyclohexane-1,4-dione (8 mg, 0.07 mmol) was added to the stirred solution of **9b** (35 mg, 0.14 mmol) in THF (1 mL). To the reaction mixture, 15% of KOH (0.1 mL) was added. The reaction mixture was allowed to stir at room temperature for overnight. The reaction mixture was cooled using dry ice and filtered at cold through a frit of medium porosity. The residue was washed with water (2 mL) followed by cold ethyl ether (5 mL) and dried under vacuum to give dark solid. The crude product was purified by chromatography on silica with dichloromethane as eluent. The first yellow fraction was collected, volatiles were removed *in vacuo* to give **10b** (26 mg, 65%) as a yellow powder. The analytically

pure product was obtained by recrystallization through chloroform. **MP:** 220-240 °C (dec). **^{1}H NMR (400 MHz, $CDCl_3$, ppm):** δ 5.35 (t, 2H, ^{3}J = 2.9 Hz, CHC*H*CH), 5.49 (d, 4H, ^{3}J = 2.9 Hz, C*H*CHC*H*), 8.66 (s, 4H, Ar). **^{13}C{^{1}H} NMR (100 MHz, $CDCl_3$, ppm):** δ 74.4 (CH*C*HCH), 93.1 (*C*HCH*C*H), 104.2 (*ipso*-Cp), 129.9 (Ar), 130.7 (*ipso*-Ar), 180.7 (*C*O), 223.3 (M-*C*≡O). **IR (KBr, cm^{-1}):** 1670 (C=O), 1928, 1953, 2025 (C≡O).

Synthesis of [Mn(η^5-1,2-$C_5H_3CHCH_2$)(CO)$_3$]$_2$ (11b): In a 50-mL Schlenk flask, borane (3 mL, 1 M solution in THF, 3 mmol) was added to the stirred solution of **10b** (50 mg, 0.11 mmol) in THF (5 mL). The reaction mixture was allowed to stir at room temperature for overnight. Water (2 mL) was added and the product was extracted with ethyl ether (2 x 10 mL). The volatiles were removed *in vacuo* to give **10b** (46 mg, 90%) as a yellow powder. ^{1}H NMR analysis of the product showed the presence of two isomers in a ca. 1:1 ratio which were separated by chromatography on silica with hexane:ethyl ether (3:1) as eluent. The first yellow fraction was found to be *anti* isomer of **11b**. **^{1}H NMR (400 MHz, acetone-d$_6$, ppm):** δ 3.97 (s, 4H, CH_2), 5.16 (t, 2H, ^{3}J = 2.8 Hz, CHC*H*CH), 5.41 (d, 4H, ^{3}J = 2.8 Hz, C*H*CHC*H*), 7.50 (s, 4H, Ar). **^{13}C{^{1}H} NMR (100 MHz, acetone-d$_6$, ppm):** δ 38.3 (*C*H$_2$), 72.6 (*C*HCH*C*H), 89.1 (CH*C*HCH), 104.8 (*ipso*-Cp), 122.1 (*ipso*-Ar), 138.3 (Ar), 226.5 (*C*≡O). The second yellow fraction of the column was found to be *syn* isomer of **11b**. **^{1}H NMR (400 MHz, acetone-d$_6$, ppm):** δ 3.88 (AB, 2H, ^{2}J = 16 Hz, CH_2), 4.00 (AB, 2H, ^{2}J = 16 Hz, C*H*$_2$), 5.14 (t, 2H, ^{3}J = 2.8 Hz, CHC*H*CH), 5.40 (d, 4H, ^{3}J = 2.8 Hz, C*H*CHC*H*), 7.49 (s, 4H, Ar). **^{13}C{^{1}H} NMR (100 MHz, acetone-d$_6$, ppm):** δ 38.4 (*C*H$_2$), 72.7

(*C*HCH*C*H), 88.8 (CH*C*HCH), 104.9 (*ipso*-Cp), 122.0 (*ipso*-Ar), 138.4 (Ar), 226.5 (*C*≡O).

Synthesis of [Mn(η^5-1,2-$C_5H_3C_{12}H_6O_2$)(CO)$_3$] (12b): In a 50-mL Schlenk flask, naphthalene-1,4-diol (68 mg, 0.39 mmol) was added to the stirred solution of **9b** (100 mg, 0.39 mmol) in ethyl alcohol (2.0 mL). To the reaction mixture, 15% of KOH (0.1 mL) was added. The reaction mixture was allowed to stir at room temperature for overnight. The reaction mixture was cooled using dry ice and filtered at cold through a frit of medium porosity. The residue was washed with water (2 mL) followed by cold ethyl ether (5 mL) and dried under vacuum to give dark solid. The crude product was purified by chromatography on silica with dichloromethane as eluent. The first yellow fraction was collected, volatiles were removed *in vacuo* to give **12b** (36 mg, 25%) as a yellow powder. **^{1}H NMR (400 MHz, acetone-d$_6$, ppm):** δ 5.67 (t, 1H, ^{3}J = 2.8 Hz, CHC*H*CH), 5.94 (d, 2H, ^{3}J = 2.8 Hz, C*H*CHC*H*), 7.93-7.96 (m, 2H, Ar), 8.32-8.34 (m, 2H, Ar), 8.73 (s, 2H, Ar). The complex was fully characterized by Ketcham.

Synthesis of [Mn(η^5-1,2-$C_5H_3C_{16}H_8O_2$)(CO)$_3$] (13b): In a 50-mL Schlenk flask, anthracene-1,4-diol (57 mg, 0.27 mmol) was added to the stirred solution of **9b** (70 mg, 0.27 mmol) in ethyl alcohol (2.0 mL). To the reaction mixture, 15% of NaOH (0.1 mL) was added. The reaction mixture was allowed to stir at room temperature for overnight. The reaction mixture was cooled using dry ice and filtered at cold through a frit of medium porosity. The residue was washed with water (2 mL) followed by cold ethyl ether (5 mL) and dried under vacuum to give dark solid. The crude product was re-dissolved in dichloromethane, filtered and

filtrate was collected. The volatiles were removed *in vacuo* to give **13b** (58 mg, 49%) as a dark purple solid. **^{1}H NMR (400 MHz, $CDCl_3$, ppm):** δ 5.32 (br, 1H, CHC*H*CH), 5.52 (d, 2H, C*H*CHC*H*), 7.69 (br, 2H, Ar), 8.10 (br, 2H, Ar), 8.19 (s, 2H, Ar), 8.90 (br, 2H). **IR (ATR, cm^{-1}):** 1668 (C=O), 1928, 2017 (C≡O).

4.2.2. Results and discussion

4.2.2.1. Synthesis. Bis(1,2-dicarbophenoxy)pentamethylruthenocene **2a** and bis(1,2-dicarbophenoxy)cymantrene **2b** are the starting materials for the synthesis of mono-nuclear and binuclear quinone complexes as shown in Scheme 4.6. The 1',2',3',4',5'-pentamethylruthenocene-1,2-dimethanol **8a** was prepared in sufficiently high yield (95%) by the reduction of **2a** with lithium aluminum hydride (1 M solution in THF) at room temperature for 12 h. We observed a complete reduction of carbophenoxy to methyl group in the presence of $LiAlH_4$ over extended time of 32 h showing the electrophilicity of carbon atom at α-position of metallocene. Our attempts to reduce **2b** to diol **8b** with $LiAlH_4$ were unsuccessful leading to immediate decomposition of complex giving black solid. The reduction of 1,2-dicarbophenoxy cymantrene complex **8b**, however, was successful in the presence of DIBAL-H at -78 °C by following literature procedure[148] to give desired diol in 58% yield. The phenolic impurities formed during reduction were removed by extraction with NaOH solution.

The two hydroxymethyl substituents of **8a** and **8b** exhibit AB pattern expected from diastereotopic geminal hydrogens in ^{1}H NMR. The geminal protons signals in **8a** were found to be broadened in proton NMR even though

there is no intramolecular hydrogen bonding as evidenced in its molecular structure. The variable temperature NMR also did not make the signal sharper. The reduction of **2a** in the presence of DIBAL-H was not successful even until 20 h at room temperature. This might be due to steric interaction of two isobutyl groups with the methyl groups of Cp* ligand.

The pentamethylruthenocene-1,2-dialdehyde (**9a**, 52%) and cymantrene-1,2-dialdehyde (**9b**, 58%) were synthesized through a mild oxidation of corresponding bis(hydroxymethyl) metal complexes with activated manganese dioxide.[149] The disappearance of AB pattern of geminal coupling and appearance of peaks at 9.82-10.04 ppm in ^{1}H NMR indicates the oxidation of dialcohols to dialdehydes. Scaling up of the oxidation reaction resulted in the poor yield of product. The partial oxidation of diols always results in formation of formyl alcohol complexes. An attempt to oxidize the Ru-diol under Swern conditions resulted in the demetalation of the complex.

Scheme 4.6. Synthesis of Cp-capped mononuclear and binuclear quinone complexes

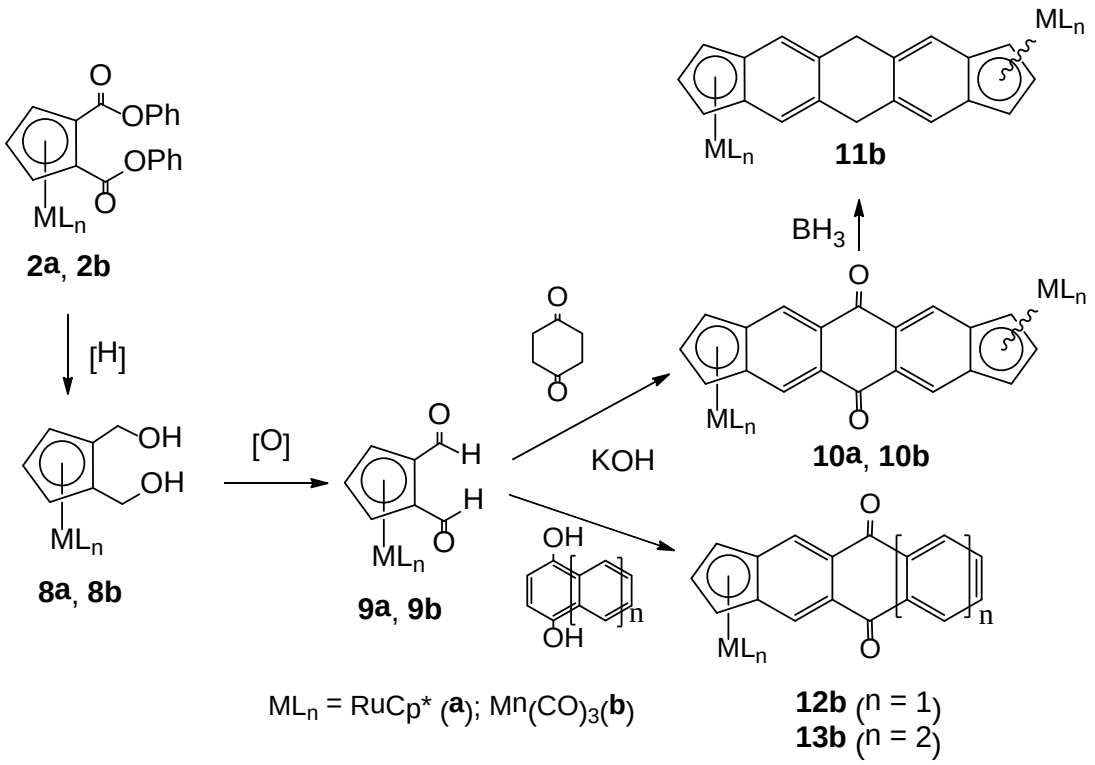

Aldol condensations of 1,2-diformyl complexes were carried out by following the literature procedures.[150] Diformyl complexes of ruthenium and manganese were treated with cyclohexane-1,4-dione in a 2:1 ratio in the presence of sodium hydroxide to give binuclear quinone complexes of ruthenium (**10a**, 68%) and manganese (**10b**, 65%). The *syn* and *anti* isomers of the reaction were indistinguishable on the basis of physical methods of characterization. However, the ratio of peak integration in ^{1}H NMR of the mixture shows that *syn* and *anti* isomers of **10a** and **10b** are formed in roughly 1:2 and 1:1 ratios, respectively. We were unable to separate the isomers. The cymantrene-fused mononuclear complexes were synthesized by treating 1,2-diformylcymantrene

with naphthalene- and anthracene-1,4-diol to give quinone complexes **12b** (25%) and **13b** (49%) respectively. The aldol reactions of these metal complexes, in general, give a black solid impurity, from which quinones are separated by running a short column.

The reaction of isomeric mixture **10b** using borane in THF at room temperature reduced ketonic group to methylene (**11b**, 90% combined yield). At this step, we were able to separate *syn* and *anti* isomers by means of column chromatography. The *syn* isomer is distinctive with AB pattern of its methylene proton while anti isomer have singlet for the corresponding protons in ^{1}H NMR. An attempt of dehydrogenation of **11b** using DDQ gave a mixture of different products; the ^{1}H NMR analysis of some of the products corresponds to the demetalated ones.

4.2.2.2. Spectroscopy. All new complexes were characterized with ^{1}H NMR, ^{13}C NMR, IR and mass spectroscopy with the exception of **10a** and **10b**. These two complexes were characterized with ^{1}H NMR only due to the inseparability of isomeric mixture. The selected spectroscopic data of complexes **8**-**11** are shown in table 4.8. As usual, the protons at 3,5-positions of Cp resonate as doublet and the proton at 4-position resonate as triplet with an integration of 2:1 ratio showing the symmetry of ligand. In general, the chemical shift values ^{1}H and ^{13}C resonances of ruthenocene complexes are in higher fields than that of corresponding manganese complexes. This might be due to the increased electron-donating effect of RuCp* in comparison to $Mn(CO)_3$. The electronic effect of metal ligand environment can also be observed in the IR band due to

carbonyl group. For example, the IR absorbance due to carbonyl group of **9a** is in lower energy than **9b** by 10 cm^{-1}.

Table 4.8. Selected data of ^{1}H NMR, ^{13}C NMR and IR of complexes **8-13**

Complex	CP-4 δ_H	CP-3,5 δ_H	Cp-4 δ_C	Cp-3,5 δ_C	Cp-1,2 δ_C	CO δ_C	CO (cm^{-1})
8a[1]	4.13	4.16	73.3	74.8	88.7	-	-
8b[1]	4.58	4.76	78.7	83.2	84.9	-	-
9a[1]	4.78	4.99	80.2	89.6	84.3	190.1	1674
9b[1]	4.93	5.64	82.3	90.7	93.8	188.1	1684
11b[2](*anti*) **11b**[2](*syn*)	5.16 5.14	5.41 5.40	72.6 72.7	89.1 88.8	104.8 104.9	-	-

1 = $CDCl_3$; **2** = acetone-d_6

4.2.2.3. Structure. A thermal ellipsoid plot of the molecular structure of [Ru{η^5-$C_5H_3(CH_2OH)_2$-1,2}(Cp*)] **8a** is shown in Figure 4.10 with atom numbering scheme. The crystal structure and refinement data for compound **8a** can be found in Table 4.9. Selected bond distances and angles are given in Table 4.10. The structure shows typical ruthenocene geometries with nearly linear centroid-Ru-centroid geometry. The average carbon-ruthenium bond distance is shorter by about 0.02 Å to the Cp* ligand compared to the Cp ligand, probably due to electron releasing effect of the Cp* ligand. The effect is similar to that seen in ruthenocene complexes reported in previous chapter. Both five-membered rings (η^5) coordinated to the ruthenium with average ruthenium–to-carbon bond distances of 2.188(3) Å and 2.173(3) Å for Cp and Cp*, respectively. The Ru-C bond distances of all five carbons in Cp are almost equal. The side-chain methylene carbons are almost coplanar with the five carbon atoms of Cp. The

oxygen atoms of the two methanolic side chain are, however, oriented away from each other on opposite faces of Cp plane; O1 -0.091 Å and O2 1.423 Å; thus there is no intramolecular H-bonding between these two OH groups. However, two hydroxymethyl groups are held together by a network of intermolecular hydrogen bond with O-H-O distances ranging from 2.688(3) to 2.731(3) Å.

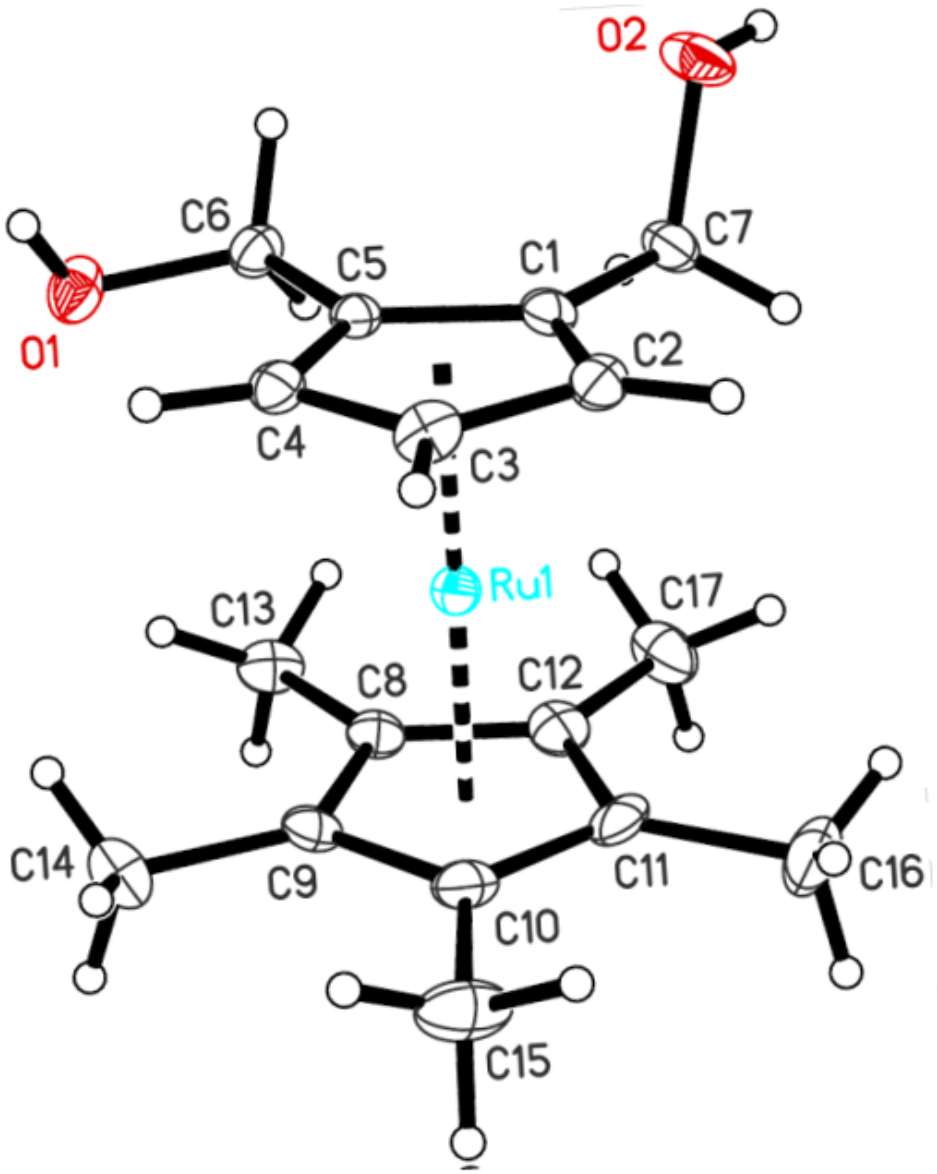

Figure 4.10. Molecular structure of [Ru{η^5-$C_5H_3(CH_2OH)_2$-1,2}(Cp*)] **(8a)**

Table 4.9. Crystal Data and Structure Refinement for Compound **8a**

Formula	$C_{17}H_{24}O_2Ru$
Formula wt (amu)	361.43
T, K	90.0(2)
Crystal system	Monoclinic
Space group	$P2_1/c$
Z	4
a, Å	13.4100(1)
b, Å	13.9712(2)
c, Å	8.3027(2)
α,(deg)	90
β, (deg)	90.7969(7)
γ, (deg)	90
V, $Å^3$	1553.69(5)
d_{calc}, Mg/m^3	1.545
F(000)	744
Crystal size (mm^3)	0.10 x 0.09 x 0.08
Radiation	Mo Kα (λ = 0.71073 Å)
Monochromator	Graphite
Absorption coef m (mm^{-1})	1.008
Diffractometer	Nonius KappaCCD diffractometer
q range (deg)	2.11 to 26.00
Limiting indices	$-16 \le h \le 16$
	$-17 \le k \le 17$
	$-10 \le l \le 10$
Reflections collected	25323
Independent reflections	3046 (R_{int} = 0.0408)
Absorption correction	Semi-empirical from equivalents
Refinement program	SHELXL-97
Refinement method	Full-matrix least-squares on F^2
Data/restraints/parameters	3046 / 0 / 188
Goodness-of-fit on F^2	1.129
Final R indices [I>2s(I)]	R_1 = 0.0281, wR_2 = 0.0610
R indices (all data)	R_1 = 0.0350, wR_2 = 0.0643
Largest diff. peak and hole, e•$Å^{-3}$	1.450 and -0.731

Table 4.10. Bond Distances (Å) and bond angles [°] for **8a**

Ru1-C8	2.170(2)
Ru1-C12	2.170(3)
Ru1-C9	2.174(2)
Ru1-C11	2.176(3)
Ru1-C1	2.178(3)
Ru1-C10	2.179(3)
Ru1-C2	2.184(2)
Ru1-C5	2.184(2)
Ru1-C3	2.197(3)
Ru1-C4	2.200(3)
O1-C6	1.423(3)
O2-C7	1.441(3)
C7-C1	1.483(4)
C1-C2	1.433(4)
C1-C5	1.441(4)
C2-C3	1.422(4)
C3-C4	1.426(4)
C4-C5	1.429(4)
C5-C6	1.502(4)
C8-C12	1.436(4)
C8-C9	1.439(4)
C8-C13	1.500(4)
C9-C10	1.434(4)
C9-C14	1.494(4)
C10-C11	1.428(4)
C10-C15	1.498(4)
C11-C12	1.437(4)
C11-C16	1.503(4)
C12-C17	1.504(4)
C8-Ru1-C12	38.65(10)
C8-Ru1-C9	38.68(10)
C12-Ru1-C9	64.69(10)
C8-Ru1-C11	64.50(10)
C12-Ru1-C11	38.63(11)
C9-Ru1-C11	64.24(10)
C8-Ru1-C1	125.49(10)
C12-Ru1-C1	110.57(10)

C9-Ru1-C1	160.36(10)
C11-Ru1-C1	125.14(10)
C8-Ru1-C10	64.67(10)
C12-Ru1-C10	64.66(11)
C9-Ru1-C10	38.47(10)
C11-Ru1-C10	38.27(11)
C1-Ru1-C10	159.20(10)
C8-Ru1-C2	161.13(10)
C12-Ru1-C2	127.81(10)
C9-Ru1-C2	159.60(10)
C11-Ru1-C2	113.82(10)
C1-Ru1-C2	38.37(10)
C10-Ru1-C2	126.87(10)
C8-Ru1-C5	109.74(10)
C12-Ru1-C5	123.02(10)
C9-Ru1-C5	126.12(10)
C11-Ru1-C5	157.54(10)
C1-Ru1-C5	38.56(9)
C10-Ru1-C5	161.60(10)
C2-Ru1-C5	64.03(10)
C8-Ru1-C3	157.87(10)
C12-Ru1-C3	163.10(10)
C9-Ru1-C3	126.02(10)
C11-Ru1-C3	129.71(10)
C1-Ru1-C3	63.95(10)
C10-Ru1-C3	114.23(10)
C2-Ru1-C3	37.88(10)
C5-Ru1-C3	63.76(10)
C8-Ru1-C4	123.78(10)
C12-Ru1-C4	156.53(11)
C9-Ru1-C4	112.14(10)
C11-Ru1-C4	163.56(11)
C1-Ru1-C4	63.93(10)
C10-Ru1-C4	128.72(10)
C2-Ru1-C4	63.43(10)
C5-Ru1-C4	38.03(9)
C3-Ru1-C4	37.84(10)

Table 4.10 continued

O2-C7-C1	108.9(2)
C2-C1-C5	107.4(2)
C2-C1-C7	126.1(2)
C5-C1-C7	126.5(2)
C2-C1-Ru1	71.02(14)
C5-C1-Ru1	70.95(14)
C7-C1-Ru1	125.15(18)
C3-C2-C1	108.5(2)
C3-C2-Ru1	71.57(15)
C1-C2-Ru1	70.61(14)
C2-C3-C4	108.0(2)
C2-C3-Ru1	70.55(14)
C4-C3-Ru1	71.19(14)
C3-C4-C5	108.3(2)
C3-C4-Ru1	70.96(14)
C5-C4-Ru1	70.39(14)
C4-C5-C1	107.8(2)
C4-C5-C6	126.0(2)
C1-C5-C6	126.1(2)
C4-C5-Ru1	71.58(14)
C1-C5-Ru1	70.49(14)
C6-C5-Ru1	126.52(18)
O1-C6-C5	112.0(2)
C12-C8-C9	107.9(2)
C12-C8-C13	126.5(2)
C9-C8-C13	125.5(2)
C12-C8-Ru1	70.68(14)

C9-C8-Ru1	70.83(14)
C13-C8-Ru1	125.73(18)
C10-C9-C8	108.1(2)
C10-C9-C14	126.2(2)
C8-C9-C14	125.7(2)
C10-C9-Ru1	70.93(15)
C8-C9-Ru1	70.49(14)
C14-C9-Ru1	126.35(19)
C11-C10-C9	107.8(2)
C11-C10-C15	126.2(3)
C9-C10-C15	125.8(3)
C11-C10-Ru1	70.76(15)
C9-C10-Ru1	70.60(14)
C15-C10-Ru1	127.69(19)
C10-C11-C12	108.5(2)
C10-C11-C16	125.3(3)
C12-C11-C16	126.1(3)
C10-C11-Ru1	70.97(15)
C12-C11-Ru1	70.46(15)
C16-C11-Ru1	126.94(19)
C8-C12-C11	107.6(2)
C8-C12-C17	125.6(3)
C11-C12-C17	126.7(3)
C8-C12-Ru1	70.67(14)
C11-C12-Ru1	70.91(15)
C17-C12-Ru1	125.77(19)

4.2.4. Summary

Bis(1,2-dicarbophenoxy)pentamethylruthenocene **2a** and bis(1,2-dicarbophenoxy)cymantrene **2b** are the starting materials for the synthesis of mono-nuclear and binuclear quinone complexes. The diester complex of ruthenium **2a** was reduced to diol **8a** (95%) using $LiAlH_4$ while analogous

reduction of manganese **2b** to **8b** (58%) was done in the presence of DIBAL-H[148] by following literature procedure. The analysis of molecular structure of pentamentylruthenocene-1,2-dimethoanol showed that there is no intramolecular H-bond between alcohol groups. Both diol complexes were oxidized in the presence of activated MnO_2 to yield diformyl complexes **9a** (52%) and **9b** (73%).

Aldol condensation of diformyl complexes with cyclohexane-1,4-dione gave binuclear complexes of ruthenium **10a** (68%) and manganese **10b** (65%). The *syn*/*anti* isomers of quinones were inseparable by physical technique. The carbonyl groups of quinone **10b** were reduced to methylene in the presence of BH_3/THF to give **11b** (90%) whose *syn* and *anti* isomers were separated by chromatography. Our attempts to dehydrogenate the complex **11b** using DDQ failed. Similarly, aldol condensation of **9b** with 1,4-dihydroxynaphthalene or dihydroxyanthracene gave mononuclear complexes **12b** (25%) and **13b** (49%).

Chapter 5: Synthesis and Characterization of Ferrocene-Fused Acene-Quinone Complexes

5.1. Introduction

The physical and optoelectronic properties of organic acenes might be tuned by incorporating a redox-active metal center. One way of introducing transition metals on acenes is through a cyclopentadienyl ring linearly fused with an acene backbone. The building of an acene framework starting from the cyclopentadienylmetal complexes satisfies the requirements of both the Cp moiety and the metal center as a pendant group attached *via* π-bonds. As chemistry of metallocenes has a close relationship with the aromatic organic compounds, the Friedel-Crafts acylation of metallocenes with phthalic anhydride or naphthalene-1,2-dicarboxylic anhydride can give the desired frameworks.

The single-step Friedel-Crafts acylation of organic aromatics with phthalic anhydride is a common quinone-forming reaction.[151-154] While the reactions of ferrocene are parallel to those of aromatic compounds,[126] analogous quinone-forming reactions of ferrocene with phthalic anhydride have not been reported. This might be because the second acylation is difficult due to the deactivation of the Cp carbons by the presence of a ketone group at alpha position.[155,156] The activation of the Cp ring for the second Friedel-Crafts acylation, however, can be done by reducing the carbonyl group to a methylene as demonstrated by Weiβensteiner *et al.*[157]

Ferrocene is a well-known transition-metal complex with reversible electrochemistry. Unlike other cyclopentadienyl metal complexes, ferrocene is a cheap, readily available metallocene showing compatibility with various reagents. Although the Nesmeyanov group reported the synthesis of a ferrocene-fused naphthoquinone long ago, a detailed experimental procedure and characterization data are not available.[158] We have recently published a route to pentamethylruthocene-fused acenequinones *via* single-step Friedel-Crafts acylation between ruthenocene-1,2-diacyl chloride and organic or organometallic aromatics.[78]

To come up with similar targets by reducing the cost of starting materials, we decided to switch the functionality of two Friedel-Crafts substrates in our earlier work.[78] We are interested in exploring the synthesis of Fc-anthrone and Fc-naphthacenone analogs (**I**) (Scheme 5.1), replacing terminal 1,2-phenylenes with 1,2-ferrocenylenes (Fc) in anthrone and naphthacenone. This can be done by two successive acylations of ferrocene with phthalic or naphthalic anhydrides, or their synthetic equivalents. Similarly, ferrocene-capped quinones (Fc-naphthoquinone) and (Fc-anthraquinone) homologues (**II**) can be synthesized by the oxidation of anthrones (**I**). That not only gives us an opportunity to design ferrocene-fused naphthalene homolog (**III**), but it also helps to understand the influence of the iron center on the stability of the extended metallocenes. While the synthesis of indenyl complexes of iron[53] was reported long ago, there are no reports of benz[*f*]indenyl complexes of iron. We are interested in exploring the chemistry of benzannulated indenyl complexes of iron.

Herein, we report the synthesis and characterization of Fc-anthrone, Fc-naphthacenone and derivatives *en route* to benzannulated ferrocene.

Scheme 5.1. Target Fc-fused acenes and their synthetic precursors

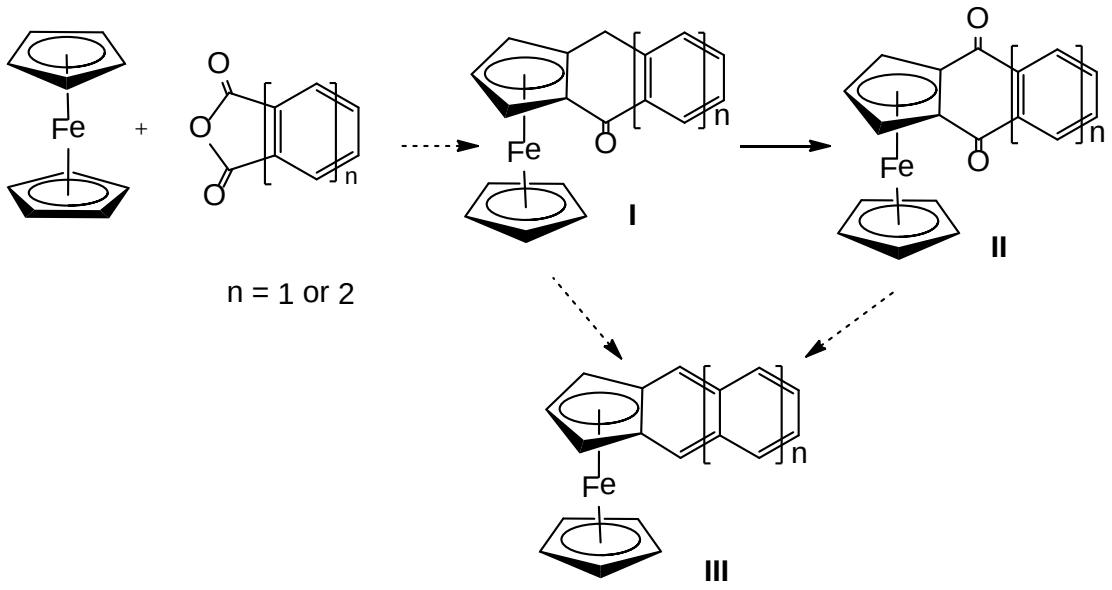

5.2. Experimental

Chapter 2 lists the general conditions for all experiments. Ferrocene, manganese(IV)oxide, and N-phenylmaleimide (Acros), naphthalene-2,3-carboxylic anhydride (TCI), thionyl chloride, benzyl chloride, trifluoroacetic anhydride, piperidine, lithium diisopropylamide, lithium hexamethyldisilazide (LiHDMS), cyclohexanol, potassium iodide, lithium aluminum hydride and chlorotrimethylsilane (Aldrich), aluminum chloride and aluminum powder (Alfa Aesar), zinc powder, acetic anhydride and triethylamine (Mallinckrodt), 40% aqueous fluoroboric acid, tetrabutylammonium bromide and mercuric chloride (Baker), deuterium oxide (Columbia Organic), and DMAD (AK Scientific) were

used as purchased. Phthalic anhydride (Acros) was recrystallized from chloroform before use. *o*-Carbomethoxybenzoic acid[159] and o-carbomethoxybenzoyl chloride[160] were synthesized using literature procedures. Similar procedures were followed for the corresponding 2,3-naphthalenedicarboxylic anhydride derivatives.

Synthesis of $C_{18}H_{14}FeO_3$ (1a). To a stirred solution of ferrocene (11.8 g, 63.3 mmol) in CS_2 (120 mL), a solution of 2-carbomethoxybenzoylchloride (12.03 g, 63.32 mmol) in dry ethyl ether (50 mL) was added quickly. After addition of a solution of $AlCl_3$ (17.0 g, 0.13 mol) in ethyl ether (50 mL) [Caution**:** dissolving aluminum chloride in ethyl ether is a highly exothermic reaction!], the reaction mixture was refluxed for 2 h, during which time the product separated as viscous oil. After cooling the mixture to room temperature and separation of the solvent, the residue was hydrolyzed with dil. HCl (pH = 3-4). The precipitated product was filtered off, washed with water (200 mL) and dried under vacuum to give **1a** (17.02 g, 77%) as a red-brown crystalline solid. Mp**:** 132-134 °C [Lit.[157] 139 °C]. All spectroscopic data were consistent with previous reports.[157]

Synthesis of $C_{23}H_{18}FeO_3$ (1b). In a 250-mL Schlenk flask, a solution of 2-carbomethoxynaphthaloyl chloride (7.23 g, 29.1 mmol) in ethyl ether (50 mL) was added dropwise to a stirred solution of ferrocene (5.4 g, 29 mmol) in CS_2 (50 mL) at room temperature. To the reaction mixture, anhydrous $AlCl_3$ (7.74 g, 58.2 mmol) dissolved in ethyl ether (25 mL) [Caution**:** dissolving $AlCl_3$ in ethyl ether is a highly exothermic reaction!] was added. The reaction mixture was refluxed overnight, during which time the product separated as a viscous oil. After cooling

the mixture and separation of the solvent, the residue was hydrolyzed with dilute HCl. The precipitate was filtered off, washed with water (150 mL) and dried under vacuum to give **1b** (10.32 g, 89%) as a dark red, crystalline solid. **Mp:** 152 °C. **^{1}H NMR (400 MHz, $CDCl_3$, ppm):** δ 3.69 (s, 3H, OC*H*$_3$), 4.22 (s, 5H, Cp), 4.50 (t, 2H, ^{3}J = 2.0 Hz) 4.64 (t, 2H, ^{3}J = 2.0 Hz), 7.61–7.68 (m, 2H, Ar), 7.97 (dd, 2H, ^{3}J = 8 Hz, ^{4}J = 1.2 Hz), 8.13 (s, 1H, Ar), 8.46 (s, 1H, Ar). **^{13}C{^{1}H} NMR (100 MHz, $CDCl_3$, ppm):** δ 52.5 (O*C*H$_3$), 70.35 (Cp), 70.38 (C3, C4-Cp), 72.57 (C2, C5-Cp), 80.39 (C1-Cp), 127.4, 128.2, 128.3, 128.6, 129.1, 129.2, 131.5, 133.0, 134.3, 138.9 (Ar), 167.4 (*C*O, ester), 199.6 (*C*O, ketone). **IR (ATR, cm^{-1}):** 1652 (C=O, ketone), 1716 (C=O, ester). **MS (EI):** m/z 184 (M^+).

Synthesis of $C_{18}H_{18}FeO_2$ (4a) and $C_{18}H_{18}FeO_3$ (4'a). Amalgamated zinc was prepared by shaking for ten minutes a mixture of zinc (3.3 g), mercuric chloride (0.33 g), water (5.2 mL) and conc. HCl (0.2 mL) in a 200-mL Schlenk flask. The solution was decanted and washed with distilled water. To the amalgamated zinc, water (2.0 mL), conc. HCl (4.84 mL), toluene (12.0 mL) and 2-carbomethoxybenzoylferrocene **1a** (2.72 g, 7.81 mmol) were added in the given order and the resultant mixture was refluxed for 8 h. The mixture was cooled to room temperature and filtered. The layers were separated and the aqueous layer was extracted with ethyl ether (3 x 30 mL). The combined organic extracts were dried over $MgSO_4$, filtered and volatiles were removed *in vacuo*. The crude product was purified by column chromatography on silica with ethyl acetate as eluent to collect a dark-yellow band. Evaporation of the solvents to dryness gave **4a** (1.84 g, 70.5%) as a yellow powder. The analytically pure

product was obtained by crystallization through hot hexane. **Mp:** 58 °C. **^{1}H NMR (400 MHz, $CDCl_3$, ppm):** δ 3.89 (s, OC*H*$_3$), 4.05 (t, 2H, ^{3}J = 1.6 Hz 2,5-Cp), 4.09 (m, 4H, 3,4-Cp and C*H*$_2$), 4.12 (s, 5H, Cp), 7.16–7.21(m, 2H, Ar), 7.33–7.37 (m, 1H, Ar), 7.81–7.83 (, 1H, Ar). **^{13}C{^{1}H} NMR (100 MHz, $CDCl_3$, ppm):** δ 33.9 (O*C*H$_3$), 52.1 (*C*H$_2$), 67.7, 68.9, 69.2, 87.8 (Cp), 126.1, 129.2, 130.5, 130.6, 143.7, 132.2 (Ar), 168.4 (*C*O). **IR (ATR, cm^{-1}):** 1709 (CO). **MS (EI):** m/z 334 (M$^+$). The byproduct of the reaction was found to contain partially reduced ketone, **4'a**, (412 mg, 15%) as a yellow solid. **Mp:** 208 °C. **^{1}H NMR (400 MHz, $CDCl_3$, ppm):** δ 3.51 (s, OC*H*$_3$), 3.58 (br, 1H), 3.71 (br, 1H), 3.84 (br, 1H), 3.88 (s, 5H, Cp), 3.95 (br, 1H), 5.30 (s, 1H, C*H*OH), 7.16–7.20 (m, 1H), 7.45–7.49 (m, 1H, Ar), 7.63 (d, 1H, ^{3}J = 7.6 Hz, Ar), 7.69 (dd, 1H, ^{3}J = 7.6 Hz, ^{4}J = 1.2 Hz, Ar). **^{13}C{^{1}H} NMR (100 MHz, $CDCl_3$, ppm):** δ 46.7 (O*C*H3), 52.1(*C*HOH), 66.0, 66.8, 67.5, 68.5, 70.9, 94.6 (Cp), 125.8, 129.8, 130.0, 130.3, 131.2, 146.5 (Ar), 168.8 (*C*O). **IR (ATR, cm^{-1}):** 1714 (CO), 3326 (OH). **MS (EI):** m/z 334 (M$^+$ - OH).

Synthesis of $C_{18}H_{14}FeO_3$ (2a). Method A: To a suspension of anhydrous aluminum chloride (15.5 g, 0.116 mmol) in dichloromethane (140 mL), a solution of ferrocene (20 g, 110 mmol) and phthalic anhydride (7.95 g, 53.8 mmol) in dichloromethane (130 mL) was added dropwise over the period of 45 min. The reaction mixture was stirred for additional 12 h at room temperature and then poured into ice. The pH was adjusted to 3-4 by adding conc. HCl, and the organic layer was separated. The aqueous layer was extracted with dichloromethane (3 x 100 mL). The combined organic layers were concentrated to approximately 400 mL and extracted with 2 M aqueous NaOH (2 x 200 mL).

The aqueous phase was collected and precipitated by slow addition of conc. HCl at 0 °C. The precipitate was filtered off, washed with water and dried to give **1a** (2.44 g, 14%) as a brown solid. **Mp:** 186 °C [Lit[161] 186 °C]. **^{1}H NMR (400 MHz, acetone-d, ppm):** δ 4.22 (s, 5H, Cp) 4.53 (s, 4H, Cp), 7.62–7.66 (m, 1H, Ar), 7.72–7.79 (m, 2H, Ar), 7.98 (dd, 1H, ^{3}J = 7.6 Hz, ^{4}J = 0.8 Hz, Ar). **^{13}C{^{1}H} NMR (100 MHz, acetone-d$_6$, ppm):** δ 70.7, 70.8, 72.9, 81.4 (Cp), 128.9, 130.3, 130.6, 130.7, 133.0, 143.8 (Ar), 167.7 (*C*OOH), 200.1 (*C*O). **IR (ATR, cm^{-1}):** 1652 (C=O), 1688 (C=O), 2600-3200 (OH). The full characterization of the complex was done by Li *et al.*[162]

Method B. To a stirred solution of keto-ester **1a** (3.36 g, 9.65 mmol) in methanol (20 mL), KOH (1.08 g, 18.9 mmol) was added. The reaction mixture was allowed to reflux for 4 h. The reaction mixture was cooled to room temperature and water (20 mL) was added. The unreacted neutral components were extracted with ethyl ether (2 x 20 mL). The aqueous phase was acidified with conc. HCl and precipitate was collected by filtration. The residue was washed with water and dried under vacuum to give **2a** (3.13 g, 97.0%) as a dark brown solid. All physical and spectroscopic data were consistent with the previously prepared complex.

Synthesis of $C_{22}H_{16}FeO_3$ (2b). To a stirred solution of keto-ester **1b** (4.72 g, 12.3 mmol) in methanol (20 mL), KOH (1.37 g, 24.6 mmol) was added. After the reaction mixture was refluxed for 4 h, starting materials were completely consumed and precipitate began to appear. The reaction mixture was cooled to room temperature and water (50 mL) was added. The neutral unreacted

materials were extracted with ethyl ether (2 x 20 mL). The aqueous phase was acidified with conc. HCl and precipitate was collected by filtration. The residue was washed with water and dried under vacuum to give **2b** (4.42 g, 97.0%) as a dark brown solid. **Mp: ^{1}H NMR (400 MHz, acetone-d$_6$, ppm):** δ 4.25 (s, 5H, Cp), 4.54 (t, 2H, ^{3}J = 1.6 Hz), 4.62 (t, 2H, ^{3}J = 1.6 Hz), 7.69–7.77 (m, 2H, Ar), 8.15–1.20 (m, 2H, Ar), 8.28 (s, 1H, Ar), 8.56 (s, 1H, Ar). **^{13}C{^{1}H} NMR (100 MHz, CDCl$_3$, ppm):** δ 70.9, 71.1, 72.8, 81.6 (Cp), 128.8, 129.0, 129.4, 129.8, 129.9, 131.8, 133.7, 137.1, 139.8 (Ar), 167.9 (*C*OOH), 199.6 (*C*O). **IR (ATR, cm^{-1}):** 1655 (C=O, ketone), 1684 (C=O), 3200–2500 (O-H). **MS (EI):** m/z 384 (M^{+})

Synthesis of $C_{18}H_{16}FeO_2$ (3a). Method A: In a 250-mL Schlenk flask, powder zinc (44 g) was activated by stirring it in a solution of $CuSO_4$ (1.5 g) in water (40 mL) for 20 minutes. The solution was decanted, and the residue was washed with water. To the activated zinc, keto-acid **2a** (4.68 g, 14.0 mmol) in NaOH solution (11 g in 150 mL of water) was added. The reaction mixture was allowed to reflux for 12 h and then cooled to room temperature. The reaction mixture was filtered and the filtrate was acidified with conc. HCl. The resulting precipitate was collected, washed with water and dried to give **3a** (3.96 g, 89.0%) as a yellow powder. **Mp:** 178-179 °C [Lit.[161] 174 °C]. **^{1}H NMR (400 MHz, acetone-d, ppm):** δ 4.04 (t, 2H, ^{3}J = 1.6 Hz, 2,5-Cp) 4.12 (s, 5H, Cp), 4.16 (br, 4H, C*H*$_2$ and 3,4-Cp), 7.25–7.31 (m, 2H, Ar), 7.42–7.46 (m, 1H, Ar), 7.87- 7.90 (m, 1H, Ar). The acidic proton was found to be exchanged with water at 2.8 ppm. **^{13}C{^{1}H} NMR (100 MHz, acetone-d$_6$, ppm):** δ 34.2 (*C*H$_2$), 68.1, 69.2, 69.4, 69.7

(Cp), 126.8, 130.5, 131.4, 131.6, 132.7, 144.6 (Ar), 169.1 (*C*O). **IR (ATR, cm^{-1}):** 1682 (C=O) 3300–2500 (OH).

Method B. A suspension of **4a** (1.80 g, 5.39 mmol) in 25% aqueous KOH (25 mL) was refluxed for 24 h. The reaction mixture was cooled to room temperature, filtered and the filtrate was acidified with conc. HCl. The precipitate was separated by filtration. The crude product was chromatographed on silica with ethyl acetate**:** petroleum ether (1**:**1) as eluent to collect a yellow band. Evaporation of the solvent gave **3a** (0.95 g, 55%) as a yellow solid. The melting point and spectroscopic data were consistent with the previously synthesized complex.

Synthesis of $C_{18}H_{16}FeO_3$ (3'a). Amalgamated zinc was prepared by shaking for 10 min a mixture of zinc (3.52 g), mercuric chloride (0.35 g), water (6.0 mL) and conc. HCl (1.0 mL) in a 200-mL Schlenk flask. The solution was decanted and washed with distilled water. To the amalgamated zinc, water (1.0 mL), conc. HCl (4.0 mL), methanol (10 mL) and **2a** (2.60 g, 8.22 mmol) were added in the given order and the resultant mixture was refluxed for 8 h. The reaction mixture was cooled to room temperature, filtered, and the residue was washed with ethyl ether. The organic phase was separated and the aqueous phase was extracted with ethyl ether (2 x 10 mL). The combined ether extracts were dried over $MgSO_4$. Volatiles were removed *in vacuo* and the product was triturated with cold pentane to give **3'a** (1.85 g, 71.0%) as a light yellow powder. **Mp:** 124-126 °C. **^{1}H NMR (400 MHz, $CDCl_3$, ppm):** δ 4.17 (s, 5H, Cp), 4.18-4.21 (m, 4H, Cp), 6.25 (s, 1H, C*H*OH), 7.52-7.55 (m, 2H, Ar), 7.65-7.69 (m, 1H, Ar),

7.91-7.92 (m, 1H, Ar). **$^{13}C\{^1H\}$ NMR (100 MHz, $CDCl_3$, ppm):** δ 66.5 (Cp), 67.2 (Cp), 68.5 (Cp), 69.2 (Cp unsubstituted), 80.1 (*C*HOH), 84.8 (*C*-Ar), 122.7, 125.9, 126.2, 129.5, 134.1, 149.6 (Ar), 170.7 (*C*OOH). **IR (ATR, cm^{-1}):** 1740 (C=O), 1685 (C=C), 3100–2500 (OH). Same product was isolated during basic Clemmensen used for preparation of **3a** within 30 min (*vide infra*).

Synthesis of $C_{22}H_{18}FeO_2$ (3b). Zinc powder (1.1 g) was activated by stirring it in a solution of $CuSO_4$ (360 mg) in water (30 mL) for 30 min. The solution was decanted, and the residue was washed with water. To the activated zinc, keto-acid **2b** (1.0 g, 2.7 mmol) and aqueous NaOH (2.7 g in 45 mL of water) were added. The reaction mixture was heated at 60 °C for 12 h and then cooled to room temperature and filtered. The filtrate was collected and acidified with conc. HCl. The resulting precipitate was filtered, washed with water and dried to give **3b** (0.56 g, 58%) as a yellow powder. **Mp:** 175-180 °C (dec). **^1H NMR (400 MHz, acetone-d, ppm):** δ 4.06 (br, 2H, Cp) 4.14 (s, 5H, Cp), 4.20 (br, 2H, Cp), 4.31 (br, 2H, CH_2), 7.49–7.59 (m, 2H, Ar), 7.75 (s, 1H, Ph), 7.84 (d, 1H, ^3J = 8.4 Hz, Ar), 7.98 (d, 1H, ^3J = 8.4 Hz, Ar), 8.50 (s, 1H, Ar). The acidic proton was found to be exchanged with water at 2.8 ppm. **$^{13}C\{^1H\}$ NMR (100 MHz, acetone-d_6, ppm):** δ 34.5 (*C*H_2), 68.2, 69.8, 69.5, 69.9 (Cp), 127.0, 128.1 129.1, 129.3, 129.5, 129.9, 132.1, 132.5, 135.5, 135.9, 140.5 (Ar), 169.2 (*C*O). **IR (ATR, cm^{-1}):** 1682 (C=O) 3315–2555 (OH). **MS (EI):** m/z 370 (M^+).

Synthesis of $C_{18}H_{16}FeO_2$ (3a) and $C_{36}H_{26}Fe_2O_4$ (5a). Amalgamated zinc was prepared by shaking for 10 min a mixture of zinc (2.0 g), mercuric chloride (0.2 g), water (3.0 mL) and conc. HCl (0.1 mL) in a 200-mL Schlenk flask. The

solution was decanted and washed with distilled water. To the amalgamated zinc, water (1.0 mL), conc. HCl (2.4 mL), toluene (10 mL) and **2a** (1.0 g, 2.9 mmol) were added in the given order and the resultant mixture was refluxed for 24 h. The mixture was cooled to room temperature, filtered and residue was washed with ethyl ether. Two layers were separated. The aqueous layer was extracted with ethyl ether and the combined ether extracts were evaporated to dryness. The solid was again filtered through a thin pad of silica and washed with ethyl acetate. The volatiles were removed *in vacuo* to give a yellow solid. The ^{1}HNMR analysis of the product shows the desired *o*-carboxybenzylferrocene **3a** and a dimerized lactone **5a** in a 5**:**2 ratio. The mixture was separated by column chromatography on silica with ethyl acetate**:**hexane (1**:**4) as eluent. The first yellow band was collected and volatiles were removed *in vacuo*. The analytically pure product was prepared by recrystallization from a mixture of ethyl ether and hexane to give **5a** (88 mg, 9.0%) as an orange solid. **Mp:** 124 °C (dec). **^{1}H NMR (400 MHz, acetone-d, ppm):** δ 3.49 (s, 5H, Cp) 3.80–3.82 (m, 2H), 4.06–4.08 (m, 2H), 4.27–4.29 (m, 1H), 4.49–4.50 (m, 2H), 7.54–7.58 (m, 2H, 7.67 (d, 2H, ^{3}J = 8 Hz), 7.72–7.78 (m, 4H). **^{13}C{^{1}H} NMR (100 MHz, $CDCl_3$, ppm):** δ 67.4, 68.2, 68.6, 68.9, 69.5, 85.6, 90.0, 123.5, 125.7, 126.8, 129.8, 133.9, 150.2 (Ar), 169.8 (*C*O). **IR (ATR, cm^{-1}):** 1768 (C=O). **MS (EI):** m/z 634 (M^+), 317 (M^+/2). The product was characterized by X-ray diffraction. The second band of the column was found to contain carboxylic acid **4a** (0.22 g, 23%). All spectroscopic and physical data were consistent with the previously prepared complex.

Synthesis of $C_{23}H_{20}FeO_2$ (4b) and **$C_{44}H_{30}Fe_2O_4$ (5b).** Amalgamated zinc was prepared by shaking for five minutes a mixture of zinc (3.0 g), mercuric chloride (0.3 g), water (4.0 mL) and conc. HCl (0.16 mL) in a 200-mL Schlenk flask. The solution was decanted and washed with distilled water (20 mL). To the amalgamated zinc, water (2.0 mL), conc. HCl (4.0 mL), toluene (10 mL) and **1b** (1.0 g, 3.0 mmol) were added in the given order and the resultant mixture was refluxed for 5 h. The mixture was cooled to room temperature and conc. HCl (2.0 mL) was added. The mixture was refluxed for another 5 h. The reaction mixture was cooled to room temperature and layers were separated. The aqueous layer was diluted with water (20 mL) and extracted with ethyl ether (3 x 30 mL). The toluene layer and the ether extracts were combined, washed with water (20 mL), and dried over anhydrous $MgSO_4$. The volatiles were removed *in vacuo* and the crude product was separated by chromatography on silica with ethyl acetate**:**hexane (1**:**4) as eluent to collect a yellow band as a first fraction. The evaporation of solvents gave **4b** (0.42 g, 44 %) as a yellow powder. **Mp:** 126-128 °C. **^{1}H NMR (400 MHz, $CDCl_3$, ppm):** δ 3.94 (s, 3H, OC*H*$_3$), 4.07 (t, 2H, ^{3}J = 2 Hz, Cp), 4.13 (t, 2H, ^{3}J = 2 Hz, Cp), 4.14 (s, 5H, Cp), 4.24 (br, 2H, C*H*$_2$), 7.41–7.51 (m, 2H, Ar), 7.54 (s, 1H, Ar), 7.70 (d, 1H, Ar), 7.82 (d, 1H, Ar), 7.39 (s, 1H, Ar). **^{13}C{^{1}H} NMR (100 MHz, acetone-d_6, ppm):** δ 34.2 (O*C*H$_3$), 52.29 (*C*H$_2$), 67.8 (Cp), 68.9 (Cp), 69.4 (Cp), 87.9 (Cp), 126.3, 127.5, 127.9, 128.3, 128.8, 129.0 131.2, 131.9, 135.1, 139.4 (Ar), 168.5 (*C*OOMe). **IR (ATR, cm^{-1}):** 1720 (C=O). **MS (EI):** m/z 184 (M^+). The second chromatographic fraction of column contained dimerized lactone complex, **5b** (0.39 g, 44%), as a yellow solid.

Analytically pure product was obtained by crystallization from hexane and ethyl acetate (4:1) by cooling at -10 °C overnight. **Mp:** 240–245 °C (dec). **^{1}H NMR (400 MHz, $CDCl_3$, ppm):** 3.39 (s, 10H, Cp), 3.91 (br, 2H, Cp), 4.01–4.02 (m, 2H, Cp), 4.21–4.22 (m, 2H, Cp), 4.56 (br, 2H, Cp), 7.47–7.52 (m, 2H, Ar), 7.82 (d, 2H, ^{3}J = 8.4 Hz, Ar), 7.98 (d, 2H, ^{3}J = 8.4 Hz, Ar), 8.03 (s, 2H, Ar), 8.22 (s, 2H, Ar). **^{13}C{^{1}H} NMR (100 MHz, acetone-d, ppm):** δ 67.5, 68.4, 68.5, 68.8, 68.5, 69.0, 69.6, 122.6, 124.8, 127.1, 127.5, 129.1, 129.4, 129.8, 133.1, 135.7, 143.4, 169.8. **IR (ATR, cm^{-1}):** 1732 (C=C), 1765 (C=O). **MS (EI):** m/z 367 (M^+/2).

Synthesis of $C_{22}H_{18}FeO_2$ (3b). To a stirred solution of ester **4b** (720 mg, 1.87 mmol) in methanol (10 mL) and dichloromethane (10 mL), KOH (210 mg, 3.75 mmol) was added. The reaction mixture was refluxed for 30 h by when starting materials were completely consumed. The reaction was cooled to room temperature and water (30 mL) was added. The unreacted neutral components were extracted with ethyl ether (2 x 20 mL). The aqueous phase was acidified with conc. HCl and then extracted with ethyl ether (3 x 20 mL). The combined ether extracts were dried over $MgSO_4$, filtered and volatiles were removed *in vacuo*. The crude product was triturated with cold pentane and dried under reduced pressure to give **3b** (0.47 g, 67 %) as a light yellow powder. The melting point and spectroscopic data were consistent with the previously prepared complex.

Synthesis of $C_{18}H_{14}FeO$ (6a). The complex was prepared by Nesmeyanov *et al.*[158] without its full characterization data. In a 250-mL Schlenk flask, **3a** (5.74 g, 17.9 mmol) was dissolved in anhydrous dichloromethane (200

mL). The solution was transferred to the dropping funnel and added dropwise to the stirred suspension of trifluoroacetic anhydride (5.0 mL, 36 mmol) in dichloromethane (200 mL) and activated molecular sieves (5 g) taken in a 500-mL Schlenk flask at 0 °C. The reaction was stirred for 3 h at 0 °C and poured into water (200 mL) saturated with $NaHCO_3$. The layers were separated; the organic phase was washed with water and then dried over $MgSO_4$. The volatiles were removed *in vacuo*. The crude product was purified by chromatography on silica with ethyl acetate**:**hexane (1**:**1) as eluent to give **6a** (5.2 g, 96%) as dark red crystalline solid. Analytically pure product was obtained by recrystallization from hexane by cooling at -10 °C for 3 days. **Mp:** 98 °C [Lit.[158] 101 °C]. **^{1}H NMR ($CDCl_3$, 400 MHz, ppm):** δ 3.90 (AB, 1H, ^{2}J = 21.2 Hz), 3.93 (s, 5H, Cp), 4.07 (AB, 1H, ^{2}J = 21.2 Hz), 4.54 (t, 1H, ^{3}J = 2.4 Hz), 4.72 (ABC, 1H), 5.00 (ABC, 1H), 7.36–7.43 (m, 2H, Ar), 7.48–7.52 (m, 1H, Ar), 8.31–8.33 (dd, 1H, ^{3}J = 8.0 Hz, ^{4}J = 1.2 Hz, Ar). **^{13}C{^{1}H} NMR (100 MHz, $CDCl_3$, ppm):** δ 29.9 (*C*H_2), 65.7 (Cp), 70.3 (Cp), 71.0 (unsubstituted Cp), 71.7 (Cp), 75.6 (Cp), 88.9 (Cp), 126.9 (Ar), 127.0 (Ar), 128.9 (Ar), 131.9 (Ar), 133.4 (Ar), 140.7 (Ar), 190.5 (*C*O). **IR (ATR, cm^{-1}):** 1644 (CO), 1597 (C=C). **MS (EI):** m/z 302 (M^+). To the NMR sample dissolved in $CDCl_3$, a droplet of trifluoroacetic acid was added inside the glove box. The solution was shaken well to give purple color. The proton NMR of the purple solution is as follows**: ^{1}H NMR ($CDCl_3$, 400 MHz, ppm):** δ 3.89 (AB, 1H, ^{2}J = 21.6 Hz, CH_AH$_B$), 3.99 (s, 5H, Cp), 4.08 (AB, 1H, ^{2}J = 21.6 Hz, CH$_A$$H_B$), 4.75 (t, 1H, ^{3}J = 2.4 Hz, Cp), 4.93 (br, 1H, Cp), 5.08 (br, 1H, Cp), 7.40-7.46 (m, 2H, Ar), 7.55-7.58 (m, 1H, Ar), 8.35 (d, 1H, ^{3}J = 7.6 Hz, Ar). **^{13}C{^{1}H} NMR (100 MHz,**

$CDCl_3$, ppm): δ 29.9 (*C*H_2), 66.2 (Cp), 71.6 (Cp, unsubstituted), 72.0 (Cp), 73.7 (Cp), 77.2 (Cp), 89.8 (Cp), 127.1 (Ar), 127.2 (Ar), 129.0 (Ar), 132.9 (Ar), 134.8 (Ar), 141.5 (Ar), 195.7 (*C*O).

Synthesis of $C_{22}H_{16}FeO$ (6b). In a 200-mL Schlenk flask, a solution of **3b** (500 mg, 1.35 mmol) in dichloromethane (60 mL) was added dropwise to a stirred solution of trifluoroacetic anhydride (0.76 mL, 5.40 mmol) in dichloromethane (50 mL) at 0 °C. The reaction was stirred for 1 h at room temperature and poured into saturated aqueous $NaHCO_3$ (100 mL). The layers were separated; the organic phase was washed with water and then dried over $MgSO_4$. The volatiles were removed *in vacuo*. The crude product was triturated with cold pentane to give **6b** (0.46 g, 96%) as a light red solid. **Mp:** 140–145 °C (dec) **^{1}H NMR ($CDCl_3$, 400 MHz, ppm):** δ 3.92 (s, 5H, Cp), 4.08 (AB, 1H, ^{2}J = 20.8 Hz), 4.22 (AB, 1H, ^{2}J = 20.8 Hz), 4.61 (t, 1H, ^{3}J = 2.4 Hz, CHC*H*CH), 4.76 (ABC, 1 H, Cp), 4.05 (ABC, 1H, Cp), 7.48–7.52 (m, 1H, Ar), 7.55–7.59 (m, 1H, Ar), 7.83 (s, 1H, Ar), 7.84 (d, 1H, 3J = 7.6 Hz, Ar), 8.04 (d, 1H, 3J = 7.6 Hz, Ar), 8.90 (s, 1H, Ar). **^{13}C{^{1}H} NMR (100 MHz, $CDCl_3$, ppm):** δ 29.7 (*C*H_2), 65.9 (Cp), 70.6 (Cp), 71.2 (Cp), 72.0 (Cp), 75.6 (Cp), 89.5 (Cp), 126.3 (Ar), 127.3 (Ar), 127.8 (Ar), 128.4 (Ar), 129.9 (Ar), 131.7 (Ar), 132.1 (Ar), 134.9 (Ar), 136.1 (Ar), 190.6 (*C*O). **IR (ATR, cm^{-1}):** 1623 (C=C), 1650 (CO). **MS (EI):** m/z 352 (M^+).

Synthesis of $C_{18}H_{12}FeO_2$ (7a). The complex was prepared by Nesmeyanov *et al.*[163] without full characterization. To the stirred solution of **6a** (45 mg, 0.14 mmol) in chloroform (5.0 mL), activated MnO_2 (940 mg) was added. The reaction mixture was stirred for 30 min at room temperature and then filtered

through a thin pad of silica. The filtrate was collected and volatiles were removed *in vacuo*. Analytically pure product was obtained by crystallization from a mixture of hexane and ethyl ether to give **6a** (39 mg, 88%) as a dark purple crystals. **Mp:** 192 °C. **^{1}H NMR ($CDCl_3$, 400 MHz, ppm):** δ 4.17 (s, 5H, Cp), 5.10 (t, 1H, ^{3}J = 2.8 Hz, CHC*H*CH), 5.47 (d, 2H, ^{3}J = 2.8 Hz, C*H*CHC*H*), 7.67–7.69 (m, 2H, Ar), 8.21–8.23 (m, 2H, Ar). **^{13}C{^{1}H} NMR (100 MHz, $CDCl_3$, ppm):** δ 72.8, 73.6 (Cp, unsubstituted), 76.5, 78.1(Cp), 126.7, 133.4, 135.3 (Ar), 188.6 (*C*O). **IR (ATR, cm^{-1}):** 1651(C=O). **MS (EI):** m/z 316 (M^+). The complex was characterized by X-ray diffraction. To the NMR sample dissolved in $CDCl_3$, a droplet of trifluoroacetic acid was added inside the glove box. The solution was shaken well to give a deep-purple color. The proton NMR of the purple solution is as follows**: ^{1}H NMR ($CDCl_3$, 400 MHz, ppm):** δ 4.28 (s, 5H, Cp), 5.38 (t, 1H, ^{3}J = 2.0 Hz, Cp), 5.67 (d, 2H, ^{3}J = 2.0 Hz, Cp), 7.74 (br, 2H, Ar), 8.23 (br, 2H, Ar). **^{13}C{^{1}H} NMR (100 MHz, $CDCl_3$, ppm):** δ 74.6, 75.1 (Cp, unsubstituted), 76.9 (Cp), 79.2 (Cp), 127.4, 134.5, 135.1 (Ar), 191.1 (*C*O).

Synthesis of $C_{22}H_{14}FeO_2$ (7b). To a stirred solution of **6b** (100 mg, 0.28 mmol) in dichloromethane (20 mL), activated MnO_2 (490 mg) was added. The reaction mixture was stirred for 2 h at room temperature and then filtered through a thin pad of Celite. The filtrate was collected and volatiles were removed *in vacuo*. The product was isolated by chromatography on silica with ethyl acetate**:**petroleum ether (1**:**3) as eluent to collect a pink band. Volatiles were removed *in vacuo* to give **7b** (97 mg, 93%) as a dark purple powder. Analytically pure product was obtained by recrystallization from hexane:ethyl ether (1**:**1) by

slow evaporation. **Mp:** 240-250 °C (dec). **^{1}H NMR ($CDCl_3$, 400 MHz, ppm):** δ 4.17 (s, 5H, Cp), 5.1 (t, 1H, ^{3}J = 2.4 Hz, CHC*H*CH), 5.51 (d, 2H, ^{3}J = 2.4 Hz, C*H*CHC*H*), 7.64–7.66 (m, 2H, Ar), 8.04–8.07 (m, 2H, Ar), 8.76 (s, 2H, Ar). **^{13}C{^{1}H} NMR (100 MHz, $CDCl_3$, ppm):** δ 72.8 (Cp), 73.5 (Cp), 76.8 (Cp), 78.1(Cp), 128.6 (Ar), 129.3 (Ar), 130.2 (Ar), 131.8 (Ar), 134.9 (Ar), 188.5 (*C*O). **IR (ATR, cm^{-1}):** 1666 (C=O), 1657 (C=C). **MS (EI):** m/z 366 (M^+). The complex was characterized by X-ray diffraction.

Synthesis of $C_{18}H_{16}FeO$ (8a). In a 125-mL Schlenk flask, **7a** (500 mg, 1.65 mmol) dissolved in ethyl ether (10 mL) was added dropwise to the stirred suspension of $LiAlH_4$ (80 mg, 2.1 mmol) at 0 °C. The reaction mixture was stirred for 1.5 h at the same temperature. Water (5 mL) was added and the mixture was passed through a thin pad of Celite. The filtrate was collected and layers were separated. The aqueous layer was extracted with ethyl ether (10 mL). The ether extracts were combined and dried over $MgSO_4$. The volatiles were removed *in vacuo* and product was isolated by chromatography on silica with dichloromethane**:**hexane (1**:**1) as eluent. Volatiles were removed *in vacuo* to give **8a** (434 mg, 86%) as a yellow semi-solid. **^{1}H NMR (400 MHz, $CDCl_3$, ppm):** δ 2.16 (d, 1H, ^{3}J = 11.2 Hz, CHO*H*), 3.63 (br, 2H, CH_2), 3.84 (s, 5H, Cp), 4.14 (t, 1H, ^{3}J = 1.6 Hz, CHC*H*CH), 4.33–4.36 (m, 2H, C*H*CHC*H*), 5.22 (d, 1H, ^{3}J = 10.8 Hz, C*H*OH), 7.24–7.28 (m, 2H, Ar), 7.32–7.36 (m, 1H, Ar), 7.83 (d, 1H, ^{3}J = 7.6 Hz). **^{13}C{^{1}H} NMR (100 MHz, $CDCl_3$, ppm):** δ 30.1 (*C*H2), 63.4, 65.4, 66.5, 66.8, 68.8, 90.6 (Cp), 84.4 (*C*HOH), 126.6, 126.7, 127.1, 128.2, 134.5, 140.1 (Ar). **^{1}H NMR (400 MHz, acetone-d_6, ppm):** δ 3.51 (AB, 1H, ^{2}J = 18.0 Hz, C$H_A$$H_B$), 3.68

(AB, 1H, ^2J = 18.0 Hz, $CH_A\mathit{H}_B$), 3.78 (s, 5H, Cp), 4.07 (t, 1H, ^3J = 2.3 Hz, CHC*H*CH), 4.27–4.28 (m, 2H, C*H*CHC*H*), 4.36 (d, 1H, ^3J = 8.1 Hz, CHO*H*), 5.25 (d, 1H, ^3J = 8.1 Hz, C*H*OH), 7.22–7.25 (m, 1H, Ar), 7.29–7.32 (m, 2H, Ar), 7.81 (d, 1H, ^3J = 8.1 Hz). **$^{13}C\{^1H\}$ NMR (100 MHz, acetone-d_6, ppm):** δ 30.6 (*C*H2), 63.9, 65.8, 66.7, 66.8, 69.6, 84.5 (Cp), 91.8 (*C*HOH), 126.3, 126.8, 127.2, 128.7, 136.0, 142.1 (Ar). **IR (ATR, cm^{-1}):** 3338 (vb, OH).

Synthesis of $C_{18}H_{18}Fe$ (9a). In a 125-Schlenk flask, **6a** (100 mg, 0.33 mmol) was added to the stirred suspension of powder zinc (1.0 g), mercuric chloride (0.1 g), conc. HCl (2 mL) and THF (20 mL). The reaction was allowed to reflux for 3 h, cooled to room temperature, and then filtered. The filtrate was collected and layers were separated. The aqueous layer was extracted with ethyl ether (2 x 10 mL). The combined organic phase was dried over $MgSO_4$ and volatiles were removed *in vacuo*. The product was isolated by chromatography on silica with ethyl ether**:**hexane (1**:**1) as eluent. The volatiles were removed *in vacuo* to give **9a** (68 mg, 71%) as a light yellow solid. Analytically pure product was obtained by recrystallization from hot hexane. **Mp:** 132 °C. **^1H NMR ($CDCl_3$, ppm):** δ 3.65 (s, 5H, Cp), 3.74 (s, 4H, CH_2), 4.04 (t, 1H, ^3J = 2.4 Hz, CHC*H*CH), 4.17 (d, 2H, ^3J = 2.4 Hz, C*H*CHC*H*), 7.18–7.26 (m, 4H, Ar). **$^{13}C\{^1H\}$ NMR (100 MHz, $CDCl_3$, ppm):** δ 30.5 (CH_2), 57.0, 66.4 (1, 2-Cp), 66.4 (Cp), 66.0 (CH*C*HCH), 69.2 (*C*HCH*C*H), 126.0, 126.5, 128.4, 128.5, 128.7, 129.6 (Ar). **MS (EI):** m/z 290 (M^+). The complex was characterized by X-ray diffraction.

Synthesis of $C_{36}H_{28}Fe_2$ (11a). In a 125-mL Schlenk flask, a mixture of powder aluminum (89 mg, 3.3 mmol), $HgCl_2$ (7 mg), cyclohexanol (4.5 mL) and

carbon tetrachloride (13 µL) was refluxed for 3 h. The mixture was cooled to room temperature and **6a** (100 mg, 0.33 mmol) was added. The reaction was again allowed to reflux for 2 h. The reaction was cooled to room temperature and conc. HCl (3.0 mL) and ethyl alcohol (3.0 mL) were added. The mixture was filtered and the filtrate was washed with water. The organic layer was separated and dried over $MgSO_4$. The volatiles were removed *in vacuo*. The crude product was triturated with cold methanol and dried to give **11a** (67 mg, 71%). The ^{1}H NMR analysis of the product showed the formation of multiple isomers. However, careful crystallization of the mixture from hot hexane gave single crystal of anti-isomer. **^{1}H NMR ($CDCl_3$, 400 MHz, ppm):** δ 3.52–3.53 (m, 4H), 3.59–3.61 (m, 6H), 6.62–6.64 (m, 2H), 6.96–6.98 (m, 2H), 7.37–7.43 (m, 2H), 7.76 (s, 2H), 7.79–7.85 (m, 4H). The complex was characterized by X-ray diffraction.

Synthesis of $C_{18}H_{13}DFeO$ (12a) and $C_{18}H_{16}FeO_2$ (13a). In a 50-mL Schlenk flask, LDA (120 µL of 2 M solution in heptane/tetrahydrofuran/ethylbenzene, 0.25 mmol) was slowly added to the stirred solution of **6a** (50 mg, 0.17 mmol) in THF (10 mL) at -78 °C. The mixture was allowed to stir for 1 h and quenched with deuterium oxide (2 mL). The mixture was slowly warmed to room temperature and stirred for an additional 1 h. Water (10 mL) was added and the product was extracted with ethyl ether (2 x 10 mL). The combined ether layers were dried over anhydrous $MgSO_4$, filtered and volatiles were removed *in vacuo*. The crude product was chromatographed on silica with ethyl ether**:**hexane (1**:**1) as eluent to give a yellow-red band as a first fraction. The removal of volatiles gave **12a** (12 mg, 24%) as a red solid. **^{1}H NMR**

($CDCl_3$, 400 MHz, ppm): δ 3.93 (s, 5H, Cp), 4.19 (t, 1H, ^2J = 5.2 Hz, C*H*D), 4.54 (br, 1H, Cp), 4.72 (br, 1H, Cp), 5.00 (br, 1H, Cp), 7.48-7.51 (m, 1H, Ar), 7.68 (br, 1H, Ar), 8.32 (d, 1H, ^3J = 7.6 Hz, Ar). The second chromatographic fraction yielded keto-alcohol **13a** (20 mg, 38%). **Mp:** 132 °C. **^{1}H NMR ($CDCl_3$, 400 MHz, ppm):** δ 1.99 (d, 1H, ^3J = 8 Hz, C*H*OH), 3.97 (s, 5H, Cp), 4.67 (t, 1H, 3J = 2.4 Hz, Cp), 4.97 (ABC, 1H, Cp), 5.08 (ABC, 1H, Cp), 5.75 (d, 1H, ^3J =7.6 Hz, CHO*H*), 4.47–4.51 (m, 1H, Ar), 4.58–7.62 (m, 1H, Ar), 7.67 (d, 1H, ^3J = 7.6 Hz, Ar), 7.26 (d, 1H, ^3J = 8 Hz). **^{13}C{^{1}H} NMR (100 MHz, $CDCl_3$, ppm):** δ 67.0, 67.4, 71.5, 72.4, 73.1, 77.4 (Cp), 89.8 (*C*HOH), 126.6, 129.1, 129.8, 132.5, 132.8, 142.4 (Ar), 189.3 (*C*O). **IR (ATR, cm^{-1}):** 1645 (C=O), 3490 (vb, OH). **MS (EI):** m/z 318 (M^+), 302 (M^+-H_2O).

Synthesis of $C_{25}H_{20}FeO$ (14a) and $C_{32}H_{26}FeO$ (15a). A mixture of **6a** (100 mg, 0.33 mmol), benzyl chloride (42 mg, 0.17 mmol), potassium hydroxide (100 mg, 1.78 mmol), tetrabutylammonium bromide (5 mg, 0.02 mmol) and potassium iodide (4 mg, 0.02 mmol) in dry acetone (20 mL) was heated at 60 °C for 4 h. The volatiles were removed *in vacuo* and the residue was dissolved in ethyl ether (20 mL) and washed with water (2 x 20 mL). The organic layer was collected and dried over $MgSO_4$. The volatiles were removed *in vacuo*. The crude product was chromatographed on silica with ethyl ether**:**hexane (3**:**1) as eluent. The product was collected as the second red band. Volatiles were removed *in vacuo* to give red viscous mass (108 mg). The analysis of the product with ^{1}H NMR showed the presence of monosubstituted **14a** (48 mg, 37 %) and disubstituted **15a** (60 mg, 37%) products in a 1**:**1 ratio. The mixture was

dissolved in hot pentane and cooled at -10 °C for 5 days to give **14a** as yellow crystals. **Mp:** 114 °C. **^{1}H NMR ($CDCl_3$, 400 MHz, ppm):** δ 2.73 (dd, 1H, ^{2}J = 13.2, ^{3}J = 8.0 Hz, C*H*$_A$H$_B$), 3.12 (dd, 1H, ^{2}J = 13.2, ^{3}J = 5.0 Hz, CH$_A$*H*$_B$), 3.82 (s, 5H, Cp), 4.22-4.23 (ABC, 1H, Cp), 4.26 (dd, 1H, ^{3}J = 5.0 Hz, ^{3}J = 8.0 Hz, C*H*), 4.45 (t, 1H, 2.4 Hz, Cp), 4.90(ABC, 1H, Cp), 6.69-6.71 (m, 2H, Ar), 7.09-7.14 (m, 3H, Ar), 7.37-7.42 (m, 2H, Ar), 7.50 (td, 1H, ^{3}J = 7.6 Hz, ^{4}J = 1.6 Hz, Ar), 8.22 (dd, 1H, ^{3}J = 8 Hz, ^{4}J = 1.2 Hz, Ar). **^{13}C{^{1}H} NMR (100 MHz, $CDCl_3$, ppm):** δ 43.5 (*C*H$_2$), 48.9 (*C*H), 65.7 (Cp), 70.9 (Cp), 71.1 (Cp unsubstituted), 71.5 (Cp), 75.2 (Cp-ipso), 92.5 (Cp-ipso), 126.5, 126.6, 127.2, 128.1, 128.7, 129.9, 131.7, 133.6, 138.0, 144.8 (Ar), 190.1 (*C*O). **IR (ATR, cm^{-1}):** 1646 (C=O). The product was characterized with an X-ray crystallography. The mother liquor was concentrated and cooled at -10 °C again for another 3 days to collect **15a** as dark-yellow crystals. **^{1}H NMR ($CDCl_3$, 400 MHz, ppm):** δ 3.01 (AB, 2H, ^{2}J = 12.4, C*H*$_A$H$_B$), 3.18 (AB, 2H, ^{2}J = 12.4 Hz, CH$_A$*H*$_B$), 3.95 (s, 5H, Cp), 4.48 (ABC, 1H, Cp), 4.60 (t, 1H, 2.8 Hz, Cp), 4.92 (ABC, 1H, Cp), 5.86 (d, 2H, ^{3}J = 8.4 Hz, Ar), 6.69-6.73 (m, 3H, Ar), 6.88 (t, 1H, ^{3}J =7.2 Hz, Ar), 7.34-7.36 (m, 3H, Ar), 7.55-7.59 (m, 3H, Ar), 8.08 (dd, 2H, ^{3}J = 7.6 Hz, ^{4}J = 1.6 Hz, Ar). **^{13}C{^{1}H} NMR (100 MHz, $CDCl_3$, ppm):** δ 45.5 (*C*H$_2$), 48.1 (*C*H$_2$), 53.7 (C), 65.3 (Cp), 70.5 (Cp), 70.9 (Cp unsubstituted), 71.8 (Cp), 75.2 (Cp-ipso), 99.3 (Cp-ipso), 126.4, 126.5, 126.9, 127.1, 127.2, 127.8, 128.5, 130.2, 131.5, 132.1, 134.2, 135.8, 138.9, 147.0 (Ar), 188.7 (*C*O). **IR (ATR, cm^{-1}):** 1643 (C=O). The product was characterized by an X-ray crystallography.

Attempted synthesis of $C_{21}H_{22}FeOSi$ (16a). In an oven-dried 125-mL Schlenk flask, LiHMDS (2 mL of 1 M solution in hexane, 2 mmol) and TMSCl (0.1 mL, 0.8 mmol) were added to the stirred solution of **6a** (200 mg, 0.66 mmol) in THF (10 mL) at -78 °C. The reaction was slowly allowed to warm to room temperature and stirred for 4 h. The volatiles were removed *in vacuo*. The green gum was dissolved in dry hexane and filtered under nitrogen. The filtrate was collected and volatiles were removed *in vacuo*. The ^{1}H NMR of the green gum showed multiple impurities, mainly the aliphatic. The hexane-soluble green mass, possibly **16a**, was chromatographed on silica with ethyl ether**:**hexane (1**:**1) as eluent. Exposure to air changed the product's color from green to dark red. The first light yellow fraction showed the presence of starting materials. The ^{1}H NMR analysis of the second red fraction showed the formation of two stereoisomers: (*R,S*) and *meso* of dimerized anthrone ($C_{36}H_{26}Fe_2O_2$) **17a** (83 mg, 42%) in a 4:1 ratio. The two compounds of the second fraction were inseparable with column chromatography. The analysis of the single crystals of the mixture showed the presence of dimerized Fc-anthrone (*R,S*) as major component and the meso form as minor component. Dimerized Fc-anthrone **17a** (*R,S*) isomer**: ^{1}H NMR ($CDCl_3$, 400 MHz, ppm):** δ 3.75 (s, 10 H, Cp), 4.26 (ABC, 2H, Cp), 4.41 (s, 2H, C*H*), 4.47 (t, 2H, ^{3}J = 2.4 Hz, Cp), 4.75 (ABC, 2H, Cp), 6.77 (dd, 2H, ^{3}J = 7.2 Hz, ^{4}J = 1.6 Hz, Ar), 7.29–7.37 (m, 4H, Ar), 8.01 (dd, 2H, ^{3}J = 7.6 Hz, ^{4}J = 1.6 Hz, Ar). **^{13}C{^{1}H} NMR (100 MHz, $CDCl_3$, ppm):** δ 51.7 (*C*H), 65.6, 71.0, 71.1, 71.7, 76.4, 89.4 (Cp), 126.0, 127.8, 128.4, 131.2, 134.7, 140.7 (Ar), 189.2 (*C*O). **IR (ATR, cm^{-1}):** 1646, 1656 (C=O). **MS (EI):** m/z 602 (weak, M^+), 301 (M^+/2). **17a**

The *meso* form**: ^{1}H NMR ($CDCl_3$, 400 MHz, ppm):** δ 3.29 (ABC, 2H, Cp), 3.68 (s, 10 H, Cp), 4.23 (t, 2H, ^{3}J = 2.8 Hz, Cp), 4.48 (s, 2H, C*H*), 4.65 (ABC, 2H, Cp), 7.28-7.34 (m, 2H, Ar), 7.49-7.50 (m, 4H, Ar), 7.65 (d, 2H, ^{3}J =7.6 Hz, Ar), 8.19 (d, 2H, ^{3}J = 8 Hz, Ar). The third red fraction of the column was Fc-hydroxyanthrone $C_{18}H_{14}FeO_2$, **13a** (47 mg, 22%) The fourth fraction of column contained Fc-quinone **7a.**

Synthesis of $C_{31}H_{29}FeNO_3Si$ (18a). In an oven-dried 125-mL Schlenk flask, LDA (0.24 mL of 2 M solution in heptanes/tetrahydrofuran/benzene, 0.50 mmol) was added to the stirred solution of **6a** (100 mg, 0.33 mmol) in ethyl ether (10 mL) at -78 °C. The reaction mixture was stirred for 2 h and TMSCl (84 µL, 0.66 mmol) was added. The reaction mixture was allowed to warm to room temperature and stirred for an additional 1 h to give dark green solution. The volatiles were removed *in vacuo*. The green gum was dissolved in THF (5 mL) and N-phenylmaleimide (58 mg, 0.33 mmol) was added. The solution turned to light yellow immediately. The reaction mixture was stirred at room temperature for 30 min and volatiles were removed *in vacuo*. The crude product was chromatographed on silica with ethyl ether**:**hexane (1**:**1) as eluent. The second reddish-yellow fraction was collected and volatiles were removed *in vacuo* to give **18a** (79 mg, 44%) as a light yellow solid. Analytically pure product was obtained by recrystallization from pentane by cooling overnight at -10 °C. **Mp:** 212 °C. **^{1}H NMR ($CDCl_3$, 400 MHz, ppm):** δ 0.45 (s, 9H, Si(CH_3)$_3$), 3.18 (ABX, 1H, J_{AB} = 8.4 Hz, J_{BX} = 2.8 Hz, C*H*), 3.20 (ABX, 1H, J_{AB} = 8.4 Hz, J_{BX} = 3.2 Hz, C*H*), 3.55 (s, 5H, Cp), 3.96 (ABC, 1H, Cp), 4.21 (ABC, 1H, Cp), 4.32 (ABC, 1H, Cp), 4.36 (d,

1H, ^3J = 2.8 Hz, C*H*), 6.42–6.44 (m, 2H, Ar), 7.22–7.23 (m, 3H, Ar), 7.27–7.28 (m, 2H, Ar), 7.32–7.36 (m, 1H, Ar), 7.61 (d, 1H, ^3J = 7.2 Hz). **$^{13}C\{^1H\}$ NMR (100 MHz, $CDCl_3$, ppm):** δ 2.9 (SiCH_3)$_3$, 40.3, 50.6, 52.3 (*C*H), 62.9, 64.3, 64.7 (C3-C5 Cp), 69.2 (Cp), 79.5 (*C*-OSi), 90.7, 93.7 (C1-C2 Cp), 121.3, 123.8, 126.8, 126.9, 127.0, 128.8, 129.2, 131.7, 137.9, 141.6 (Ar), 173.2, 175.5 (*C*O). **IR (ATR, cm^{-1}):** 1715 (C=O). **MS (EI):** m/z 547 (M^+), 374 (M^+-N-phenylmaleimide).

Synthesis of $C_{27}H_{28}FeO_5Si$ (19a). In an oven-dried 125-mL Schlenk flask, LDA (0.25 mL of 2 M solution in heptanes/tetrahydrofuran/benzene, 0.50 mmol) was added to the stirred solution of **6a** (100 mg, 0.33 mmol) in ethyl ether (10 mL) at -78 °C. The reaction mixture was stirred for 2 h and TMSCl (84 µL, 0.66 mmol) was added. The reaction mixture was allowed to warm to room temperature and stirred for an additional 1 h to give dark green solution. DMAD (60 µL, 0.49 mmol) was added and the reaction mixture was stirred for an additional 1 h at room temperature. The volatiles were removed *in vacuo*. The crude product was chromatographed on silica with ethyl ether**:**hexane (1**:**1) as eluent. The second reddish-yellow fraction was collected and volatiles were removed *in vacuo* to give **19a** (82 mg, 48%) as a light red solid. Analytically pure product was obtained by recrystallization from pentane by cooling overnight at -10 °C. **Mp:** 188-190 °C. **^1H NMR ($CDCl_3$, 400 MHz, ppm):** δ 0.44 (s, 9H, Si(CH_3)$_3$), 3.53 (s, 5H, Cp), 3.64 (s, 3H, OCH_3), 3.71 (s, 3H, OCH_3), 3.89 (ABC, 1H, Cp), 4.17 (ABC, 1H, Cp), 4.22 (ABC, 1H, Cp), 5.06 (s, 1H, C*H*), 7.11 (dt, 1H, ^3J = 7.6 Hz, ^2J = 1.2 Hz, Ar), 7.18 (dt, 1H, ^3J = 7.6 Hz, ^2J = 1.2 Hz, Ar), 7.36 (d, 1H, ^3J = 7.2 Hz, Ar), 7.50 (d, 1H, ^3J = 7.2 Hz, Ar). **$^{13}C\{^1H\}$ NMR (100 MHz,**

$CDCl_3$, ppm): δ 2.9 (SiCH_3)$_3$, 43.3 (*C*H), 52.1 (O*C*H_3), 52.5 (O*C*H_3), 63.5, 63.7, 64.3 (C3-C5 Cp), 69.5 (Cp), 84.2 (*C*-OSi), 97.6, 97.8 (C1-C2 Cp), 119.8, 122.7, 125.1, 125.5, 139.4, 144.1 (Ar), 148.6, 160.1 (*C*=*C*), 164.0, 166.4 (*C*O). **IR (ATR, cm^{-1}):** 1734, 1704 (C=O), 1655 (C=C). **MS (EI):** m/z 516 (M^+), 374 (M^+-DMAD).

Synthesis of $[C_{18}H_{15}Fe]BF_4$ (20a). A solution prepared by adding of 40% aqueous fluoroboric acid (2 mL) to acetic anhydride (9 mL) at 0 °C was added to a solution of Fc-carbinol **8a** (434 mg, 1.43 mmol) in acetic anhydride (2 mL). The reaction mixture was allowed to stand at room temperature for 15 min. Ethyl ether (100 mL), purged with nitrogen for 5 min, was added and olive-green precipitate was obtained. The supernatant liquid was decanted and the residue was dried under vacuum to give **20a** (320 mg, 60%) as an olive-green solid. Attempts to recrystallize of the product failed. **Mp:** does not melt up to 250 °C. **^{1}H NMR (acetone-d_6, 400 MHz, ppm):** δ 3.35 (AB, 1H, ^{2}J = 21.6 Hz, C$H_A$$H_B$), 3.66 (AB, 1H, ^{2}J = 21.6 Hz, $CH_A$$H_B$), 4.84 (s, 5H, Cp), 5.01 (br, 1H, Cp), 6.36 (t, 1H, ^{3}J = 2.8 Hz, Cp), 6.75 (br, 1H, Cp), 7.40 (d, 1H, ^{3}J = 7.2 Hz, Ar), 7.46-7.50 (m, 1H, Ar), 7.54-7.56 (m, 1H, Ar), 8.10 (d, 1H, ^{3}J = 7.6 Hz, Ar), 8.44 (s, 1H, C^+*H*). **^{1}H NMR (CD_2Cl_2, 400 MHz, ppm):** δ 3.22 (AB, 1H, ^{2}J = 21.6 Hz, C$H_A$$H_B$), 3.45 (AB, 1H, ^{2}J = 21.6 Hz, $CH_A$$H_B$), 4.66 (s, 5H, Cp), 4.82 (br, 1H, Cp), 6.09 (br, 1H, Cp), 6.51 (br, 1H, Cp), 7.30 (d, 1H, ^{3}J = 7.2 Hz, Ar), 7.41-7.45 (m, 1H, Ar), 7.49-7.52 (m, 1H, Ar), 7.93 (d, 1H, ^{3}J = 7.6 Hz, Ar), 8.19 (s, 1H, C^+*H*). **^{13}C{^{1}H} NMR (100 MHz, CD_2Cl_2, ppm):** δ 29.3 (*C*H_2), 76.78 (Cp-4), 82.8 (Cp), 90.1, 90.2 (Cp-3,5), 98.6, 98.8 (CC), 118.1 (C^+), 128.9, 130.0, 131.4, 132.4, 132.6, 137.1 (Ar). There was no signal of proton and carbon resonances on the same NMR sample taken

after 24 h. **IR (ATR, cm^{-1}):** 1062 (BF_4). The dry sample changed its color from olive green to dark green on storage for 24 h. We were unable to measure the ^{1}H and ^{13}C NMR of the resultant sample due to its paramagnetism. The resultant compound was expected to be converted to its dimeric form, $[C_{36}H_{28}Fe_2][BF_4]_2$ **(21a)**.

Synthesis of $C_{23}H_{25}FeN$ (23a). To a solution of **20a** (230 mg, 0.61 mmol) in dichloromethane (12 mL), piperidine (0.1 mL, 1.0 mmol) was added at room temperature. The solution changed its color from olive green to light yellow. The reaction was stirred for 5 min. The volatiles were removed *in vacuo* and the product was extracted in pentane. The volatiles were again removed *in vacuo* to give **23a** (0.18 g, 78%) as a light yellow solid. **Mp:** 88-90 °C. **^{1}H NMR ($CDCl_3$, 400 MHz, ppm):** δ 1.21-1.24 (m, 2H, CH_2), 1.39-1.43 (m, 4H, CH_2), 2.25-2.28 (m, 4H, CH_2), 3.56 (AB, 1H, ^{2}J = 21.2 Hz, CH_AH$_B$), 3.64 (AB, 1H, ^{2}J = 21.2 Hz, CH$_A$$H_B$), 3.66 (s, 5H, Cp), 4.09 (t, 1H, ^{3}J = 2.4 Hz, Cp), 4.25 (br, 2H, Cp), 4.61 (br, 1H, C*H*N), 7.20-7.23 (m, 2H, Ar), 7.24-7.27 (m, 1H, Ar), 7.46 (d, 1H, ^{3}J = 6.8 Hz, Ar), **^{13}C{^{1}H} NMR (100 MHz, $CDCl_3$, ppm):** δ 24.6 (*C*H$_2$), 26.4 (*C*H$_2$), 31.0 (*C*H$_2$), 45.2 (*C*H$_2$N), 49.8 (*C*HN), 65.4, 66.0, 66.5, 67.4, 69.4, 86.3 (Cp), 126.1, 126.6, 127.8, 130.7, 137.3, 138.3 (Ar). **IR (ATR, cm^{-1}):** 2930 (C-H), **MS (EI):** m/z 371 (M^+), 286 (M^+-$C_5H_{10}N$).

Attempted synthesis of $C_{18}H_{14}Fe$ (10a):

Method A. To a stirred solution of **9a** (40 mg, 0.14 mmol) in benzene (5 mL), DDQ (64 mg, 0.28 mmol) was added. The reaction mixture changed the color from light yellow to dark immediately. The mixture was stirred for 1 h and then volatiles were removed *in vacuo.* The crude product was purified by column chromatography on silica with ethyl ether**:**hexane (1**:**1) as eluent to collect a dark band. Removal of volatiles *in vacuo* showed the formation of quinone **7a** (26 mg, 59%).

Method B. In a nitrogen-purged 125-mL Schlenk flask, of hydroxyanthrone **8a** (100 mg, 0.33 mmol) was dissolved in acetic anhydride (5 mL). The mixture was refluxed for 8 h. The reaction slowly changed the color from light yellow to red. TLC analysis of the product showed the formation of Fc-anthrone along with starting materials.

Method C. To a solution of freshly prepared **20a** (150 mg, 0.40 mmol) in dichloromethane (10 mL), triethylamine (0.1 mL, 0.71 mmol) was slowly added at 0 °C. The solution changed its color from olive green to light yellow. The reaction was stirred for 15 minutes. The volatiles were removed *in vacuo* and the crude product was chromatographed on silica with ethyl ether**:**hexane (1**:**3) as eluent. The first light yellow band was collected and volatiles were removed *in vacuo* to give $C_{36}H_{30}Fe_2$, **20a** (63 mg, 55%) as a light yellow solid. Analytically pure product was obtained by cooling concentrated solution in hexane at -10 °C for 24 h. **Mp:** 140-142 °C. **^{1}H NMR (acetone-d$_6$, 400 MHz, ppm):** δ 2.28 (AB, 1H, ^{2}J =

17.2 Hz, CH_AH$_B$), 3.15 (AB, 1H, ^{2}J = 17.2 Hz, CH$_A$$H_B$), 3.30 (ABC, 1H, Cp), 3.54 (s, 5H, Cp), 3.82 (t, 1H, ^{3}J = 2.4 Hz, Cp), 3.98 (ABC, 1H, Cp), 4.20 (s, 1H, C*H*), 7.07 (d, 1H, ^{3}J = 6.8 Hz, Ar), 7.18-7.23 (m, 2H, Ar), 7.36 (d, 1H, ^{3}J = 6.8 Hz, Ar). **^{13}C{^{1}H} NMR (100 MHz, acetone-d$_6$, ppm):** δ 30.8 (*C*H$_2$), 52.0 (*C*H), 66.0, 66.4, 67.4, 69.6, 85.1, 87.0 (Cp), 126.3, 126.7, 128.5, 129.8, 139.4, 139.7 (Ar). **MS (EI):** m/z 574 (M$^+$), 287 (M$^+$/2). The complex was characterized by X-ray diffraction as the (*R,R*)/(*S,S*) stereoisomer. The second chromatographic fraction yielded the *meso* stereoisomer (22 mg, 10%). **^{1}H NMR (acetone-d$_6$, 400 MHz, ppm):** δ 2.12 (AB, 1H, ^{2}J = 17.6 Hz, CH_AH$_B$), 3.08 (AB, 1H, ^{2}J = 17.6 Hz, CH$_A$$H_B$), 3.56 (s, 5H, Cp), 3.88 (br, 1H, Cp), 3.96 (t, 1H, ^{3}J = 2.4 Hz, Cp), 4.02 (br, 1H, Cp), 4.15 (s, 1H, C*H*), 6.83 (d, 1H, ^{3}J = 8.0 Hz, Ar), 6.99-7.05 (m, 1H, Ar), 7.12-7.17 (m, 2H, ^{3}J = 6.8 Hz, Ar).

Reduction of [C$_{36}$H$_{28}$Fe$_2$][BF$_4$]$_2$. To the suspension of **21a** (50 mg, 0.07 mmol) in acetic acid (5 mL), excess zinc powder (200 mg, 3.05 mmol) was added. The reaction was stirred for 15 min at room temperature. Water (10 mL) was added and the product was extracted with ethyl ether (2 x 10 mL). The combined ether layer was washed with saturated aqueous NaHCO$_3$ (3 x 5 mL). The organic layer was collected and dried over MgSO$_4$. Volatiles were removed *in vacuo* and the resulted viscous mass was dissolved in pentane. Evaporation of pentane to dryness gave **22a** (34 mg) as a light yellow viscous mass. Analytically pure product was not obtained. However, the analysis of the crude product with ^{1}H NMR showed the formation of two isomers of **22a** along with other impurities.

The analysis of the crude products with high-resolution mass spectroscopy also indicated the formation of two expected product.

5.3. Results and Discussion

5.3.1. Synthesis and Characterization. Several routes of synthesis of ferrocene-fused quinone complexes **7a** and **7b** are shown in Scheme 5.2 and Scheme 5.3. The Friedel-Crafts acylation of ferrocene with phthalic anhydride in the presence of $AlCl_3$ by following the conditions reported for the analogous reaction between ferrocene and cyclohexane-1,2-dicarboxylic anhydride[162] gave *o*-carboxybenzoylferrocene **2a** consistently less than 15% yield. To improve the yield of the reaction, phthalic anhydride was converted to *o*-carbomethoxybenzoic acid by refluxing in anhydrous methanol[159] and then treated with thionyl chloride to give *o*-carbomethoxybenzoyl chloride.[160] The Friedel-Crafts acylation of *o*-carbomethoxy benzoyl chloride with ferrocene in the presence of $AlCl_3$ using a mixture of carbon disulfide and ethyl ether as a solvent[157] gave 2-carbomethoxybenzoylferrocene **1a** (77%). Similarly 2,3-naphthalenedicarboxylic anhydride was treated with methanol to obtain 2-carbomethoxynaphthanoic acid, which was in turn converted to monomethyl 2-naphthalate chloride using $SOCl_2$. The reaction of ferrocene with the resultant acid chloride under Friedel-Crafts condition gave keto-ester complex **2b** (89%).

For the activation of carbon atom at 2-positon of substituted Cp requires the conversion of α-carbonyl group to methylene. The conventional way of reducing carbonyl group at α-position of ferrocenyl group is the Clemmensen

reduction of α-ferrocenyl ketone.[164-167] However, our attempts to reduce keto-ester **1a, 1b** and keto-acid **2a** under acidic Clemmensen conditions following literature procedure[157,168] was not result oriented. Our first attempt to reduce *o*-carboxybenzoylferrocene **2a** in the presence of activated zinc/HCl with toluene as cosolvent gave us desired *o*-carboxybenzylferrocene **3a** (72%) within 4 h.

Scheme 5.2. Synthesis of ferrocene-fused quinone complexes

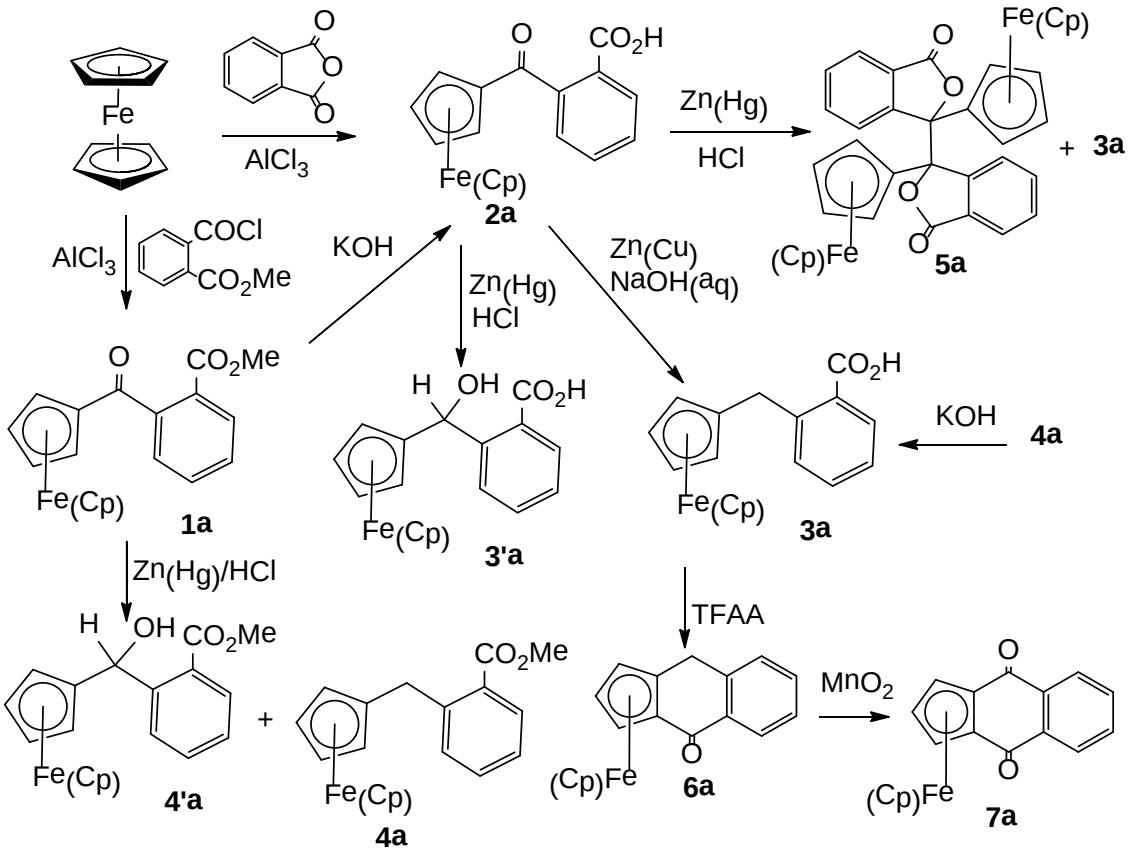

However, we were unable to reproduce the procedure in other preparations. Surprisingly, when the scale of the reaction was increased by five, we recovered ferrocenylcarbinol **3'a** (71%) even after 8 h of reflux. Similarly, reduction of keto-ester **1a** in the presence of Zn/HCl using methanol as

cosolvent,[157] we isolated desired **4a** (70.5%) and carbinol **4'a** (15%). Formation of secondary alcohol is evidenced by singlet resonance at δ 6.25 ppm (**3'a**) and 5.30 ppm (**4'a**) due to methine proton. Further reduction of the carbinol with longer reaction time and additional amount of reagents also could not give the desired result. The extra stability of secondary alcohol might be due to intramolecular H-bonding with the carbonyl group of carboxylic group. The ester **4a** was saponified to carboxylic acid **3a** (55%) in the presence of 25% aqueous KOH. Similarly, ester **4b** was saponified using KOH/MeOH to carboxylic acid **3b** (67%).

When reaction time for reduction of ketone was increased for 24 h while refluxing in toluene, we isolated desired **3a** (23%) along with dimerized lactone **5a** (9%). Under similar reaction conditions, keto-ester **1b** gave methylene ester **4b** (44%) and dimerized lactone **5b** (44%). The formation of the lactone was evidenced by IR stretching (**5a**, 1768 cm^{-1}; **5b**, 1765 cm^{-1}) at higher wavenumber due to carbonyl group than the corresponding keto-acid (**1a**, 1652 cm^{-1}) and keto-ester (**1b**, 1655 cm^{-1}). The four protons of substituted Cp in the ^{1}H spectra of **5a** and **5b** gave separate signals, indicating the chiral center at α-carbon atom. The mass spectra of dimeric lactone complex showed base peaks at 317 (**5a)** and 367 (**5b**) corresponding to half the molecular ion peak to indicate homolytic cleavage of the dimer. The dimerization was further evidenced by an X-ray crystallography.

Nesmeyanov *et al*. suggest that *o*-carboxybenzoylferrocene exists in solution in the forms of two isomers as shown in Scheme 5.4. This is due to its

capability of ring-chain tautomerism. Out of two tautomers, only one is active in some transformation depending upon the polarity of solvent.[163] On the similar lines of arguments, the Simenel group rationalized the formation of 3-(N-imidazolyl)-3-ferrocenylisobenzofuran-1(3*H*)-one as an unexpected but the exclusive product from a reaction between *o*-carboxybenzoylferrocene and N,N'-carbonyldiimidazole in an attempt to form an amide linkage.[169]

Scheme 5.3. Synthesis of Fc-anthraquinone by two-step Friedel-Crafts acylation

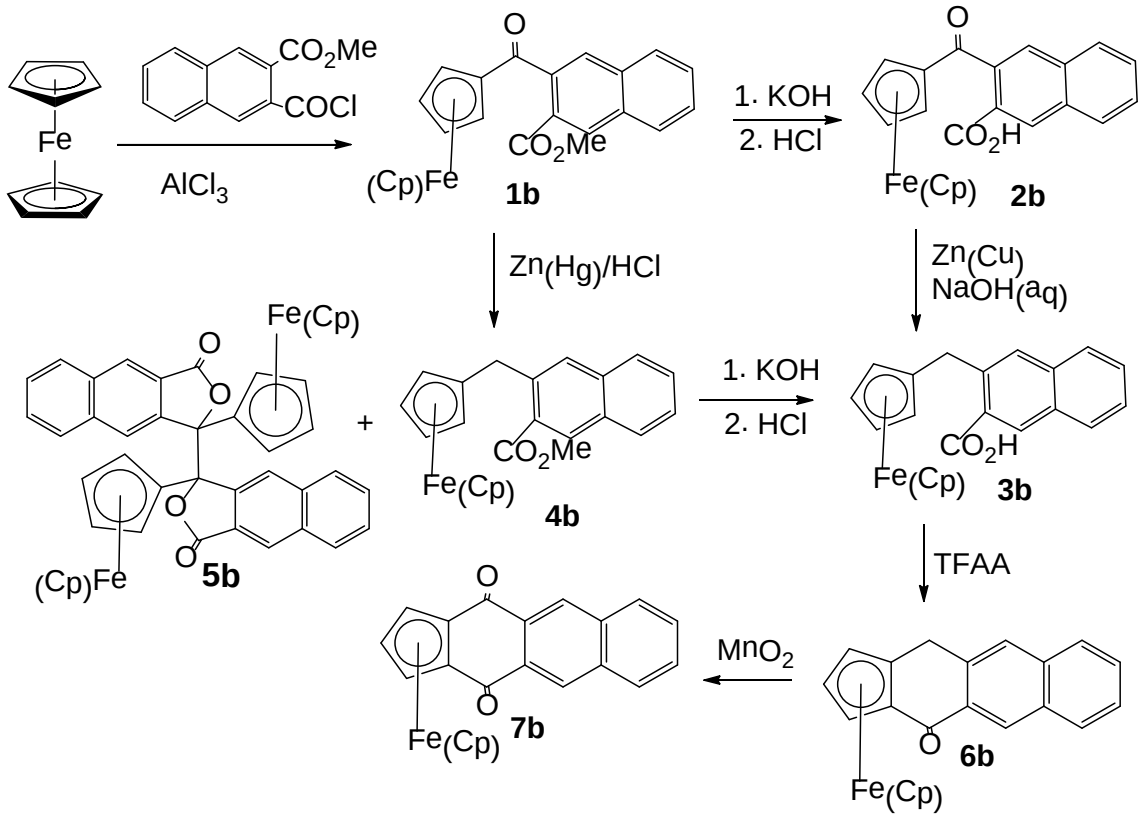

We obtained the contradictory results of these reports as the ring-chain isomerism is not possible in case of carbomethoxy ester **4b**. Our results showed that dimerized lactone is formed in higher proportion (**5b**, 44%) than the dimer (**5a**, 9%) from keto-acid **4a**. We rationalize the results of dimerization on the

basis of involvement of ketyl free radical. The nucleophilic attack of O-atom on carbonyl center of ester and departure of alkoxy or hydroxyl groups in form of alcohol or water in acidic media gives lactone. The free radical at 3° free radical alpha to two aromatic rings is sufficiently stable to dimerize (Scheme 5.5)

Scheme 5.4. Equilibration of *o*-carboxybenzoylferrocene and its cyclic tautomer

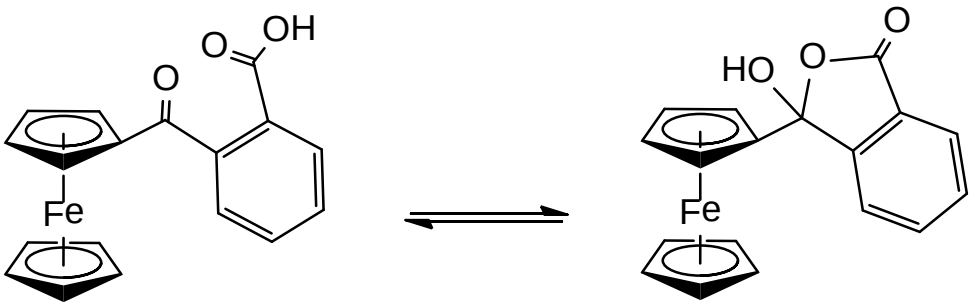

The keto-ester **1a** and **1b** were saponified under basic conditions to give keto acids in nearly quantitative yields (**2a**, 97%; **2b**, 97%). When the keto-acids were subjected to Clemmensen reduction by using zinc and aqueous sodium hydroxide for 24 h by following literature procedure[170], we obtained excellent results to yield **3a** (89%) and **3b** (58%). This result also indicates the role of acidic media for the formation of lactone. When reaction of **3a** was stopped within 30 min, α-carbinol **3'a** was isolated as an exclusive product.

The carboxylic acid complexes **3a** and **3b** gave Fc-anthrone **6a** (96%) and Fc-anthracenone **6b** (96%) in almost quantitative yields in the presence of trifluoroacetic anhydride[171] even in gram-scale reactions. The Fc-anthrone and Fc-anthracenone complexes have distinctive AB pattern of resolution in ^{1}H NMR with high coupling constant (20-21 Hz) due to geminal coupling of methylene

protons. Similarly, substituted Cp gives three distinct ABC resonances, showing breaking in symmetry of the molecule.

Scheme 5.5. Proposed mechanism of dimerization of keto-acid under acidic condition

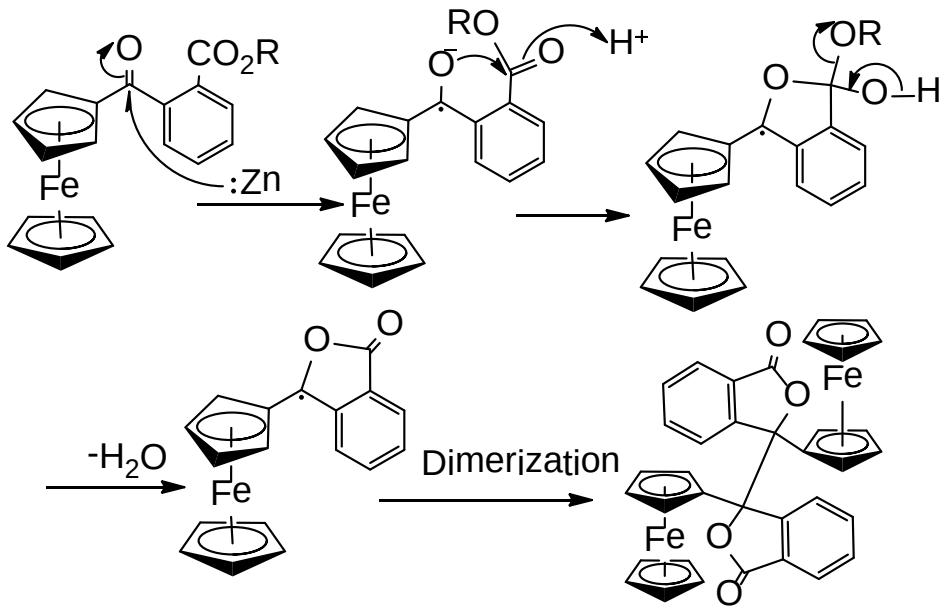

When a tiny drop of trifluoroacetic acid was added to the solution of **6a** in $CDCl_3$ in NMR tube, it changed color from dark red to deep purple. The color change of the sample was accompanied by the deshielding of protons and carbon resonances. We observed minimal shifts in proton and carbon resonances of methylene and arene signals. The shifts in ppm due to proton**:** 3-H (0.21), 4-H (0.21), 5-H (0.07) and Cp (0.09); and carbon**:** 1-C (0.9 ppm), 2-C (-0.8 ppm), 3-C (1.7 ppm), C-4 (0.5 ppm), C-5 (2.0 ppm) resonances are in support of protonation of carbonyl oxygen. There is significant shift (5.0 ppm) in carbon resonance due to carbonyl carbon. The downfield shift of proton and carbon signals along with color change of the solution indicates the delocalization of

positive charge in different positions as shown in Figure 5.1. As the effects of protonation on ferrocenyl moiety is higher than that of arene moiety, it appeared that structures **I** and **II** are more contributing than structures **III** and **IV**. This might be due to the higher electronic density of Cp than that of arene and the tendency of arene to retain its aromaticity. In all canonical structures iron retains its coordinatively saturated electronic configuration to minimize the effect of paramagnetism, however, there was a slight broadening of proton and carbon signals after acidification.

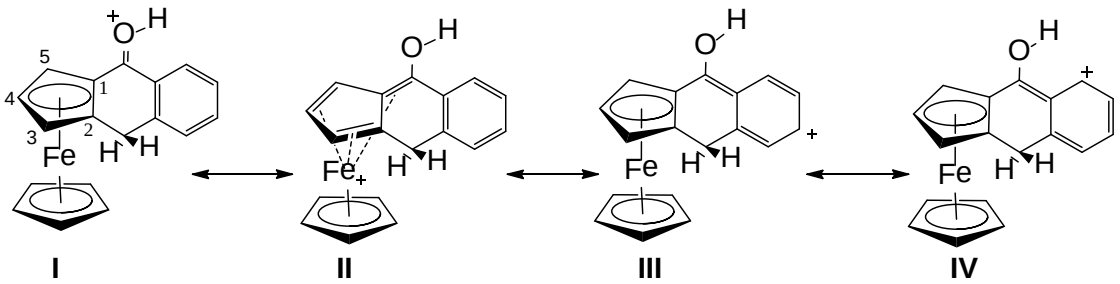

Figure 5.1. Delocalization of positive charge on acidified Fc-anthrone

The ketone complexes **6a** and **6b** slowly undergo oxidation with air during storage to Fc-quinones. The intentional oxidation of those ketones with MnO_2 in chloroform gave ferrocene-fused quinones **7a** (88%) and **7b** (97%) within 30 min at room temperature. The loss of asymmetry of substituted Cp and disappearance of signals due to methylene protons and carbons in NMR indicated the formation of quinones. The X-ray crystal structure analysis of both quinones displayed a slight proximity of *ipso* carbons towards Fe center in comparison to remaining three carbons of Cp. This unusual bonding mode of substituted Cp indicates the interaction of electron deficient *ipso* carbons, caused by the inductive effect of carbonyl, with electron-rich Fe center.

We studied the effect of acids on proton and carbon resonances of quinone **7a** under NMR conditions. The shifts in ppm due to resonances of Cp protons 3,5-H (0.20), 4-H (0.28) and unsubstituted Cp (0.09); and carbons 1,2-C (1.1), 3,5-C (0.4), 4-C (1.8) reveals the effects of protonation of ketonic oxygen. Similar deshielding was observed in proton and carbon resonances of arene moiety as well but they were less obvious than that of Cp. The most significant shift (2.5 ppm) was observed in carbonyl carbon. We assume that there is fast exchange of protons between two carbonyl O-atoms as shown in the contributing structures **I-IV** (Figure 5.2) to retain the symmetry of the molecules. Similarly, delocalization of positive charge over different atoms is responsible for the deepening of color after acidification.

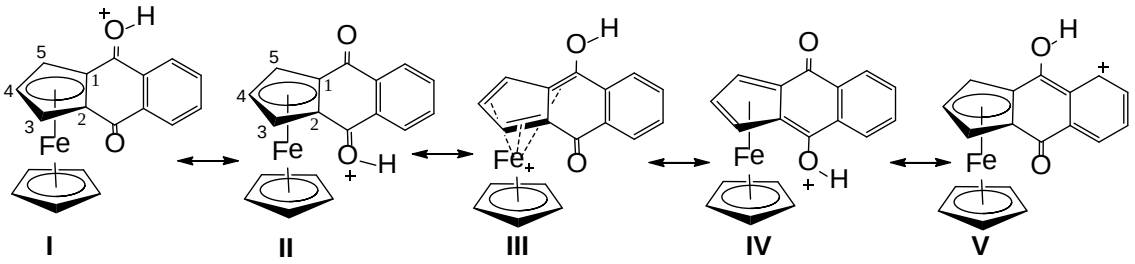

Figure 5.2. Delocalization of positive charge on acidified Fc-quinone

Various reactions of Fc-anthrone are shown in Scheme 5.6. The carbonyl group of **6a** was reduced to alcohol using $LiAlH_4$ to give α-carbinol **8a** (86%). ^1H and ^{13}C NMR analysis of the product shows only one isomer of alcohol, most probably the *endo* one due to the nucleophilic attack of hydride from *exo* to the Fe center. The secondary alcohol readily oxidizes back to ketone upon exposure to air in solution. In an attempt to dehydrate complex **8a**, we used milder to

harsher reaction condition starting from anhydrous $CuSO_4$,[55] and molecular sieves to Ac_2O but our all attempts to give benz[*f*]indene complex **10a** failed.

Scheme 5.6. Reactions of Fc-anthrone

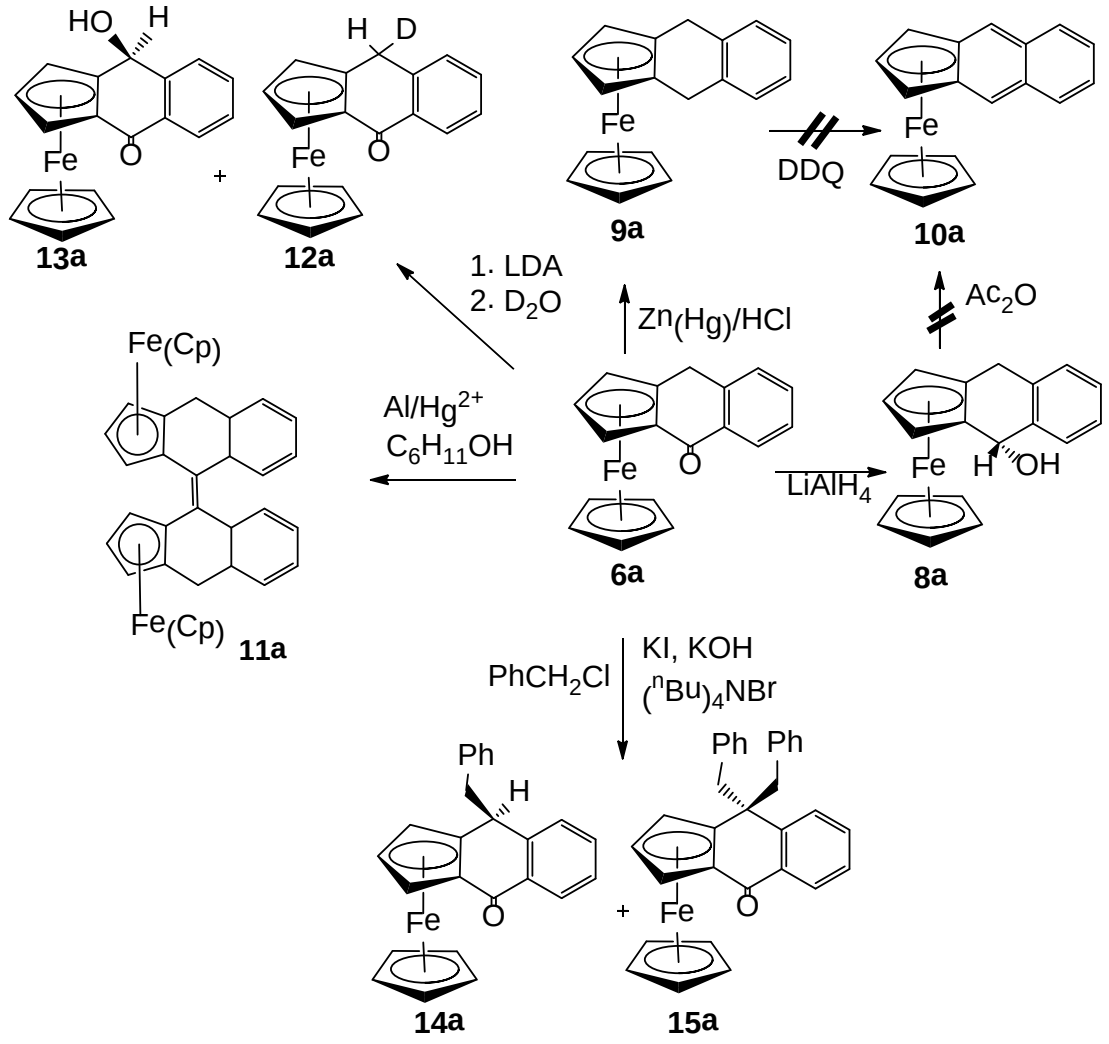

The reduction of Fc-anthrone **6a** under acidic Clemmensen conditions[168] gave methylene complex **9a** (71%) which was evidenced by a singlet (δ 3.74 ppm) resonance in ^{1}H NMR integrating four protons due to two methylene groups. An X-ray crystallographic analysis of the complex revealed a bending of Cp-fused ligand at methylene C-atoms with respect to Cp plane towards the Fe-

center by an angle of 27.93°. Our attempt to dehydrogenate the complex using DDQ[172] gave quinone complex **7a** along with other intractable products.

Treatment of **6a** under Meerwein-Ponndorf-Verley conditions[143] gave McMurry-type reductive coupling product **11a** (71%). The separation of the isomers by physical methods failed. However, slow crystallization from hexane gave single crystals of *anti*-isomers with *cis* configuration. The bridging C-C bond is 1.350 (5) Å long showing the formation of double bond. Fc-anthrone did not react under standard McMurry conditions[173] even after 24 h. We suggest that either the aluminum ketyl of anthrone **6a** undergoes coupling followed by loss of aluminum oxide (Scheme 5.7), or the anthrone ligand was reduced to benz[*f*]indenyl by Al/Hg, subsequently dimerization with the migration of two hydrogen atoms.

Scheme 5.7. Proposed mechanism of reductive coupling

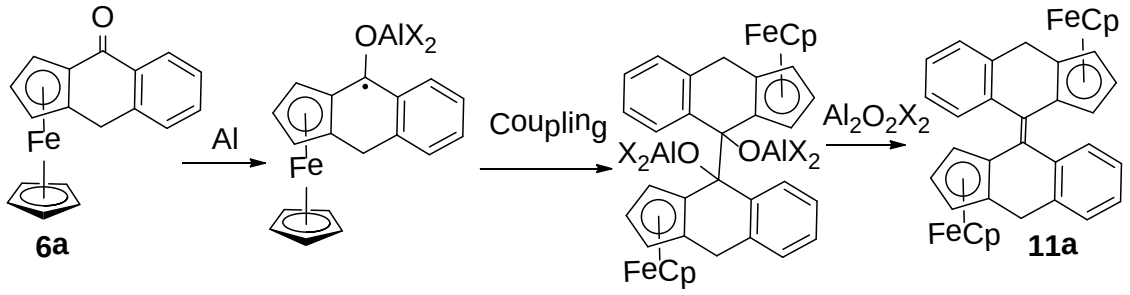

To probe the acidity of the methylene protons in **6a**, the complex was treated with LDA at -78 °C and quenched with heavy water. The anion produced by LDA gave a deep purple solution, suggesting extensive delocalization of the negative charge. The analysis of the final products after chromatographic separation revealed the formation of the deuterium exchanged product **12a**

(24%). The deuterium exchange was evidenced by the loss of the AB pattern due to geminal coupling of methylene protons and appearance of a triplet (δ 4.19 ppm, J = 5.2 Hz) due to geminal deuterium coupling in ^{1}H NMR.

Another byproduct of the reaction was the single isomer of Fc-hydroxyanthrone **13a** (38%) along with some quinone **7a**. Two doublets in ^{1}H NMR resonating at δ 1.99 ppm and 5.75 ppm with a coupling constant of 8.0 Hz showed the formation of the secondary alcohol. Mass spectra of the product showed a base peak at 302, which is corresponds to the loss of a water molecule from its parent peak. An X-ray crystallographic analysis of **13a** showed that the position of hydroxyl group is *exo* with respect to the Fe center.

The C-alkylation of the Fc-anthrone was performed by using benzyl chloride in the presence of KOH as a base and tetrabutylammonium bromide as a phase-transfer catalyst[174] to give benzyl (**14a**) and dibenzyl (**15a**) anthrone complexes in ca. 1**:**1 ratio. Our attempts to synthesize **14a** by controlling the stoichiometry of reagents failed. The analytically pure products were separated from the mixture by fractional crystallization. The monobenzyl derivative was distinguished by its three double-doublet resonances in ^{1}H NMR with coupling constants, ^{2}J = 13.2 Hz; ^{3}J = 5.0 Hz, 8.0 Hz corresponding to methylene protons of benzylic group and methine proton of the anthrone backbone. Similarly, the dibenzyl derivative is characterized by two AB resonances centered at δ 3.01 ppm and 3.18 ppm with a coupling constant of 12.4 Hz due to the benzylic protons.

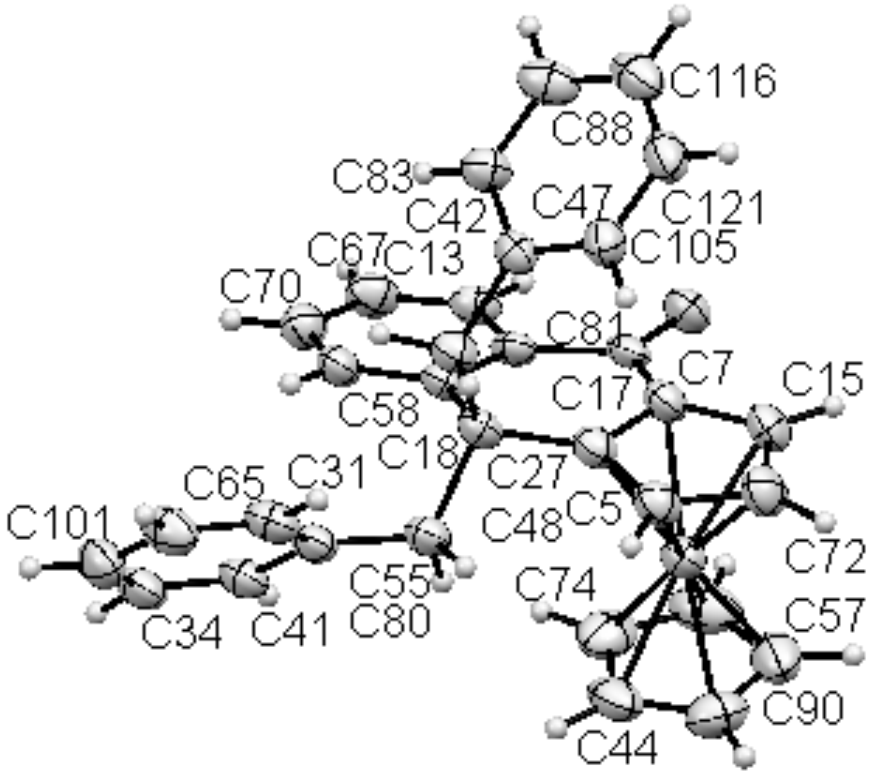

Figure 5.5. ORTEP diagram of C32H26FeO **(15a)**

One of the protons of benzene ring of **15a** resonates as a doublet centered at δ 5.86 ppm, ^{3}J = 8.4 Hz in $CDCl_3$. This unusual upfield shift of the aromatic proton might be due to the effect of the ring current in addition to the inductive effect. The ORTEP diagram of **15a** reveals that the proton attached to C58 of the anthrone backbone falls directly on the face of benzene ring of benzyl substituent to experience the effect of ring current (Figure 5.5). The X-ray crystallographic analysis of **14a** reveals that the benzyl group is oriented *exo* with respect to the Fe center.

Scheme 5.8. The oxidative coupling and cycloaddition of trimethylsilyl enol ether

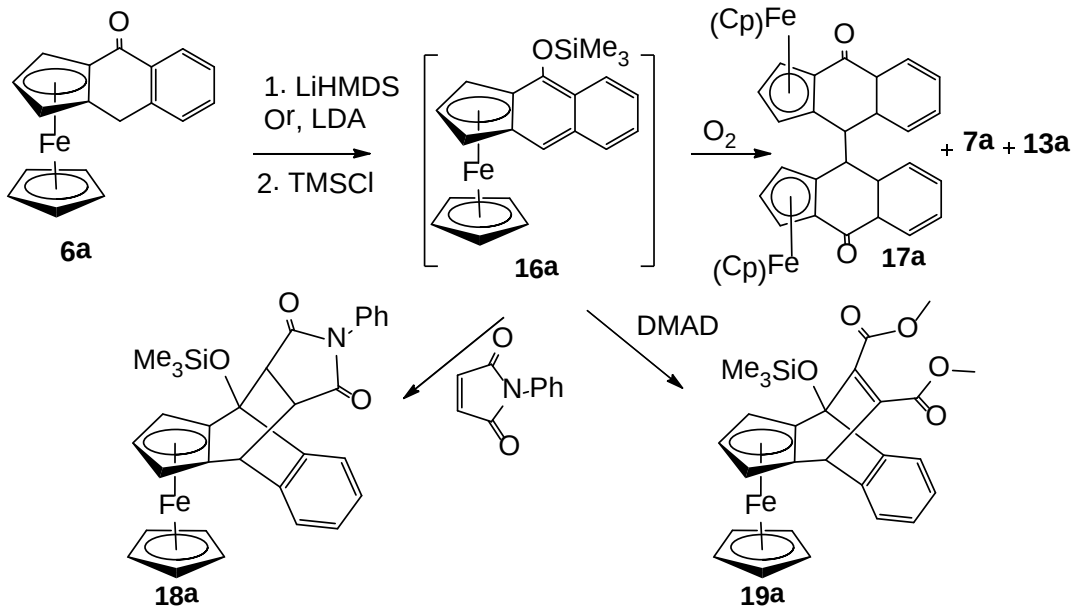

In an attempt to form the O-silyl ether of the Fc-anthrone, we treated **6a** with lithium hexamethyldisilazide at -78 °C and then quenched with trimethylsilyl chloride (Scheme 5.8). After removal of the volatiles, the deep-green product was extracted with scrupulously dry hexane under nitrogen. Although the hexane-soluble, deep-green complex may be the desired trimethylsilyl enol ether **16a**, we were unable to obtain an analytically pure product. ^{1}H NMR of the green gum showed impurities of aliphatic hydrocarbons. The green compound is surprisingly sensitive towards oxidation; it decomposes upon exposure to air forming red byproducts. The final aerobic work-up of the complex by column chromatography on silica showed oxidatively coupled products Fc-anthrone dimer **17a** (42%), Fc-hydroxyanthrone **7a** (22%), Fc-quinone **13a** and starting material **6a**.

As shown in the crystal structure of coupled product **17a** (Figure 5.3), the absolute configuration of the two chiral centers in the major isomer are (*R,S*) and (*S,R*). The minor product was *meso* with absolute configuration of (*R,R*) and (*S,S)*. The *meso* stereoisomer shows an interesting shift of one of the Cp protons to a significantly upfield position (δ 3.29 ppm in $CDCl_3$) in ^1H NMR. This might be due to the effect of a ring current in one of the arene ring. The mass spectra of the dimer show a very weak molecular ion peak but a base peak corresponding to half of the molecular ion, showing homolytic cleavage of the bridging C-C bond. Similar dimerization was reported in planar enolizable ketones fused with ferrocene.[175]

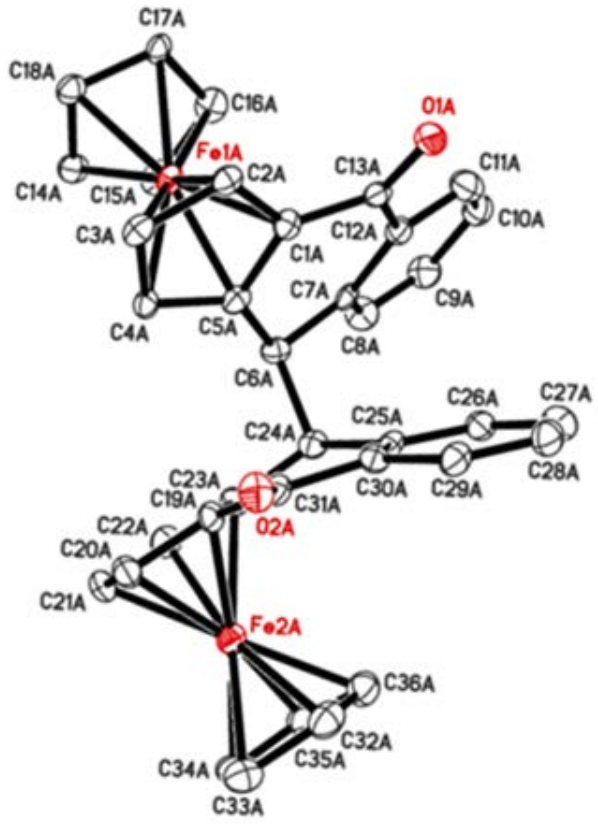

Figure 5.3. X-ray crystal structure of $C_{36}H_{26}Fe_2O_2$ (**17a)**

The results of the enolization reaction indicate that the deep green enol-silyl ether **16a** acquires a diradical (triplet) character at carbon atoms alpha to the ferrocenyl group. Although there is not much quantitative study of ferrocenylmethyl-type free radicals, its involvement has been mentioned in the photolysis of ferrocenyl olefins and ethers.[176] The Creary group proposes that the ferrocenyl group stabilizes the free radical at the α-position due to the involvement of iron d-orbitals. Even though the spin delocalization involving iron is uncertain, the stability of the ferrocenylmethyl free radical is due to different canonical structures involving ferrocenium Fe(III) form and an Fe(I) η^4 form as shown in Figure 5.4.[177]

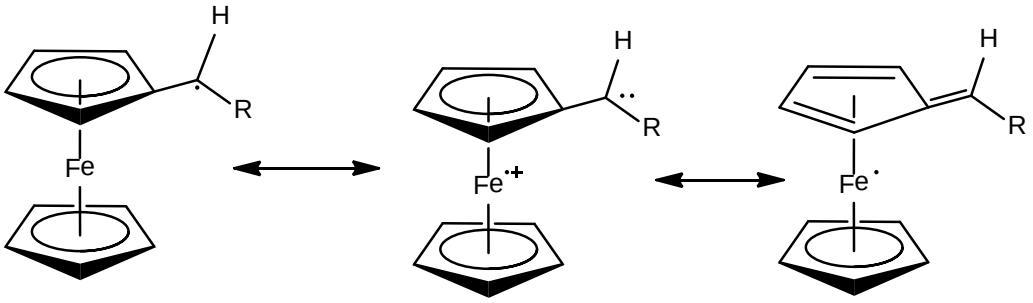

Figure 5.4. Canonical structures of ferrocenylmethyl free radical

On the similar lines of arguments, we assume that the trimethylsilyl enol ether **16a** is sufficiently stable in the absence of oxygen but undergoes immediate decomposition giving dimerized Fc-anthrone **17a** and Fc-hydroxyanthrone **13a** as major products and Fc-quinone **7a** and Fc-anthrone as minor products. The decomposition of silyl-enol ether can be explained on the basis of formation of [4+2] cycloaddition product between electron rich butadiene

like six-membered middle ring of **16a** with oxygen molecule giving endoperoxide.[178] The hemolytic cleavage of O-O bond and subsequent loss of Me_3SiOH gives complex **13a** and **7a** (Scheme 5.9). Similarly cleavage at C-O bond gives rise to the formation of peroxide radical with an unpaired electron at stable α-position to the ferrocenyl moiety to dimerize. The subsequent loss of trimethylsilyl peroxide can justify the formation of coupled product **17a.**

Scheme 5.9. The proposed mechanism of oxidative coupling and cycloaddition of **16a**

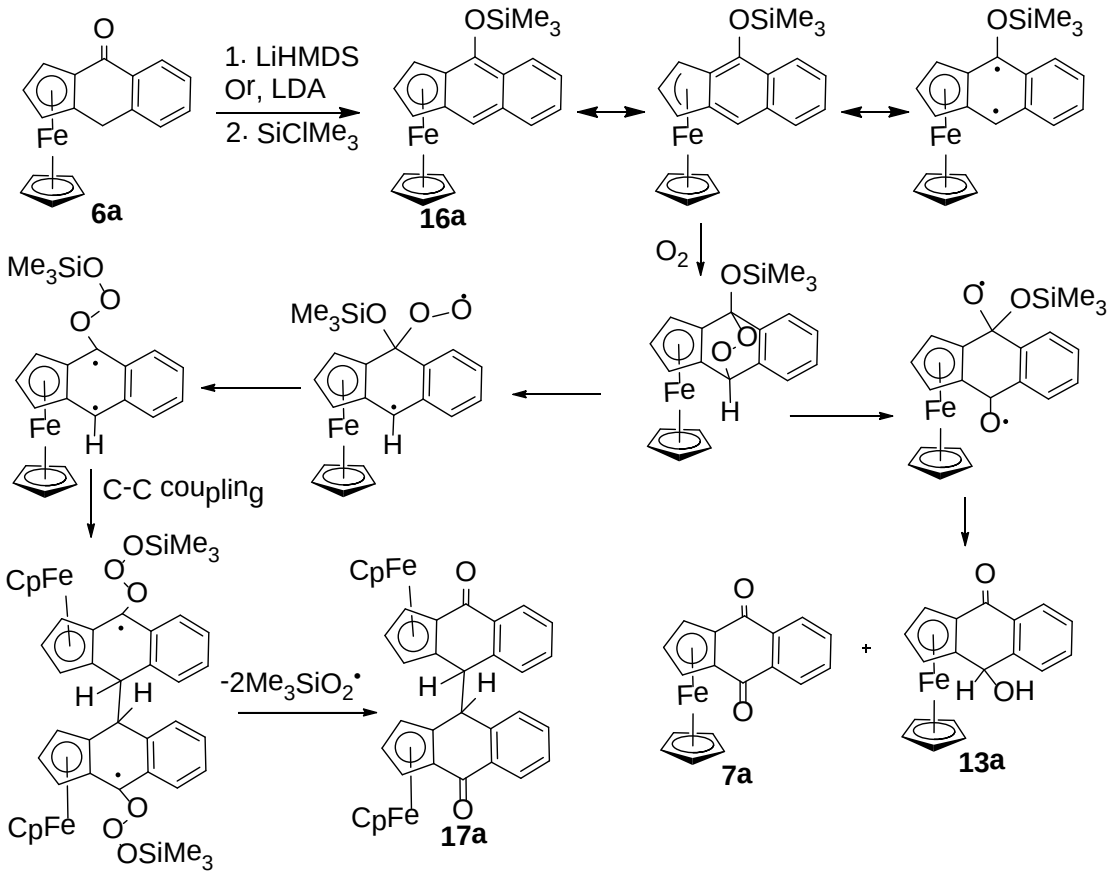

As the silyl enol ether **16a** is stable only in the in the absence of aerobic conditions, we decided to trap the product in the presence of dienophiles under

Diels-Alder conditions. Considering that the middle six-member ring of the **16a** (Scheme 5.8) exhibit a reactive butadiene-like character, one may anticipate cycloaddition reaction of **16a** with dienophiles. The Wang group reported the Diels-Alder reaction of benzyne with indenyl iron complexes[179] as well as indenyl and fluorenyl complexes of ruthenium[180] and confirmed that six-membered ring of the indenyl ligand is reactive towards dienophile. However, there is no report of Diels-Alder cycloaddition of η^5-benz[*f*]indenyl metal complexes with dienophiles. Our assumption was corroborated by the formation of adduct between *in situ* generated trimethylsilyl enol ether with N-phenylmaleimide and DMAD at room temperature to give cycloadducts **18a** (44%) and **19a** (48%).

The cycloadducts were accompanied by silyl ether group as evidenced by a singlet around 0.4 ppm integrating nine protons in ^{1}H NMR. The three methine protons of **18a** exhibit ABX spin system (J_{AB} = 8.4 Hz, J_{BX} = 2.8 Hz). Two of the protons of the aromatic ring of **18a** shields appearing at 6.42-6.44 ppm as a multiplet possibly due to ring current of one of the arene moiety. The IR stretches at 1734 cm^{-1} and 1704 cm^{-1} corresponds to the presence of two carbonyl groups of ester in **19a**. Similarly, a strong band was observed at 1715 cm^{-1} due to carbonyl group of amide. The high resolution mass spectra of both cycloadducts show base peak corresponding to the loss of dienophiles moiety from their molecular ion peaks indicating the stability silyl enol ether. The molecular structures of both adducts **18a** and **19a** were analyzed with an X-ray crystallographic analysis. It was observed that cycloaddition was taken place at

the middle ring with dienophile oriented *exo* with respect to Fe center on both cases.

Cais *et al*. studied the solvolysis of 2,3-ferroindenol to benzopentalenecyclopentadienyliron, which underwent an extremely fast internal oxidation-reduction process, resulting in the formation of the cation radical. They proved the formation of dimerized ferrocenium-type dication by reducing the paramagnetic salt with ascorbic acid as shown in Scheme 5.10.[132] We simulated their reaction conditions to solvolyze ferrocenylcarbinol **8a** to give α-ferrocenylcarbenium tetrafluoroborate **20a** (60%) as an olive-green product (Scheme 5.11). Our attempts to crystallize the freshly prepared salt under nitrogen failed. However, unlike the fluoroborate salt of benzopentalenecyclopentadienyliron π-complex[132] prepared by Cais group, we were able to characterize the product with ^{1}H NMR and ^{13}C NMR.

Scheme 5.10. Solvolysis of 2,3-ferroindenol and subsequent dimerization[132]

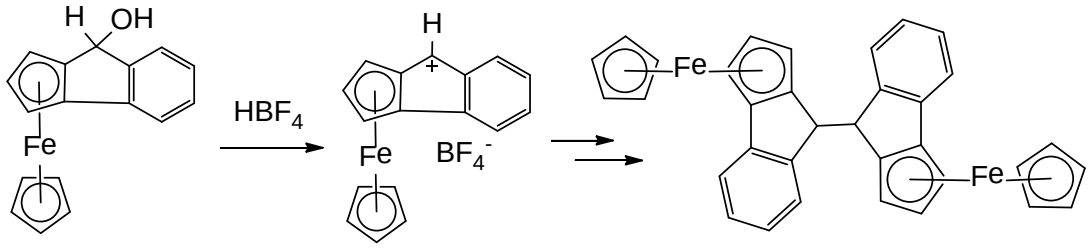

Figure 5.6 shows the ^{1}H NMR spectra of freshly prepared α-ferrocenylcarbenium salt (Spectrum A). Surprisingly, the same NMR sample

turned to paramagnetic over the period of 12 h, which resulted in the complete disappearance of signals (Spectrum B).

Scheme 5.11. Solvolysis of carbinol and reactions of ferrocenylcarbenium ion

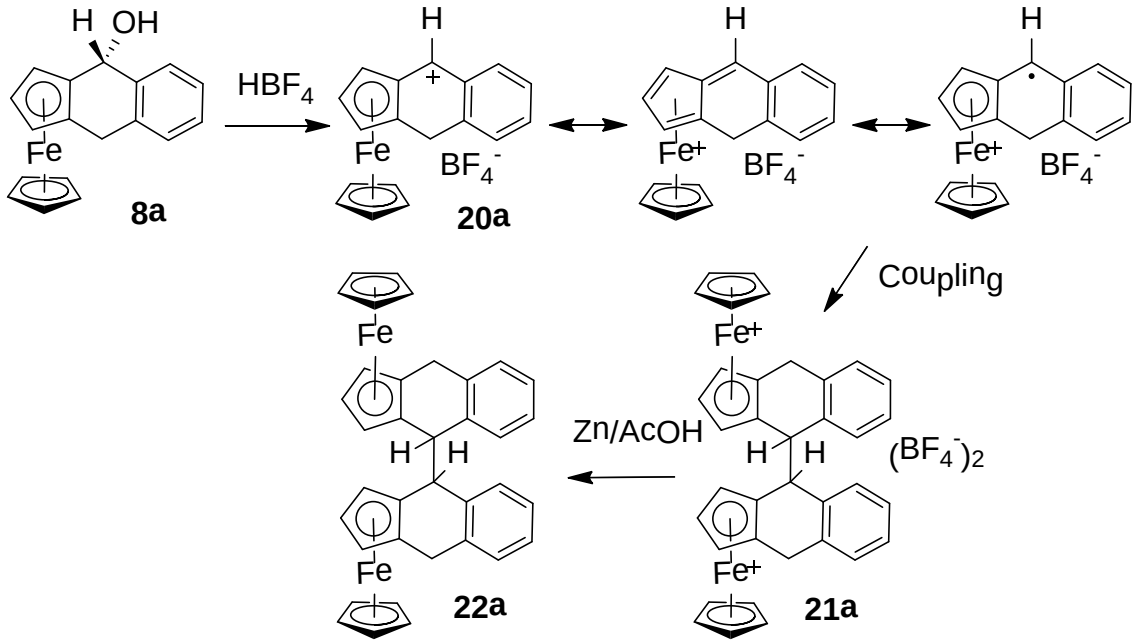

The solid sample of **20a** turned darker on overnight storage on bench-top conditions and displayed similar paramagnetic behaviors. On the basis of literature precedents,[132,133,181] we suggest that the darker paramagnetic complex is diferrocenylcarbenium tetrafluoroborate **21a,** which might be formed due to oxidation of iron atom to reduce cationic center giving the radical cation **20a** followed by dimerization. The salt underwent immediate reduction in the presence of zinc with acetic acid giving a mixture of two diastereoisomers of **20a** along with some intractable products.

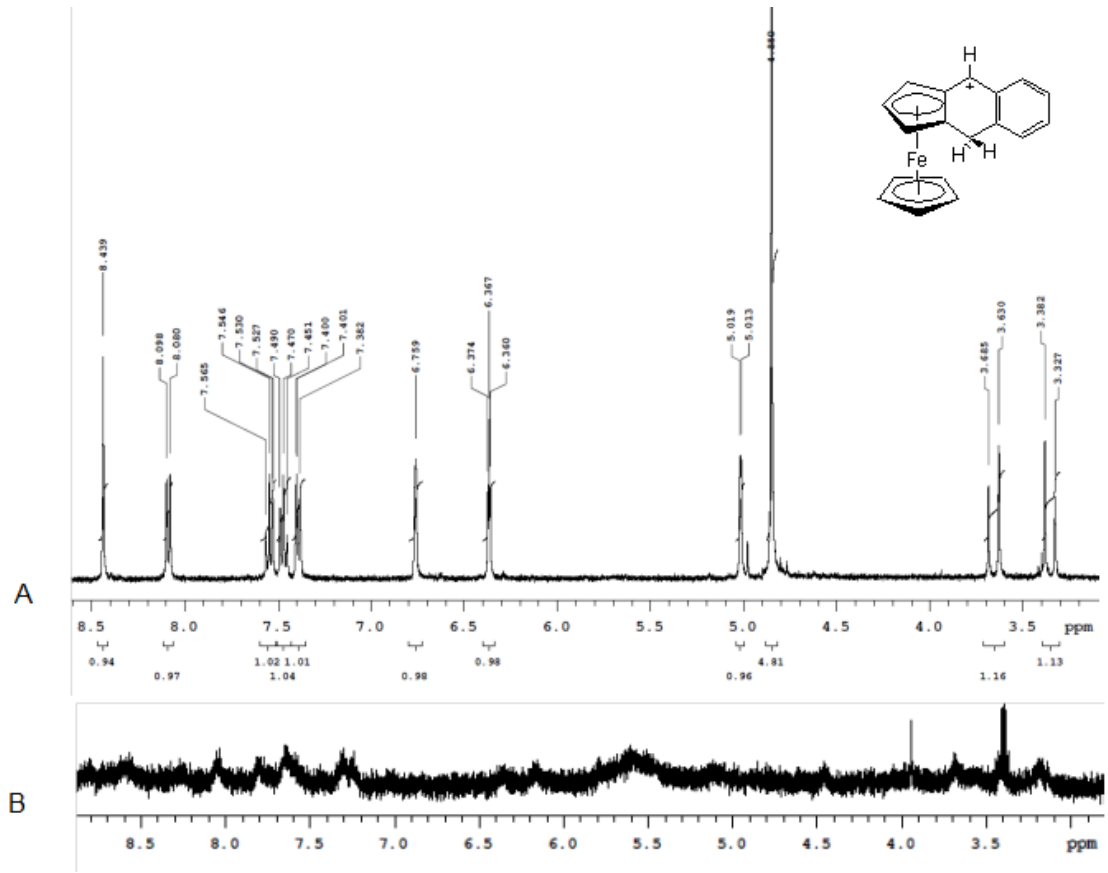

Figure 5.6. ^{1}H NMR of **20a** in acetone-d_6. (A) Freshly prepared compound; (B) the same sample after 12 h.

As shown in Figure 6, the signals of the substituted ring protons of **20a** appeared at δ 5.01 ppm (1H), 6.36 (1H) and 6.75 (1H) as an ABX resonance. Table 5.1 shows the comparison of chemical shift values of peak resonances of the ferrocenylcarbinol **8a** and the ferrocenyl carbenium ion **20a**. After solvolysis, there is a significant deshielding in resonances of protons [Δδ ppm = 1.06 (Cp), 0.94 (C1), 2.08-2.47 (C2-C3), 3.19 (C4)] and carbon [Δδ ppm = 13.2 (Cp), 12.9-23.6 (C1-C3), 7.1-14.3 (*ipso*), 33.6 (C4)] (The numbering scheme is shown in Figure 5.7). The greatest shift was observed on the signals of the H (2, 3) of the

substituted ring, while the H (1) is less deshielded. This might be due to the inductive effects of the carbocation. The proton and carbon of the cationic center of **20a** are greatly deshielded (^{1}H, δ 8.10 ppm; ^{13}C δ 118 ppm). The shift in the resonances is analogous to the ^{1}H and ^{13}C NMR of α-ferrocenylphenylmethylcarbenium fluoroborate and is in good agreement to the values reported in literature.[182,183] Even though there is some shift in proton and carbon signals of the arene, the shifts are not as significant as the ferrocenyl moiety. It can be inferred from the comparison of peak values in NMR that the structures **I** and **II** are more contributing than the structure **III** and **IV** to stabilize the positive charge at C4 (Figure 5.5).

Table 5.1. Comparison of ^{1}H and ^{13}C NMR of carbinol **8a** and carbenium ion **20a**

	C9*H*A	C9*H*B	Cp*H*	C1*H*	C2,3*H*	C4*H*	C8*H*	C6,7*H*	C8*H*
8a	3.51	3.68	3.78	4.07	4.28	5.25	7.24	7.3	7.81
20a	3.35	3.66	4.84	5.01	6.36,6.75	8.44	7.40	7.47,7.54	8.10
	C9	CpC	C1-C3	C3'	C9'	C4	C5-C8	C8'	C4'
8a	30.6	69.6	63.9, 65.8, 66.7	66.7	91.7	84.5	126.3,126.8, 127.2,128.7	136	142.1
20a	29.3	82.8	76.8,90.1,90.3	98.7	98.8	118.1	128.9,130.0, 131.4,132.4	132.6	137.1

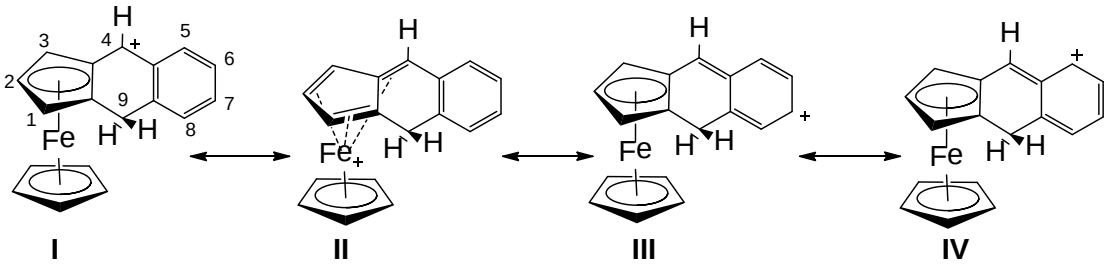

Figure 5.7. Canonical structures of ferrocenylcarbenium ion **20a**$^{+}$

The factors stabilizing the carbenium ion center in the α-ferrocenyl cation have been the subject of study and debate for some time. It has been argued that the conjugation with π-electrons is the source of unusual stability of α-ferrocenyl cation.[184] Similarly, donor-acceptor interaction between nonbonding e_{2g} metal orbital with the vacant p-orbital of carbocationic center has been documented to show the unusual stability of α-metallocenylcarbenium ion.[185-189] Sime and Sime studied the crystal structure of ferrocenyldiphenylcyclopropenium tetrafluoroborate and established that the stability of the cation is due to the interaction of metal d-orbitals and empty p-orbitals of the cyclopropenium moiety.[190] The results of cationic dimerization of the ferrocenylphenylmethylcarbenium ion[191] has ruled out the necessity of the planarity of the carbenium ion for the dimerization of the α-ferrocenylcarbenium salt. However, the sluggishness in the electronic rearrangements in our system might be due to the larger size of the ring that keeps iron d-orbitals away from empty p-orbitals of the cyclohexanium moiety.

Scheme 5.12. Attempts to deprotonate of α-ferrocenylcarbenium salt **20a**

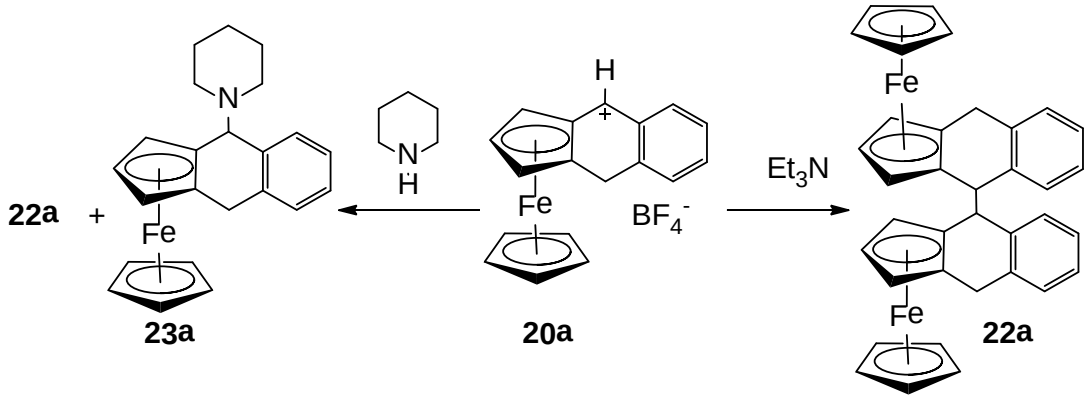

In an attempt to deprotonate **20a** using piperidine, we isolated an adduct between the α-ferrocenylcarbenium ion and piperidine **23a** (78%) showing high electrophilicity of positively charged center. The adduct was accompanied by two diastereoisomers of **20a** (Scheme 5.12). The proportion of dimer increased when piperidine was added slowly at 0 °C. When we switched from piperidine to triethylamine in order to reduce the nucleophilic addition, two diastereoisomers of **20a** were obtained in 65% combined yield. The dimers were characterized with an AB pattern (δ 2.12-3.15 ppm, ^{2}J = 17.2-17.6 Hz in acetone-d_6) due to methylene protons. Similarly the methine protons appear as singlet in the range of δ 4.15–4.20 ppm. The X-ray crystallographic analysis of the one isomer indicated that the major diastereomer was (*R,R*)/(*S,S*) and the minor was (*R,S*). An interesting feature of the (*R,R*)/(*S,S*) isomer is that one of the protons of the substituted Cp is shielded to δ 3.30 ppm, possibly due to the effect of the ring current of arene ring. As shown in the ORTEP diagram of complex **20a** (Figure 8), H2 and H16 lie on the face of arene ring to shield their signals to upfield.

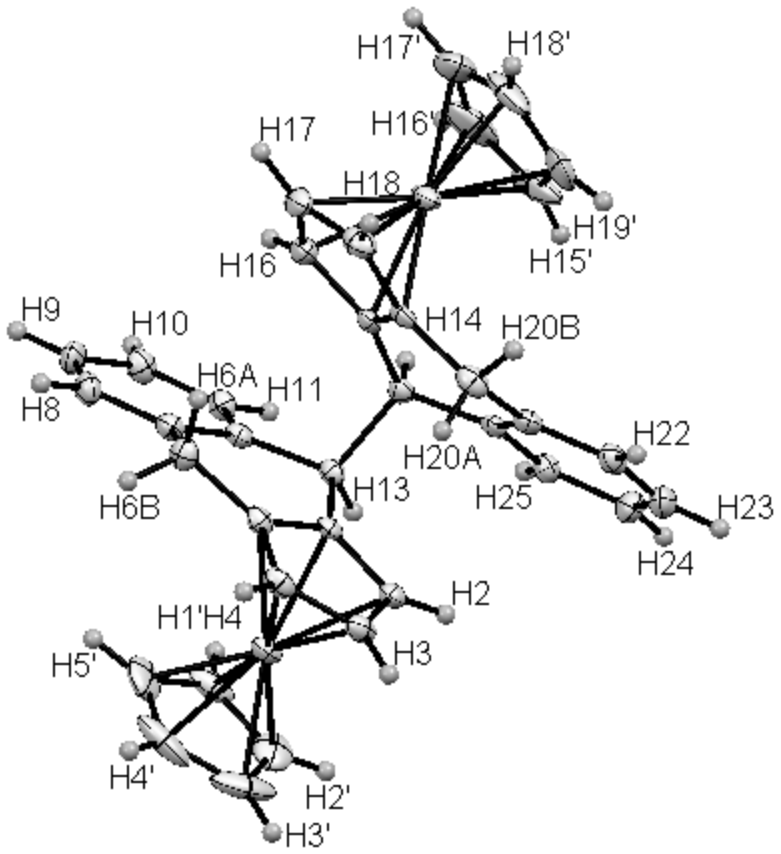

Figure 5.8. ORTEP diagram of complex $C_{36}H_{30}Fe_2$ (**22a)**

Our results of facile dimerization of the α-ferrocenylcarbenium ion in the presence of non-nucleophilic bases can be rationalized on the basis of reactions as shown in the scheme 5.13. The base removes the most acidic methylene proton giving benz[*f*]indenyl complex of iron **10a.** To maintain the aromaticity of the terminal benzene ring and coupling with t_{2g} set of d-orbitals,[177] the incipient **10a** acquires triplet configuration giving an easy access to dimerize. The homocoupling of two free radicals in the absence of air and abstraction of hydrogen radicals gives two different diastereoisomeric products of **20a**. Our

attempt to trap an adduct of *in situ* generated **10a** and the dimethylacetylenedicarboxylate trap failed.

Scheme 5.13. Proposed mechanism of coupling of benz[*f*]indenyl complex of iron

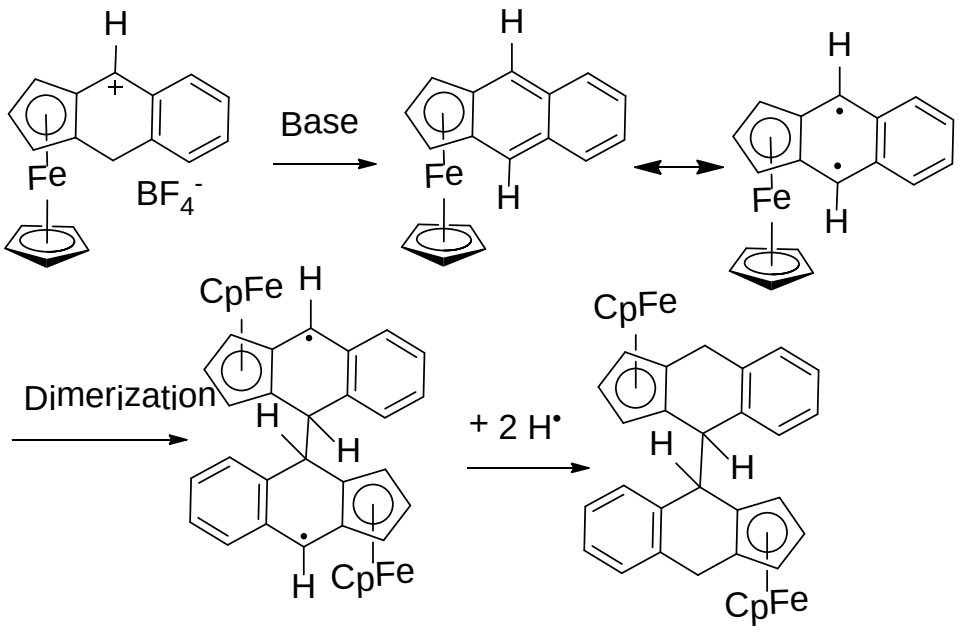

5.3.2. Electrochemistry. The cyclic voltammetry of the quinone complexes **7a** and **7b** was carried out at room temperature under nitrogen at 25-50 mV s^{-1} in a 0.1 M (Bu_4NPF_6/CH_2Cl_2) solution as the supporting electrolyte. The three electrode electrochemical cell consists of a platinum bottomed working electrode, a platinum wire counter electrode and silver wire reference electrode all connected to a potentiostat. The voltammogram for complex **7a** is exhibited in Figure 5.9 with peak numbers to show the direction of scan. The half-wave potentials of each oxidation ($E^0_{1/2,\ ox}$) and reduction ($E^0_{1/2,\ red}$) wave were

calculated by averaging the corresponding anodic (E_{pa}) and cathodic (E_{pc}) peak potentials.

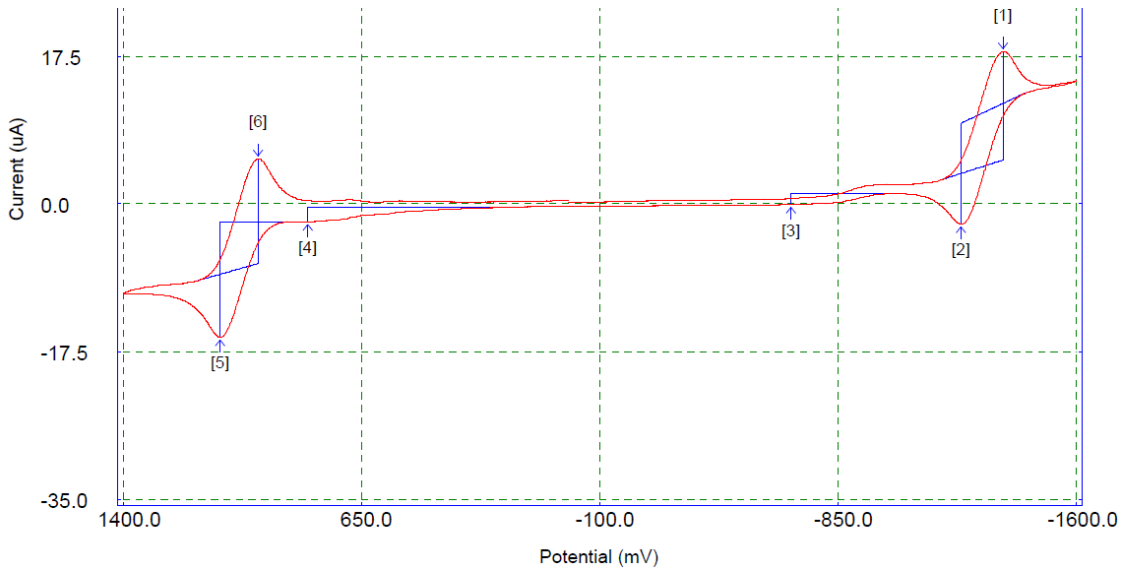

Figure 5.9. Cyclic voltammogram of $C_{18}H_{12}FeO_2$ **(7a)**

Unlike anthraquinone and 2-methylanthraquinone,[135] reduction of the complexes of Fc-quinones show only one reversible wave. This might be due to the formation of stable radical anion. The radical can delocalize over several atoms as shown in Figure 5.10 including iron d-orbitals. Electrochemical data (Table 5.2) of both complexes [$E_{1/2}$ = 1035 mV, i_{pa}/i_{pc} = 1.13, ΔE = 142 mV (**7a**), $E_{1/2}$ = 997 mV, i_{pa}/i_{pc} = 2.07, ΔE =109 mV (**7b**)] demonstrates that the oxidation peak due to Fe centers are pseudo-reversible while the reduction waves due to the quinone moiety are almost reversible. Unlike polycyclic aromatic hydrocarbons, the expansion on the π-system in quinones leads to a decrease in electron affinity. This is due to the nature of the LUMO of the quinone, which is a

π*-type orbital and the negative charge is largely located on the two oxygen atoms, but in aromatic acenes the extra electron is delocalized throughout the molecule.[192] By following the similar trend, the quinone **7a** shows a slightly higher (130 mV) reduction potential than **7b** under similar experimental conditions.

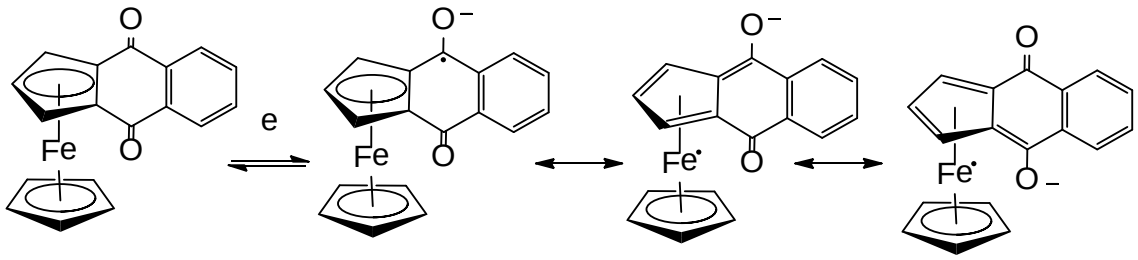

Figure 5.10. The electrochemical reduction of ferrocene-fused quinones

Table 5.2. Electrochemical data of complexes **7a** and **7b** showing half oxidation and half reduction

	Oxidation						Reduction					
	E_{pa}	E_{pc}	$E^0_{1/2,}$	i_{pa}	i_{pc}	i_{pa}/ i_{pc}	E_{pa}	E_{pc}	$E^0_{1/2}$	i_{pa}	i_{pc}	i_{pa}/ i_{pc}
7a	1106	964	1035	18.14	16.01	1.13	-1226	-1367	-1296	14.83	13.96	1.06
7b	1067	943	997	7.3	3.51	2.07	-1354	-1498	-1426	11.97	11.66	1.02

5.3.3. Structure. The structure of dimerized lactones $C_{36}H_{26}Fe_2O_4$ **(5a)** and $C_{44}H_{30}Fe_2O_4$ **(5b)**, quinones $C_{18}H_{12}FeO_2$ **(7a)** and $C_{22}H_{14}FeO_2$ **(7b)**, reduced quinone $C_{18}H_{18}Fe$ **(9a)**, reductively coupled $C_{36}H_{28}Fe_2$ **(11a)**, hydroxyl Fc-anthrone $C_{18}H_{16}FeO_2$ **(13a)**, monobenzyl substituted anthrone $C_{25}H_{20}FeO$ **(14a)**, dimerized Fc-anthrone $C_{36}H_{26}Fe_2O_2$ **(17a)** and coupled benz[*f*]indenyl $C_{36}H_{30}Fe_2$ **(20a)** complexes were determined by X-ray crystallography. Ellipsoid plots with

numbering schemes for **5a**, **5b, 7a, 7b, 9a, 11a, 13a, 14a, 17a and 20a** are shown in Figures 5.12-5.21. The structure of **17a** was of poor quality as a result of twinning by non-merohedry. Although the atom connectivities are established well enough, the overall structure refinements of the crystal structure is not of high enough quality for publication. The crystal structure and refinement data and bond length and bond angle data for compounds **5b, 7a, 7b, 9a, 11a, 13a, 14a and 20a** can be found in Tables 5.3-5.7 and Tables 5.8-5.18 respectively.

5.3.3.1. Dimerized lactones. The molecular structures of **5a** and **5b** each have a chemical C_2 rotation axes, but in the crystal structure of **5a** the molecules occupy a general position. In the structure of **5b** the main molecules occupy a crystallographic 2-fold rotation axis. The two halves of each species are related by a C-C single bond [**5a**, 1.578 (3) Å; **5b**, 1.566(6) Å]. The analogous bridging C-C bond distance in *meso*-3,3'-di(-*p*-chlorophenyl)bi-3-phthalidyl[193] is 1.547(2) Å. The slight bond elongation seems to be caused by steric repulsion between two ferrocenyl and lactone moieties group at 3, 3' position. The crystal structure of **5b** also contained a solvent molecule (ethyl acetate). Both molecules adopt conformations in which the two halves are staggered. The structure of **5a** is centrosymmetric (space group $P2_1/c$), which necessarily means that equal amounts of both (*R,R*) and (*S,S*) configurations are present. The structure of **5b** is non-centrosymmetric, but since the space group (*Aba2*) includes glide planes, there must also be equal amounts of both (*R,R*) and (*S,S*) configurations present. In complex **5a**, the ferrocenyl moiety containing Fe1 is largely eclipsed while the

moiety containing Fe2 is more staggered while in **5b** both of them appear to be disordered over two orientations.

The lactone groups in both molecules are virtually co-planar with the arene moiety. In **5b**, the C-O bonds about O1 show the expected asymmetry, the one adjacent to the C=O bond being 0.051 Å less than the other. The length of C15-O1 signifies partial double bond character. However, the C15-O2 length of 1.184(5) Å agrees well with the typical lactone C=O bond of 1.19 Å within experimental error. Similar features were observed in the crystal structure of **5a** as well. In both structures, the 5-membered lactone ring of makes an angle of ca. 111.5° at O-atom.

5.3.3.2. Quinones. Both quinone complexes possess typical metallocene geometry with the angles between the Fe and the two Cp ring centroids being near to 180°. The centroids of both Cp lie roughly equidistance from Fe. For example, the distance of Fe from the centroid of quinone-fused Cp and the centroid of unsubstituted Cp in **7b** are 1.649 Å and 1.657 Å. However, the bridging carbons (C1 and C5) of quinone-fused Cp are slightly nearer to the Fe center then other three (C2, C3 and C4) on both structures. The average distortion in **7a** and **7b** are 0.019 Å and 0.027 Å respectively. Similarly, the distance of the ketonic carbon from Cp is slightly shorter than from arene. For instance, the average distance of *ipso* carbons of Cp to carbonyl carbon in **7a** is less than the distance of carbonyl carbon from *ipso* carbons (C7, C12) of arene by 0.04 (3) Å. Similar effects have been observed in the structure of benzoylferrocene[194]. The partial double nature of the bond between carbonyl

group and Cp might be due to fulvenoid character of the Cp moiety. The C-C bonds in the subsutituted cyclopentadienyl ring are in the same range 1.424-1.443(4) Å.

In both structures the quinone moiety is slightly tilted towards the iron center. The dihedral angles between the plane defined by the five Cp carbons and the plane including rest of the quinone in **7a** are 0.67° and **7b** is 3.83°. The bending is prominent at the carbonyl carbon in both structures, which was evidenced by the torsional angle of C2-C1-C5-C6 (-173.8°) and C4-C5-C1-C13 (174.2°) in **7a**. The analogous bending in **7b** are C2-C1-C5-C6 (-171.1°) and C4-C5-C1-C17 (179.8°). The distance of carbonyl carbon from the plane of Cp are as follows**: 7a** (C6, 0.125 Å; C13, 0.117 Å), **7b** (C6, 0.190Å; C17, 0.003 Å). In both structures two Cp are largely in eclipsed conformations.

Figure 5.11 shows the packing of quinone molecules along the a-axis. The two quinone molecules are arranged in anti-parallel orientation with an interplanar face-to-face distance of 3.468 Å between two closest neighbors. The electron-rich aromatic moiety of one molecule interacts with the electron-deficient carbonyl group of its neighboring molecule. The ferrocenyl groups of two molecules are oriented on the opposite face of the plane, thereby avoiding steric interactions.

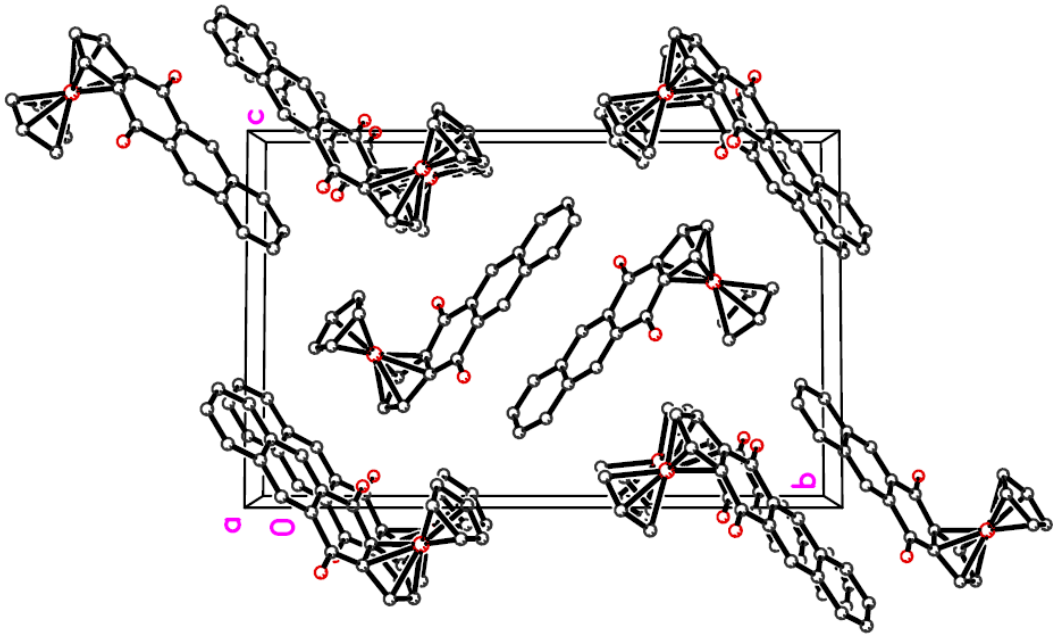

Figure 5.11. Packing of quinone **7b** molecules on their lattice along a-axis

5.3.3.3. Reduced quinones. All C-C bonds of substituted Cp in **9a** are symmetrically bonded, ranging from 1.426-1.429(15) Å. The Fe centroid distances to substituted and unsubstituted Cp rings are 1.643 Å and 1.646 Å respectively. The bonding pattern of Cp carbons in **9a** is opposite than quinones **7a** and **7b**. Unlike quinones, the two tetrahedral carbon centers at α-ferrocenyl positions are essentially coplanar with the Cp moiety. The bending of Cp-fused ligand at methylene C-atoms with respect to Cp plane towards the Fe-center is 27.93°. The *ipso* carbons (C1, C5) of Cp are slightly further away from Fe than remaining three carbons (C2-C5), the average distortion is 0.005 (15) Å. This is in agreement with the electron-releasing effect of saturated tetrahedral center towards the ferrocene moieties. The methylene carbons are symmetrically bonded to the *ipso* carbons of both Cp and Ar, the average distance from Cp and

arene being 1.495(2) Å and 1.518(2) Å, respectively. The Cp moieties are fully eclipsed.

The molecular diagram of complex **11a** shows the centrosymmetric arrangement between the two halves of the molecule, where two reduced anthrone moieties are linked by a C-C double bond of 1.351 Å Similar to the structure of **9a**, bending at carbon atoms (C6, C13) adjacent to Cp was observed in the structure of **11a** as well. However, the the folding is not as symmetrical as **9a** due to the nature of hybridization of bridging carbons. The folding angle between the mean square plane of Cp including α-carbons (C6 and C13) and rest of the arene moiety is 42.04°. The Cp moieties are fully eclipsed.

5.3.3.4. Fc-Hydroxyanthrone. Two independent molecules are included in the asymmetric unit of hydroxy Fc-complex **13a**. The folding angle between the plane including 5-carbons of Cp and the remaining carbons of the substituted Cp ligand is 5.99°. Much folding is observed at C5 and C13 which makes an angle of 10.20°. The folding is not symmetrical like the one in **9a** due to difference in hybridization of α-ferrocenyl carbons atoms. The hydroxy group is positioned *exo* with respect to Fe. The carbon bearing hydroxy group is slightly above (0.037 Å) the least-squares plane of Cp while the carbonyl carbon is slightly below (0.186 Å). The hydroxy groups are linked with a network of intermolecular H-bonding ranging from 2.790(2) Å to 2.838(2) Å.

The five carbon atoms of the substituted Cp are not bonded to Fe symmetrically and bond length ranges from 2.023(2) to 2.063(2) Å, the *ipso*

carbon joining carbonyl group is shortest of all. The distance of carbonyl carbon from Cp (1.458 Å) is slightly shorter than the distance from Ar (1.487 Å) displaying the electron releasing effect of ferrocenyl moiety. In both structures the two Cp are eclipsed.

5.3.3.5. Monobenzyl anthrone. The structure of monobenzyl anthrone **14a** is closely similar to hydroxy Fc-anthrone with benzyl substituent projecting *exo* with respect to Fe. The folding angle between the plane containing five carbons of Cp and rest of the plane comprasing rest of the carbons is 13.53° and bending is towards the center of the molecule. The majority of the folding takes place at C1 and C6. The carbonyl carbon is below the plane of substituted Cp by 0.108 Å while the tetrahedral carbon center C6 is 0.011 Å

In the structure of **20a** is the two halves of the molecule are connected by a C-C bond of 1.579 (3) Å. The bond length is roughly the same as the dimeric lactones **5a** and **5b**. Two tetrahedral centers at the α-ferrocenyl carbon are essentially co-planar to the cyclopentadienyl ring. However, the plane including rest of the C-atoms makes an angle of 21.45° and 23.50° at the tetrahedral centers with respect to the substituted Cp plane. The folding is more regular in both monomeric units due to the similar nature of hybridization of both tetrahedral centers.

The effect of the saturated carbon center at α-ferrocenyl position can be observed on the bonding modes of Cp-carbons with iron. The C-Fe bond adjacent to the electron releasing carbon center is slightly longer than rest of the

C-Fe bonds. For instance, the average distance of Fe1 from *ipso* carbons (C1, C5) is larger than the remaining three carbons (C2-C4) by 0.012(2) Å. The average distance of tetrahedral carbon from the ipso carbons of Cp and arene are 1.497 (3) Å and 1.519(3) Å respectively. The average distances of Fe from the centroids of substituted Cp and unsubstituted one are 1.641 Å and 1.650 Å respectively showing electron richness of the substituted Cp. The angle between centroids of two Cp and Fe are 179.27° and 179.26°. The two Cp moieties bonded to Fe1 exhibit perfectly eclipsed conformation while the Cp's bonded to Fe2 are oriented with skewed conformation. The absolute configuration of the two chiral centers was found to be (*R,S*) and the tetrahedral centers are oriented with staggered conformation.

5.3.3.6. Trimethylsilyl enol ether adducts. Structures of both cycloaddition products of the trimethylsilyl enol ether of Fc-anthrone, **18a** and **19a,** exhibit similar bonding pattern. As expected the dienophiles reacted with middle six-membered ring of benz[*f*]indenyl group from the outside of the indenyl plane possibly due to steric effects. The terminal benzene ring in both complexes bend towards the Fe center. The bridgehead carbon atoms in**18a** and **19a** fold with an angle of 7.08° and 7.85° from the mean plane of Cp on the opposite direction of Fe center. The C14-C15 bond length in the complex **18a** is 1.544(3) Å and analogous bond length between C7-C8 in the complex **19a** is 1.337(3) Å suggesting that the butadiene like middle six-member rings undergo Diels-Alder reaction with C-C triple bond of dimethylacetylenedicarboxylate and C-C double bond of N-phenylmaleimide. An eclipsed conformation of two hydrogen atoms

from diene moiety in the adduct **18a** shows cycloaddition reaction with *syn* configuration.The folding angle between two planes comprising C6-C7-C8-C9 and C9-C10-C11-C6 in **19a** is 59.92°. The benzene ring is oriented with an angle of 57.60° with respect to plane of imide in the complex **18a**. The unsubstituted Cp of **19a** is disordered.

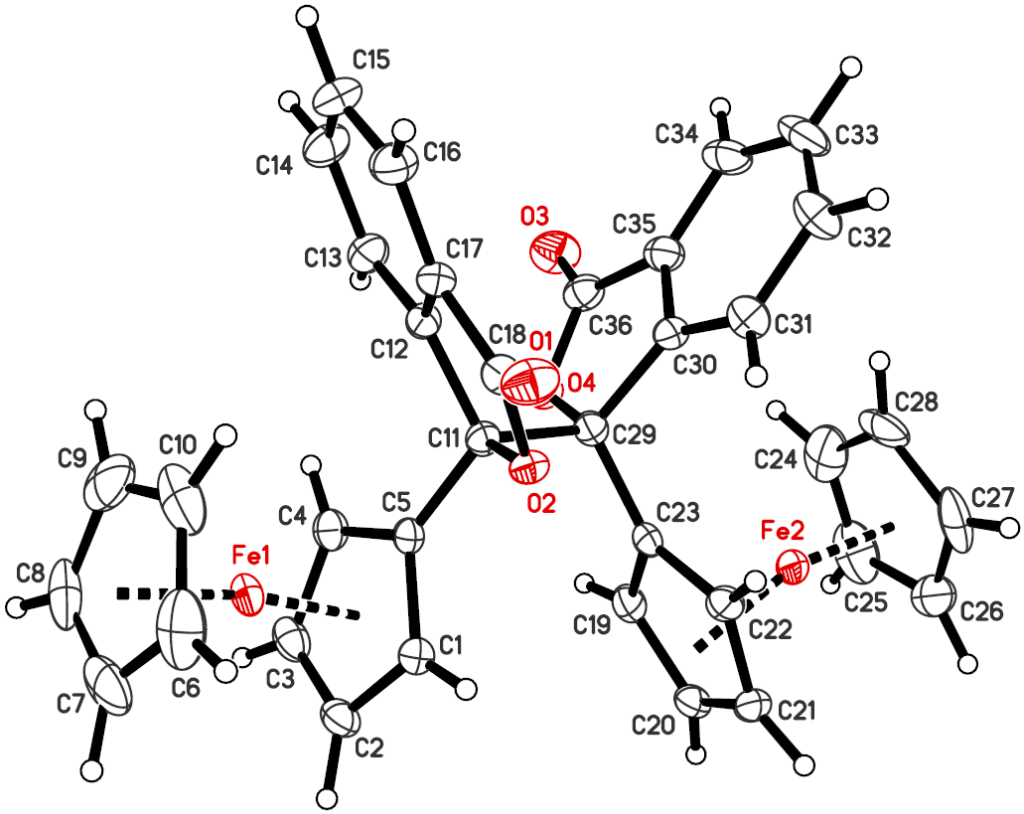

Figure 5.12. Molecular structure of $C_{36}H_{26}Fe_2O_4$ **(5a)**

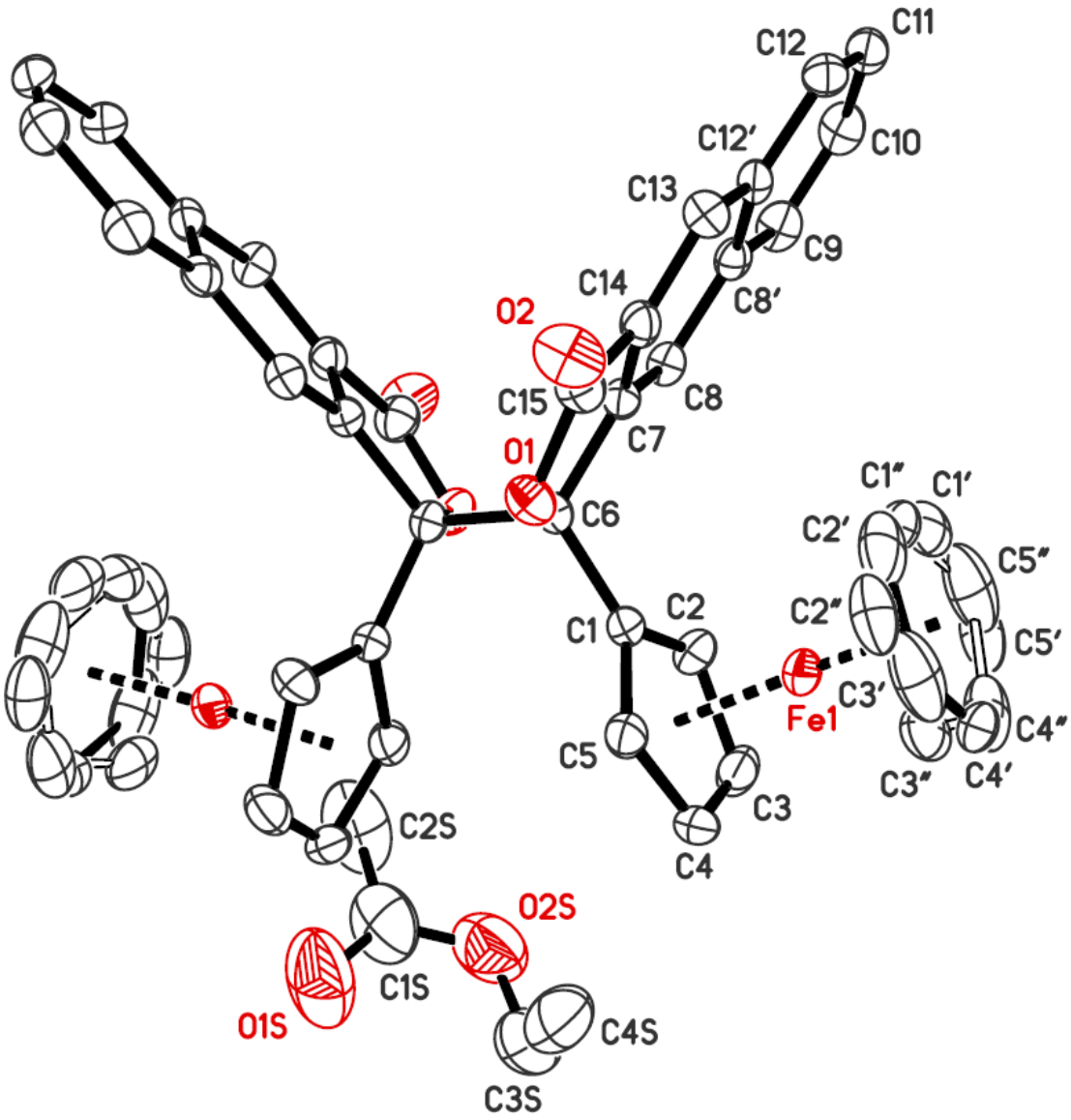

Figure 5.13. Molecular structure of $C_{44}H_{30}Fe_2O_4$ **(5b)**

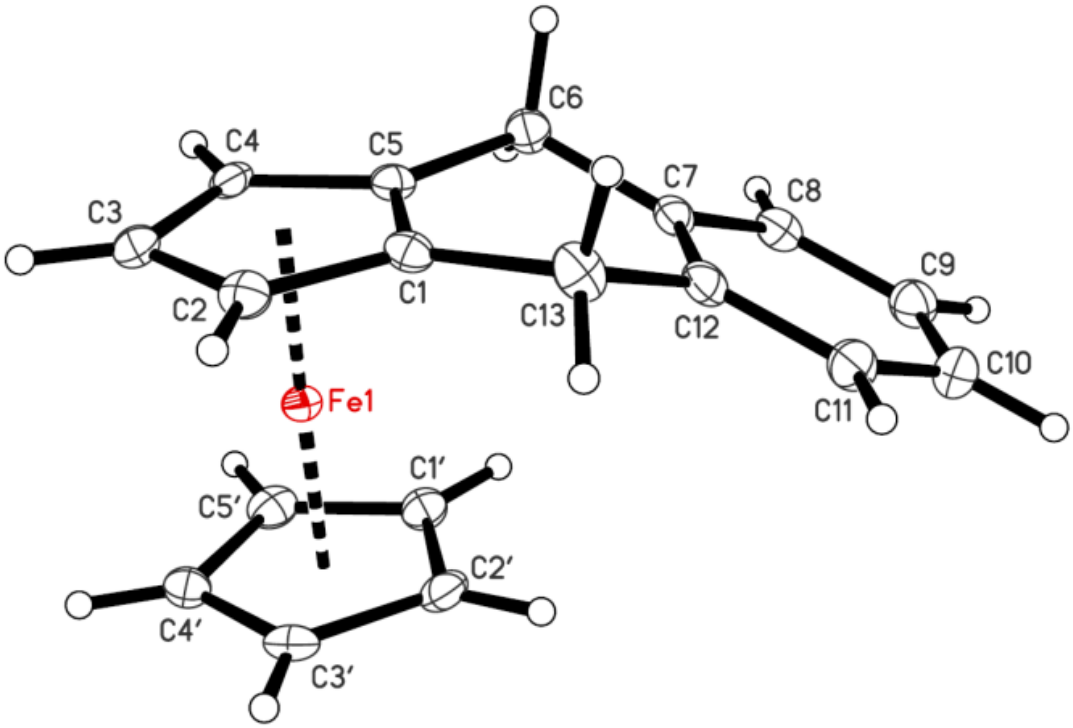

Figure 5.14. Molecular structure of $C_{18}H_{18}Fe$ **(9a)**

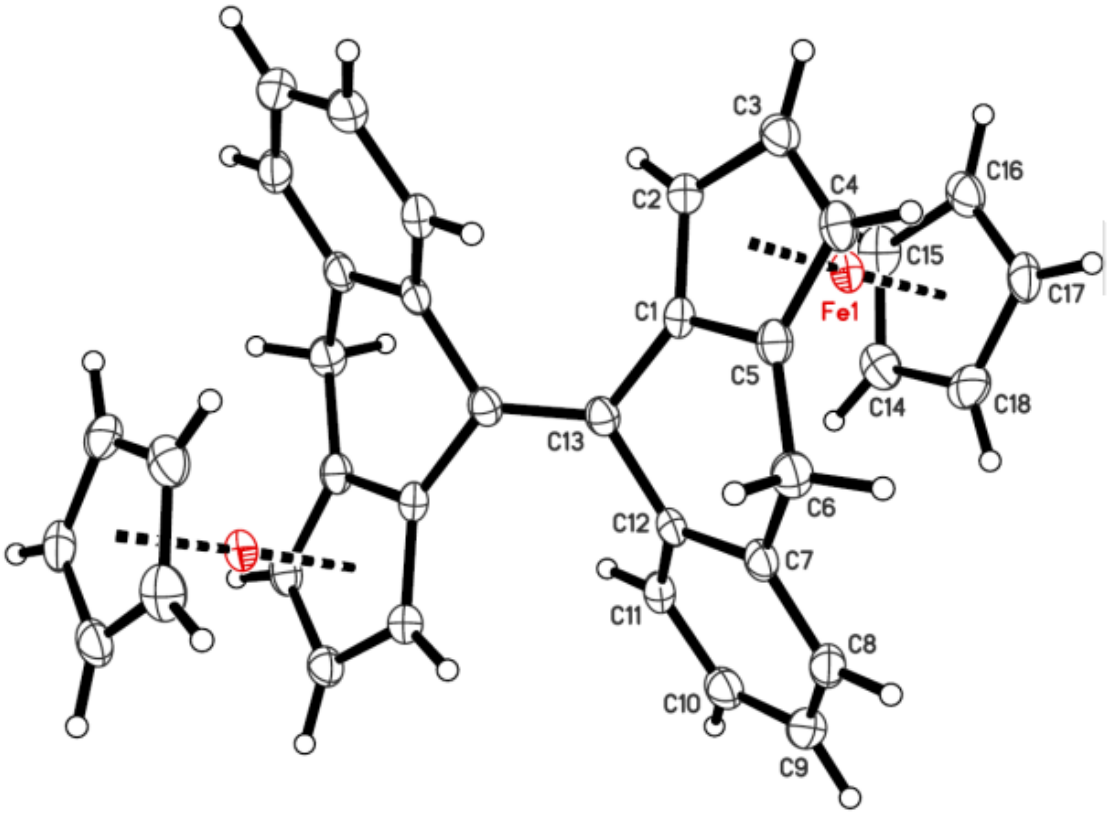

Figure 5.15. Molecular structure of $C_{36}H_{28}Fe_2$ **(11a)**

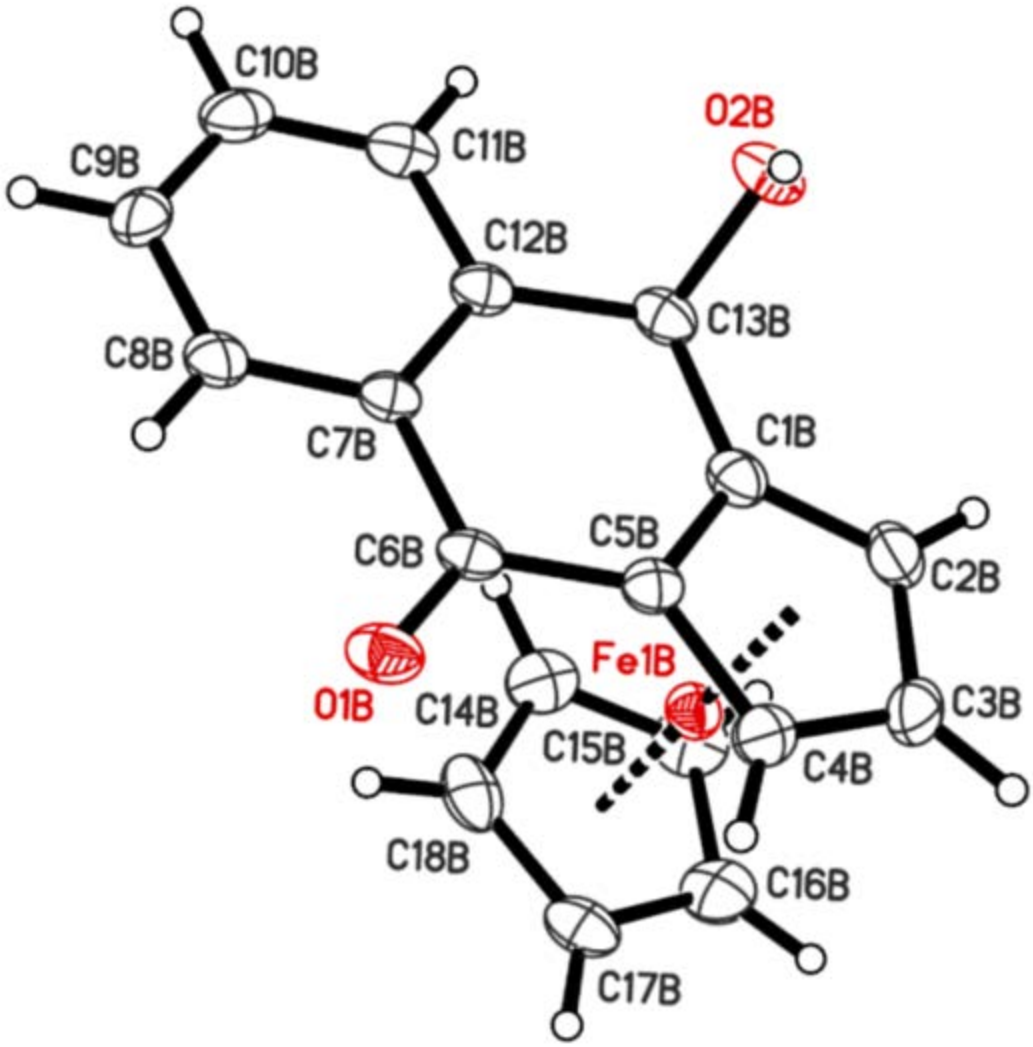

Figure 5.16. Molecular structure of $C_{18}H_{16}FeO_2$ **(13a)**

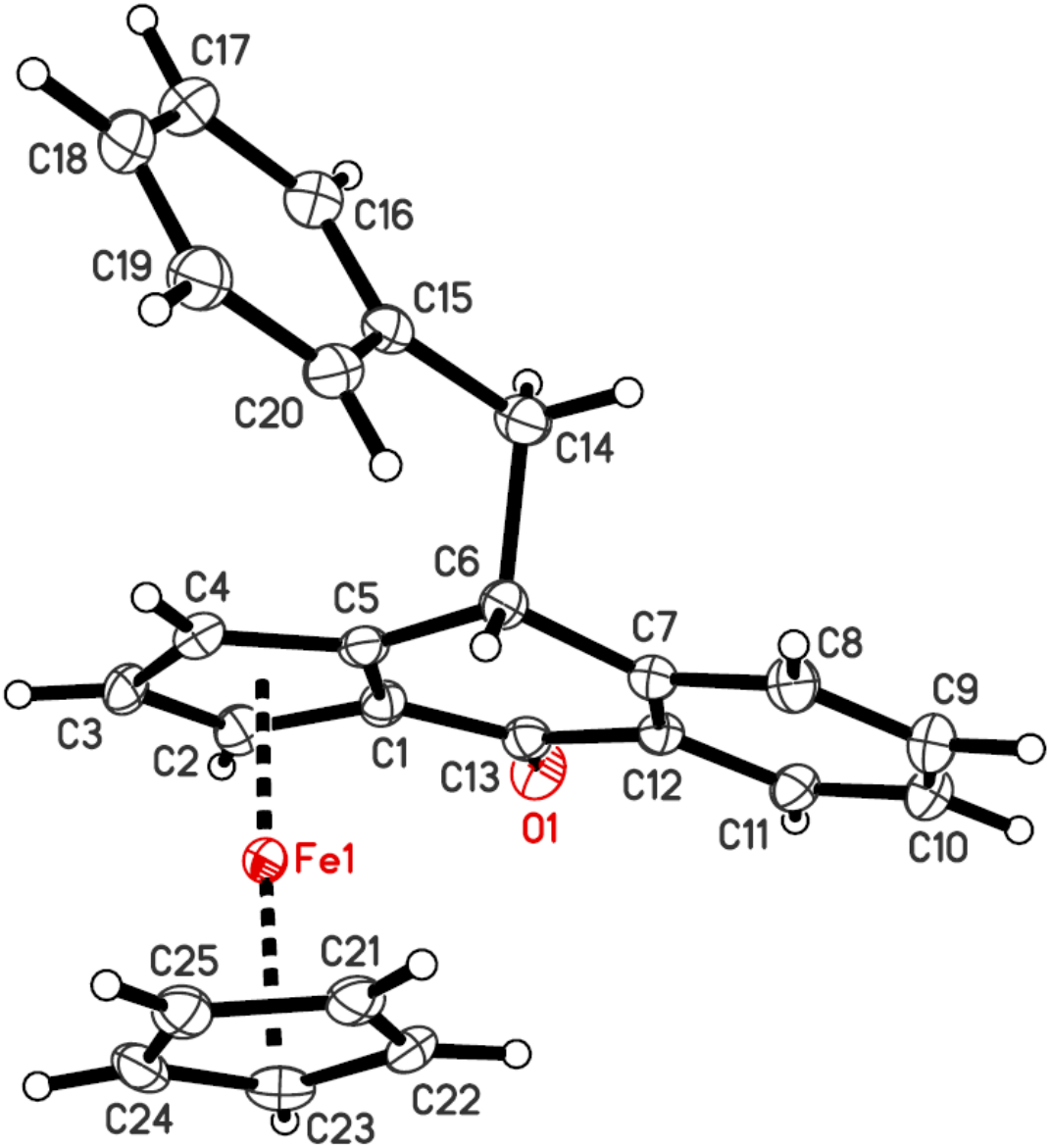

Figure 5.17. Molecular structure of $C_{25}H_{20}FeO$ **(14a)**

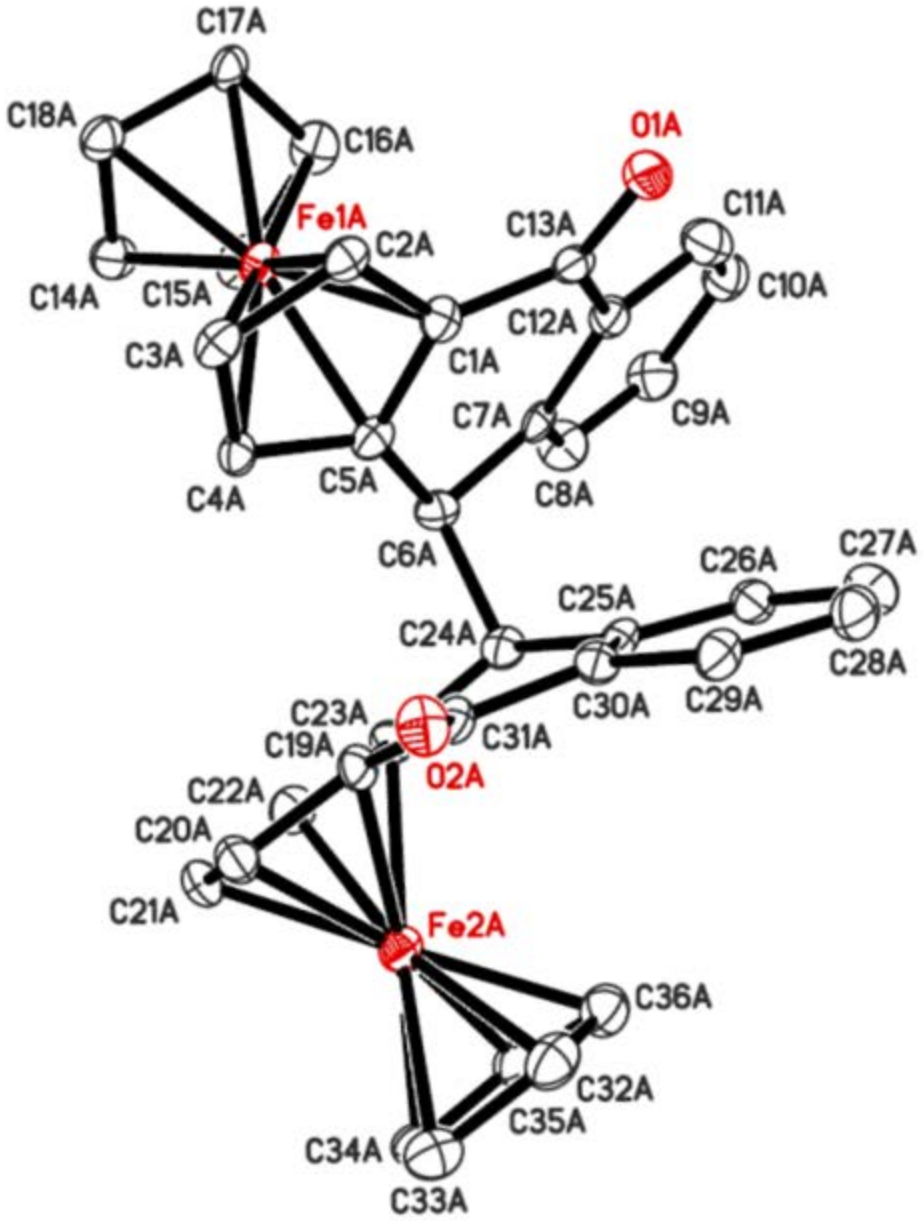

Figure 5.18. Molecular structure of $C_{36}H_{26}Fe_2O_2$ **(17a)**

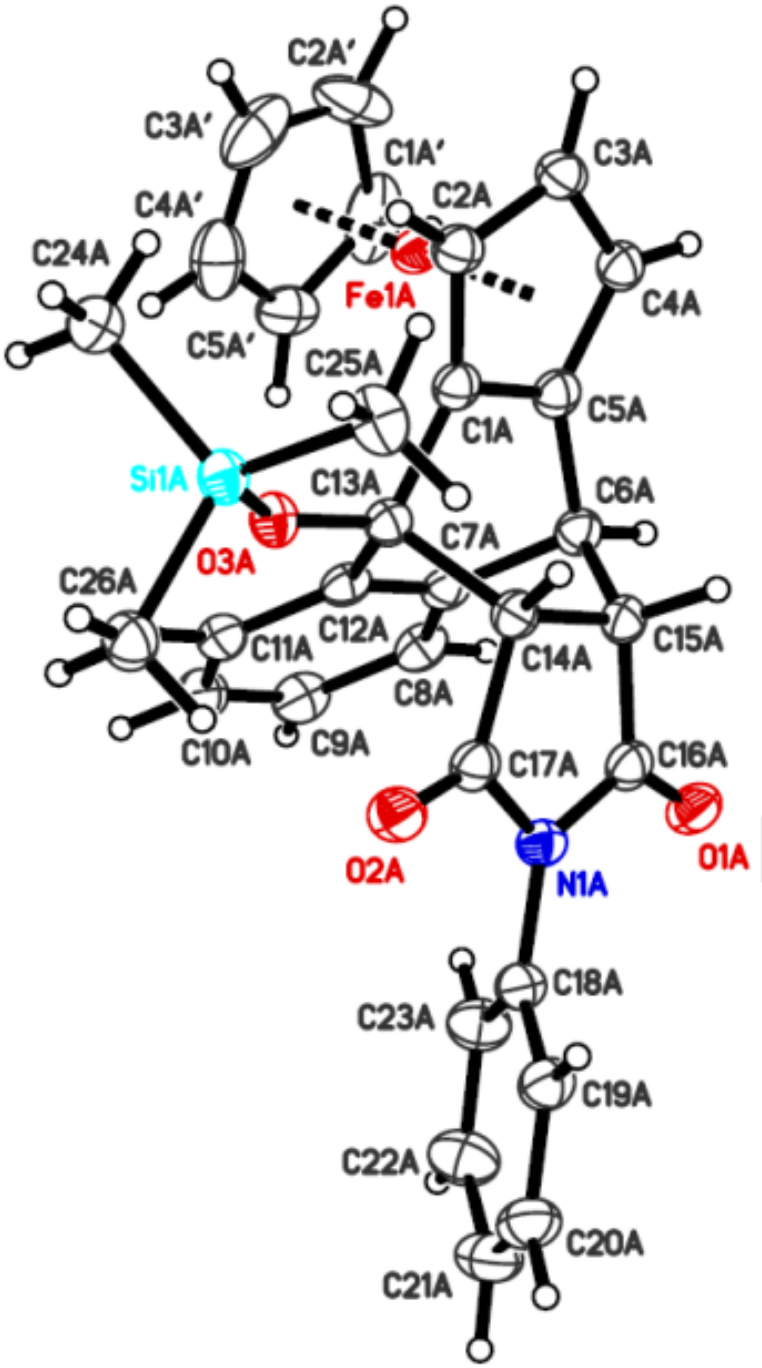

Figure 5.19. Molecular structure of $C_{31}H_{29}FeNO_3Si$ **(18a)**

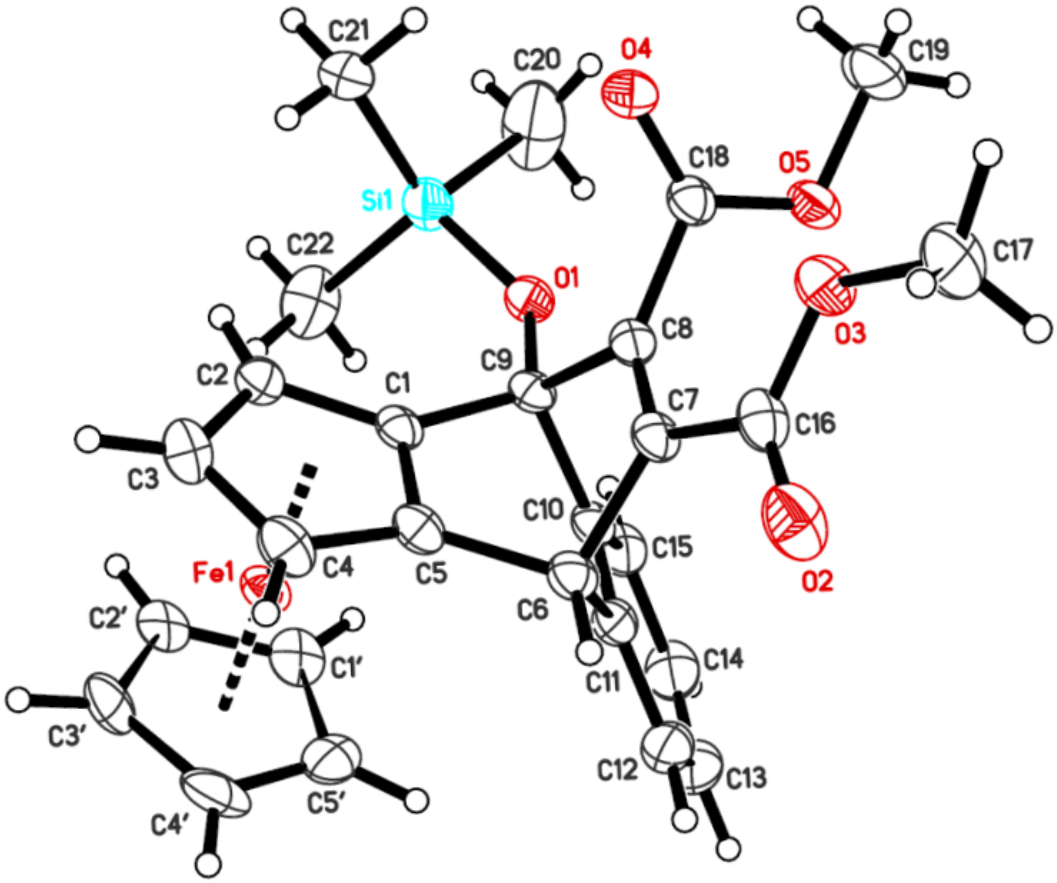

Figure 5.20. Molecular structure of $C_{27}H_{28}FeO_5Si$ (**19a**)

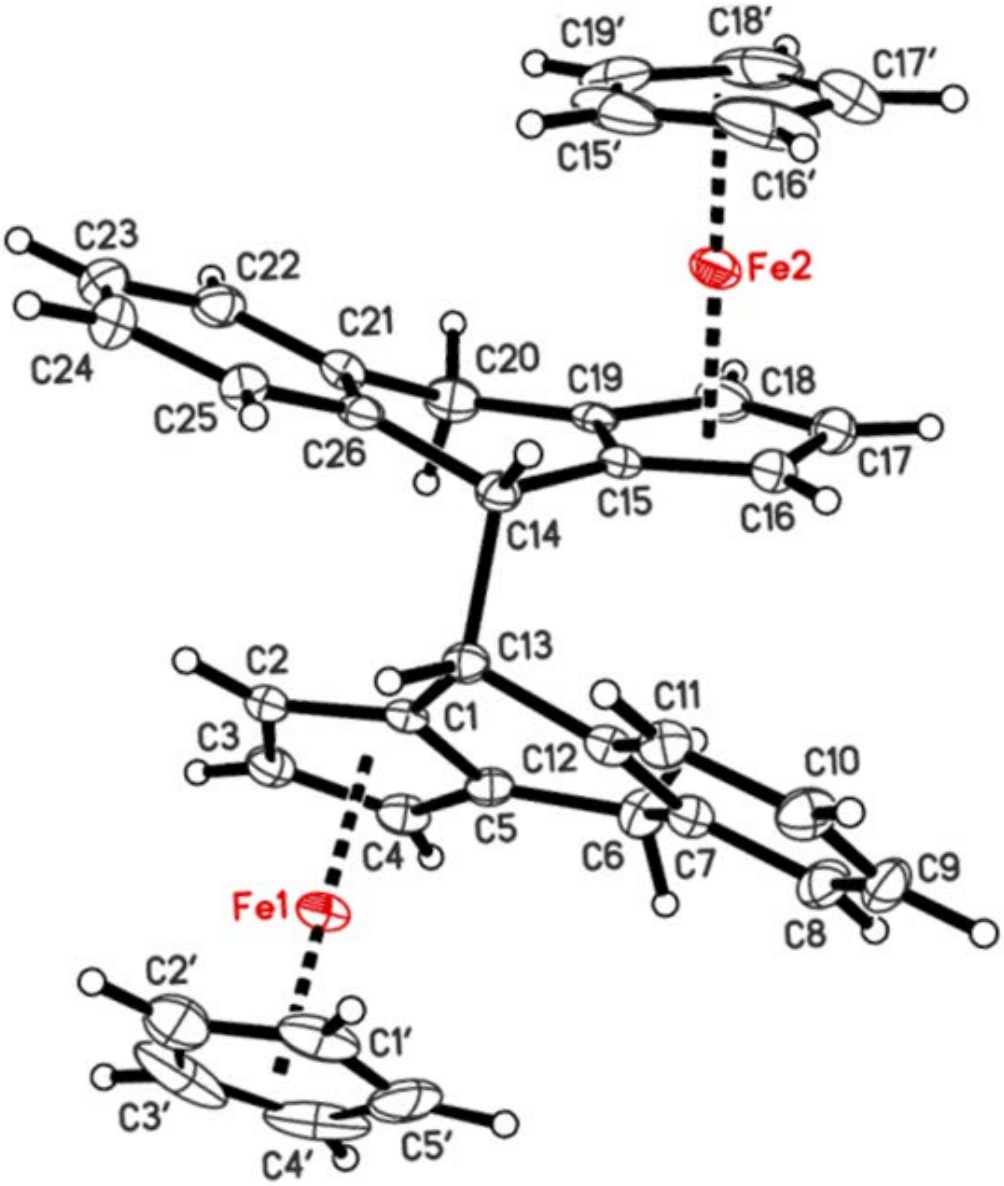

Figure 5.21. Molecular structure of $C_{36}H_{26}Fe_2O_2$ **(20a)**

Table 5.3. Crystal Data and Structure Refinement for Compounds **5a** and **5b**

	5a	**5b**
Identification code	x11018	x10200
Formula	$C_{36}H_{26}Fe_2O_4$	$C_{52}H_{46}Fe_2O_8$
Formula wt (amu)	634.27	910.59
T, K	90.0(2)	90.0(2)
Wavelength (Å)	1.54178	1.54178
Crystal system, space group	Monoclinic, $P2_1/c$	Orthorhombic, *Aba2*
a, Å	16.0357(3)	22.1332(4)
b, Å	10.8621(2)	17.3047(3)
c, Å	16.4588(3)	11.1104(3)
α,(deg)	90	90
β, (deg)	110.334	90
γ, (deg)	90	90
V, $Å^3$	2688.16(9)	4255.38(16)
Z, d_{calc}, Mg/m^3	4, 1.567	4, 1.421
Absorption coef μ (mm^{-1})	8.998	5.935
F(000)	1304	1896
Crystal size (mm^3)	0.18 x 0.04 x 0.03	0.10 x 0.04 x 0.04
2θ range (deg)	2.94 to 68.52	3.99 to 68.59
Limiting indices	$-19 \le h \le 19$, $-10 \le k \le 12$, $-19 \le l \le 19$	$-26 \le h \le 26$, $-20 \le k \le 20$, $-13 \le l \le 13$
Reflections collected / unique	38001/4912 [R(int) = 0.0627]	28004/3852 [R(int) = 0.0618]
Absorption correction	Semi-empirical from equivalents	Semi-empirical from equivalents
Max. and min. transmission	0.774 and 0.294	0.797 and 0.624
Refinement method	Full-matrix least-squares on F^2	Full-matrix least-squares on F^2
Data/restraints/parameters	4912 / 0 / 379	3852 / 31 / 298
Goodness-of-fit on F^2	1.046	1.089
Final *R* indices [$I>2\sigma(I)$]	R_1 = 0.0384, wR_2 = 0.0954	R_1 = 0.0477, wR_2 = 0.1218
R indices (all data)	R_1 = 0.0484, wR_2 = 0.1016	R_1 = 0.0535, wR_2 = 0.1255
Largest diff. peak and hole $e.A^{-3}$	1.014 and -0.479	0.532 and -0.409

Table 5.4. Crystal Data and Structure Refinement for Compounds **7a and 7b**

	7a	**7b**
Identification code	k10242	k11001
Formula	$C_{18}H_{12}FeO_2$	$C_{22}H_{14}Fe\ O_2$
Formula wt (amu)	316.13	366.18
T, K	90.0(2)	90.0(2)
Wavelength (Å)	0.71073	0.71073
Crystal system, space group	Tetragonal, $I4_1/a$	Monoclinic, $P2_1/c$
a, Å	15.0346(3)	6.1744(1)
b, Å	15.0346(3)	19.6997(3)
c, Å	22.7894(5)	12.5042(2)
α,(deg)	90	90
β, (deg)	90	94.5748(7)
γ, (deg)	90	90
V, $Å^3$	5151.30(18)	1516.09(4)
Z, d_{calc}, Mg/m^3	16, 1.630	4, 1.604
Absorption coef μ (mm^{-1})	1.171	1.007
F(000)	2592	752
Crystal size (mm^3)	0.22 x 0.22 x 0.22	0.30 x 0.30 x 0.25
2θ range (deg)	1.62 to 27.50	1.93 to 27.48
Limiting indices	$-19 \le h \le 19$, $-13 \le k \le 13$, $-29 \le l \le 29$	$-8 \le h \le 8$, $-25 \le k \le 25$, $-16 \le l \le 16$
Reflections collected / unique	42334 / 2964 [R(int) = 0.0680]	22328 / 3463 [R(int) = 0.0380]
Absorption correction	Semi-empirical from equivalents	Semi-empirical from equivalents
Max. and min. transmission	0.783 and 0.783	0.787 and 0.752
Refinement method	Full-matrix least-squares on F^2	Full-matrix least-squares on F^2
Data/restraints/parameters	2964/0/190	3463/0 /226
Goodness-of-fit on F^2	1.051	1.076
Final R indices [I>2σ(I)]	R_1 = 0.0410, wR_2 = 0.1094	R_1 = 0.0330, wR_2 = 0.0815
R indices (all data)	R_1 = 0.0533, wR_2 = 0.1175	R_1 = 0.0413, wR_2 = 0.0860
Largest diff. peak and hole $e.A^{-3}$	0.635 and -0.660	0.531 and -0.408

Table 5.5. Crystal Data and Structure Refinement for Compounds **9a** and **11a**

	9a	**11a**
Identification code	k10237	k11046
Formula	$C_{18}H_{16}Fe$	$C_{36}H_{28}Fe_2$
Formula wt (amu)	288.16	572.28
T, K	90.0(2)	90.0(2)
Wavelength (Å)	0.71073	0.71073
Crystal system, space group	Monoclinic, $P2_1/c$	Monoclinic, $P\ 2_1/c$
a, Å	13.7820(2)	12.3682(3)
b, Å	7.53329(10)	10.6085(3)
c, Å	12.6706(2)	10.2639(4)
α,(deg)	90	90
β, (deg)	97.5581(6)	113.6668(13)
γ, (deg)	90	90
V, $Å^3$	1304.08(3)	1233.44(7)
Z, d_{calc}, Mg/m^3	4, 1.468	2, 1.541
Absorption coef μ (mm^{-1})	1.137	1.202
F(000)	600	592
Crystal size (mm^3)	0.22 x 0.20 x 0.05	0.16 x 0.14 x 0.10
2θ range (deg)	1.49 to 27.48	1.80 to 27.49
Limiting indices	$-17 \le h \le 17$, $-9 \le k \le 9$, $-16 \le l \le 16$	$-16 \le h \le 16$, $-13 \le k \le 13$, $-13 \le l \le 13$
Reflections collected / unique	33154 / 2990 [R(int) = 0.0390]	19747 / 2823 [R(int) = 0.0540]
Absorption correction	Semi-empirical from equivalents	Semi-empirical from equivalents
Max. and min. transmission	0.945 and 0.788	0.889 and 0.831
Refinement method	Full-matrix least-squares on F^2	Full-matrix least-squares on F^2
Data/restraints/parameters	2990 /0/172	2823 /0/172
Goodness-of-fit on F^2	1.054	1.040
Final R indices [I>2σ(I)]	R_1 = 0.0264, wR_2 = 0.0653	R_1 = 0.0422, wR_2 = 0.1073
R indices (all data)	R_1 = 0.0326, wR_2 = 0.0686	R_1 = 0.0584, wR_2 = 0.1149
Largest diff. peak and hole $e.A^{-3}$	0.410 and -0.273	0.996 and -0.554

Table 5.6. Crystal Data and Structure Refinement for Compounds **13a, 14a** and **20a**

	13a	**14a**	**20a**
Identification code	k11035	x11084	k11165-sr
Formula	$C_{18}H_{14}Fe\ O_2$	$C_{25}H_{20}FeO$	$C_{36}H_{30}\ Fe_2$
Formula wt (amu)	318.14	392.26	574.3
T, K	90.0(2)	90.0(2)	90.0(2)
Wavelength (Å)	0.71073	1.54178	0.71073
Crystal system, space group	Triclinic, *P-1*	Monoclinic, $P2_1/n$	Monoclinic, $P2_1/n$
a, Å	10.8436(2)	14.4479(5)	13.5359(1)
b, Å	11.1812(2)	6.8518(3)	17.4907(2)
c, Å	11.7245(2)	19.4426(7)	12.8842(2)
α,(deg)	87.8260(6)	90	90
β, (deg)	69.9284(6)	108.560(2)	103.6078(5)
γ, (deg)	86.5328(6)	90	90
V, $Å^3$	1332.53(4)	1824.60(12)	2964.74(6)
Z, d_{calc}, Mg/m^3	4, 1.586	4, 1.428	4, 1.287
Absorption coef μ (mm^{-1})	1.132	6.701	1.000
F(000)	656	816	1192
Crystal size (mm^3)	0.22 x 0.18 x 0.16	0.12 x 0.10 x 0.06	0.28 x 0.25 x 0.11
2θ range (deg)	1.82 to 27.50	3.35 to 69.65	1.55 to 27.48
Limiting indices	$-14\le h\le 14$, $-14\le k\le 14$, $-15\le l\le 15$	$-17\le h\le 17$, $-8\le k\le 8$, $-23\le l\le 23$	$-17\le h\le 17$, $-22\le k\le 22$, $-16\le l\le 16$
Reflections collected / unique	34510 / 6113 [R(int) = 0.0410]	23970 / 3355 [R(int) = 0.0721]	69576 / 6801 [R(int) = 0.0355]
Absorption correction	Semi-empirical from equivalents	Semi-empirical from equivalents	Semi-empirical from equivalents
Max. and min. transmission	0.840 and 0.789	0.753 and 0.512	0.898 and 0.767
Refinement method	Full-matrix least-squares on F^2	Full-matrix least-squares on F^2	Full-matrix least-squares on F^2
Data/restraints/parameters	6113 /0/381	3355 /0/244	6801/0 /344
Goodness-of-fit on F^2	1.058	1.057	1.036
Final R indices [I>2σ(I)]	R_1 = 0.0352, wR_2 = 0.0850	R_1 = 0.0275, wR_2 = 0.0757	R_1 = 0.0424, wR_2 = 0.1083
R indices (all data)	R_1 = 0.0496, wR_2 =	R_1 = 0.0666, wR_2 =	R_1 = 0.0626, wR_2 =

	0.0920	0.0790	0.1165
Largest diff. peak and hole e.A^{-3}	0.625 and -0.658	0.372 and -0.276	1.049 and -0.448

Table 5.7. Crystal Data and Structure Refinement for Compounds **18a** and **19a**

	18a	**19a**
Identification code	x12047sx	x12039
Formula	$C_{31}H_{29}FeNO_3Si$	$C_{27}H_{28}FeO_5Si$
Formula wt (amu)	547.49	516.43
T, K	90.0(2)	90.0(2)
Wavelength (Å)	1.54178	1.54178
Crystal system, space group	Triclinic, *P-1*	Triclinic, *P-1*
a, Å	10.2174(2)	8.1026(2)
b, Å	15.1625(2)	10.2704(2)
c, Å	17.5849(3)	16.6542(4)
α,(deg)	77.770(1)	106.026(1)
β, (deg)	86.965(1)	91.887(1)
γ, (deg)	83.976(1)	110.826(1)
V, $Å^3$	2646.42(8)	1231.69(5)
Z, d_{calc}, Mg/m^3	4, 1.374	2, 1.392
Absorption coef μ (mm^{-1})	5.269	5.673
F(000)	1144	540
Crystal size (mm^3)	0.16 x 0.12 x 0.08	0.14 x 0.08 x 0.02
2θ range (deg)	2.57 to 67.99	2.79 to 68.00
Limiting indices	$-12 \le h \le 12$, $-18 \le k \le 18$, $-20 \le l \le 21$	$-9 \le h \le 8$, $-12 \le k \le 12$, $-20 \le l \le 20$
Reflections collected / unique	38198 / 9547 [R(int) = 0.0356]	17259 / 4409 [R(int) = 0.0449]
Absorption correction	Semi-empirical from equivalents	Semi-empirical from equivalents
Max. and min. transmission	0.678 and 0.452	0.896 and 0.612
Refinement method	Full-matrix least-squares on F^2	Full-matrix least-squares on F^2
Data/restraints/parameters	9547 /0/673	4409/90/328
Goodness-of-fit on F^2	1.021	1.035
Final R indices [$I>2\sigma(I)$]	*R1* = 0.0349, *wR2* = 0.0930	*R1* = 0.0385, *wR2* = 0.1041
R indices (all data)	*R1* = 0.0380, *wR2* = 0.0955	*R1* = 0.0440, *wR2* = 0.1085
Largest diff. peak and hole $e.A^{-3}$	1.365 and -0.392	0.423 and -0.457

Table 5.8. Bond Distances (Å) and Bond Angles [°] for **5a**

Fe1-C7	2.038(3)
Fe1-C5	2.039(3)
Fe1-C9	2.041(3)
Fe1-C6	2.041(3)
Fe1-C10	2.042(3)
Fe1-C4	2.043(3)
Fe1-C8	2.044(3)
Fe1-C3	2.053(3)
Fe1-C2	2.053(3)
Fe1-C1	2.057(3)
Fe2-C26	2.039(3)
Fe2-C20	2.041(3)
Fe2-C25	2.041(3)
Fe2-C24	2.043(3)
Fe2-C23	2.045(3)
Fe2-C28	2.045(3)
Fe2-C27	2.047(3)
Fe2-C19	2.047(3)
Fe2-C21	2.049(3)
Fe2-C22	2.052(3)
O1-C18	1.195(3)
O2-C18	1.372(3)
O2-C11	1.457(3)
O3-C36	1.201(3)
O4-C36	1.356(3)
O4-C29	1.456(3)
C1-C2	1.421(4)
C1-C5	1.432(4)
C2-C3	1.414(4)
C3-C4	1.418(4)
C4-C5	1.429(4)
C5-C11	1.491(4)
C6-C7	1.397(5)
C6-C10	1.415(6)
C7-C8	1.406(5)
C8-C9	1.399(5)
C9-C10	1.411(5)
C11-C12	1.515(4)
C11-C29	1.578(3)
C12-C17	1.379(4)
C12-C13	1.389(4)
C13-C14	1.386(4)

C14-C15	1.387(5)
C15-C16	1.379(4)
C16-C17	1.387(4)
C17-C18	1.466(4)
C19-C20	1.422(4)
C19-C23	1.430(4)
C20-C21	1.414(4)
C21-C22	1.419(4)
C22-C23	1.424(4)
C23-C29	1.500(4)
C24-C25	1.385(6)
C24-C28	1.388(6)
C25-C26	1.390(5)
C26-C27	1.411(5)
C27-C28	1.430(5)
C29-C30	1.502(4)
C30-C31	1.379(4)
C30-C35	1.381(4)
C31-C32	1.384(4)
C32-C33	1.397(5)
C33-C34	1.380(5)
C34-C35	1.381(4)
C35-C36	1.471(4)
C7-Fe1-C5	161.57(13)
C7-Fe1-C9	67.88(15)
C5-Fe1-C9	122.83(13)
C7-Fe1-C6	40.05(14)
C5-Fe1-C6	126.05(13)
C9-Fe1-C6	68.08(15)
C7-Fe1-C10	67.72(14)
C5-Fe1-C10	109.62(12)
C9-Fe1-C10	40.45(15)
C6-Fe1-C10	40.56(16)
C7-Fe1-C4	155.16(13)
C5-Fe1-C4	41.00(10)
C9-Fe1-C4	109.07(13)
C6-Fe1-C4	163.86(14)
C10-Fe1-C4	127.04(14)
C7-Fe1-C8	40.28(15)
C5-Fe1-C8	157.26(14)
C9-Fe1-C8	40.07(15)
C6-Fe1-C8	**67**.46(14)

Table 5.8 continued

C10-Fe1-C8	67.43(13)
C4-Fe1-C8	121.36(13)
C7-Fe1-C3	119.67(13)
C5-Fe1-C3	68.35(11)
C9-Fe1-C3	125.52(14)
C6-Fe1-C3	154.20(15)
C10-Fe1-C3	163.22(15)
C4-Fe1-C3	40.52(11)
C8-Fe1-C3	107.60(12)
C7-Fe1-C2	106.01(13)
C5-Fe1-C2	68.58(10)
C9-Fe1-C2	160.84(14)
C6-Fe1-C2	119.75(15)
C10-Fe1-C2	155.95(15)
C4-Fe1-C2	68.37(11)
C8-Fe1-C2	123.74(13)
C3-Fe1-C2	40.27(12)
C7-Fe1-C1	123.73(14)
C5-Fe1-C1	40.94(10)
C9-Fe1-C1	157.98(14)
C6-Fe1-C1	107.70(13)
C10-Fe1-C1	122.29(13)
C4-Fe1-C1	68.62(11)
C8-Fe1-C1	160.23(13)
C3-Fe1-C1	67.89(11)
C2-Fe1-C1	40.45(11)
C26-Fe2-C20	111.23(12)
C26-Fe2-C25	39.84(14)
C20-Fe2-C25	107.07(14)
C26-Fe2-C24	67.18(14)
C20-Fe2-C24	132.40(15)
C25-Fe2-C24	39.66(16)
C26-Fe2-C23	177.10(13)
C20-Fe2-C23	68.77(10)
C25-Fe2-C23	143.06(13)
C24-Fe2-C23	115.10(13)
C26-Fe2-C28	67.70(13)
C20-Fe2-C28	172.10(15)
C25-Fe2-C28	66.82(15)
C24-Fe2-C28	39.70(16)
C23-Fe2-C28	112.73(12)
C26-Fe2-C27	40.42(14)
C20-Fe2-C27	142.80(14)

C25-Fe2-C27	67.46(14)
C24-Fe2-C27	67.80(14)
C23-Fe2-C27	138.08(13)
C28-Fe2-C27	40.91(15)
C26-Fe2-C19	140.82(13)
C20-Fe2-C19	40.72(11)
C25-Fe2-C19	111.52(13)
C24-Fe2-C19	109.07(13)
C23-Fe2-C19	40.90(11)
C28-Fe2-C19	135.44(14)
C27-Fe2-C19	176.34(14)
C26-Fe2-C21	109.51(12)
C20-Fe2-C21	40.45(11)
C25-Fe2-C21	132.96(14)
C24-Fe2-C21	171.55(15)
C23-Fe2-C21	68.50(10)
C28-Fe2-C21	147.43(15)
C27-Fe2-C21	115.19(13)
C19-Fe2-C21	68.19(11)
C26-Fe2-C22	136.47(13)
C20-Fe2-C22	68.19(11)
C25-Fe2-C22	173.37(14)
C24-Fe2-C22	146.97(14)
C23-Fe2-C22	40.67(10)
C28-Fe2-C22	118.31(13)
C27-Fe2-C22	113.21(13)
C19-Fe2-C22	68.24(11)
C21-Fe2-C22	40.47(11)
C18-O2-C11	111.13(19)
C36-O4-C29	111.1(2)
C2-C1-C5	107.8(2)
C2-C1-Fe1	69.64(16)
C5-C1-Fe1	68.86(15)
C3-C2-C1	108.1(2)
C3-C2-Fe1	69.85(16)
C1-C2-Fe1	69.91(15)
C2-C3-C4	108.7(2)
C2-C3-Fe1	69.88(16)
C4-C3-Fe1	69.35(16)
C3-C4-C5	107.7(2)
C3-C4-Fe1	70.13(16)
C5-C4-Fe1	69.36(15)
C4-C5-C1	1**07**.7(2)

Table 5.8 continued

C4-C5-C11	126.5(2)
C1-C5-C11	125.5(2)
C4-C5-Fe1	69.64(15)
C1-C5-Fe1	70.20(15)
C11-C5-Fe1	131.03(18)
C7-C6-C10	107.9(3)
C7-C6-Fe1	69.86(19)
C10-C6-Fe1	69.74(19)
C6-C7-C8	108.1(3)
C6-C7-Fe1	70.09(18)
C8-C7-Fe1	70.08(18)
C9-C8-C7	108.6(3)
C9-C8-Fe1	69.83(18)
C7-C8-Fe1	69.63(18)
C8-C9-C10	107.6(3)
C8-C9-Fe1	70.10(18)
C10-C9-Fe1	69.81(19)
C9-C10-C6	107.9(3)
C9-C10-Fe1	69.74(18)
C6-C10-Fe1	69.71(19)
O2-C11-C5	108.4(2)
O2-C11-C12	103.7(2)
C5-C11-C12	116.4(2)
O2-C11-C29	105.82(19)
C5-C11-C29	110.4(2)
C12-C11-C29	111.3(2)
C17-C12-C13	120.1(2)
C17-C12-C11	108.2(2)
C13-C12-C11	131.7(3)
C14-C13-C12	117.4(3)
C13-C14-C15	122.1(3)
C16-C15-C14	120.5(3)
C15-C16-C17	117.3(3)
C12-C17-C16	122.6(3)
C12-C17-C18	109.2(2)
C16-C17-C18	128.2(3)
O1-C18-O2	121.1(2)
O1-C18-C17	131.2(3)
O2-C18-C17	107.7(2)
C20-C19-C23	108.0(2)
C20-C19-Fe2	69.41(15)
C23-C19-Fe2	69.47(15)
C21-C20-C19	108.1(2)

C21-C20-Fe2	70.10(15)
C19-C20-Fe2	69.87(15)
C20-C21-C22	108.2(2)
C20-C21-Fe2	69.45(15)
C22-C21-Fe2	69.88(15)
C21-C22-C23	108.3(2)
C21-C22-Fe2	69.65(15)
C23-C22-Fe2	69.38(15)
C22-C23-C19	107.4(2)
C22-C23-C29	127.6(2)
C19-C23-C29	125.0(2)
C22-C23-Fe2	69.95(15)
C19-C23-Fe2	69.63(15)
C29-C23-Fe2	128.29(18)
C25-C24-C28	108.4(3)
C25-C24-Fe2	70.1(2)
C28-C24-Fe2	70.21(19)
C24-C25-C26	108.9(3)
C24-C25-Fe2	70.3(2)
C26-C25-Fe2	70.00(18)
C25-C26-C27	108.2(3)
C25-C26-Fe2	70.17(19)
C27-C26-Fe2	70.10(17)
C26-C27-C28	106.4(3)
C26-C27-Fe2	69.49(18)
C28-C27-Fe2	69.47(17)
C24-C28-C27	108.1(3)
C24-C28-Fe2	70.09(19)
C27-C28-Fe2	69.62(17)
O4-C29-C23	108.0(2)
O4-C29-C30	104.3(2)
C23-C29-C30	114.6(2)
O4-C29-C11	104.63(19)
C23-C29-C11	112.5(2)
C30-C29-C11	111.9(2)
C31-C30-C35	120.5(3)
C31-C30-C29	131.6(2)
C35-C30-C29	107.9(2)
C30-C31-C32	117.8(3)
C31-C32-C33	121.1(3)
C34-C33-C32	121.2(3)
C33-C34-C35	116.8(3)
C34-C35-C30	1**22**.6(3)

Table 5.8 continued

C34-C35-C36	128.5(3)
C30-C35-C36	108.9(2)
O3-C36-O4	121.5(3)

O3-C36-C35	130.6(3)
O4-C36-C35	107.9(2)

Table 5.9. Bond Distances (Å) and Bond Angles [°] for **5b**

Fe1-C3'	2.020(7)
Fe1-C4'	2.033(14)
Fe1-C2	2.037(4)
Fe1-C2'	2.037(9)
Fe1-C1	2.039(4)
Fe1-C5"	2.04(2)
Fe1-C3	2.042(4)
Fe1-C5	2.048(4)
Fe1-C4"	2.05(5)
Fe1-C1"	2.05(3)
Fe1-C1'	2.059(8)
Fe1-C5'	2.060(7)
O1-C15	1.384(5)
O1-C6	1.435(4)
O2-C15	1.184(5)
C1-C5	1.429(5)
C1-C2	1.434(5)
C1-C6	1.502(5)
C2-C3	1.431(6)
C3-C4	1.421(7)
C4-C5	1.427(6)
C6-C7	1.506(5)
C6-C6#1	1.566(6)
C7-C8	1.365(5)
C7-C14	1.402(5)
C8'-C9	1.413(5)
C8'-C8	1.419(5)
C8'-C12'	1.424(5)
C9-C10	1.360(6)
C10-C11	1.412(6)
C11-C12	1.366(6)
C12-C12'	1.414(6)
C12'-C13	1.411(5)
C13-C14	1.374(5)
C14-C15	1.460(5)
C1'-C5'	1.382(12)
C1'-C2'	1.434(13)
C2'-C3'	1.394(16)
C3'-C4'	1.390(13)
C4'-C5'	1.420(11)
C1"-C5"	1.37(2)
C1"-C2"	1.43(2)

C2"-C3"	1.39(2)
C3"-C4"	1.387(19)
C4"-C5"	1.417(19)
O2S-C1S	1.325(9)
O2S-C3S	1.419(9)
O1S-C1S	1.197(8)
C1S-C2S	1.502(12)
C3S-C4S	1.481(11)
C3'-Fe1-C4'	40.1(4)
C3'-Fe1-C2	174.5(4)
C4'-Fe1-C2	142.5(4)
C3'-Fe1-C2'	40.2(5)
C4'-Fe1-C2'	67.9(5)
C2-Fe1-C2'	134.4(4)
C3'-Fe1-C1	136.6(3)
C4'-Fe1-C1	175.2(3)
C2-Fe1-C1	41.22(15)
C2'-Fe1-C1	111.7(3)
C3'-Fe1-C5"	60.3(7)
C4'-Fe1-C5"	46.9(11)
C2-Fe1-C5"	117.2(7)
C2'-Fe1-C5"	50.7(10)
C1-Fe1-C5"	136.9(11)
C3'-Fe1-C3	144.3(5)
C4'-Fe1-C3	111.9(4)
C2-Fe1-C3	41.09(16)
C2'-Fe1-C3	171.8(5)
C1-Fe1-C3	69.18(16)
C5"-Fe1-C3	122.7(11)
C3'-Fe1-C5	112.7(2)
C4'-Fe1-C5	134.6(3)
C2-Fe1-C5	68.81(16)
C2'-Fe1-C5	117.8(3)
C1-Fe1-C5	40.95(15)
C5"-Fe1-C5	168.5(12)
C3-Fe1-C5	68.48(18)
C3'-Fe1-C4"	45.6(9)
C4'-Fe1-C4"	8.1(11)
C2-Fe1-C4"	136.3(9)
C2'-Fe1-C4"	68.4(9)
C1-Fe1-C4"	176.7(11)
C5"-Fe1-C4"	40.5(8)

Table 5.9 continued

C3-Fe1-C4"	110.2(8)
C5-Fe1-C4"	142.1(11)
C3'-Fe1-C1"	51.5(9)
C4'-Fe1-C1"	69.1(7)
C2-Fe1-C1"	123.2(9)
C2'-Fe1-C1"	16.3(10)
C1-Fe1-C1"	112.0(7)
C5"-Fe1-C1"	39.2(7)
C3-Fe1-C1"	155.6(13)
C5-Fe1-C1"	129.4(11)
C4"-Fe1-C1"	67.2(11)
C3'-Fe1-C1'	67.4(3)
C4'-Fe1-C1'	67.1(4)
C2-Fe1-C1'	108.4(3)
C2'-Fe1-C1'	41.0(4)
C1-Fe1-C1'	116.0(2)
C5"-Fe1-C1'	22.5(11)
C3-Fe1-C1'	131.0(4)
C5-Fe1-C1'	148.7(4)
C4"-Fe1-C1'	61.8(9)
C1"-Fe1-C1'	25.2(10)
C3'-Fe1-C5'	67.6(3)
C4'-Fe1-C5'	40.6(3)
C2-Fe1-C5'	111.6(2)
C2'-Fe1-C5'	67.9(3)
C1-Fe1-C5'	144.1(3)
C5"-Fe1-C5'	18.4(10)
C3-Fe1-C5'	106.3(3)
C5-Fe1-C5'	172.0(4)
C4"-Fe1-C5'	32.7(10)
C1"-Fe1-C5'	57.5(9)
C1'-Fe1-C5'	39.2(3)
C15-O1-C6	111.5(3)
C5-C1-C2	107.4(3)
C5-C1-C6	125.7(3)
C2-C1-C6	126.7(3)
C5-C1-Fe1	69.9(2)
C2-C1-Fe1	69.3(2)
C6-C1-Fe1	130.6(3)
C3-C2-C1	107.9(4)
C3-C2-Fe1	69.7(2)
C1-C2-Fe1	69.5(2)
C4-C3-C2	108.3(4)

C4-C3-Fe1	70.5(3)
C2-C3-Fe1	69.2(2)
C3-C4-C5	107.8(4)
C3-C4-Fe1	69.0(2)
C5-C4-Fe1	69.1(2)
C4-C5-C1	108.6(4)
C4-C5-Fe1	70.2(2)
C1-C5-Fe1	69.2(2)
O1-C6-C1	107.8(3)
O1-C6-C7	103.8(3)
C1-C6-C7	113.8(3)
O1-C6-C6#1	106.4(3)
C1-C6-C6#1	110.9(2)
C7-C6-C6#1	113.4(2)
C8-C7-C14	119.9(3)
C8-C7-C6	131.1(3)
C14-C7-C6	108.9(3)
C9-C8'-C8	121.0(3)
C9-C8'-C12'	118.4(3)
C8-C8'-C12'	120.6(3)
C7-C8-C8'	119.1(3)
C10-C9-C8'	121.0(4)
C9-C10-C11	120.7(4)
C12-C11-C10	120.0(4)
C11-C12-C12'	120.6(4)
C13-C12'-C12	121.8(3)
C13-C12'-C8'	118.8(3)
C12-C12'-C8'	119.3(3)
C14-C13-C12'	118.6(3)
C13-C14-C7	122.9(3)
C13-C14-C15	129.6(3)
C7-C14-C15	107.5(3)
O2-C15-O1	120.7(4)
O2-C15-C14	131.2(4)
O1-C15-C14	108.2(3)
C5'-C1'-C2'	108.7(7)
C5'-C1'-Fe1	70.4(4)
C2'-C1'-Fe1	68.7(4)
C3'-C2'-C1'	106.3(7)
C3'-C2'-Fe1	69.2(5)
C1'-C2'-Fe1	70.3(4)
C4'-C3'-C2'	109.5(7)
C4'-C3'-Fe1	70.5(7)

Table 5.9 continued

C2'-C3'-Fe1	70.6(5)
C3'-C4'-C5'	107.8(8)
C3'-C4'-Fe1	69.4(6)
C5'-C4'-Fe1	70.7(6)
C1'-C5'-C4'	107.6(7)
C1'-C5'-Fe1	70.3(4)
C4'-C5'-Fe1	68.7(6)
C5"-C1"-C2"	106.8(14)
C5"-C1"-Fe1	69.9(16)
C2"-C1"-Fe1	72.3(15)
C3"-C2"-C1"	108.2(15)
C3"-C2"-Fe1	69.1(14)
C1"-C2"-Fe1	67.5(16)
C4"-C3"-C2"	108.0(16)

C4"-C3"-Fe1	69(2)
C2"-C3"-Fe1	72.2(14)
C3"-C4"-C5"	107.8(15)
C3"-C4"-Fe1	71.4(19)
C5"-C4"-Fe1	69.3(18)
C1"-C5"-C4"	109.0(15)
C1"-C5"-Fe1	70.9(16)
C4"-C5"-Fe1	70(2)
C1S-O2S-C3S	117.8(6)
O1S-C1S-O2S	121.3(8)
O1S-C1S-C2S	125.4(8)
O2S-C1S-C2S	113.3(6)
O2S-C3S-C4S	114.7(7)

Table 5.10. Bond Distances (Å) and Bond Angles [°] for **7a**

Fe1-C5	2.030(2)
Fe1-C1	2.031(2)
Fe1-C2	2.044(2)
Fe1-C5'	2.044(2)
Fe1-C4	2.047(2)
Fe1-C4'	2.047(3)
Fe1-C1'	2.052(2)
Fe1-C3	2.057(2)
Fe1-C2'	2.060(3)
Fe1-C3'	2.061(2)
O1-C6	1.229(3)
O2-C13	1.231(3)
C1-C2	1.431(3)
C1-C5	1.443(3)
C1-C13	1.457(3)
C2-C3	1.424(3)
C3-C4	1.422(3)
C4-C5	1.433(3)
C5-C6	1.461(3)
C6-C7	1.500(3)
C7-C8	1.392(3)
C7-C12	1.415(3)
C8-C9	1.383(4)
C9-C10	1.389(3)
C10-C11	1.388(4)
C11-C12	1.392(3)
C12-C13	1.496(3)
C1'-C2'	1.424(4)
C1'-C5'	1.428(4)
C2'-C3'	1.420(4)
C3'-C4'	1.417(3)
C4'-C5'	1.428(3)
C5-Fe1-C1	41.62(9)
C5-Fe1-C2	69.59(10)
C1-Fe1-C2	41.10(9)
C5-Fe1-C5'	120.68(10)
C1-Fe1-C5'	158.87(10)
C2-Fe1-C5'	157.31(10)
C5-Fe1-C4	41.15(10)
C1-Fe1-C4	69.36(9)
C2-Fe1-C4	69.05(10)
C5'-Fe1-C4	104.52(10)

C5-Fe1-C4'	155.10(10)
C1-Fe1-C4'	160.01(9)
C2-Fe1-C4'	121.56(10)
C5'-Fe1-C4'	40.86(10)
C4-Fe1-C4'	118.19(10)
C5-Fe1-C1'	108.80(10)
C1-Fe1-C1'	124.75(10)
C2-Fe1-C1'	160.36(10)
C5'-Fe1-C1'	40.80(11)
C4-Fe1-C1'	123.43(10)
C4'-Fe1-C1'	68.43(10)
C5-Fe1-C3	68.69(10)
C1-Fe1-C3	68.54(10)
C2-Fe1-C3	40.63(9)
C5'-Fe1-C3	120.66(10)
C4-Fe1-C3	40.55(10)
C4'-Fe1-C3	104.39(10)
C1'-Fe1-C3	158.44(10)
C5-Fe1-C2'	126.91(10)
C1-Fe1-C2'	110.92(10)
C2-Fe1-C2'	123.88(10)
C5'-Fe1-C2'	68.38(10)
C4-Fe1-C2'	161.86(11)
C4'-Fe1-C2'	68.09(10)
C1'-Fe1-C2'	40.52(11)
C3-Fe1-C2'	157.48(11)
C5-Fe1-C3'	163.57(10)
C1-Fe1-C3'	125.84(9)
C2-Fe1-C3'	107.64(10)
C5'-Fe1-C3'	68.27(10)
C4-Fe1-C3'	154.35(10)
C4'-Fe1-C3'	40.36(10)
C1'-Fe1-C3'	68.04(10)
C3-Fe1-C3'	120.44(10)
C2'-Fe1-C3'	40.31(10)
C2-C1-C5	108.0(2)
C2-C1-C13	129.4(2)
C5-C1-C13	122.2(2)
C2-C1-Fe1	69.94(13)
C5-C1-Fe1	69.14(13)
C13-C1-Fe1	121.08(16)
C3-C2-C1	107.5(2)

Table 5.10 continued

C3-C2-Fe1	70.17(13)
C1-C2-Fe1	68.95(13)
C4-C3-C2	109.1(2)
C4-C3-Fe1	69.33(14)
C2-C3-Fe1	69.20(13)
C3-C4-C5	107.7(2)
C3-C4-Fe1	70.12(14)
C5-C4-Fe1	68.79(13)
C4-C5-C1	107.6(2)
C4-C5-C6	129.8(2)
C1-C5-C6	122.3(2)
C4-C5-Fe1	70.06(14)
C1-C5-Fe1	69.24(13)
C6-C5-Fe1	121.13(16)
O1-C6-C5	122.9(2)
O1-C6-C7	121.5(2)
C5-C6-C7	115.52(19)
C8-C7-C12	119.0(2)
C8-C7-C6	119.0(2)
C12-C7-C6	121.9(2)
C9-C8-C7	121.1(2)
C8-C9-C10	119.8(2)
C11-C10-C9	120.1(2)

C10-C11-C12	120.7(2)
C11-C12-C7	119.2(2)
C11-C12-C13	118.8(2)
C7-C12-C13	122.0(2)
O2-C13-C1	122.6(2)
O2-C13-C12	121.7(2)
C1-C13-C12	115.7(2)
C2'-C1'-C5'	108.0(2)
C2'-C1'-Fe1	70.05(14)
C5'-C1'-Fe1	69.31(14)
C3'-C2'-C1'	108.0(2)
C3'-C2'-Fe1	69.88(14)
C1'-C2'-Fe1	69.43(14)
C4'-C3'-C2'	108.3(2)
C4'-C3'-Fe1	69.29(14)
C2'-C3'-Fe1	69.81(14)
C3'-C4'-C5'	108.1(2)
C3'-C4'-Fe1	70.34(14)
C5'-C4'-Fe1	69.46(14)
C1'-C5'-C4'	107.6(2)
C1'-C5'-Fe1	69.89(14)
C4'-C5'-Fe1	69.68(13)

Table 5.11. Bond Distances (Å) and Bond Angles [°] for **7b**

Fe1-C5	2.0242(18)
Fe1-C1	2.0407(18)
Fe1-C4	2.0489(18)
Fe1-C5'	2.0496(18)
Fe1-C4'	2.0497(19)
Fe1-C3'	2.050(2)
Fe1-C2'	2.055(2)
Fe1-C1'	2.0562(19)
Fe1-C2	2.0651(18)
Fe1-C3	2.0655(18)
O1-C6	1.230(2)
O2-C17	1.225(2)
C1-C2	1.429(3)
C1-C5	1.445(3)
C1-C17	1.462(3)
C2-C3	1.424(3)
C3-C4	1.427(3)
C4-C5	1.428(3)
C5-C6	1.456(2)
C6-C7	1.499(2)
C7-C8	1.377(2)
C7-C16	1.434(2)
C8-C9	1.416(3)
C9-C10	1.421(3)
C9-C14	1.431(2)
C10-C11	1.372(3)
C11-C12	1.411(3)
C12-C13	1.370(3)
C13-C14	1.415(3)
C14-C15	1.412(2)
C15-C16	1.374(3)
C16-C17	1.498(2)
C1'-C2'	1.421(3)
C1'-C5'	1.425(3)
C2'-C3'	1.422(3)
C3'-C4'	1.423(3)
C4'-C5'	1.422(3)
C5-Fe1-C1	41.63(7)
C5-Fe1-C4	41.04(7)
C1-Fe1-C4	69.03(8)
C5-Fe1-C5'	107.24(8)
C1-Fe1-C5'	123.13(8)

C4-Fe1-C5'	123.15(8)
C5-Fe1-C4'	120.23(8)
C1-Fe1-C4'	157.76(8)
C4-Fe1-C4'	105.59(8)
C5'-Fe1-C4'	40.59(8)
C5-Fe1-C3'	155.41(8)
C1-Fe1-C3'	160.93(8)
C4-Fe1-C3'	119.66(8)
C5'-Fe1-C3'	68.30(8)
C4'-Fe1-C3'	40.62(8)
C5-Fe1-C2'	162.30(8)
C1-Fe1-C2'	125.41(8)
C4-Fe1-C2'	155.93(8)
C5'-Fe1-C2'	68.12(8)
C4'-Fe1-C2'	68.16(8)
C3'-Fe1-C2'	40.54(8)
C5-Fe1-C1'	125.05(8)
C1-Fe1-C1'	109.38(8)
C4-Fe1-C1'	160.89(8)
C5'-Fe1-C1'	40.62(8)
C4'-Fe1-C1'	68.30(8)
C3'-Fe1-C1'	68.28(8)
C2'-Fe1-C1'	40.45(8)
C5-Fe1-C2	69.32(7)
C1-Fe1-C2	40.72(7)
C4-Fe1-C2	68.60(7)
C5'-Fe1-C2	159.11(8)
C4'-Fe1-C2	159.21(8)
C3'-Fe1-C2	123.52(8)
C2'-Fe1-C2	108.56(8)
C1'-Fe1-C2	123.45(8)
C5-Fe1-C3	68.72(8)
C1-Fe1-C3	68.20(7)
C4-Fe1-C3	40.58(7)
C5'-Fe1-C3	159.31(8)
C4'-Fe1-C3	122.53(8)
C3'-Fe1-C3	106.47(8)
C2'-Fe1-C3	121.77(8)
C1'-Fe1-C3	157.97(8)
C2-Fe1-C3	40.32(7)
C2-C1-C5	108.09(16)
C2-C1-C17	129.33(17)

Table 5.11 continued

C5-C1-C17	122.57(16)
C2-C1-Fe1	70.55(10)
C5-C1-Fe1	68.58(10)
C17-C1-Fe1	125.41(13)
C3-C2-C1	107.62(16)
C3-C2-Fe1	69.85(10)
C1-C2-Fe1	68.72(10)
C2-C3-C4	108.85(17)
C2-C3-Fe1	69.82(10)
C4-C3-Fe1	69.09(10)
C3-C4-C5	107.91(16)
C3-C4-Fe1	70.33(11)
C5-C4-Fe1	68.55(10)
C4-C5-C1	107.53(16)
C4-C5-C6	129.50(17)
C1-C5-C6	122.38(16)
C4-C5-Fe1	70.41(10)
C1-C5-Fe1	69.80(10)
C6-C5-Fe1	118.30(12)
O1-C6-C5	123.08(17)
O1-C6-C7	121.19(16)
C5-C6-C7	115.72(15)
C8-C7-C16	119.70(17)
C8-C7-C6	118.76(16)
C16-C7-C6	121.53(16)
C7-C8-C9	121.77(17)
C8-C9-C10	122.84(17)
C8-C9-C14	118.43(16)
C10-C9-C14	118.73(17)

C11-C10-C9	120.47(18)
C10-C11-C12	120.59(18)
C13-C12-C11	120.44(18)
C12-C13-C14	120.61(17)
C15-C14-C13	121.98(17)
C15-C14-C9	118.84(16)
C13-C14-C9	119.16(17)
C16-C15-C14	122.06(17)
C15-C16-C7	119.17(16)
C15-C16-C17	118.61(16)
C7-C16-C17	122.21(16)
O2-C17-C1	122.68(16)
O2-C17-C16	122.10(16)
C1-C17-C16	115.18(15)
C2'-C1'-C5'	107.73(17)
C2'-C1'-Fe1	69.73(11)
C5'-C1'-Fe1	69.44(11)
C1'-C2'-C3'	108.28(18)
C1'-C2'-Fe1	69.82(11)
C3'-C2'-Fe1	69.53(11)
C2'-C3'-C4'	107.89(18)
C2'-C3'-Fe1	69.92(11)
C4'-C3'-Fe1	69.69(11)
C5'-C4'-C3'	107.99(17)
C5'-C4'-Fe1	69.70(11)
C3'-C4'-Fe1	69.69(11)
C4'-C5'-C1'	108.12(17)
C4'-C5'-Fe1	69.71(11)
C1'-C5'-Fe1	69.94(10)

Table 5.12. Bond Distances (Å) and Bond Angles [°] for **9a**

Fe1-C3	2.0391(15)
Fe1-C1'	2.0400(15)
Fe1-C2'	2.0404(15)
Fe1-C4	2.0413(14)
Fe1-C3'	2.0443(16)
Fe1-C2	2.0445(15)
Fe1-C5'	2.0460(15)
Fe1-C1	2.0462(14)
Fe1-C5	2.0470(15)
Fe1-C4'	2.0530(16)
C1-C5	1.426(2)
C1-C2	1.427(2)
C1-C13	1.495(2)
C2-C3	1.428(2)
C3-C4	1.429(2)
C4-C5	1.433(2)
C5-C6	1.495(2)
C6-C7	1.520(2)
C7-C8	1.397(2)
C7-C12	1.401(2)
C8-C9	1.392(2)
C9-C10	1.386(2)
C10-C11	1.387(2)
C11-C12	1.396(2)
C12-C13	1.516(2)
C1'-C2'	1.425(2)
C1'-C5'	1.427(2)
C2'-C3'	1.428(2)
C3'-C4'	1.426(2)
C4'-C5'	1.426(2)
C3-Fe1-C1'	158.68(7)
C3-Fe1-C2'	159.56(7)
C1'-Fe1-C2'	40.89(6)
C3-Fe1-C4	40.99(6)
C1'-Fe1-C4	121.70(6)
C2'-Fe1-C4	157.51(7)
C3-Fe1-C3'	123.76(6)
C1'-Fe1-C3'	68.82(7)
C2'-Fe1-C3'	40.92(6)
C4-Fe1-C3'	160.20(6)
C3-Fe1-C2	40.95(6)
C1'-Fe1-C2	158.34(6)

C2'-Fe1-C2	122.44(7)
C4-Fe1-C2	69.00(6)
C3'-Fe1-C2	107.57(7)
C3-Fe1-C5'	123.17(6)
C1'-Fe1-C5'	40.89(6)
C2'-Fe1-C5'	68.81(6)
C4-Fe1-C5'	107.28(6)
C3'-Fe1-C5'	68.74(7)
C2-Fe1-C5'	159.55(6)
C3-Fe1-C1	68.73(6)
C1'-Fe1-C1	121.69(6)
C2'-Fe1-C1	106.23(6)
C4-Fe1-C1	68.80(6)
C3'-Fe1-C1	122.18(6)
C2-Fe1-C1	40.83(6)
C5'-Fe1-C1	158.32(6)
C3-Fe1-C5	68.97(6)
C1'-Fe1-C5	105.88(6)
C2'-Fe1-C5	120.97(6)
C4-Fe1-C5	41.05(6)
C3'-Fe1-C5	157.61(6)
C2-Fe1-C5	68.90(6)
C5'-Fe1-C5	122.33(6)
C1-Fe1-C5	40.77(6)
C3-Fe1-C4'	108.59(6)
C1'-Fe1-C4'	68.59(6)
C2'-Fe1-C4'	68.62(6)
C4-Fe1-C4'	123.75(6)
C3'-Fe1-C4'	40.74(7)
C2-Fe1-C4'	123.49(6)
C5'-Fe1-C4'	40.70(7)
C1-Fe1-C4'	159.01(7)
C5-Fe1-C4'	159.46(6)
C5-C1-C2	108.47(13)
C5-C1-C13	121.16(13)
C2-C1-C13	130.36(14)
C5-C1-Fe1	69.65(8)
C2-C1-Fe1	69.52(8)
C13-C1-Fe1	126.98(11)
C1-C2-C3	107.73(13)
C1-C2-Fe1	69.65(8)
C3-C2-Fe1	69.32(8)

Table 5.12 continued

C2-C3-C4	108.20(13)
C2-C3-Fe1	69.73(8)
C4-C3-Fe1	69.59(8)
C3-C4-C5	107.87(13)
C3-C4-Fe1	69.42(8)
C5-C4-Fe1	69.69(8)
C1-C5-C4	107.73(13)
C1-C5-C6	121.10(13)
C4-C5-C6	131.17(14)
C1-C5-Fe1	69.58(8)
C4-C5-Fe1	69.26(8)
C6-C5-Fe1	127.00(11)
C5-C6-C7	111.83(13)
C8-C7-C12	119.39(14)
C8-C7-C6	119.47(14)
C12-C7-C6	121.13(14)
C9-C8-C7	120.72(15)
C10-C9-C8	119.91(15)
C9-C10-C11	119.64(15)
C10-C11-C12	121.20(15)

C11-C12-C7	119.14(14)
C11-C12-C13	119.67(14)
C7-C12-C13	121.19(14)
C1-C13-C12	111.97(12)
C2'-C1'-C5'	108.09(14)
C2'-C1'-Fe1	69.57(9)
C5'-C1'-Fe1	69.79(9)
C1'-C2'-C3'	107.98(14)
C1'-C2'-Fe1	69.54(9)
C3'-C2'-Fe1	69.69(9)
C4'-C3'-C2'	107.89(14)
C4'-C3'-Fe1	69.96(9)
C2'-C3'-Fe1	69.39(9)
C5'-C4'-C3'	108.15(14)
C5'-C4'-Fe1	69.39(9)
C3'-C4'-Fe1	69.30(9)
C4'-C5'-C1'	107.88(14)
C4'-C5'-Fe1	69.91(9)
C1'-C5'-Fe1	69.33(9)

Table 5.13. Bond Distances (Å) and Bond Angles [°] for **11a**

Fe1-C3	2.031(3)
Fe1-C4	2.033(3)
Fe1-C17	2.038(3)
Fe1-C16	2.041(3)
Fe1-C18	2.041(3)
Fe1-C5	2.043(3)
Fe1-C15	2.050(3)
Fe1-C14	2.053(3)
Fe1-C2	2.054(3)
Fe1-C1	2.079(3)
C1-C2	1.425(4)
C1-C5	1.437(4)
C1-C13	1.479(3)
C2-C3	1.431(4)
C3-C4	1.438(4)
C4-C5	1.430(4)
C5-C6	1.496(4)
C6-C7	1.521(4)
C7-C8	1.393(4)
C7-C12	1.402(4)
C8-C9	1.381(4)
C9-C10	1.391(4)
C10-C11	1.382(4)
C11-C12	1.405(4)
C12-C13	1.494(4)
C13-C13#1	1.350(5)
C14-C15	1.417(4)
C14-C18	1.425(4)
C15-C16	1.417(4)
C16-C17	1.425(4)
C17-C18	1.419(4)
C3-Fe1-C4	41.44(11)
C3-Fe1-C17	119.37(11)
C4-Fe1-C17	103.85(12)
C3-Fe1-C16	105.09(11)
C4-Fe1-C16	120.23(11)
C17-Fe1-C16	40.88(12)
C3-Fe1-C18	155.83(12)
C4-Fe1-C18	120.09(12)
C17-Fe1-C18	40.71(12)
C16-Fe1-C18	68.59(12)
C3-Fe1-C5	69.26(11)

C4-Fe1-C5	41.08(11)
C17-Fe1-C5	121.28(11)
C16-Fe1-C5	157.21(11)
C18-Fe1-C5	107.08(11)
C3-Fe1-C15	122.81(12)
C4-Fe1-C15	157.82(12)
C17-Fe1-C15	68.41(12)
C16-Fe1-C15	40.53(12)
C18-Fe1-C15	68.38(12)
C5-Fe1-C15	160.62(12)
C3-Fe1-C14	160.48(12)
C4-Fe1-C14	157.90(12)
C17-Fe1-C14	68.38(11)
C16-Fe1-C14	68.22(12)
C18-Fe1-C14	40.73(12)
C5-Fe1-C14	124.00(11)
C15-Fe1-C14	40.41(12)
C3-Fe1-C2	41.00(11)
C4-Fe1-C2	69.34(11)
C17-Fe1-C2	156.68(11)
C16-Fe1-C2	122.02(11)
C18-Fe1-C2	161.86(11)
C5-Fe1-C2	68.98(11)
C15-Fe1-C2	109.11(12)
C14-Fe1-C2	125.77(11)
C3-Fe1-C1	68.30(11)
C4-Fe1-C1	68.61(10)
C17-Fe1-C1	159.58(12)
C16-Fe1-C1	159.33(11)
C18-Fe1-C1	125.40(11)
C5-Fe1-C1	40.79(10)
C15-Fe1-C1	125.41(11)
C14-Fe1-C1	111.13(11)
C2-Fe1-C1	40.32(10)
C2-C1-C5	108.3(2)
C2-C1-C13	133.5(2)
C5-C1-C13	118.1(2)
C2-C1-Fe1	68.89(15)
C5-C1-Fe1	68.27(14)
C13-C1-Fe1	128.43(18)
C1-C2-C3	107.8(2)
C1-C2-Fe1	**70**.78(15)

Table 5.13 continued

C3-C2-Fe1	68.62(15)
C2-C3-C4	108.3(2)
C2-C3-Fe1	70.38(15)
C4-C3-Fe1	69.37(15)
C5-C4-C3	107.6(2)
C5-C4-Fe1	69.85(15)
C3-C4-Fe1	69.19(15)
C4-C5-C1	107.9(2)
C4-C5-C6	132.6(2)
C1-C5-C6	119.5(2)
C4-C5-Fe1	69.07(15)
C1-C5-Fe1	70.94(15)
C6-C5-Fe1	126.47(19)
C5-C6-C7	110.0(2)
C8-C7-C12	118.8(3)
C8-C7-C6	121.4(2)
C12-C7-C6	119.7(2)
C9-C8-C7	121.5(3)
C8-C9-C10	119.8(3)
C11-C10-C9	119.7(3)
C10-C11-C12	120.8(3)

C7-C12-C11	119.3(2)
C7-C12-C13	118.6(2)
C11-C12-C13	121.9(2)
C13#1-C13-C1	124.0(3)
C13#1-C13-C12	124.8(3)
C1-C13-C12	111.1(2)
C15-C14-C18	108.0(3)
C15-C14-Fe1	69.66(16)
C18-C14-Fe1	69.16(16)
C16-C15-C14	108.2(3)
C16-C15-Fe1	69.39(16)
C14-C15-Fe1	69.93(16)
C15-C16-C17	108.0(3)
C15-C16-Fe1	70.08(16)
C17-C16-Fe1	69.47(16)
C18-C17-C16	107.9(3)
C18-C17-Fe1	69.74(16)
C16-C17-Fe1	69.64(15)
C17-C18-C14	107.9(3)
C17-C18-Fe1	69.54(16)
C14-C18-Fe1	70.10(15)

Table 5.14. Bond Distances (Å) and Bond Angles [°] for **13a**

Fe1A-C5A	2.0232
Fe1A-C1A	2.031(2)
Fe1A-C14A	2.042(2)
Fe1A-C15A	2.044(2)
Fe1A-C16A	2.047(2)
Fe1A-C4A	2.050(2)
Fe1A-C18A	2.051(2)
Fe1A-C17A	2.054(2)
Fe1A-C2A	2.055(2)
Fe1A-C3A	2.063(2)
O1A-C6A	1.236(2)
O2A-C13A	1.428(2)
C1A-C2A	1.420(3)
C1A-C5A	1.440(3)
C1A-C13A	1.494(3)
C2A-C3A	1.424(3)
C3A-C4A	1.424(3)
C4A-C5A	1.429(3)
C5A-C6A	1.458(3)
C6A-C7A	1.487(3)
C7A-C8A	1.405(3)
C7A-C12A	1.410(3)
C8A-C9A	1.381(3)
C9A-C10A	1.390(3)
C10A-C11A	1.383(3)
C11A-C12A	1.388(3)
C12A-C13A	1.525(3)
C14A-C15A	1.422(3)
C14A-C18A	1.424(3)
C15A-C16A	1.417(3)
C16A-C17A	1.424(3)
C17A-C18A	1.418(3)
Fe1B-C5B	2.0226(19)
Fe1B-C1B	2.036(2)
Fe1B-C18B	2.037(2)
Fe1B-C14B	2.039(2)
Fe1B-C4B	2.039(2)

Fe1B-C16B	2.046(2)
Fe1B-C17B	2.046(2)
Fe1B-C15B	2.049(2)
Fe1B-C3B	2.057(2)
Fe1B-C2B	2.061(2)
O1B-C6B	1.235(2)
O2B-C13B	1.427(2)
C1B-C2B	1.414(3)
C1B-C5B	1.440(3)
C1B-C13B	1.493(3)
C2B-C3B	1.426(3)
C3B-C4B	1.414(3)
C4B-C5B	1.431(3)
C5B-C6B	1.456(3)
C6B-C7B	1.488(3)
C7B-C8B	1.398(3)
C7B-C12B	1.412(3)
C8B-C9B	1.385(3)
C9B-C10B	1.384(3)
C10B-C11B	1.381(3)
C11B-C12B	1.391(3)
C12B-C13B	1.517(3)
C14B-C15B	1.409(3)
C14B-C18B	1.428(3)
C15B-C16B	1.414(3)
C16B-C17B	1.423(3)
C17B-C18B	1.415(3)
C5A-Fe1A-C1A	41.62(8)
C5A-Fe1A-C14A	122.34(9)
C1A-Fe1A-C14A	106.26(9)
C5A-Fe1A-C15A	157.97(9)
C1A-Fe1A-C15A	120.79(9)
C14A-Fe1A-C15A	40.74(9)
C5A-Fe1A-C16A	160.19(9)
C1A-Fe1A-C16A	157.00(9)
C14A-Fe1A-C16A	68.23(9)
C15A-Fe1A-C16A	40.53(9)

Table 5.14 continued

C5A-Fe1A-C4A	41.08(8)
C1A-Fe1A-C4A	69.63(8)
C14A-Fe1A-C4A	158.99(9)
C15A-Fe1A-C4A	159.12(9)
C16A-Fe1A-C4A	123.52(9)
C5A-Fe1A-C18A	107.93(9)
C1A-Fe1A-C18A	123.18(9)
C14A-Fe1A-C18A	40.73(9)
C15A-Fe1A-C18A	68.46(9)
C16A-Fe1A-C18A	68.13(9)
C4A-Fe1A-C18A	123.20(9)
C5A-Fe1A-C17A	123.85(8)
C1A-Fe1A-C17A	160.14(9)
C14A-Fe1A-C17A	68.33(9)
C15A-Fe1A-C17A	68.42(9)
C16A-Fe1A-C17A	40.62(9)
C4A-Fe1A-C17A	108.17(9)
C18A-Fe1A-C17A	40.42(9)
C5A-Fe1A-C2A	68.73(8)
C1A-Fe1A-C2A	40.65(8)
C14A-Fe1A-C2A	122.39(9)
C15A-Fe1A-C2A	106.51(9)
C16A-Fe1A-C2A	122.02(9)
C4A-Fe1A-C2A	68.67(8)
C18A-Fe1A-C2A	159.18(9)
C17A-Fe1A-C2A	158.42(9)
C5A-Fe1A-C3A	68.32(8)
C1A-Fe1A-C3A	68.56(8)
C14A-Fe1A-C3A	158.79(9)
C15A-Fe1A-C3A	122.86(9)
C16A-Fe1A-C3A	108.04(9)
C4A-Fe1A-C3A	40.50(8)
C18A-Fe1A-C3A	159.17(9)
C17A-Fe1A-C3A	123.37(9)
C2A-Fe1A-C3A	40.47(8)
C2A-C1A-C5A	107.20(18)
C2A-C1A-C13A	129.02(18)

C5A-C1A-C13A	123.74(18)
C2A-C1A-Fe1A	70.59(12)
C5A-C1A-Fe1A	68.87(11)
C13A-C1A-Fe1A	127.49(14)
C1A-C2A-C3A	108.35(18)
C1A-C2A-Fe1A	68.76(11)
C3A-C2A-Fe1A	70.05(12)
C4A-C3A-C2A	108.79(19)
C4A-C3A-Fe1A	69.25(12)
C2A-C3A-Fe1A	69.48(12)
C3A-C4A-C5A	107.06(18)
C3A-C4A-Fe1A	70.24(12)
C5A-C4A-Fe1A	68.43(12)
C4A-C5A-C1A	108.59(18)
C4A-C5A-C6A	129.32(19)
C1A-C5A-C6A	121.30(19)
C4A-C5A-Fe1A	70.48(12)
C1A-C5A-Fe1A	69.51(11)
C6A-C5A-Fe1A	117.81(14)
O1A-C6A-C5A	122.5(2)
O1A-C6A-C7A	121.48(19)
C5A-C6A-C7A	116.00(18)
C8A-C7A-C12A	119.0(2)
C8A-C7A-C6A	118.22(19)
C12A-C7A-C6A	122.75(19)
C9A-C8A-C7A	120.8(2)
C8A-C9A-C10A	119.7(2)
C11A-C10A-C9A	120.1(2)
C10A-C11A-C12A	121.1(2)
C11A-C12A-C7A	119.20(19)
C11A-C12A-C13A	118.07(18)
C7A-C12A-C13A	122.61(19)
O2A-C13A-C1A	110.98(17)
O2A-C13A-C12A	110.33(16)
C1A-C13A-C12A	111.91(16)
C15A-C14A-C18A	108.0(2)
C15A-C14A-Fe1A	69.70(12)

Table 5.14 continued

C18A-C14A-Fe1A	69.96(12)
C16A-C15A-C14A	107.8(2)
C16A-C15A-Fe1A	69.85(12)
C14A-C15A-Fe1A	69.56(13)
C15A-C16A-C17A	108.4(2)
C15A-C16A-Fe1A	69.62(12)
C17A-C16A-Fe1A	69.96(12)
C18A-C17A-C16A	107.8(2)
C18A-C17A-Fe1A	69.66(12)
C16A-C17A-Fe1A	69.42(12)
C17A-C18A-C14A	108.1(2)
C17A-C18A-Fe1A	69.92(12)
C14A-C18A-Fe1A	69.31(12)
C5B-Fe1B-C1B	41.56(8)
C5B-Fe1B-C18B	107.36(9)
C1B-Fe1B-C18B	125.38(9)
C5B-Fe1B-C14B	121.54(9)
C1B-Fe1B-C14B	107.96(9)
C18B-Fe1B-C14B	41.01(9)
C5B-Fe1B-C4B	41.24(8)
C1B-Fe1B-C4B	69.54(8)
C18B-Fe1B-C4B	120.44(9)
C14B-Fe1B-C4B	156.76(9)
C5B-Fe1B-C16B	161.11(9)
C1B-Fe1B-C16B	155.88(9)
C18B-Fe1B-C16B	68.24(10)
C14B-Fe1B-C16B	68.04(10)
C4B-Fe1B-C16B	123.79(9)
C5B-Fe1B-C17B	124.12(8)
C1B-Fe1B-C17B	162.13(9)
C18B-Fe1B-C17B	40.56(10)
C14B-Fe1B-C17B	68.52(9)
C4B-Fe1B-C17B	106.40(9)
C16B-Fe1B-C17B	40.70(9)
C5B-Fe1B-C15B	156.89(9)
C1B-Fe1B-C15B	121.10(9)
C18B-Fe1B-C15B	68.36(10)

C14B-Fe1B-C15B	40.32(10)
C4B-Fe1B-C15B	160.85(9)
C16B-Fe1B-C15B	40.40(10)
C17B-Fe1B-C15B	68.34(9)
C5B-Fe1B-C3B	68.29(9)
C1B-Fe1B-C3B	68.32(9)
C18B-Fe1B-C3B	155.58(10)
C14B-Fe1B-C3B	161.86(10)
C4B-Fe1B-C3B	40.37(9)
C16B-Fe1B-C3B	107.66(10)
C17B-Fe1B-C3B	120.55(10)
C15B-Fe1B-C3B	125.11(10)
C5B-Fe1B-C2B	68.62(8)
C1B-Fe1B-C2B	40.36(8)
C18B-Fe1B-C2B	162.40(10)
C14B-Fe1B-C2B	125.29(10)
C4B-Fe1B-C2B	68.62(9)
C16B-Fe1B-C2B	121.13(9)
C17B-Fe1B-C2B	155.88(9)
C15B-Fe1B-C2B	108.20(10)
C3B-Fe1B-C2B	40.51(9)
C2B-C1B-C5B	107.54(19)
C2B-C1B-C13B	129.04(19)
C5B-C1B-C13B	123.35(18)
C2B-C1B-Fe1B	70.77(12)
C5B-C1B-Fe1B	68.71(11)
C13B-C1B-Fe1B	128.11(15)
C1B-C2B-C3B	108.07(19)
C1B-C2B-Fe1B	68.87(12)
C3B-C2B-Fe1B	69.60(12)
C4B-C3B-C2B	108.98(19)
C4B-C3B-Fe1B	69.13(12)
C2B-C3B-Fe1B	69.88(13)
C3B-C4B-C5B	107.27(19)
C3B-C4B-Fe1B	70.50(13)
C5B-C4B-Fe1B	68.75(11)
C4B-C5B-C1B	108.14(18)

Table 5.14 continued

C4B-C5B-C6B	129.24(18)
C1B-C5B-C6B	122.03(18)
C4B-C5B-Fe1B	70.01(11)
C1B-C5B-Fe1B	69.73(11)
C6B-C5B-Fe1B	118.97(14)
O1B-C6B-C5B	123.18(19)
O1B-C6B-C7B	120.99(19)
C5B-C6B-C7B	115.83(17)
C8B-C7B-C12B	119.75(19)
C8B-C7B-C6B	118.01(18)
C12B-C7B-C6B	122.20(18)
C9B-C8B-C7B	120.3(2)
C10B-C9B-C8B	119.9(2)
C11B-C10B-C9B	120.3(2)
C10B-C11B-C12B	121.1(2)
C11B-C12B-C7B	118.57(19)
C11B-C12B-C13B	117.95(18)
C7B-C12B-C13B	123.43(18)

O2B-C13B-C1B	111.43(18)
O2B-C13B-C12B	110.53(17)
C1B-C13B-C12B	112.33(16)
C15B-C14B-C18B	108.0(2)
C15B-C14B-Fe1B	70.23(13)
C18B-C14B-Fe1B	69.42(13)
C14B-C15B-C16B	108.1(2)
C14B-C15B-Fe1B	69.45(13)
C16B-C15B-Fe1B	69.68(13)
C15B-C16B-C17B	108.3(2)
C15B-C16B-Fe1B	69.92(13)
C17B-C16B-Fe1B	69.66(12)
C18B-C17B-C16B	107.6(2)
C18B-C17B-Fe1B	69.37(12)
C16B-C17B-Fe1B	69.64(12)
C17B-C18B-C14B	108.0(2)
C17B-C18B-Fe1B	70.07(13)
C14B-C18B-Fe1B	69.57(13)

Table 5.15. Bond Distances (Å) and bond angles [°] for **14a**

Fe1-C5	2.0335(15)
Fe1-C1	2.0370(13)
Fe1-C2	2.0477(14)
Fe1-C21	2.0489(14)
Fe1-C25	2.0500(14)
Fe1-C4	2.0527(15)
Fe1-C22	2.0575(18)
Fe1-C23	2.0586(14)
Fe1-C3	2.0597(15)
Fe1-C24	2.0604(15)
O1-C13	1.2301(17)
C1-C2	1.435(2)
C1-C5	1.4390(18)
C1-C13	1.457(2)
C2-C3	1.420(2)
C3-C4	1.432(2)
C4-C5	1.420(2)
C5-C6	1.503(2)
C6-C7	1.511(2)
C6-C14	1.5518(18)
C7-C8	1.399(2)
C7-C12	1.412(2)
C8-C9	1.384(2)
C9-C10	1.393(2)
C10-C11	1.383(2)
C11-C12	1.394(2)
C12-C13	1.489(2)
C14-C15	1.510(2)
C15-C16	1.390(2)
C15-C20	1.399(2)
C16-C17	1.384(2)
C17-C18	1.391(2)
C18-C19	1.383(3)
C19-C20	1.389(3)
C21-C25	1.419(2)
C21-C22	1.422(2)
C22-C23	1.425(2)
C23-C24	1.422(3)
C24-C25	1.429(2)
C5-Fe1-C1	41.41(5)
C5-Fe1-C2	69.62(5)
C1-Fe1-C2	41.13(6)

C5-Fe1-C21	104.24(6)
C1-Fe1-C21	125.80(6)
C2-Fe1-C21	165.41(7)
C5-Fe1-C25	124.93(5)
C1-Fe1-C25	163.48(6)
C2-Fe1-C25	153.69(6)
C21-Fe1-C25	40.51(6)
C5-Fe1-C4	40.68(7)
C1-Fe1-C4	68.55(6)
C2-Fe1-C4	68.68(6)
C21-Fe1-C4	115.85(6)
C25-Fe1-C4	106.92(6)
C5-Fe1-C22	115.74(7)
C1-Fe1-C22	107.19(7)
C2-Fe1-C22	129.08(6)
C21-Fe1-C22	40.52(6)
C25-Fe1-C22	68.13(7)
C4-Fe1-C22	149.39(7)
C5-Fe1-C23	151.21(7)
C1-Fe1-C23	119.29(6)
C2-Fe1-C23	110.46(6)
C21-Fe1-C23	68.19(6)
C25-Fe1-C23	68.20(6)
C4-Fe1-C23	167.93(7)
C22-Fe1-C23	40.52(7)
C5-Fe1-C3	68.87(6)
C1-Fe1-C3	68.39(6)
C2-Fe1-C3	40.46(6)
C21-Fe1-C3	151.09(6)
C25-Fe1-C3	119.27(6)
C4-Fe1-C3	40.75(6)
C22-Fe1-C3	168.05(6)
C23-Fe1-C3	130.93(6)
C5-Fe1-C24	164.39(6)
C1-Fe1-C24	153.99(6)
C2-Fe1-C24	120.87(6)
C21-Fe1-C24	68.23(6)
C25-Fe1-C24	40.68(6)
C4-Fe1-C24	128.88(7)
C22-Fe1-C24	68.07(8)
C23-Fe1-C24	40.41(7)
C3-Fe1-C24	110.69(7)

Table 5.15 continued

C2-C1-C5	108.32(14)
C2-C1-C13	128.78(13)
C5-C1-C13	122.50(14)
C2-C1-Fe1	69.83(8)
C5-C1-Fe1	69.17(8)
C13-C1-Fe1	121.06(10)
C3-C2-C1	107.50(12)
C3-C2-Fe1	70.23(8)
C1-C2-Fe1	69.04(8)
C2-C3-C4	108.37(13)
C2-C3-Fe1	69.31(9)
C4-C3-Fe1	69.36(8)
C5-C4-C3	108.48(13)
C5-C4-Fe1	68.94(9)
C3-C4-Fe1	69.89(8)
C4-C5-C1	107.31(13)
C4-C5-C6	130.66(13)
C1-C5-C6	122.03(15)
C4-C5-Fe1	70.39(8)
C1-C5-Fe1	69.43(8)
C6-C5-Fe1	126.03(10)
C5-C6-C7	112.00(12)
C5-C6-C14	110.20(12)
C7-C6-C14	109.73(11)
C8-C7-C12	117.76(15)
C8-C7-C6	118.80(13)
C12-C7-C6	123.41(13)
C9-C8-C7	121.38(14)
C8-C9-C10	120.42(15)
C11-C10-C9	119.19(16)
C10-C11-C12	120.88(14)

C11-C12-C7	120.35(14)
C11-C12-C13	118.22(13)
C7-C12-C13	121.38(14)
O1-C13-C1	122.33(14)
O1-C13-C12	121.83(15)
C1-C13-C12	115.83(12)
C15-C14-C6	114.25(11)
C16-C15-C20	118.03(15)
C16-C15-C14	121.22(13)
C20-C15-C14	120.72(15)
C17-C16-C15	121.41(15)
C16-C17-C18	120.02(16)
C19-C18-C17	119.38(17)
C18-C19-C20	120.43(15)
C19-C20-C15	120.73(16)
C25-C21-C22	108.16(14)
C25-C21-Fe1	69.79(8)
C22-C21-Fe1	70.07(9)
C21-C22-C23	107.95(15)
C21-C22-Fe1	69.41(9)
C23-C22-Fe1	69.78(10)
C24-C23-C22	108.07(14)
C24-C23-Fe1	69.87(9)
C22-C23-Fe1	69.70(9)
C23-C24-C25	107.78(15)
C23-C24-Fe1	69.73(8)
C25-C24-Fe1	69.27(8)
C21-C25-C24	108.04(14)
C21-C25-Fe1	69.70(8)
C24-C25-Fe1	70.05(8)

Table 5.16. Bond Distances (Å) and bond angles [°] for **18a**

Fe1A-C2A'	2.027(2)
Fe1A-C3A'	2.027(3)
Fe1A-C3A	2.030(2)
Fe1A-C1A	2.0321(19)
Fe1A-C2A	2.035(2)
Fe1A-C1A'	2.041(2)
Fe1A-C5A'	2.046(2)
Fe1A-C4A'	2.046(2)
Fe1A-C5A	2.0536(19)
Fe1A-C4A	2.055(2)
Si1A-O3A	1.6408(14)
Si1A-C26A	1.855(2)
Si1A-C25A	1.860(2)
Si1A-C24A	1.865(2)
N1A-C16A	1.397(3)
N1A-C17A	1.400(3)
N1A-C18A	1.437(3)
O1A-C16A	1.208(2)
O2A-C17A	1.205(2)
O3A-C13A	1.392(2)
C1A-C5A	1.421(3)
C1A-C2A	1.425(3)
C1A-C13A	1.512(3)
C1A'-C5A'	1.408(4)
C1A'-C2A'	1.469(4)
C2A-C3A	1.432(3)
C2A'-C3A'	1.389(5)
C3A-C4A	1.429(3)
C3A'-C4A'	1.355(4)
C4A-C5A	1.422(3)
C4A'-C5A'	1.367(4)
C5A-C6A	1.505(3)
C6A-C7A	1.511(3)
C6A-C15A	1.567(3)
C7A-C8A	1.386(3)
C7A-C12A	1.399(3)
C8A-C9A	1.394(3)
C9A-C10A	1.383(3)
C10A-C11A	1.397(3)
C11A-C12A	1.384(3)
C12A-C13A	1.520(3)
C13A-C14A	1.585(3)

C14A-C17A	1.517(3)
C14A-C15A	1.544(3)
C15A-C16A	1.508(3)
C18A-C23A	1.382(3)
C18A-C19A	1.384(3)
C19A-C20A	1.388(3)
C20A-C21A	1.382(3)
C21A-C22A	1.382(3)
C22A-C23A	1.387(3)
Fe1B-C3B	2.025(2)
Fe1B-C2B'	2.029(2)
Fe1B-C3B'	2.029(2)
Fe1B-C2B	2.029(2)
Fe1B-C1B	2.0335(19)
Fe1B-C1B'	2.041(2)
Fe1B-C4B	2.052(2)
Fe1B-C4B'	2.054(2)
Fe1B-C5B'	2.059(2)
Fe1B-C5B	2.0611(19)
Si1B-O3B	1.6539(15)
Si1B-C26B	1.854(2)
Si1B-C24B	1.855(2)
Si1B-C25B	1.864(2)
N1B-C16B	1.393(3)
N1B-C17B	1.407(3)
N1B-C18B	1.435(3)
O1B-C16B	1.208(2)
O2B-C17B	1.207(3)
O3B-C13B	1.392(2)
C1B-C2B	1.425(3)
C1B-C5B	1.430(3)
C1B-C13B	1.512(3)
C1B'-C5B'	1.400(4)
C1B'-C2B'	1.422(4)
C2B-C3B	1.442(3)
C2B'-C3B'	1.416(3)
C3B-C4B	1.434(3)
C3B'-C4B'	1.414(3)
C4B-C5B	1.421(3)
C4B'-C5B'	1.413(4)
C5B-C6B	1.508(3)
C6B-C7B	1.509(3)

Table 5.16 continued

C6B-C15B	1.566(3)
C7B-C8B	1.388(3)
C7B-C12B	1.398(3)
C8B-C9B	1.390(3)
C9B-C10B	1.382(3)
C10B-C11B	1.392(3)
C11B-C12B	1.385(3)
C12B-C13B	1.522(3)
C13B-C14B	1.584(3)
C14B-C17B	1.510(3)
C14B-C15B	1.540(3)
C15B-C16B	1.513(3)
C18B-C19B	1.384(3)
C18B-C23B	1.387(3)
C19B-C20B	1.388(3)
C20B-C21B	1.387(4)
C21B-C22B	1.383(4)
C22B-C23B	1.387(3)
C2A'-Fe1A-C3A'	40.06(13)
C2A'-Fe1A-C3A	107.55(9)
C3A'-Fe1A-C3A	113.28(10)
C2A'-Fe1A-C1A	165.97(13)
C3A'-Fe1A-C1A	127.68(11)
C3A-Fe1A-C1A	68.85(8)
C2A'-Fe1A-C2A	127.50(11)
C3A'-Fe1A-C2A	104.12(10)
C3A-Fe1A-C2A	41.27(8)
C1A-Fe1A-C2A	41.01(8)
C2A'-Fe1A-C1A'	42.34(13)
C3A'-Fe1A-C1A'	68.58(12)
C3A-Fe1A-C1A'	133.77(11)
C1A-Fe1A-C1A'	149.19(11)
C2A-Fe1A-C1A'	169.76(11)
C2A'-Fe1A-C5A'	67.96(10)
C3A'-Fe1A-C5A'	66.06(11)
C3A-Fe1A-C5A'	174.09(9)
C1A-Fe1A-C5A'	116.46(8)
C2A-Fe1A-C5A'	144.48(9)
C1A'-Fe1A-C5A'	40.32(11)
C2A'-Fe1A-C4A'	66.86(12)
C3A'-Fe1A-C4A'	38.85(12)
C3A-Fe1A-C4A'	143.73(10)
C1A-Fe1A-C4A'	107.51(10)

C2A-Fe1A-C4A'	111.74(10)
C1A'-Fe1A-C4A'	67.49(11)
C5A'-Fe1A-C4A'	39.04(10)
C2A'-Fe1A-C5A	151.99(12)
C3A'-Fe1A-C5A	167.87(11)
C3A-Fe1A-C5A	68.47(8)
C1A-Fe1A-C5A	40.69(8)
C2A-Fe1A-C5A	68.84(8)
C1A'-Fe1A-C5A	119.61(10)
C5A'-Fe1A-C5A	113.51(9)
C4A'-Fe1A-C5A	133.17(10)
C2A'-Fe1A-C4A	118.12(10)
C3A'-Fe1A-C4A	147.77(11)
C3A-Fe1A-C4A	40.95(8)
C1A-Fe1A-C4A	68.68(8)
C2A-Fe1A-C4A	69.26(8)
C1A'-Fe1A-C4A	112.77(9)
C5A'-Fe1A-C4A	137.03(9)
C4A'-Fe1A-C4A	173.37(10)
C5A-Fe1A-C4A	40.51(8)
O3A-Si1A-C26A	106.10(9)
O3A-Si1A-C25A	113.93(9)
C26A-Si1A-C25A	109.89(10)
O3A-Si1A-C24A	106.46(9)
C26A-Si1A-C24A	111.10(10)
C25A-Si1A-C24A	109.32(11)
C16A-N1A-C17A	112.86(16)
C16A-N1A-C18A	122.99(17)
C17A-N1A-C18A	124.15(16)
C13A-O3A-Si1A	142.54(13)
C5A-C1A-C2A	108.64(17)
C5A-C1A-C13A	114.11(17)
C2A-C1A-C13A	136.79(18)
C5A-C1A-Fe1A	70.47(11)
C2A-C1A-Fe1A	69.62(11)
C13A-C1A-Fe1A	130.93(13)
C5A'-C1A'-C2A'	104.6(2)
C5A'-C1A'-Fe1A	70.04(13)
C2A'-C1A'-Fe1A	68.33(14)
C1A-C2A-C3A	106.98(18)
C1A-C2A-Fe1A	69.38(11)
C3A-C2A-Fe1A	69.17(11)
C3A'-C2A'-C1A'	106.6(2)

Table 5.16 continued

C3A'-C2A'-Fe1A	69.98(15)
C1A'-C2A'-Fe1A	69.33(14)
C4A-C3A-C2A	108.63(18)
C4A-C3A-Fe1A	70.45(11)
C2A-C3A-Fe1A	69.56(11)
C4A'-C3A'-C2A'	109.8(3)
C4A'-C3A'-Fe1A	71.33(15)
C2A'-C3A'-Fe1A	69.96(15)
C5A-C4A-C3A	107.37(17)
C5A-C4A-Fe1A	69.71(11)
C3A-C4A-Fe1A	68.60(11)
C3A'-C4A'-C5A'	109.3(3)
C3A'-C4A'-Fe1A	69.83(15)
C5A'-C4A'-Fe1A	70.48(14)
C1A-C5A-C4A	108.36(17)
C1A-C5A-C6A	114.12(17)
C4A-C5A-C6A	136.84(18)
C1A-C5A-Fe1A	68.84(11)
C4A-C5A-Fe1A	69.78(11)
C6A-C5A-Fe1A	133.13(14)
C4A'-C5A'-C1A'	109.7(2)
C4A'-C5A'-Fe1A	70.49(14)
C1A'-C5A'-Fe1A	69.64(14)
C5A-C6A-C7A	108.62(16)
C5A-C6A-C15A	104.38(16)
C7A-C6A-C15A	104.10(15)
C8A-C7A-C12A	120.01(19)
C8A-C7A-C6A	125.76(18)
C12A-C7A-C6A	114.09(17)
C7A-C8A-C9A	119.4(2)
C10A-C9A-C8A	120.4(2)
C9A-C10A-C11A	120.4(2)
C12A-C11A-C10A	119.13(19)
C11A-C12A-C7A	120.57(18)
C11A-C12A-C13A	124.52(18)
C7A-C12A-C13A	114.84(17)
O3A-C13A-C1A	116.20(16)
O3A-C13A-C12A	109.56(15)
C1A-C13A-C12A	108.57(16)
O3A-C13A-C14A	114.14(15)
C1A-C13A-C14A	102.56(15)
C12A-C13A-C14A	105.04(15)
C17A-C14A-C15A	104.58(16)

C17A-C14A-C13A	113.02(16)
C15A-C14A-C13A	109.76(15)
C16A-C15A-C14A	105.41(16)
C16A-C15A-C6A	109.65(16)
C14A-C15A-C6A	111.45(15)
O1A-C16A-N1A	124.92(19)
O1A-C16A-C15A	126.63(18)
N1A-C16A-C15A	108.44(16)
O2A-C17A-N1A	124.29(19)
O2A-C17A-C14A	127.32(19)
N1A-C17A-C14A	108.39(16)
C23A-C18A-C19A	121.3(2)
C23A-C18A-N1A	118.81(18)
C19A-C18A-N1A	119.92(19)
C18A-C19A-C20A	118.9(2)
C21A-C20A-C19A	120.3(2)
C22A-C21A-C20A	120.3(2)
C21A-C22A-C23A	119.9(2)
C18A-C23A-C22A	119.3(2)
C3B-Fe1B-C2B'	113.75(10)
C3B-Fe1B-C3B'	104.02(9)
C2B'-Fe1B-C3B'	40.86(10)
C3B-Fe1B-C2B	41.66(8)
C2B'-Fe1B-C2B	102.56(9)
C3B'-Fe1B-C2B	122.93(9)
C3B-Fe1B-C1B	69.15(8)
C2B'-Fe1B-C1B	125.11(9)
C3B'-Fe1B-C1B	161.91(9)
C2B-Fe1B-C1B	41.06(8)
C3B-Fe1B-C1B'	149.12(11)
C2B'-Fe1B-C1B'	40.90(10)
C3B'-Fe1B-C1B'	68.43(9)
C2B-Fe1B-C1B'	115.83(10)
C1B-Fe1B-C1B'	108.37(9)
C3B-Fe1B-C4B	41.16(8)
C2B'-Fe1B-C4B	149.56(9)
C3B'-Fe1B-C4B	117.51(9)
C2B-Fe1B-C4B	69.83(8)
C1B-Fe1B-C4B	69.04(8)
C1B'-Fe1B-C4B	168.88(10)
C3B-Fe1B-C4B'	126.64(9)
C2B'-Fe1B-C4B'	68.31(10)
C3B'-Fe1B-C4B'	40.53(9)

Table 5.16 continued

C2B-Fe1B-C4B'	162.38(9)
C1B-Fe1B-C4B'	156.38(9)
C1B'-Fe1B-C4B'	67.79(10)
C4B-Fe1B-C4B'	109.96(9)
C3B-Fe1B-C5B'	166.29(10)
C2B'-Fe1B-C5B'	67.97(10)
C3B'-Fe1B-C5B'	67.89(9)
C2B-Fe1B-C5B'	152.01(10)
C1B-Fe1B-C5B'	121.88(9)
C1B'-Fe1B-C5B'	39.94(11)
C4B-Fe1B-C5B'	131.48(10)
C4B'-Fe1B-C5B'	40.18(10)
C3B-Fe1B-C5B	68.44(8)
C2B'-Fe1B-C5B	165.34(9)
C3B'-Fe1B-C5B	153.80(9)
C2B-Fe1B-C5B	68.98(8)
C1B-Fe1B-C5B	40.86(8)
C1B'-Fe1B-C5B	130.82(9)
C4B-Fe1B-C5B	40.41(8)
C4B'-Fe1B-C5B	123.00(9)
C5B'-Fe1B-C5B	113.62(9)
O3B-Si1B-C26B	106.32(10)
O3B-Si1B-C24B	106.01(10)
C26B-Si1B-C24B	111.03(11)
O3B-Si1B-C25B	113.18(9)
C26B-Si1B-C25B	108.73(12)
C24B-Si1B-C25B	111.46(11)
C16B-N1B-C17B	112.28(16)
C16B-N1B-C18B	123.79(17)
C17B-N1B-C18B	123.91(17)
C13B-O3B-Si1B	137.76(13)
C2B-C1B-C5B	108.49(17)
C2B-C1B-C13B	137.35(18)
C5B-C1B-C13B	113.90(17)
C2B-C1B-Fe1B	69.30(11)
C5B-C1B-Fe1B	70.61(11)
C13B-C1B-Fe1B	129.55(14)
C5B'-C1B'-C2B'	108.1(2)
C5B'-C1B'-Fe1B	70.72(13)
C2B'-C1B'-Fe1B	69.08(13)
C1B-C2B-C3B	106.93(18)
C1B-C2B-Fe1B	69.64(11)
C3B-C2B-Fe1B	69.02(11)

C3B'-C2B'-C1B'	107.5(2)
C3B'-C2B'-Fe1B	69.58(12)
C1B'-C2B'-Fe1B	70.03(13)
C4B-C3B-C2B	108.67(18)
C4B-C3B-Fe1B	70.44(11)
C2B-C3B-Fe1B	69.32(11)
C4B'-C3B'-C2B'	108.1(2)
C4B'-C3B'-Fe1B	70.70(12)
C2B'-C3B'-Fe1B	69.56(12)
C5B-C4B-C3B	107.24(17)
C5B-C4B-Fe1B	70.13(11)
C3B-C4B-Fe1B	68.40(11)
C5B'-C4B'-C3B'	107.7(2)
C5B'-C4B'-Fe1B	70.09(13)
C3B'-C4B'-Fe1B	68.77(12)
C4B-C5B-C1B	108.66(17)
C4B-C5B-C6B	137.17(18)
C1B-C5B-C6B	113.79(17)
C4B-C5B-Fe1B	69.46(11)
C1B-C5B-Fe1B	68.53(11)
C6B-C5B-Fe1B	132.11(14)
C1B'-C5B'-C4B'	108.6(2)
C1B'-C5B'-Fe1B	69.34(13)
C4B'-C5B'-Fe1B	69.73(13)
C5B-C6B-C7B	108.04(16)
C5B-C6B-C15B	104.72(15)
C7B-C6B-C15B	105.20(15)
C8B-C7B-C12B	120.51(18)
C8B-C7B-C6B	125.70(18)
C12B-C7B-C6B	113.76(17)
C7B-C8B-C9B	119.2(2)
C10B-C9B-C8B	120.2(2)
C9B-C10B-C11B	120.9(2)
C12B-C11B-C10B	119.10(19)
C11B-C12B-C7B	120.01(18)
C11B-C12B-C13B	124.93(18)
C7B-C12B-C13B	115.06(17)
O3B-C13B-C1B	116.64(16)
O3B-C13B-C12B	110.16(15)
C1B-C13B-C12B	107.42(16)
O3B-C13B-C14B	113.08(15)
C1B-C13B-C14B	103.47(15)
C12B-C13B-C14B	105.25(15)

Table 5.16 continued

C17B-C14B-C15B	105.12(16)
C17B-C14B-C13B	112.27(16)
C15B-C14B-C13B	110.19(15)
C16B-C15B-C14B	104.95(15)
C16B-C15B-C6B	109.19(16)
C14B-C15B-C6B	111.13(15)
O1B-C16B-N1B	124.78(19)
O1B-C16B-C15B	126.36(18)
N1B-C16B-C15B	108.83(16)
O2B-C17B-N1B	124.08(19)

O2B-C17B-C14B	127.53(19)
N1B-C17B-C14B	108.39(16)
C19B-C18B-C23B	120.9(2)
C19B-C18B-N1B	120.36(19)
C23B-C18B-N1B	118.72(19)
C18B-C19B-C20B	119.0(2)
C21B-C20B-C19B	120.5(2)
C22B-C21B-C20B	120.0(2)
C21B-C22B-C23B	120.0(2)
C18B-C23B-C22B	119.6(2)

Table 5.17. Bond Distances (Å) and bond angles [°] for **19a**

Fe1-C1"	1.892(13)
Fe1-C2"	1.89(3)
Fe1-C5"	1.946(10)
Fe1-C3	2.036(2)
Fe1-C3'	2.046(14)
Fe1-C2	2.049(2)
Fe1-C4	2.053(2)
Fe1-C5	2.056(2)
Fe1-C1	2.059(2)
Fe1-C4"	2.062(11)
Fe1-C4'	2.068(5)
Fe1-C3"	2.07(3)
Si1-O1	1.6452(16)
Si1-C20	1.854(3)
Si1-C22	1.856(3)
Si1-C21	1.861(3)
O1-C9	1.389(2)
O2-C16	1.204(3)
O3-C16	1.331(3)
O3-C17	1.451(3)
O4-C18	1.203(3)
O5-C18	1.334(3)
O5-C19	1.447(3)
C1-C2	1.423(3)
C1-C5	1.426(3)
C1-C9	1.527(3)
C2-C3	1.425(3)
C3-C4	1.426(3)
C4-C5	1.417(3)
C5-C6	1.513(3)
C1'-C5'	1.416(6)
C1'-C2'	1.417(7)
C2'-C3'	1.417(7)
C3'-C4'	1.430(7)
C4'-C5'	1.414(7)
C1"-C5"	1.400(11)
C1"-C2"	1.425(13)
C2"-C3"	1.418(13)
C3"-C4"	1.423(13)
C4"-C5"	1.409(11)
C6-C11	1.527(3)
C6-C7	1.528(3)

C7-C8	1.338(3)
C7-C16	1.485(3)
C8-C18	1.484(3)
C8-C9	1.556(3)
C9-C10	1.536(3)
C10-C15	1.378(3)
C10-C11	1.389(3)
C11-C12	1.383(3)
C12-C13	1.395(4)
C13-C14	1.374(4)
C14-C15	1.407(3)
C1"-Fe1-C2"	44.2(5)
C1"-Fe1-C5"	42.8(4)
C2"-Fe1-C5"	72.0(8)
C1"-Fe1-C3	164.6(4)
C2"-Fe1-C3	121.0(6)
C5"-Fe1-C3	146.9(4)
C1"-Fe1-C3'	62.9(5)
C2"-Fe1-C3'	38.5(9)
C5"-Fe1-C3'	60.4(4)
C3-Fe1-C3'	109.1(3)
C1"-Fe1-C2	131.5(4)
C2"-Fe1-C2	108.6(7)
C5"-Fe1-C2	170.9(4)
C3-Fe1-C2	40.82(9)
C3'-Fe1-C2	125.9(2)
C1"-Fe1-C4	154.4(4)
C2"-Fe1-C4	155.2(6)
C5"-Fe1-C4	114.6(3)
C3-Fe1-C4	40.81(10)
C3'-Fe1-C4	121.8(3)
C2-Fe1-C4	68.90(9)
C1"-Fe1-C5	125.1(4)
C2"-Fe1-C5	163.5(6)
C5"-Fe1-C5	108.5(3)
C3-Fe1-C5	67.90(9)
C3'-Fe1-C5	156.3(3)
C2-Fe1-C5	68.26(9)
C4-Fe1-C5	40.36(9)
C1"-Fe1-C1	115.1(4)
C2"-Fe1-C1	126.6(7)
C5"-Fe1-C1	131.7(4)

Table 5.17 continued

C3-Fe1-C1	68.13(8)
C3'-Fe1-C1	162.2(2)
C2-Fe1-C1	40.53(8)
C4-Fe1-C1	68.44(8)
C5-Fe1-C1	40.56(8)
C1"-Fe1-C4"	71.0(4)
C2"-Fe1-C4"	70.1(7)
C5"-Fe1-C4"	41.0(4)
C3-Fe1-C4"	110.8(3)
C3'-Fe1-C4"	35.8(5)
C2-Fe1-C4"	148.0(3)
C4-Fe1-C4"	98.6(3)
C5-Fe1-C4"	121.6(3)
C1-Fe1-C4"	162.0(3)
C1"-Fe1-C4'	55.0(4)
C2"-Fe1-C4'	65.5(8)
C5"-Fe1-C4'	23.9(3)
C3-Fe1-C4'	128.5(2)
C3'-Fe1-C4'	40.7(2)
C2-Fe1-C4'	164.7(2)
C4-Fe1-C4'	110.06(18)
C5-Fe1-C4'	121.55(17)
C1-Fe1-C4'	154.5(2)
C4"-Fe1-C4'	17.9(3)
C1"-Fe1-C3"	71.5(7)
C2"-Fe1-C3"	41.6(6)
C5"-Fe1-C3"	69.3(6)
C3-Fe1-C3"	99.7(6)
C3'-Fe1-C3"	9.6(8)
C2-Fe1-C3"	117.4(6)
C4-Fe1-C3"	116.1(6)
C5-Fe1-C3"	154.7(6)
C1-Fe1-C3"	156.5(5)
C4"-Fe1-C3"	40.2(5)
C4'-Fe1-C3"	48.4(6)
O1-Si1-C20	102.18(12)
O1-Si1-C22	109.51(11)
C20-Si1-C22	111.13(17)
O1-Si1-C21	113.30(11)
C20-Si1-C21	108.89(17)
C22-Si1-C21	111.48(12)
C9-O1-Si1	139.98(13)
C16-O3-C17	115.40(19)

C18-O5-C19	114.56(18)
C2-C1-C5	107.88(18)
C2-C1-C9	139.14(19)
C5-C1-C9	112.24(18)
C2-C1-Fe1	69.38(12)
C5-C1-Fe1	69.59(11)
C9-C1-Fe1	132.55(14)
C1-C2-C3	107.32(19)
C1-C2-Fe1	70.10(12)
C3-C2-Fe1	69.08(13)
C2-C3-C4	109.01(19)
C2-C3-Fe1	70.11(13)
C4-C3-Fe1	70.24(13)
C5-C4-C3	106.96(19)
C5-C4-Fe1	69.92(12)
C3-C4-Fe1	68.94(13)
C4-C5-C1	108.84(19)
C4-C5-C6	136.4(2)
C1-C5-C6	114.13(18)
C4-C5-Fe1	69.72(12)
C1-C5-Fe1	69.85(12)
C6-C5-Fe1	132.61(15)
C5'-C1'-C2'	107.9(5)
C5'-C1'-Fe1	69.3(2)
C2'-C1'-Fe1	70.2(6)
C1'-C2'-C3'	108.3(6)
C1'-C2'-Fe1	71.2(5)
C3'-C2'-Fe1	66.8(7)
C2'-C3'-C4'	107.6(5)
C2'-C3'-Fe1	73.7(7)
C4'-C3'-Fe1	70.5(5)
C5'-C4'-C3'	107.7(5)
C5'-C4'-Fe1	72.1(3)
C3'-C4'-Fe1	68.8(6)
C4'-C5'-C1'	108.4(4)
C4'-C5'-Fe1	68.4(3)
C1'-C5'-Fe1	71.9(3)
C5"-C1"-C2"	106.1(9)
C5"-C1"-Fe1	70.7(6)
C2"-C1"-Fe1	67.9(13)
C3"-C2"-C1"	109.4(11)
C3"-C2"-Fe1	76.0(15)
C1"-C2"-Fe1	67.9(10)

Table 5.17 continued

C2"-C3"-C4"	106.5(10)
C2"-C3"-Fe1	62.4(14)
C4"-C3"-Fe1	69.5(10)
C5"-C4"-C3"	107.8(9)
C5"-C4"-Fe1	65.1(6)
C3"-C4"-Fe1	70.3(12)
C1"-C5"-C4"	109.9(8)
C1"-C5"-Fe1	66.6(6)
C4"-C5"-Fe1	73.9(7)
C5-C6-C11	106.23(16)
C5-C6-C7	104.25(17)
C11-C6-C7	104.51(16)
C8-C7-C16	125.8(2)
C8-C7-C6	114.43(18)
C16-C7-C6	119.66(18)
C7-C8-C18	128.35(19)
C7-C8-C9	114.79(18)
C18-C8-C9	116.84(17)
O1-C9-C1	119.73(17)
O1-C9-C10	111.76(16)

C1-C9-C10	106.35(16)
O1-C9-C8	110.32(16)
C1-C9-C8	103.72(15)
C10-C9-C8	103.50(16)
C15-C10-C11	121.0(2)
C15-C10-C9	125.2(2)
C11-C10-C9	113.82(18)
C12-C11-C10	120.4(2)
C12-C11-C6	125.9(2)
C10-C11-C6	113.69(18)
C11-C12-C13	119.1(2)
C14-C13-C12	120.5(2)
C13-C14-C15	120.6(2)
C10-C15-C14	118.4(2)
O2-C16-O3	124.3(2)
O2-C16-C7	123.3(2)
O3-C16-C7	112.34(19)
O4-C18-O5	124.5(2)
O4-C18-C8	123.26(19)
O5-C18-C8	112.13(17)

Table 5.18. Bond Distances (Å) and Bond Angles [°] for **20a**

Fe1-C5'	2.025(2)
Fe1-C1'	2.028(2)
Fe1-C2'	2.031(2)
Fe1-C3	2.031(2)
Fe1-C4	2.034(2)
Fe1-C4'	2.037(3)
Fe1-C2	2.040(2)
Fe1-C3'	2.041(3)
Fe1-C5	2.045(2)
Fe1-C1	2.0485(19)
Fe2-C17	2.027(2)
Fe2-C15'	2.033(3)
Fe2-C19'	2.034(3)
Fe2-C16	2.034(2)
Fe2-C18'	2.038(2)
Fe2-C18	2.040(2)
Fe2-C17'	2.041(3)
Fe2-C15	2.043(2)
Fe2-C16'	2.043(3)
Fe2-C19	2.050(2)
C1-C5	1.422(3)
C1-C2	1.429(3)
C1-C13	1.494(3)
C2-C3	1.426(3)
C3-C4	1.413(3)
C4-C5	1.422(3)
C5-C6	1.496(3)
C1'-C2'	1.401(4)
C1'-C5'	1.413(4)
C2'-C3'	1.391(4)
C3'-C4'	1.398(5)
C4'-C5'	1.402(4)
C6-C7	1.514(3)
C7-C8	1.394(3)
C7-C12	1.403(3)
C8-C9	1.385(3)
C9-C10	1.393(3)
C10-C11	1.379(3)
C11-C12	1.395(3)
C12-C13	1.526(3)
C13-C14	1.579(3)
C14-C15	1.504(3)

C14-C26	1.522(3)
C15-C19	1.416(3)
C15-C16	1.427(3)
C16-C17	1.424(3)
C17-C18	1.417(3)
C18-C19	1.431(3)
C19-C20	1.497(3)
C15'-C16'	1.396(5)
C15'-C19'	1.409(4)
C16'-C17'	1.391(4)
C17'-C18'	1.391(5)
C18'-C19'	1.408(4)
C20-C21	1.516(3)
C21-C22	1.396(3)
C21-C26	1.402(3)
C22-C23	1.389(3)
C23-C24	1.380(3)
C24-C25	1.391(3)
C25-C26	1.391(3)
C5'-Fe1-C1'	40.81(10)
C5'-Fe1-C2'	67.92(11)
C1'-Fe1-C2'	40.38(11)
C5'-Fe1-C3	157.83(11)
C1'-Fe1-C3	159.95(10)
C2'-Fe1-C3	124.03(10)
C5'-Fe1-C4	121.91(10)
C1'-Fe1-C4	158.00(11)
C2'-Fe1-C4	159.83(11)
C3-Fe1-C4	40.69(9)
C5'-Fe1-C4'	40.38(11)
C1'-Fe1-C4'	68.17(10)
C2'-Fe1-C4'	67.59(12)
C3-Fe1-C4'	122.45(10)
C4-Fe1-C4'	107.47(10)
C5'-Fe1-C2	159.59(11)
C1'-Fe1-C2	123.34(9)
C2'-Fe1-C2	108.39(10)
C3-Fe1-C2	41.00(8)
C4-Fe1-C2	68.66(8)
C4'-Fe1-C2	158.67(12)
C5'-Fe1-C3'	67.58(13)
C1'-Fe1-C3'	67.67(11)

Table 5.18 continued

C2'-Fe1-C3'	39.95(12)
C3-Fe1-C3'	108.43(11)
C4-Fe1-C3'	123.78(11)
C4'-Fe1-C3'	40.09(13)
C2-Fe1-C3'	123.40(13)
C5'-Fe1-C5	106.84(10)
C1'-Fe1-C5	122.02(9)
C2'-Fe1-C5	158.46(11)
C3-Fe1-C5	68.79(8)
C4-Fe1-C5	40.82(8)
C4'-Fe1-C5	122.86(12)
C2-Fe1-C5	68.81(8)
C3'-Fe1-C5	159.35(12)
C5'-Fe1-C1	122.95(10)
C1'-Fe1-C1	107.48(9)
C2'-Fe1-C1	123.29(11)
C3-Fe1-C1	68.75(8)
C4-Fe1-C1	68.43(8)
C4'-Fe1-C1	159.02(13)
C2-Fe1-C1	40.91(8)
C3'-Fe1-C1	159.15(13)
C5-Fe1-C1	40.64(8)
C17-Fe2-C15'	164.46(13)
C17-Fe2-C19'	153.53(12)
C15'-Fe2-C19'	40.54(12)
C17-Fe2-C16	41.05(9)
C15'-Fe2-C16	126.51(12)
C19'-Fe2-C16	164.31(11)
C17-Fe2-C18'	119.67(10)
C15'-Fe2-C18'	67.59(11)
C19'-Fe2-C18'	40.46(12)
C16-Fe2-C18'	153.36(12)
C17-Fe2-C18	40.77(9)
C15'-Fe2-C18	153.50(13)
C19'-Fe2-C18	119.38(12)
C16-Fe2-C18	68.84(9)
C18'-Fe2-C18	108.88(11)
C17-Fe2-C17'	108.69(11)
C15'-Fe2-C17'	67.21(12)
C19'-Fe2-C17'	67.63(13)
C16-Fe2-C17'	119.33(12)
C18'-Fe2-C17'	39.89(13)
C18-Fe2-C17'	128.03(12)

C17-Fe2-C15	68.93(9)
C15'-Fe2-C15	107.49(9)
C19'-Fe2-C15	126.67(10)
C16-Fe2-C15	40.98(8)
C18'-Fe2-C15	164.96(12)
C18-Fe2-C15	68.75(9)
C17'-Fe2-C15	153.02(13)
C17-Fe2-C16'	127.32(13)
C15'-Fe2-C16'	40.04(13)
C19'-Fe2-C16'	67.75(13)
C16-Fe2-C16'	107.79(12)
C18'-Fe2-C16'	67.18(13)
C18-Fe2-C16'	165.07(13)
C17'-Fe2-C16'	39.83(13)
C15-Fe2-C16'	118.93(11)
C17-Fe2-C19	68.70(9)
C15'-Fe2-C19	119.07(11)
C19'-Fe2-C19	108.05(10)
C16-Fe2-C19	68.58(9)
C18'-Fe2-C19	128.15(12)
C18-Fe2-C19	40.97(8)
C17'-Fe2-C19	165.72(12)
C15-Fe2-C19	40.48(8)
C16'-Fe2-C19	152.78(12)
C5-C1-C2	108.15(18)
C5-C1-C13	122.88(18)
C2-C1-C13	128.97(19)
C5-C1-Fe1	69.55(11)
C2-C1-Fe1	69.23(11)
C13-C1-Fe1	127.16(14)
C3-C2-C1	107.60(19)
C3-C2-Fe1	69.17(12)
C1-C2-Fe1	69.86(12)
C4-C3-C2	108.03(19)
C4-C3-Fe1	69.74(12)
C2-C3-Fe1	69.82(12)
C3-C4-C5	108.60(18)
C3-C4-Fe1	69.58(12)
C5-C4-Fe1	70.03(12)
C1-C5-C4	107.62(18)
C1-C5-C6	121.18(18)
C4-C5-C6	131.16(19)
C1-C5-Fe1	69.81(11)

Table 5.18 continued

C4-C5-Fe1	69.15(12)
C6-C5-Fe1	127.79(15)
C2'-C1'-C5'	107.2(2)
C2'-C1'-Fe1	69.92(14)
C5'-C1'-Fe1	69.48(14)
C3'-C2'-C1'	108.5(3)
C3'-C2'-Fe1	70.41(15)
C1'-C2'-Fe1	69.69(14)
C2'-C3'-C4'	108.5(3)
C2'-C3'-Fe1	69.64(15)
C4'-C3'-Fe1	69.78(16)
C3'-C4'-C5'	107.8(3)
C3'-C4'-Fe1	70.13(15)
C5'-C4'-Fe1	69.37(14)
C4'-C5'-C1'	108.0(3)
C4'-C5'-Fe1	70.25(15)
C1'-C5'-Fe1	69.72(14)
C5-C6-C7	112.54(17)
C8-C7-C12	119.0(2)
C8-C7-C6	119.11(19)
C12-C7-C6	121.84(19)
C9-C8-C7	121.5(2)
C8-C9-C10	119.5(2)
C11-C10-C9	119.3(2)
C10-C11-C12	121.9(2)
C11-C12-C7	118.77(19)
C11-C12-C13	119.31(18)
C7-C12-C13	121.86(18)
C1-C13-C12	111.60(17)
C1-C13-C14	112.07(16)
C12-C13-C14	109.17(16)
C15-C14-C26	110.93(17)
C15-C14-C13	111.69(16)
C26-C14-C13	109.70(16)
C19-C15-C16	108.06(19)
C19-C15-C14	122.66(18)
C16-C15-C14	129.3(2)
C19-C15-Fe2	70.04(12)
C16-C15-Fe2	69.18(12)
C14-C15-Fe2	126.07(14)
C17-C16-C15	107.8(2)

C17-C16-Fe2	69.21(13)
C15-C16-Fe2	69.84(12)
C18-C17-C16	108.3(2)
C18-C17-Fe2	70.08(13)
C16-C17-Fe2	69.75(12)
C17-C18-C19	107.8(2)
C17-C18-Fe2	69.15(13)
C19-C18-Fe2	69.92(12)
C15-C19-C18	108.08(19)
C15-C19-C20	121.69(19)
C18-C19-C20	130.2(2)
C15-C19-Fe2	69.48(11)
C18-C19-Fe2	69.11(12)
C20-C19-Fe2	126.94(15)
C16'-C15'-C19'	108.3(3)
C16'-C15'-Fe2	70.37(17)
C19'-C15'-Fe2	69.75(15)
C17'-C16'-C15'	108.0(3)
C17'-C16'-Fe2	69.98(17)
C15'-C16'-Fe2	69.60(16)
C16'-C17'-C18'	108.5(3)
C16'-C17'-Fe2	70.19(16)
C18'-C17'-Fe2	69.96(16)
C17'-C18'-C19'	108.2(3)
C17'-C18'-Fe2	70.16(15)
C19'-C18'-Fe2	69.62(15)
C18'-C19'-C15'	107.0(3)
C18'-C19'-Fe2	69.93(15)
C15'-C19'-Fe2	69.71(16)
C19-C20-C21	111.77(18)
C22-C21-C26	119.1(2)
C22-C21-C20	119.0(2)
C26-C21-C20	121.85(19)
C23-C22-C21	121.3(2)
C24-C23-C22	119.5(2)
C23-C24-C25	119.8(2)
C24-C25-C26	121.4(2)
C25-C26-C21	118.89(19)
C25-C26-C14	118.78(19)
C21-C26-C14	122.25(19)

5.4. Summary

In order to investigate the chemistry of ferrocene-fused quinones and their reduction derivatives, Friedel-Crafts acylation of ferrocene with phthalic anhydride was our first entry. Since we were not able to improve the yield of the reaction more than 15% in several attempts, we opened the ring of the phthalic anhydride using methanol and the resultant *o*-carbomethoxybenzoic acid was treated with thionyl chloride to give *o*-carbomethoxy benzoyl chloride. When o-carbomethoxybenzoyl chloride was treated with ferrocene in the presence of $AlCl_3$, using a mixture of dry ethyl ether and CS_2,[157] we isolated 2-carbomethoxybenzoylferrocene **1a** in 77% yield. In order to homologate the benzene ring of our final target, we followed the similar procedure starting from naphthalene-1,2-dicarboxyic anhydride and isolated **1b** (89%) in Friedel-Crafts step.

We were unable to obtain the clean products from the Clemmensen reduction of the keto-acid or keto-ester in the presence of HCl. Our reactions stop in the form of secondary alcohol (**3'a**, **4'a**) on milder reaction conditions or dimerized lactones (**5a** and **5b**) on harsher conditions. In order to obtain the clean product, we saponified the keto-esters (**1a** and **1b**) under basic media[87] to give keto acids (**2a,** 97%; **2b,** 97%). The keto group was reduced to methylene by using zinc, activated with the copper sulfate, in the presence of aqueous sodium hydroxide[170] to give the desired acids (**3a**, 89%; **3b**, 58%).

The carboxylic acids **3a** and **3b** were used to give Fc-anthrone **6a** (96%) and Fc-anthracenone **6b** (96%) in the presence of trifluoroacetic anhydride. The mono-ketone complexes underwent a facile oxidation in the presence of MnO_2 at room temperature to give quinones **7a** (88%) and **7b** (98%). The quinone planes of both complexes were coplanar with Cp in their single-crystal X-ray structures.

The Fc-anthrone **6a** was reduced to ferrocenylcarbinol **8a** (86%) by $LiAlH_4$. Our attempts to dehydrate the carbinol using mild dehydrating agents such as anhydrous $CuSO_4$[55] and stronger agents like acetic anhydride were unsuccessful. The reduction of Fc-anthrone **6a** under acidic Clemmensen conditions[195] gave methylene complex **9a** (71%) but we were unable to dehydrogenate the complex in the presence of DDQ. In another attempt, we applied Meerwein-Ponndorf-Verley condition[143] to reduce **6a** to benz[*f*]indenyl complex of iron **10a**, but we ended up with an isomeric mixture of McMurry-type reductively coupled product **11a** (71%).

The acidic behavior of the proton at α-position of ferrocenyl group of **6a** was studied by deuterium exchange. Our attempt to isolate its O-silyl ether in the presence of LiHMDS and TMSCl gave a deep-green complex **16a** but it readily decomposed to dimerized Fc-anthrone **17a** (42%), Fc-hydroxyanthrone **7a** (22%), Fc-quinone **13a** and starting material **6a** during aerobic workup. The existence of **16a** as a conjugated trimethylsilyl enol ether by using DMAD or N-phenylmaleimide as a trap to give Diels-Alder cycloaddition products. Similarly, the C-benzylation of the Fc-anthrone was performed under the literature

procedure[174] to give monobenzyl- (**14a**) and dibenzyl (**15a**) anthrone complexes in ca. 1**:**1 ratio.

The ferrocenylcarbinol **8a** was solvolyzed by following Cais[132] procedure to give α-ferrocenylcarbenium tetrafluoroborate salt **20a** (60%). The salt dimerized in the presence of air, giving paramagnetic dimer **21a**. The freshly prepared salt was found to be highly nucleophilic at its cationic center. On treatment with the piperidine, it immediately formed an adduct **23a** along with the isomeric mixtures of dimer **20a**. While we reduced the nucleophilicity of base by switching to triethylamine, we isolated two stereoisomers of **20a** (65%). We suggest that the benz[*f*]indenyl complex of iron **10a** acquires diradical character at α-position due to the presence of iron *d*-orbitals and undergoes facile dimerization.

References

(1) Anthony, J. E. *Angew. Chem. Int. Ed.* **2008**, *47*, 452.
(2) Mas-Torrent, M.; Rovira, C. *Chem. Soc. Rev.* **2008**, *37*, 827.
(3) Hains, A. W.; Liang, Z.; Woodhouse, M. A.; Gregg, B. A. *Chem. Rev.* **2010**, *110*, 6689.
(4) Farinola, G. M.; Ragni, R. *Chem. Soc. Rev.* **2011**, *40*, 3467.
(5) Allard, S.; Forster, M.; Souharce, B.; Thiem, H.; Scherf, U. *Angew. Chem. Int. Ed.* **2008**, *47*, 4070.
(6) Heywang, G.; Jonas, F. *Adv. Mater.* **1992**, *4*, 116.
(7) McCullough, R. D. *Adv. Mater.* **1998**, *10*, 93.
(8) Liang, Z.; Zhao, W.; Wang, S.; Tang, Q.; Lam, S.-C.; Miao, Q. *Org. Lett.* **2008**, *10*, 2007.
(9) Ono, K.; Totani, H.; Hiei, T.; Yoshino, A.; Saito, K.; Eguchi, K.; Tomura, M.; Nishida, J.-i.; Yamashita, Y. *Tetrahedron* **2007**, *63*, 9699.
(10) Brown, A. *J. Appl. Phys.* **1996**, *79*, 2136.
(11) Herwig, P. T.; Müllen, K. *Adv. Mater.* **1999**, *11*, 480.
(12) Afzali, A.; Dimitrakopoulos, C. D.; Breen, T. L. *J. Am. Chem. Soc.* **2002**, *124*, 8812.
(13) Weidkamp, K. P.; Afzali, A.; Tromp, R. M.; Hamers, R. J. *J. Am. Chem. Soc.* **2004**, *126*, 12740.
(14) Meng, H.; Bendikov, M.; Mitchell, G.; Helgeson, R.; Wudl, F.; Bao, Z.; Siegrist, T.; Kloc, C.; Chen, C. H. *Adv. Mater.* **2003**, *15*, 1090.
(15) Anthony, J. E.; Eaton, D. L.; Parkin, S. R. *Org. Lett.* **2002**, *4*, 15.
(16) Payne, M. M.; Parkin, S. R.; Anthony, J. E. *J. Am. Chem. Soc.* **2005**, *127*, 8028.
(17) Purushothaman, B.; Bruzek, M.; Parkin, S. R.; Miller, A.-F.; Anthony, J. E. *Angew. Chem. Int. Ed.* **2011**, *50*, 7013.
(18) Würthner, F.; Schmidt, R. *ChemPhysChem* **2006**, *7*, 793.
(19) Laquindanum, J. G.; Katz, H. E.; Lovinger, A. J. *J. Am. Chem. Soc.* **1998**, *120*, 664.
(20) Payne, M. M.; Odom, S. A.; Parkin, S. R.; Anthony, J. E. *Org. Lett.* **2004**, *6*, 3325.
(21) Li, Z.; Lim, Y.-F.; Kim, J. B.; Parkin, S. R.; Loo, Y.-L.; Malliaras, G. G.; Anthony, J. E. *Chem. Commun.* **2011**, *47*, 7617.
(22) Tylleman, B.; Vande Velde, C. M. L.; Balandier, J.-Y.; Stas, S.; Sergeyev, S.; Geerts, Y. H. *Org. Lett.* **2011**, *13*, 5208.
(23) Jurchescu, O. D. *Appl. Phys. Lett.* **2008**, *92*, 132103.
(24) Klein, A.; Lavastre, O.; Fiedler, J. *Organometallics* **2005**, *25*, 635.
(25) Fox, M. A.; Farmer, J. D.; Roberts, R. L.; Humphrey, M. G.; Low, P. J. *Organometallics* **2009**, *28*, 5266.
(26) Fox, M. A.; Roberts, R. L.; Baines, T. E.; Le Guennic, B.; Halet, J.-F.; Hartl, F.; Yufit, D. S.; Albesa-Jové, D.; Howard, J. A. K.; Low, P. J. *J. Am. Chem. Soc.* **2008**, *130*, 3566.
(27) Packheiser, R.; Ecorchard, P.; Rüffer, T.; Lohan, M.; Bräuer, B. r.; Justaud, F. d. r.; Lapinte, C.; Lang, H. *Organometallics* **2008**, *27*, 3444.
(28) Lohan, M.; Ecorchard, P.; Rüffer, T.; Justaud, F. d. r.; Lapinte, C.; Lang, H. *Organometallics* **2009**, *28*, 1878.
(29) Kowalski, K.; Winter, R. F. *J. Organomet. Chem.* **2009**, *694*, 1041.
(30) Santi, S.; Orian, L.; Durante, C.; Bencze, E. Z.; Bisello, A.; Donoli, A.; Ceccon, A.; Benetollo, F.; Crociani, L. *Chemistry – A European Journal* **2007**, *13*, 7933.

(31) Williams, K. A.; Boydston, A. J.; Bielawski, C. W. *Chem. Soc. Rev.* **2007**, *36*, 729.
(32) G. Alt, H.; Samuel, E. *Chem. Soc. Rev.* **1998**, *27*, 323.
(33) Kirillov, E.; Saillard, J.-Y.; Carpentier, J.-F. *Coord. Chem. Rev.* **2005**, *249*, 1221.
(34) King, R. B.; Efraty, A.; Douglas, W. M. *J. Organomet. Chem.* **1973**, *56*, 345.
(35) Decken, A.; MacKay, A. J.; Brown, M. J.; Bottomley, F. *Organometallics* **2002**, *21*, 2006.
(36) Samuel, E.; Setton, R. *J. Organomet. Chem.* **1965**, *4*, 156.
(37) Kowala, C.; Wailes, P. C.; Weigold, H.; Wunderlich, J. A. *J. Chem. Soc., Chem. Commun.* **1974**, 993.
(38) Gassman, P. G.; Winter, C. H. *J. Am. Chem. Soc.* **1988**, *110*, 6130.
(39) Bazinet, P.; Tupper, K. A.; Tilley, T. D. *Organometallics* **2006**, *25*, 4286.
(40) Price, C. J.; Zeits, P. D.; Reibenspies, J. H.; Miller, S. A. *Organometallics* **2008**, *27*, 3722.
(41) Borovkov, I. A.; Fukin, G. K.; Trifonov, A. A. *Russ. Chem. Bull.* **2008**, *57*, 541.
(42) Johnson, J. W.; Treichel, P. M. *J. Am. Chem. Soc.* **1977**, *99*, 1427.
(43) Moss, J.; Thomas, J.; Ashley, A.; Cowley, A. R.; O'Hare, D. *Organometallics* **2006**, *25*, 4279.
(44) Peifer, B.; Bruce Welch, M.; Alt, H. G. *J. Organomet. Chem.* **1997**, *544*, 115.
(45) Patsidis, K.; Alt, H. G.; Milius, W.; Palackal, S. J. *J. Organomet. Chem.* **1996**, *509*, 63.
(46) Schertl, P.; Alt, H. G. *J. Organomet. Chem.* **1997**, *545*, 553.
(47) Miller, S. A.; Bercaw, J. E. *Organometallics* **2004**, *23*, 1777.
(48) Pammer, F.; Sun, Y.; May, C.; Wolmershäuser, G.; Kelm, H.; Krüger, H.-J.; Thiel, W. R. *Angew. Chem. Int. Ed.* **2007**, *46*, 1270.
(49) Schröder, K.; Haase, D.; Saak, W.; Beckhaus, R.; Kretschmer, W. P.; Lützen, A. *Organometallics* **2008**, *27*, 1859.
(50) Spaleck, W.; Kueber, F.; Winter, A.; Rohrmann, J.; Bachmann, B.; Antberg, M.; Dolle, V.; Paulus, E. F. *Organometallics* **2002**, *13*, 954.
(51) Foster, P.; Chien, J. C. W.; Rausch, M. D. *Organometallics* **1996**, *15*, 2404.
(52) Kim, D. H.; Lee, J. A.; Lee, B. Y.; Chung, Y. K. *J. Organomet. Chem.* **2005**, *690*, 1822.
(53) Pauson, P. L.; Wilkinson, G. *J. Am. Chem. Soc.* **1954**, *76*, 2024.
(54) Zhao, X.; Luo, X.; Li, B.; Song, H.; Xu, S.; Wang, B. *Eur. Polym. J.* **2008**, *44*, 3264.
(55) Tartar, A.; Cuingnet, E. *C. R. Hebd. Seances Acad. Sci., Ser. C* **1974**, *279*, 1057.
(56) Toganoh, M.; Sato, A.; Furuta, H. *Angew. Chem. Int. Ed.* **2011**, *50*, 2752.
(57) Selegue, J. P.; Swarat, K. A. *J. Am. Chem. Soc.* **1993**, *115*, 6448.
(58) Snyder, C. A.; Tice, N. C.; Sriramula, P. G.; Neathery, J. L.; Mobley, J. K.; Phillips, C. L.; Preston, A. Z.; Strain, J. M.; Vanover, E. S.; Starling, M. P.; Sahi, N. V. *Synth. Commun.* **2011**, *41*, 1357.
(59) Wallace, C. E.; Selegue, J. P.; Carrillo, A. *Organometallics* **1998**, *17*, 3390.
(60) Snyder, C. A.; Tice, N. C.; Maddox, J. B.; Emberton, E. D.; Vanover, E. S.; Hinson, D. F.; Jackson, D. C. *J. Organomet. Chem.* **2011**, *696*, 2220.
(61) Snyder, C. A.; Selegue, J. P.; Tice, N. C.; Wallace, C. E.; Blankenbuehler, M. T.; Parkin, S.; Allen, K. D. E.; Beck, R. T. *J. Am. Chem. Soc.* **2005**, *127*, 15010.
(62) Tice, N. C., University of Kentucky, 2005.
(63) Wilkinson, G.; Rosenblum, M.; Whiting, M. C.; Woodward, R. B. *J. Am. Chem. Soc.* **1952**, *74*, 2125.
(64) Sortais, J.-B.; Voss, T.; Kehr, G.; Frohlich, R.; Erker, G. *Chem. Commun.* **2009**, 7417.

(65) Wang, H. J. H.; Jaquinod, L.; Nurco, D. J.; Vicente, M. G. H.; Smith, K. M. *Chem. Commun.* **2001**.
(66) Wang, H. J. H.; Jaquinod, L.; Olmstead, M. M.; Vicente, M. G. H.; Kadish, K. M.; Ou, Z.; Smith, K. M. *Inorg. Chem.* **2007**, *46*, 2898.
(67) Jiao, L.; Courtney, B. H.; Fronczek, F. R.; Smith, K. M. *Tetrahedron Lett.* **2006**, *47*, 501.
(68) Enk, B.; Kopacka, H.; Wurst, K.; Mueller, T.; Bildstein, B. *Organometallics* **2009**, *28*, 5575.
(69) Bonini, B. F.; Fochi, M.; Comes-Franchini, M.; Ricci, A.; Thijs, L.; Zwanenburg, B. *Tetrahedron: Asymmetry* **2003**, *14*, 3321.
(70) Ryabov, A. N.; Gribkov, D. V.; Izmer, V. V.; Voskoboynikov, A. Z. *Organometallics* **2002**, *21*, 2842.
(71) Taylor, C. J.; Motevalli, M.; Richards, C. J. *Organometallics* **2006**, *25*, 2899.
(72) Herrmann, R.; Ugi, I. *Angew. Chem. Int. Ed.* **1982**, *94*, 798.
(73) Bolton, E. S.; Pauson, P. L.; Sandhu, M. A.; Watts, W. E. *J. Chem. Soc. C* **1969**, 2260.
(74) Berkessel, A.; Reichau, S.; Von, D. H. A.; Leconte, N.; Neudorfl, J.-M. *Organometallics* **2011**, *30*, 3880.
(75) Benkeser, R. A.; Fitzgerald, W. P.; Melzer, M. S. *J. Org. Chem.* **1961**, *26*, 2569.
(76) Richards, J. H.; Curphey, T. J. *Chem. Ind. (London)* **1956**, 1456.
(77) Roling, P. V.; Rausch, M. D. *J. Org. Chem.* **1974**, *39*, 1420.
(78) Pokharel, U. R.; Selegue, J. P.; Parkin, S. *Organometallics* **2011**, *30*, 3254.
(79) Busetto, L.; Cassani, M. C.; Zanotti, V.; Albano, V. G.; Sabatino, P. *Organometallics* **2000**, *20*, 282.
(80) Wallace, C. E., Kentucky, 1998.
(81) Linn, W. J.; Sharkey, W. H. *J. Am. Chem. Soc.* **1957**, *79*, 4970.
(82) Angelici, R. J. *Inorganic Synthesis*, 1990; Vol. 28.
(83) Fagan, P. J.; Ward, M. D.; Calabrese, J. C. *J. Am. Chem. Soc.* **1989**, *111*, 1698.
(84) Otwinowski, Z.; Minor, W. In *Methods Enzymol.*; Charles W. Carter, Jr., Ed.; Academic Press: 1997; Vol. 276, p 307.
(85) Sheldrick, G. M. *Acta Crystallogr A* **2008**, *64*, 112.
(86) Blankenbuehler, M. T., University of Kentucky, 1999.
(87) Khurana, J. M.; Chauhan, S.; Bansal, G. *Monatsh. Chem.* **2004**, *135*, 83.
(88) Theodorou, V.; Skobridis, K.; Tzakos, A. G.; Ragoussis, V. *Tetrahedron Lett.* **2007**, *48*, 8230.
(89) Reeves, P. C. *Organic Synthesis* **1988**, *6*, 625.
(90) Davies, D. G.; Derenberg, M.; Hodge, P. *J. Chem. Soc. C: Organic* **1971**, 455.
(91) Wang, Y.-W.; Peng, Y. *Acta Crystallographica Section E* **2008**, *64*, o160.
(92) Hua, D. H.; Lou, K.; Havens, J.; Perchellet, E. M.; Wang, Y.; Perchellet, J.-P.; Iwamoto, T. *Tetrahedron* **2004**, *60*, 10155.
(93) Du, C.; Guo, Y.; Liu, Y.; Qiu, W.; Zhang, H.; Gao, X.; Liu, Y.; Qi, T.; Lu, K.; Yu, G. *Chem. Mater.* **2008**, *20*, 4188.
(94) Bruckner, R. *Advanced Organic Chemistry Reaction Mechanism*; Harcount Academic Press, 2002.
(95) Calhorda, M. J.; Romão, C. C.; Veiros, L. F. *Chemistry – A European Journal* **2002**, *8*, 868.
(96) Zhang, Q. T.; Tour, J. M. *J. Am. Chem. Soc.* **1997**, *119*, 5065.
(97) Ramana, D. V.; Eswara, Y. T.; Ranga, R. K. *Indian J. Heterocycl. Chem.* **2002**, *12*, 103.
(98) Ando, W.; Furuhata, T.; Tsumaki, H.; Sekiguchi, A. *Chem. Lett.* **1982**, *11*, 885.
(99) Zanin, I. E.; Antipin, M. Y.; Struchkov, Y. T. *Kristallografiya* **1991**, *36*, 420.

(100) Fitzpatrick, P. J.; Le Page, Y.; Sedman, J.; Butler, I. S. *Inorg. Chem.* **1981**, *20*, 2852.
(101) Bates, R. B.; Cutler, R. S. *Acta Crystallographica Section B* **1977**, *33*, 893.
(102) Matzat, E. *Acta Crystallographica Section B* **1972**, *28*, 415.
(103) Bresciani Pahor, N.; Calligaris, M. *Acta Crystallographica Section B* **1975**, *31*, 2685.
(104) Moriarty, R. M.; Ku, Y.; Gill, U. S. *J. Chem. Soc., Chem. Commun.* **1987**, 1493.
(105) Moriarty, R. M.; Ku, Y.; Gill, U. S. *Organometallics* **1988**, *7*, 660.
(106) Moriarty, R. M.; Guo, L.; Ku, Y.; Gilardi, R. *J. Chem. Soc., Chem. Commun.* **1990**, 1765.
(107) Kamikawa, K.; Norimura, K.; Furusyo, M.; Uno, T.; Sato, Y.; Konoo, A.; Bringmann, G.; Uemura, M. *Organometallics* **2003**, *22*, 1038.
(108) Pigge, F. C.; Dhanya, R.; Hoefgen, E. R. *Angew. Chem., Int. Ed.* **2007**, *46*, 2887.
(109) Choi, M.-G.; Ho, T. C.; Angelici, R. J. *Organometallics* **2008**, *27*, 1098.
(110) Pearson, A. J.; Heo, J.-N. *Org. Lett.* **2000**, *2*, 2987.
(111) Vecchi, P. A.; Ellern, A.; Angelici, R. J. *J. Am. Chem. Soc.* **2003**, *125*, 2064.
(112) Leong, W. L. J.; Garland, M. V.; Yoong Goh, L.; Kee Leong, W. *Inorg. Chim. Acta* **2009**, *362*, 2089.
(113) Streu, C.; Carroll, P. J.; Kohli, R. K.; Meggers, E. *J. Organomet. Chem.* **2008**, *693*, 551.
(114) Doppiu, A.; Englert, U.; Salzer, A. *Inorg. Chim. Acta* **2003**, *350*, 435.
(115) Zhang, X.; Prosenc, Marc H.; Meyer-Friedrichsen, T.; Heck, J. *Eur. J. Inorg. Chem.* **2003**, *2003*, 313.
(116) Blankenbuehler, M. T.; Selegue, J. P. *J. Organomet. Chem.* **2002**, *642*, 268.
(117) Bennett, M. A.; Smith, A. K. *J. Chem. Soc., Dalton Trans.* **1974**, 233.
(118) Little, W. F.; Koestler, R. C. *J. Org. Chem.* **1961**, *26*, 3245.
(119) Eaton, D. L.; Selegue, J. P.; Anthony, J. E.; Patrick, B. O. *Heterocycles* **2002**, *57*, 2373
(120) Snyder, C. A.; Selegue, J. P.; Dosunmu, E.; Tice, N. C.; Parkin, S. *J. Org. Chem.* **2003**, *68*, 7455.
(121) Lloyd, D.; Preston, N. W. *J. Chem. Soc. C: Organic* **1969**, 2464.
(122) Cokoja, M.; Gemel, C.; Steinke, T.; Schroder, F.; Fischer, R. A. *Dalton Transactions* **2005**, 44.
(123) Chen, Z.; Swager, T. M. *Org. Lett.* **2007**, *9*, 997.
(124) Khoumeri, O.; Montana, M.; Terme, T.; Vanelle, P. *Tetrahedron* **2008**, *64*, 11237.
(125) Ishizumi, K.; Ohashi, N.; Tanno, N. *J. Org. Chem.* **1987**, *52*, 4477.
(126) Rausch, M. D. *Can. J. Chem.* **1963**, *41*, 1289.
(127) Oatis, J. E.; Walle, T.; Daniell, H. B.; Gaffney, T. E.; Knapp, D. R. *J. Med. Chem.* **1985**, *28*, 822.
(128) Chen, Z.; Amara, J. P.; Thomas, S. W.; Swager, T. M. *Macromolecules* **2006**, *39*, 3202.
(129) Zhao, C.-m.; Xu, L.; Wang, H. *Huaxue Yanjiu* **2007**, *18*, 13.
(130) Sato, M.; Suzuki, M.; Okoshi, M.; Kurusina, M.; M., W. *J. Organomet. Chem.* **2002**, *648*, 72.
(131) Winter, C. H.; Han, Y. H.; Heeg, M. J. *Organometallics* **1992**, *11*, 3169.
(132) Cais, M.; Modiano, A.; Raveh, A. *J. Am. Chem. Soc.* **1965**, *87*, 5607.
(133) Cais, M.; Eisenstadt, A. *J. Org. Chem.* **1965**, *30*, 1148.
(134) Diaz, A. F.; Mueller-Westerhoff, U. T.; Nazzal, A.; Tanner, M. *J. Organomet. Chem.* **1982**, *236*, C45.
(135) Shamsipur, M.; Siroueinejad, A.; Hemmateenejad, B.; Abbaspour, A.; Sharghi, H.; Alizadeh, K.; Arshadi, S. *J. Electroanal. Chem.* **2007**, *600*, 345.

(136) Kang, J., Meissner, R. S., de Mendeoza, J., Rebek Jr., J. *Bull. Korean Chem. Soc.* **2000**, 221.
(137) Anthony, J. E.; Gierschner, J.; Landis, C. A.; Parkin, S. R.; Sherman, J. B.; Bakus, R. C. *Chem. Commun.* **2007**, 4746
(138) Jiang, J.; Kaafarani, B. R.; Neckers, D. C. *J. Org. Chem.* **2006**, *71*, 2155.
(139) Payne, M. M.; Delcamp, J. H.; Parkin, S. R.; Anthony, J. E. *Org. Lett.* **2004**, *6*, 1609.
(140) Vets, N.; Smet, M.; Dehaen, W. *Tetrahedron Lett.* **2004**, *45*, 7287.
(141) Palayangoda, S. S.; Mondal, R.; Shah, B. K.; Neckers, D. C. *J. Org. Chem.* **2007**, *72*, 6584.
(142) Mondal, R.; Adhikari, R. M.; Shah, B. K.; Neckers, D. C. *Org. Lett.* **2007**, *9*, 2505.
(143) Reichwagen, J.; Hopf, H.; Desvergne, J.-P.; Del Guerzo, A.; Bouas-Laurent, H. *Synthesis* **2005**, *2005*, 3505.
(144) Bastin, S.; Agbossou-Niedercorn, F.; Brocard, J.; Pélinski, L. *Tetrahedron: Asymmetry* **2001**, *12*, 2399.
(145) Malfait, S.; Pélinski, L.; Maciejewski, L.; Brocard, J. *Synlett* **1997**, *1997*, 830.
(146) Picart-Goetgheluck, S.; Delacroix, O.; Maciejewski, L.; Brocard, J. *Synthesis* **2000**, *2000*, 1421.
(147) Herberhold, M.; Biersack, M. *J. Organomet. Chem.* **1995**, *503*, 277.
(148) Dalla, V.; Catteau, J. P. *Tetrahedron* **1999**, *55*, 6497.
(149) Goldberg, S. I.; Bailey, W. D. *J. Am. Chem. Soc.* **1974**, *96*, 6381.
(150) De la Cruz, P.; Martin, N.; Miguel, F.; Seoane, C.; Albert, A.; Cano, F. H.; Gonzalez, A.; Pingarron, J. M. *J. Org. Chem.* **1992**, *57*, 6192.
(151) Ishizumi, K.; Ohashi, N.; Tanno, N. *J. Org. Chem.* **1987**, *52*, 4477.
(152) Hua, D. H.; Lou, K.; Havens, J.; Perchellet, E. M.; Wang, Y.; Perchellet, J.-P.; Iwamoto, T. *Tetrahedron* **2004**, *60*, 10155.
(153) Dhananjeyan, M. R.; Milev, Y. P.; Kron, M. A.; Nair, M. G. *J. Med. Chem.* **2005**, *48*, 2822.
(154) Chen, Z.; Swager, T. M. *Org. Lett.* **2007**, *9*, 997.
(155) Rosenblum, M.; Woodward, R. B. *J. Am. Chem. Soc.* **1958**, *80*, 5443.
(156) Nesmeyanov, A. N.; Vol'kenau, N. A.; Vil'chevskaya, V. D. *Dokl. Akad. Nauk SSSR* **1956**, *111*, 362.
(157) Weißenbacher, M.; Sturm, T.; Kalchhauser, H.; Kratky, C.; Weissensteiner, W. *Monatsh. Chem.* **2002**, *133*, 991.
(158) Nesmeyanov, A. N.; Vil'chevskaya, V. D.; Kochetkova, N. S. *Izv. Akad. Nauk SSSR, Ser. Khim.* **1966**, 938.
(159) Liu, T.; Duan, G.; Zhang, Y.; Fang, J.; Zeng, Z. *Spectrochim. Acta, Part A* **2009**, *74*, 843.
(160) Raposo, M. M. M.; Sampaio, A. M. B. A.; Kirsch, G. *J. Heterocycl. Chem.* **2005**, *42*, 1245.
(161) Nesmeyanov, A. N.; Vil'chevskaya, V. D.; Kochetkova, N. S. *Dokl. Akad. Nauk SSSR* **1961**, *138*, 390.
(162) Li, Z.; Liu, S.; Wu, J.; Li, G. *Huaxue Yanjiu* **2008**, *19*, 51.
(163) Nesmeyanov, A. N.; Vil'chevskaya, V. D.; Kochetkova, N. S. *Dokl. Akad. Nauk SSSR* **1965**, *165*, 835.
(164) Weliky, N.; Gould, E. S. *J. Am. Chem. Soc.* **1957**, *79*, 2742.
(165) Rosenblum, M.; Banerjee, A. K.; Danieli, N.; Fish, R. W.; Schlatter, V. *J. Am. Chem. Soc.* **1963**, *85*, 316.
(166) Osgerby, J. M.; Pauson, P. L. *J. Chem. Soc.* **1961**, 4604.
(167) Pauson, P. L.; Watts, W. E. *J. Chem. Soc.* **1962**, 3880.
(168) Martin, E. L. *J. Am. Chem. Soc.* **1936**, *58*, 1438.

(169) Simenel, A. A.; Samarina, S. V.; Snegur, L. V.; Starikova, Z. A.; Ostrovskaya, L. A.; Bluchterova, N. V.; Fomina, M. M. *Appl. Organomet. Chem.* **2008**, *22*, 276.
(170) Lee, H.; Harvey, R. G. *J. Org. Chem.* **1986**, *51*, 3502.
(171) Delacroix, O.; Andriamihaja, B.; Picart-Goetgheluck, S.; Brocard, J. *Tetrahedron* **2004**, *60*, 1549.
(172) Takahashi, T.; Li, S.; Huang, W.; Kong, F.; Nakajima, K.; Shen, B.; Ohe, T.; Kanno, K.-i. *J. Org. Chem.* **2006**, *71*, 7967.
(173) McMurry, J. E.; Fleming, M. P. *J. Am. Chem. Soc.* **1974**, *96*, 4708.
(174) Zhang, H.; Cao, D.; Liu, W.; Jiang, H.; Meier, H. *J. Org. Chem.* **2011**, *76*, 5531.
(175) Siegel, S.; Schmalz, H.-G. *Angew. Chem. Int. Ed.* **1997**, *36*, 2456.
(176) Baker, C.; Horspool, W. M. *J. Chem. Soc., Perkin Trans. 1* **1979**, 1862.
(177) Creary, X.; Mehrsheikh-Mohammadi, M. E.; McDonald, S. *J. Org. Chem.* **1989**, *54*, 2904.
(178) Aubry, J.-M.; Pierlot, C.; Rigaudy, J.; Schmidt, R. *Acc. Chem. Res.* **2003**, *36*, 668.
(179) Wang, B.; Mu, B.; Chen, D.; Xu, S.; Zhou, X. *Organometallics* **2004**, *23*, 6225.
(180) Luo, S.; Zhao, X.; Mu, B.; Song, H.; Xu, S.; Wang, B. *Organometallics* **2009**, *28*, 4602.
(181) Fedin, E. I.; Blumenfeld, A. L.; Petrovskii, P. V.; Kreindlin, A. Z.; Fadeeva, S. S.; Rybinskaya, M. I. *J. Organomet. Chem.* **1985**, *292*, 257.
(182) Hisatome, M.; Yamakawa, K. *Tetrahedron* **1971**, *27*, 2101.
(183) Ceccon, A.; Giacometti, G.; Venzo, A.; Paolucci, D.; Benozzi, D. *J. Organomet. Chem.* **1980**, *185*, 231.
(184) Traylor, T. G.; Ware, J. C. *J. Am. Chem. Soc.* **1967**, *89*, 2304.
(185) Richards, J. H.; Hill, E. A. *J. Am. Chem. Soc.* **1959**, *81*, 3484.
(186) Hill, E. A.; Richards, J. H. *J. Am. Chem. Soc.* **1961**, *83*, 3840.
(187) Hill, E. A.; Richards, J. H. *J. Am. Chem. Soc.* **1961**, *83*, 4216.
(188) Kreindlin, A. Z.; Dolgushin, F. M.; Yanovsky, A. I.; Kerzina, Z. A.; Petrovskii, P. V.; Rybinskaya, M. I. *J. Organomet. Chem.* **2000**, *616*, 106.
(189) Kreindlin, A. Z.; Petrovskii, P. V.; Rybinskaya, M. I.; Yanovskii, A. I.; Struchkov, Y. T. *J. Organomet. Chem.* **1987**, *319*, 229.
(190) Sime, R. L.; Sime, R. J. *J. Am. Chem. Soc.* **1974**, *96*, 892.
(191) Berger, A.; McEwen, W. E.; Kleinberg, J. *J. Am. Chem. Soc.* **1961**, *83*, 2274.
(192) Heinis, T.; Chowdhury, S.; Scott, S. L.; Kebarle, P. *J. Am. Chem. Soc.* **1988**, *110*, 400.
(193) Kalyani, V.; Vijayan, M. *Acta Crystallogr., Sect. B* **1969**, *25*, 252.
(194) Butler, I. R.; Cullen, W. R.; Rettig, S. J.; Trotter, J. *Acta Crystallographica Section C* **1988**, *44*, 1666.
(195) Martin, E. L. *Org. Synth.* **1943**, *2*, 499.

Vita

Author Name: Uttam R. Pokharel

Uttam Raj Pokharel was born on 3rd of December, 1973 in Sindhuli, Nepal.

Education:

Ph. D. Inorganic Chemistry, University of Kentucky, Lexington, KY, USA
Advisor: Prof. John P. Selegue (Expected 2012)

M. Sc. Organic Chemistry, Tribhuvan University, Kathmandu, Nepal (1999)

B. Sc. Chemistry/Biology, Tribhuvan University, Kathmandu, Nepal (1996)

Teaching Experience: Organic, inorganic and general chemistry (2000-2006)

Conferences and Presentations:

Oral presentations:

2011: ACS National Meeting, Denver, CO: Synthetic Approaches to Acene Complexes of Ruthenium, Manganese and Iron

2011: ACS National Meeting, Anaheim, CA: Synthetic Approaches to Acene Complexes of Ruthenium and Manganese

2009: KAS Annual Meeting, Northern Kentucky University, KY: Synthetic Approaches to Acene Complexes of Ruthenium or Manganese

2008: KAS Annual Meeting, University of Kentucky, KY: Synthetic Approaches to Acene and Heterocycle-Fused Complexes of Ruthenium or Manganese

Poster presentations:

2011: Naff Symposium, University of Kentucky, KY: Synthesis and Characterization of Acene-Quinone Complexes of Ruthenium, Manganese and Iron

2010: Naff Symposium, University of Kentucky, KY: Synthetic Approaches to Acene Complexes of Ruthenium and Manganese

2008: Naff Symposium, University of Kentucky, KY: Thiophene or Selenophene-Fused Heterocyclic Complexes of Ruthenium or Manganese

2007: Ohio Inorganic Weekend, Miami University, Oxford, OH: Cationic, Thiophene-Fused Heterocyclic Complexes of Ruthenium

Awards:

242nd American Chemical Society (ACS) general travel awards (2011)

Professional Affiliations:

- American Chemical Society
- Kentucky Academy of Science
- Nepal Chemical Society

Publication:

Uttam Raj Pokharel, John P. Selegue, Sean Parkin, "Ruthenocene 1,2-Dicarboxylic Acid, Carboxylic Anhydride, and Acid Chloride: A Facile Route to Metallocene-Fused Acenequinones." *Organometallics*, **2011**, *30*, 3254-3256.